10-12-2015

Design Of Shape Morphing Structures Using Bistable Elements

Ahmad Alqasimi
University of South Florida, aan2309@gmail.com

Follow this and additional works at: http://scholarcommons.usf.edu/etd

Part of the Mechanical Engineering Commons

www.manaraa.com

Design of Shape Morphing Structures Using Bistable Elements

by

Ahmad Erfan Alqasimi

A dissertation submitted in partial fulfillment
of the requirements for the degree of
Doctor of Philosophy in Mechanical Engineering
Department of Mechanical Engineering
College of Engineering
University of South Florida

Major Professor: Craig Lusk, Ph.D.
Kyle Reed, Ph.D.
Daniel Hess, Ph.D.
Thomas Weller, Ph.D.
Christos P. Tsokos, Ph.D.

Date of Approval:
November 9, 2015

Keywords: Compliant Mechanism, Pseudo-Rigid-Body Model, Space-frame, Tessellation
Kinematics

بِسْمِ اللهِ الرَّحْمنِ الرَّحِيمِ

"In the name of God, the Most Gracious, the Most Merciful"

وَقُل رَّبِّ زِدْنِي عِلْمًا

"O my Lord increase me in knowledge"

اللَّهُمَّ أَعِنِّي عَلَى ذِكْرِكَ، وَشُكْرِكَ، وَحُسْنِ عِبَادَتِكَ

"Oh God, Help me to Remember You, and

Thank You, and Worship You in the Best of Manners"

اللَّهم إِنِّي أَسْأَلُك عِلمًا نافِعًا، ورزقًا طَيِّبًا، وعمَلًا متقَبَّلًا

"O God indeed I ask You for beneficial knowledge,

and Pure Bestowed, and deeds which are accepted"

DEDICATION

To my parents, Erfan Alqasimi and Yousra Hajjar

&

To my wife, Nayat

&

To Zeidan and Lidia Hammad

&

To Maria Gonzalez-Pardo (Mami)

&

To my son Faisal

....

ACKNOWLEDGMENTS

The author gratefully acknowledges the efforts and support of all those involved in making this research and dissertation possible. My utmost gratitude is devoted to my professor and advisor, Dr. Craig Lusk, who provided me with the knowledge needed for this work. I was able to achieve high standards in research thanks to his mentorship and guidance. His vast knowledge in the compliant mechanism and engineering design fields inspired me to have the vision in accomplishing this work.

My thanks to the Compliant Mechanisms Research Group for assisting me throughout this work. Special thanks to Jairo Chimento and Philip Logan for their constant help and motivation. My gratitude also extends to the Committee members for their time and effort put into reviewing this work. The author acknowledges the support of the National Science Foundation, Grant # CMMI-1053956.

I would like to warmly thank all family members who were there for me every step of the way to accomplish this dream. My parents have always been my biggest inspiration and have never hesitated to push me to excellency. I consider my father my role model, due to his constant hard work and sacrifice. I consider my mother my soul, as she has always been there for me around the clock day and night constantly giving me the voice that made me endure this journey.

Finally, I would like to thank my wife who has been my companion and supporter. Her devotion in taking care of the family made it possible to put the time needed in my research. Although not aware of their impact, my children are also the motivation behind my hard work.

TABLE OF CONTENTS

LIST OF TABLES

LIST OF FIGURES

ABSTRACT

This dissertation presents new concepts and methodology in designing shape-morphing structures using bistable elements. Developed using the Pseudo-Rigid-Body Model (PRBM), linear bistable compliant mechanism elements produce predictable and controllable length changes. Step-by-step design procedures are developed to guide the design process of these bistable elements. Two different examples of Shape-Morphing Space-frames (SMSFs) were designed and prototyped utilizing the bistable linear elements in a single-layer grid, in addition to flexures and rigid links, to morph a cylindrical space-frame into both a hyperbolic and a spherical space-frame. Moreover, bistable unit-cell compliant-mechanism elements were also developed to morph a compact structure from a specific initial shape to a final specific shape. The detailed design of those unit-cells were done using Computer-aided design (CAD) software following a novel design procedure to transform a one-degree-of-freedom mechanism into a structure with sufficient compliance within its links to toggle between two chosen stable positions. Two different design examples were investigated in this research and prototyped to demonstrate the ability to morph disks into a hemisphere or a sphere with the structure being stable in both states (disk and sphere).

CHAPTER 1: INTRODUCTION

1.1 Objective

The objective of this dissertation is to introduce two new models for bistable compliant mechanisms and design guidelines for their customization. These models are demonstrated with arrays of such mechanisms being used to produce morphing structures.

The first model is a linear bistable element. The guidelines will allow designers to follow a step-by-step procedure to design a mechanism that would produce a linear bistable mechanism (i.e., the mechanism's displacement is parallel to the applied force). In addition, two design examples are demonstrated that utilize the Linear Bistable Compliant Crank-Slider Mechanism (LBCCSM) elements to morph space-frames from a specific initial shape to a final desired shape. Placement of each element is critical, and it is dependent on the designer's choice of the specific Shape-Morphing Space-frame (SMSF).

The second, a unit-cell bistable compliant mechanism model, is introduced with a step-by-step design procedure using the Computer-aided design (CAD) Solidworks software. This allows the replacement of the LBCCSM with compact structures, which permit significant change in length when compared to their initial lengths. A novel method is developed to transform a four-bar mechanism into a bistable mechanism without the use of torsional springs at the joints. Two different examples of this novel method are modeled and prototyped demonstrating the use of unit-cell bistable elements.

1

1.2 Motivation

The motivation for this work is to develop design procedures for multiple compliant mechanism models that designers can utilize for specific applications. Having the ability to morph a space-frame or a structure from one stable position to another, by design, would impact the way engineers design their projects. To be able to achieve a possible second application from a single model is remarkable engineering by itself. The materials used to manufacture such compliant mechanisms play an important role in the design process; the compliant links will act as rigid links when no forces are applied, but once the mechanism is actuated, those links would have enough flexibility to convert the applied forces into enough potential energy that will allow such mechanism to toggle between the two states.

Common applications for bistable mechanisms include multistable switches, self-closing gates, hinges and closures [1]. On the other hand, the ability to change the surface profile upon actuation can be implemented in various applications such as deployable antennas, airplane wings' morphing, and fluid flow controllers. Having a controllable Solid-Fluid interface can be used to reduce drag, restrict the flow and many other advantages. In the automotive industry, bistable mechanisms can be used to construct the fuselage or the bumper in particular of an automobile that upon collision, the kinetic energy is absorbed into the compliant links causing it to achieve the second stable position where fixing it may only require toggling the structure into its original state. Moreover, if the SMSF were able to be manufactured at the micro-scale, it could be used in medical applications as an intravascular stent. It would have the ability to change its shape to fit into a small incision and morph its structure to assume a final shape.

1.3 Scope

The scope of this work is to describe two novel design methods and the demonstration of their ability in shape morphing. The first design method produces predictable and controllable length changes in certain mechanical systems, allowing the morphing from one specific shape into a different specific shape. The ability to specify the LBCCSM mechanism's footprint is also important and is a novel contribution of this work. This type of design can be used in the Shape-Shifting Surfaces (SSSs) [9] as an attachment to it, providing surface coverage and bistability to the space-frame. The controllable length change allows the design of a developable surface composed of single-layer grid of flexures and LBCCSMs that if arranged in certain tessellation pattern, would transform a 2D developable surface design to a variable 3D space-frame.

The second design method produces unit-cell compliant mechanism elements which can be used as an alternative to the LBCCSM in a dense structure to transform its planes or faces into bistable two dimensional shape. The ability to morph a single plane composed of a single mechanism from one specific shape into another with the use of compliant link for bistability is a novel contribution to this research. The bistable unit-cell elements can be used to construct an initial 3D shape that morph into different designed 3D shape maintaining structures' stability at both state such as morphing a disk into a hemisphere or two disks into a sphere.

1.4 Overview

Chapter 2 serves as background and prior research used in this dissertation. This includes the concept of Pseudo-Rigid-Body Model (PRBM) replacement method for both fixed-pinned and pinned- pinned cantilever beam, the concept of compliant mechanisms bistability, which is the ability to store and release the potential energy within its compliant links upon actuation and the application of graph theory in mechanisms.

Chapter 3 describes the modeling of the Linear-Bistable-Compliant Crank-Slider Mechanism (LBCCSM) along with the equations and plots used to construct the flow charts and step-by-step design guidelines. Two different approaches to the design problem are illustrated with a design example for each approach.

Chapter 4 utilizes the LBCCSM modeling to design a Shape-Morphing Space-frame (SMSF). This involves the tessellation of a single-layer grid and identifying the rigid links from the variable link within the grid through a selection process. Design algorithms and morphing strategies are discussed with two design examples in which a cylindrical space-frame is morphed to a hyperbolic space-frame and to a spherical space-frame in the other. Both example are prototyped and were compared with the theoretical analysis.

Chapter 5 introduces the SMSF using quadrilateral bistable unit-cell elements via design example of morphing a disk to a hemisphere. The strategy behind the disk tessellation is discussed and how is it reduced to a manageable segments where mechanisms' synthesis can be applied to individual planes. Each different plane was synthesized according to its type and dimensions governed by design constraints. Graph theory was also utilized to synthesize one of the mechanisms followed by the use of the Solidworks software for detailed design and validation of the mechanisms to ensure that all the constraints were met. Two prototypes were produced to demonstrate the shape morphing from a disk to a hemisphere in one arrangement. In another arrangement, disks morphed to a sphere, requiring a minor alteration to the design. The second prototype was then subjected to a tensile test to analyze its behavior under different displacement rates.

Chapter 6 investigates adding bistability to four-bar mechanisms by introducing over-constraint. Previous work on achieving bistability in four-bar mechanisms, used placing a

torsional spring at a specific joint, was limited in the second stable positions that the mechanisms could toggle to. It was found that replacing the torsional spring with a compliant link at a specific location within the mechanism, allows to specifically designing arbitrary second stable positions. The design process was carried out using the Solidworks in two stages; the first stage considers the kinematic analysis of the mechanism, where the second stage analyzes the placement of the compliant link that serves as Potential Energy Element (PEE). Both stages are illustrated using step-by-step design guidelines.

Chapter 7 concludes this research work by summarizing the contribution done to the compliant mechanism field. Recommendations are given to whom wants to utilize the designs procedures. Finally, future work ideas are given.

5

CHAPTER 2: LITERATURE REVIEW

2.1 Compliant Mechanisms

A compliant mechanism is a mechanism that derives some or all its motion (mobility) from the deflection of flexible segments, thereby removing the need for mechanical joints. The absence or reduction of mechanical joints impacts both performance and cost. The flexible segments within the mechanism are generally thinner than the rigid ones, thus they are the first to deform under the applied force or displacement. The compliant mechanisms are categorized into two types, fully compliant or partially compliant. The fully compliant mechanisms do not contain any kinematic pairs (pins), whereas the partially compliant may contain one or more joints such as sliders and pins [1].

Advantages include reduced friction and wear, increased reliability, precision, and decreased maintenance and weight [1, 20]. Moreover, cost is also affected by reduced assembly time and, in most cases, due to its hingeless design; the fabrication of such mechanisms can be produced from a single piece reducing the number of parts [2]. An increase of precision within the compliant mechanism is due to the absence of friction forces generated by pin joints, thus reducing the vibration. As a result, compliant mechanisms are widely used in high precision instruments [3,46]. Also this type of mechanism is used in commercial products such as compliant based hinges [4, 5]. Additionally, compliant mechanisms provide the designer with an effective way to achieve mechanical stability in robotic design as in [45]. On the other hand, there are disadvantages and challenges in using compliant mechanism. The compliant segments

6

can experience creep (stress relaxation) deformation if they were subjected to a high-stress high-temperature environment for a long period of time. Because the flexible segments are used as potential energy storage elements, staying within the elastic rage of the material when the mechanism experience deformation is challenging and imposes limitations the design [6].

2.2 Approaches in Designing Compliant Mechanisms

The most commonly used approach in synthesizing compliant mechanisms is the Pseudo-Rigid-Body Models (PRBMs) [1], which is the method used in this research work, as further insight will be discussed. Alternative approaches utilize topology optimization methods to produce nonlinear compliant mechanism under specific input and output displacement [47, 48]. Su [49] uses the polynomial homotopy to formulate the four-bar compliant mechanism kinematic equations, solving for specific design parameters. An interesting approach used by Limaye [50] is using a compliant mechanism kit (connector and flexible beams) that will allow the construction of a designed mechanism and correlate the behavior of that from the topology optimization. Finally, computer-aided design (CAD) software was used in [58, 59] for planar mechanism kinematics designs and synthesis, whereas in this research, CAD will be heavily used in bistable compliant mechanisms design and synthesis.

2.3 Pseudo-Rigid-Body Model (PRBM) Concept

The Pseudo-Rigid-Body Model (PRBM) was the approach used to design the LBCCSM elements, the PRBM approximations were first developed by Howell and Midha [7]. Those approximations were then compared to the Bernoulli-Euler beam equations to produce a more general approach to the PRBM as well as to quantify its accuracy [8].

The PRBM are an easier and simplified technique to analyze and characterize the nonlinear behavior of beams undergoing large deflections. This technique approximates the

flexural beam as two or more rigid links (depending on the beam's loading condition) joined by torsional springs. The location of the torsional springs, the stiffness coefficient and the length of the rigid links are all PRBM parameters, in which they describe the nonlinear behavior in the kinematic and force-deflection analysis of the mechanical system. There are different types of PRBMs developed using the compliant mechanism theory to simulate the flexural segments' behavior which includes [12-19]:

- Small-length flexural pivots or living hinges,

- Fixed-Pinned cantilever beam with a force at the free end,

- Fixed-Guided flexible segments,

- End-Moment loading on cantilever beams,

- Initially curved cantilever beams,

- Pinned-Pinned cantilever beam segments,

- Fixed-Fixed segment with force and moment,

- Fixed-Pinned 3D cantilever beam with an arbitrary force at the end, and

- Fixed-Pinned cantilever beam with forces and uniformly distributed loads acting in parallel.

This research focuses on two PRBM types, the Fixed-Pinned cantilever beam with a force at the free end and the Pinned-Pinned cantilever beam [1]. The following subsections will discuss each model individually. Both PRBMs use torsional springs modeled using small-length flexural pivots (straight joint and constant cross-section) with their stiffness derived from the mechanism's material properties [51]. Under large displacement, the compliant segments experience high stresses which limiting the range of motion of the mechanism. Analyses on

8

different types of joints (curved and semicircular) configurations were done in [52, 53] for use as large displacement hinges.

2.3.1 PRBMs for Fixed-Pinned Cantilever Beam

This PRBM considers a uniform cross section cantilever, shown in Figure 2.1 (a), with homogenous material properties. Figure 2.1 (b) shows the equivalent pseudo-rigid-body model for a large deflection with the end-point of the beam following a circular path in which the characteristic pivot is its center. The torsional spring, which the material properties determine its stiffness coefficient (K), is located at the characteristic pivot to represents the resistance of the beam upon deflection. The radius of the beam's end path is represented by the characteristic radius (γl) where (l) is the beams undeflected total length and (γ) is the characteristic radius factor. The angle between the undeflected pseudo-rigid-link and the deflected position is called the pseudo-rigid-body angle (Θ). The location of the end point of the beam (where the origin is at the fixed end) is represented by the (a) and (b) which are the x-coordinate (horizontal distance) and the y-coordinate (vertical distance), respectively. The equations describing this pseudo-rigid-body-model are [1]:

$$a/l = 1 - \gamma(1 - \cos\Theta) \tag{2.1}$$

$$b/l = \gamma \sin\Theta \tag{2.2}$$

$$\Theta = \tan^{-1}\left(\frac{b}{a - l(1-\gamma)}\right) \tag{2.3}$$

$$\gamma = \frac{\left(\frac{b}{l}\right)^2 + \left(1 - \frac{a}{l}\right)^2}{2\left(1 - \frac{a}{l}\right)} \tag{2.4}$$

$$K = \gamma K_\Theta (EI/l) \tag{2.5}$$

9
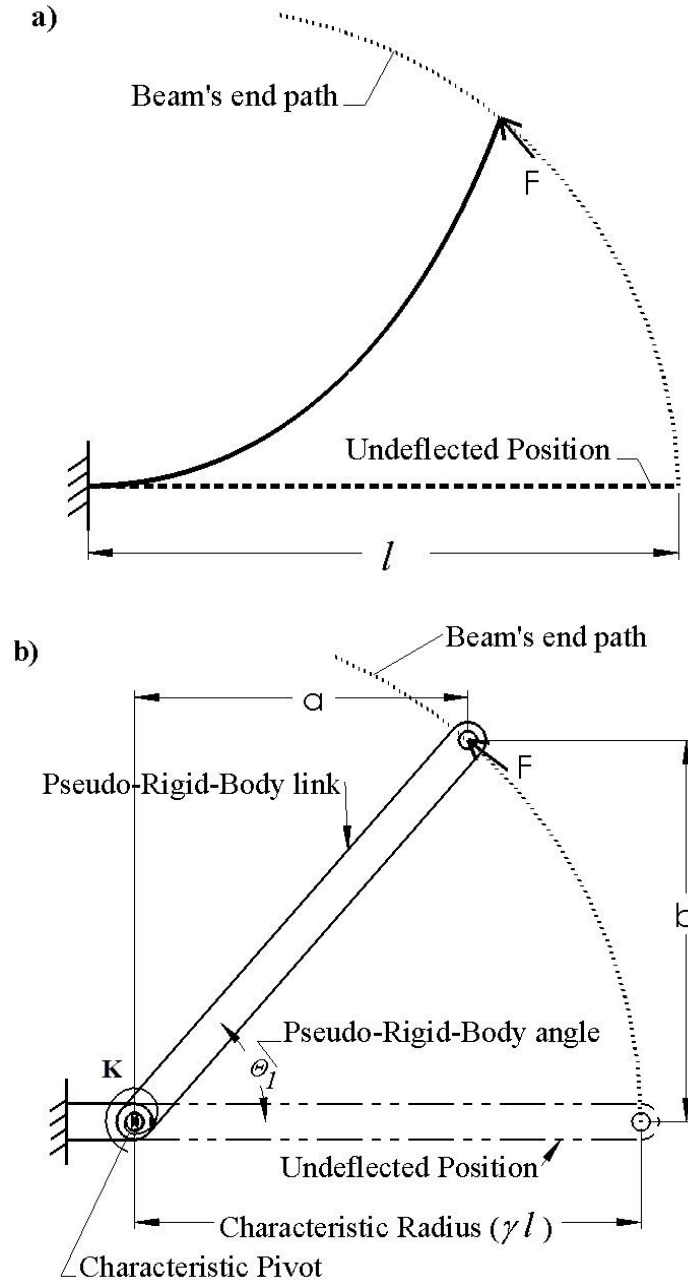
Figure 2.1 The PRBM of the Fixed-Pinned cantilever beam, adapted from [1].

2.3.2 PRBMs for Pinned-Pinned Cantilever Beam

This model was developed for initially curved beams and it was slightly modified to fit

the use of the LBCCSM discussed in Chapter 3. Figure 2.2 (a) shows a cantilever beam with

nonlinear large deflection behavior, whereas Figure 2.2 (b) represents the same beam with the

pseudo-rigid-body approximation. It uses the same definitions as the Fixed-Pinned PRBM with the following modified equations [1]:

$$a/l = 1 - \gamma + \rho \cos(\Theta) \tag{2.6}$$

$$b/l = \rho/2 \sin \Theta \tag{2.7}$$

$$K = 2 \rho K_\Theta (EI/l) \tag{2.8}$$
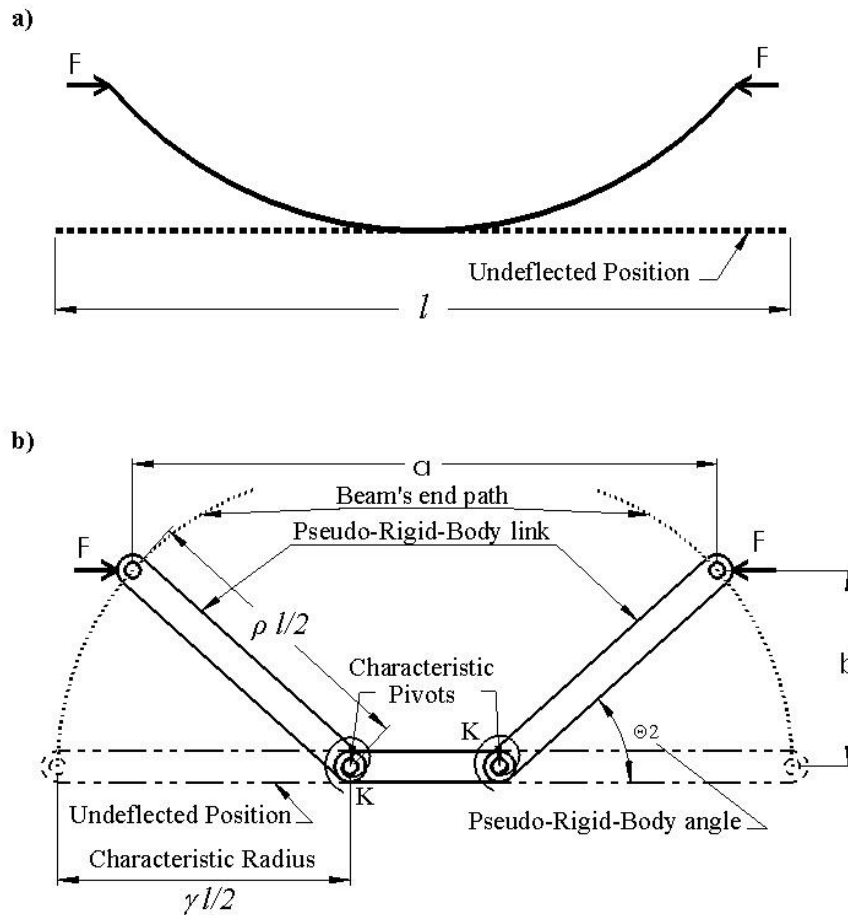
Figure 2.2 The PRBM of the Pinned-Pinned cantilever beam, adapted from [1].

2.4 Bistability in Compliant Mechanisms

A compliant bistable mechanism achieves its stability within the designed range of motion, by storing and releasing strain energy in its compliant segments [21]. Such a technique enables the mechanism to stay at its two stable positions without the need for an external

11

power/force to stay there. Energy methods, combined with Pseudo-Rigid-Body Models, can be used to analyze such compliant mechanisms [22].

2.4.1 Definition of Stability

The term *stability* in mechanisms is derived from their equilibrium state. There are two types of equilibriums, either stable or unstable; the stable equilibrium is a state where the mechanism's potential energy is at minimum and if any finite load or displacement exerted on it will cause oscillation about the point of equilibrium. On the other hand, as unstable equilibrium occurs at the maximum potential energy point on the mechanism's energy curve, and if any finite load or displacement exerted on the system will cause the mechanism to diverge to the stable equilibrium point.

This idea can be further illustrated using the "ball on the hill" analogy with the energy curve (potential energy vs. position) is correlated with the force-displacement curve for the given system shown in Figure 2.3. Starting from position 1, the ball is at stable equilibrium where the potential energy is at local minimum with no load being applied to the system as shown in the force-displacement curve. The force-displacement curve crosses the x-axis at every equilibrium points and when the derivative of the force-displacement curve is zero, this corresponds to an inflection point on the energy curve. At position 2, the ball is at unstable equilibrium state with the tendency to roll toward the first position or the third position depending on the direction of the load or displacement exerted. Position 3 of the ball is the second stable equilibrium point; this can be achieved using a hard-stop (position 3a) which holds the ball in place due to the reaction forces from the hard-stop on the ball, whereas the position 3b is the second stable equilibrium position (local minimum) by following the energy curve.

12
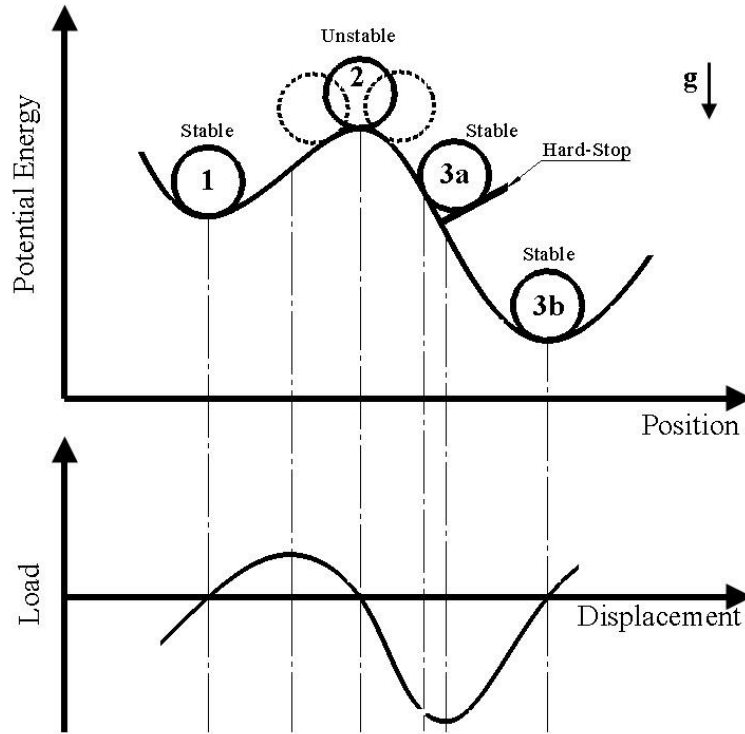
Figure 2.3 Ball on the hill analogy.

The characteristics of such bistable systems (or mechanism) can be summarized by following the ball on the hill example and correlating both curves in Figure 2.3 and I quote:

- "*A mechanism will have a stable equilibrium position when the first derivative of the potential energy curve is zero and the second derivative of the potential energy curve is positive.*

- *A mechanism will have an unstable equilibrium position when the first derivative of the potential energy curve is zero and the second derivative of the potential energy curve is negative.*

- *A mechanism will have a neutrally stable equilibrium position when the first derivative of the potential energy curve is zero and the second derivative of the potential energy curve is also zero.*

13

- *Because two local minima must always contain one local maximum between them, an unstable or neutrally stable position will always occur between any two stable states.*

- *The critical moment (the maximum load required for the mechanism to change stable states) may be found by evaluating the moment curve when the second derivative of potential energy is zero.*

- *The stiffness of a stable equilibrium position is equal to the value of the second derivative of potential energy at that position.*" [23]

2.4.2 Examples of Compliant Mechanisms' Stability

This subsection introduces work done on compliant mechanism stability by first describing examples of bistable mechanisms and then example s of multistable mechanisms.

In a wide variety of systems, bistable mechanisms are used to achieve two distinct mechanism state, such as bistable switches (on or off) and plastic caps (closed or open). The most commonly used mechanism is the four-bar linkage; an extensive study done by Howell [28] on this type of mechanisms by modeling it using the Pseudo-Rigid-Body (PRB) method. His studies concluded that by placing a torsional spring with a specific stiffness at a specific joint location will allow a four-bar mechanism to achieve bistability. The location of the spring for the Grashof mechanisms could be at either joint that is opposite to the shortest link, whereas for the non-Grashof and change-point mechanisms, the torsional spring could be located at any of the joints to produce bistable mechanisms. Similar studies were done by Schulze [29], where he incorporated the forces involved in a snap-action toggle mechanism by developing equations optimizing the actuation forces and the foot-print of the mechanism.

In micro-mechanisms (MEMS), interest in recent research has been focusing on developing micro compliant bistable mechanisms for their ability to be manufactured out of a

14

single unit without mechanical joints. Improving positioning accuracy along with energy efficiency on such mechanism was done by Jensen [33] through the development of the Young bistable mechanism and the Double-Young for tri-stable mechanisms in [56]. An in-plane rotary bistable compliant MEMS was also developed in [34] that could have potential use in micro-mechanical locks, optical shutters, and micro valves, whereas micro-sensors are developed in [35]. Out-of-plane bistable MEMS are also developed by Lusk [36] where the initial stable position is in-plane and the second stable position is out-of-plane.

Furthermore, given the fact that a bistable compliant mechanism derives its motion from the large deformation of its compliant links, incorporating bucking behavior along with the PRBM models on bistable mechanisms was first introduced by Sonmez [37] and further enhanced by Camescasse [38]. In both studies, the bucking and post-buckling behavior of the compliant links is modeled using the theories in [39-42]. Various other techniques are used with compliant mechanisms such as the torque approach used by [43] to develop a flapping mechanism to simulate the motion of insects' wings. Shape-memory-alloys are also used in [44] to actuate the bistable mechanism in a temperature controlled environment.

Arranging multiples of bistable mechanisms in certain configuration will result into tri-stable compliant system as in [54]. Ohsaki [55] also showed a multistable compliant system snap-through arrangement by shape-designing pin-jointed segments. Three-way micro-mechanisms switches are possible using the tri-stable approaches in [57].

2.5 Shape Morphing Structures

Morphing of structures is an emerging research area in recent years. They have the ability to change shape and achieve multiple stable states; they may play an important role in future designs where structures can be reconfigured, adapting to different conditions such as airplane

15

wings. Morphing wings on aircraft can improve their performance over the traditional rigid wings. The wings adapt to the airplane's flight mode by changing their aerodynamic profile [63]; interlocking actuators are arranged in linear pattern to form the wings' structure providing morphing panels (developed by Boeing) in [69], whereas in [68], the aircraft wings are made of shape-memory alloy that are attached to the hinges to produce the shape morphing. Different types of design approaches are seen in the literature; designs could be in the form of origami-based structures [64], compliant plate structures [62, 65], Rigid-body mechanisms [61] or microarchitecture [66]. Topology optimization is also used to develop a morphing roof structure space-frame in [67].

2.6 The Context of This Research in the Compliant Mechanisms Field

Gallego in [71] shows his classification system and classifies compliant mechanism literature based on its design methodology. Figure 2.4 highlights the branches that are the main focus of this research work.
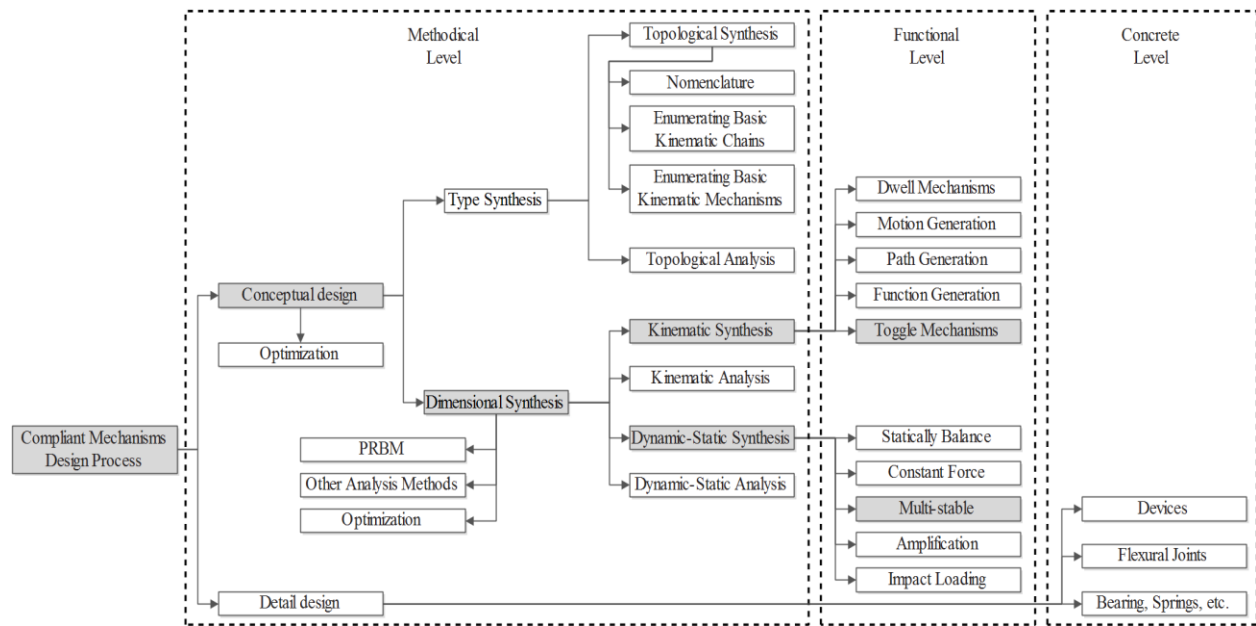
Figure 2.4 Classification for literature on compliant mechanism, adapted from [71].

16

CHAPTER 3: LINEAR BISTABLE CRANK-SLIDER-MECHANISM (LBCCSM) [*]

This chapter presents a new model for a linear bistable compliant mechanism and design guidelines for its use; the mechanism is based on the crank-slider mechanism. This model takes into account the first mode of buckling and post-buckling behavior of a compliant segment to describe the mechanism's bistable behavior. The kinetic and kinematic equations, derived from the Pseudo-Rigid-Body Model, were solved numerically and are represented in plots. This representation allows the generation of step-by-step design guidelines. The design parameters consist of maximum desired deflection, material selection, safety-factor, compliant segments' widths, maximum force required for actuator selection and maximum footprint (i.e. the maximum rectangular area that the mechanism can fit inside of and move freely without interfering with other components). Because different applications may have different input requirements, this work describes two different design approaches with different parameters subsets as inputs.

The Pseudo-Rigid-Body Model (PRBM) is an important practical approach used in this work to analyze and synthesize the LBCCSM. The approximations used in the PRBM were first developed by Howell and Midha, and works by incorporating the similar behavior between rigid-body mechanisms and compliant mechanisms [7]. The LBCCSM models based on two existing PRBMs, the Fixed-Pinned and the initially curved Pinned-Pinned PRBMs [1]. The Fixed-Pinned PRBM model was used to model the first segment (l as L_1), as shown in Figure 2.1, and the

---

[*] This chapter was published previously in [10]. Permission is included in Appendix H.

second segment (*l as L_2*) was modeled based on the initially curved Pinned-Pinned PRBM, as shown in Figure 2.2. A standard method for deriving the force-displacement equations for a compliant mechanism is the method of virtual work and the PRBM constants used are the recommended by Howell [1] as follows:

- Characteristic radius (Fixed-Pinned) $\gamma = 0.85$.

- Characteristic radius (Pinned-Pinned) $\rho = 0.85$.

- Stiffness coefficient $K_\Theta = 2.65$.

This chapter is organized as follows: First, the theory behind the LBCCSM model and how it was derived based on both PRBMs is described; second, two different design approaches with different inputs are shown using flow charts along with design charts; third, step-by-step design examples are illustrated; fourth, a brief description about the prototypes produced is given; finally, some concluding remarks regarding the design guidelines, the two proposed approaches used and future work recommendation that needed to enhance the design model.

3.1 Theory: LBCCSM Modeling

The model's equations were derived by solving both the kinematic and virtual work equations. The notations and parameters used, as well as a sketch of the model, are shown in Figure 3.1 and Figure 3.2 (a, b). The points B and C are compliant joints, and are considered small length flexural pivots, which derive their characteristic motion though bending [24]. Kinematic equations were utilized to calculate the kinematic coefficient, which was then substituted into the virtual work equations. The model's equations were then solved numerically and represented as plots. The parameters and nomenclatures used in this chapter and their definitions can be found in Appendix A.
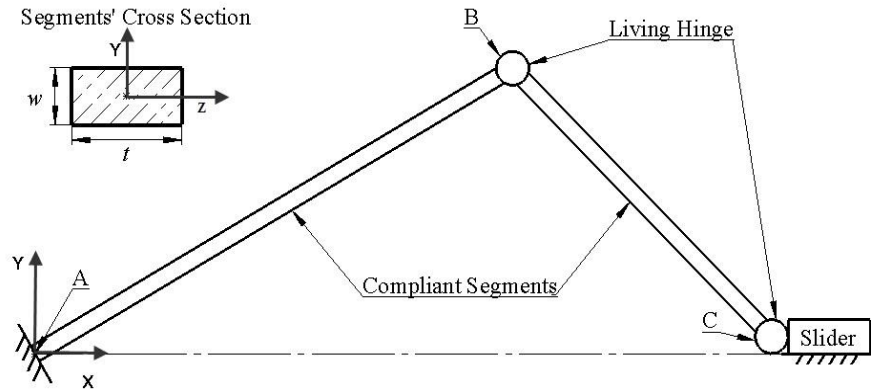
Figure 3.1 The mechanism considered, Point A is fixed, point B and C are living hinges.

The LBCCSM model behaves chosen in two different ways depending on the design parameters. In the first case, only segment 1 will experience the deflection, whereas segment 2 remains un-deflected and will only act as a force/displacement transmitter, can be seen in Figure 3.2 (a). In the second case, both segments experience some sort of deflection, i.e. bending of segment 1 and buckling of segment 2 as shown in Figure 3.2 (b). Both cases are presented with their corresponding equations, as well as the critical angles at which segment 2 buckles. Considering designs in which segment 2 buckles, allow for smaller footprints, which may be important in some applications.
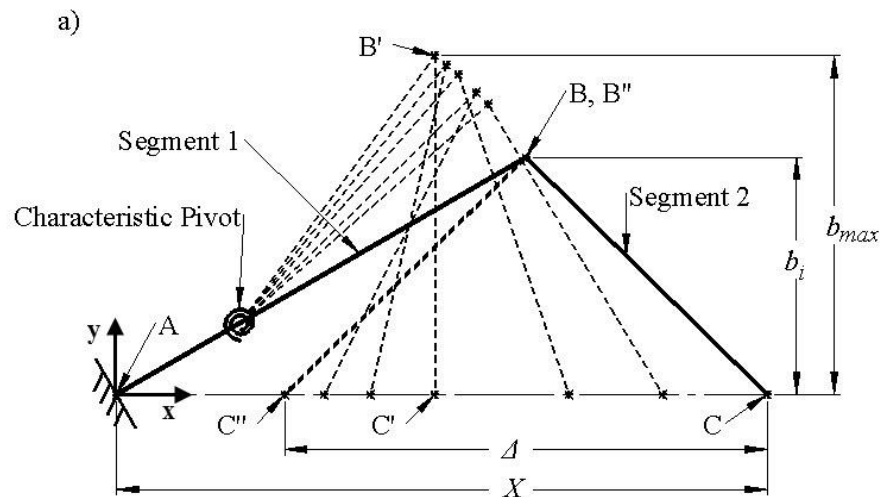
Figure 3.2 The LBCCSM model (a) 1st case, (b) 2nd case.

19

b)
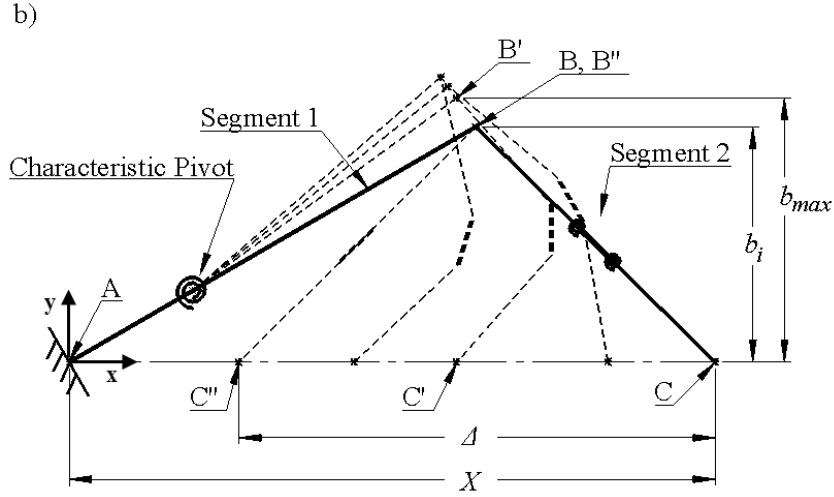
Figure 3.2 (Continued)

The notation used in this analysis and illustrates the relationship between the LBCCSM model and its equations can be shown in Figure 3.3. The Pseudo-Rigid-Body Model splits segment 1 into two parts [1]:

$$L_1 = l_{11} + l_{12} \text{ , where} \tag{3.1a}$$

$$l_{11} = (1 - \gamma)L_1 \quad and \quad l_{12} = \gamma L_1 \tag{3.1b}$$

In similar manner, segment 2 is divided into three parts when it buckles [1]:

$$L_2 = l_{21} + l_{22} + l_{23} \text{ , where} \tag{3.2a}$$

$$l_{21} = l_{23} = \gamma L_2/2 \quad and \quad l_{22} = (1 - \gamma)L_2 \tag{3.2b}$$

The characteristic stiffness associated with the Pseudo-Rigid-Body pivot in segment 1 is [1]:

$$K_1 = \gamma * K_\Theta * \frac{E*I_1}{L_1} \text{ , } where \quad I_1 = \frac{t\,w_1^3}{12} \tag{3.3}$$

The characteristic stiffness associated with the two Pseudo-Rigid-Body pivots in segment 2 when it buckles is [1]:

$$K_2 = \rho * K_\Theta * \frac{E*I_2}{L_2/2} \text{ , } where \quad I_2 = \frac{t\,w_2^3}{12} \tag{3.4}$$

20
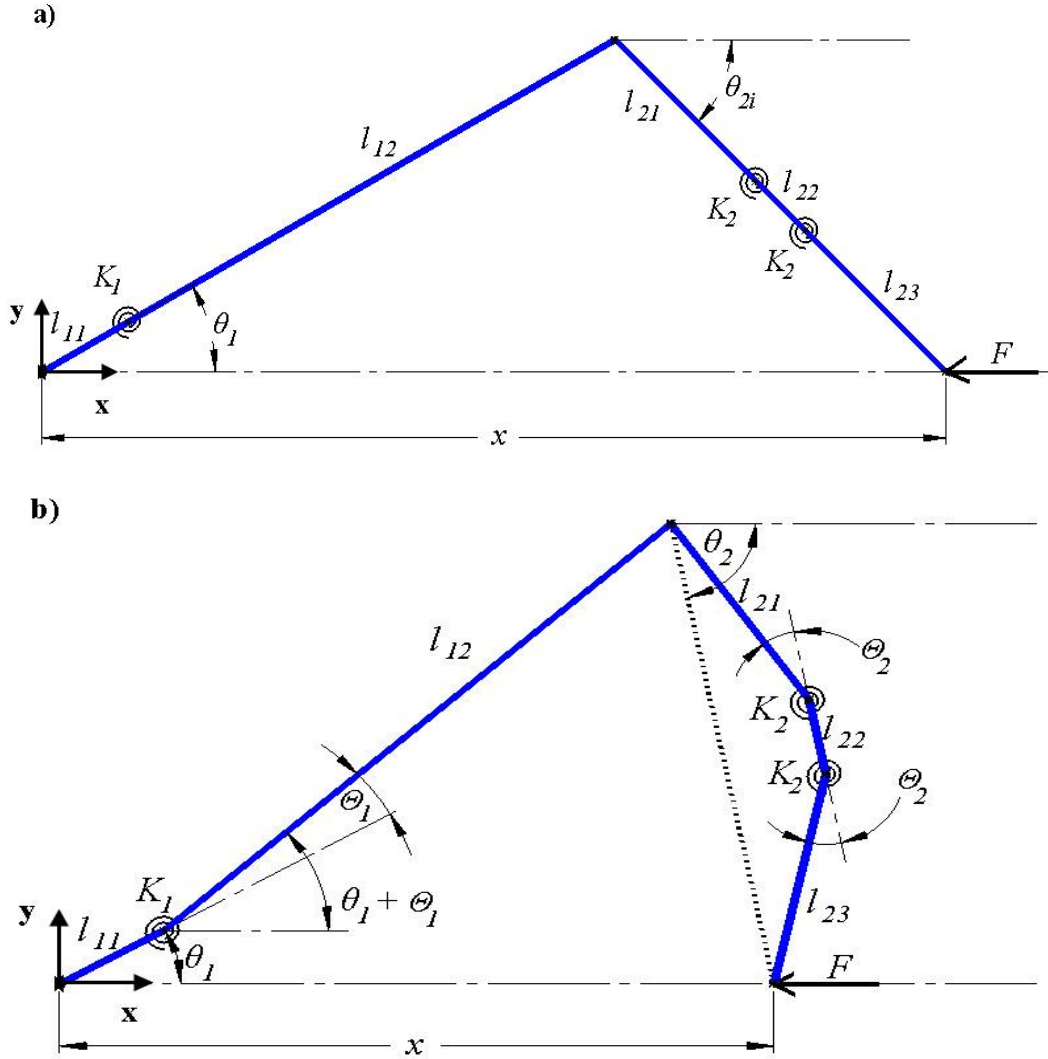
Figure 3.3 LBCCSM model at (a) Initial state, (b) Intermediate state.

3.1.1 The Buckling of Segment 2

The LBCCSM model's critical angles occur when the model switches from being solved using first case (bending only) to being solved using the second case (bending and buckling). Figure 3.4 shows the analysis of the segments' internal forces, which are then, used in the PRBM's moment equations. The moment equation for segment 1, using its characteristic pivot stiffness, is [1]:

$$M = \Theta_1 K_1 = F_t \gamma L_1 \tag{3.5}$$
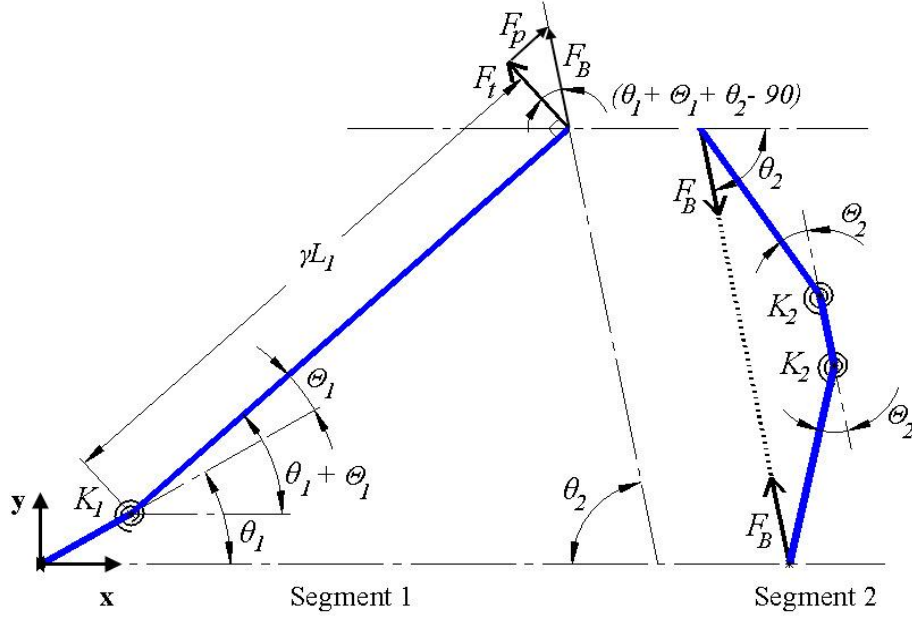
Figure 3.4 Internal force analysis.

From the force analysis illustrated in Figure 3.4:

$$F_t = F_B sin(\Theta_1 + \theta_1 + \theta_2) \tag{3.6}$$

$$F_B \geq \frac{\pi^2 E\, I_2}{L_2^2} \quad \text{for buckling} \tag{3.7}$$

Substituting equations (3.3, 3. 6 and 3.7) into equation (3.5) gives the condition for the critical value of (θ_2):

$$K_\Theta \Theta_1 = \frac{\pi^2}{2*v*m} sin(\Theta_1 + \theta_1 + \theta_2) \tag{3.8}$$

3.1.2 First Case: The Deflection of Segment 1 Only

In the first deflection mode, segment 2 does not buckle, and so the Pseudo-Rigid-Body Model looks like Figure 3.2 (a) and equations (3.2 and 3.4) do not apply. The loop closure equations for this case are:

$$-x + l_{11} cos(\theta_1) + l_{12} cos(\theta_1 + \Theta_1) + L_2 cos(\theta_2) = 0 \tag{3.9}$$

$$l_{11} sin(\theta_1) + l_{12} sin(\theta_1 + \Theta_1) - L_2 sin(\theta_2) = 0 \tag{3.10}$$

22

The virtual work equations (3.11 and 3.12) were obtained after choosing which of the unknowns is the independent variable and which are dependent variables. These equations are derived based on ($q_1 = x$ and $q_2 = \theta_2$) being the independent variables and (Θ_1, Θ_2 and F) being the dependent ones.

$$\partial w = F.dx - \frac{\partial V}{\partial q_i}\partial q_i = 0 \tag{3.11}$$

$$V = \frac{1}{2}K_1\,\Theta_1^2 + 2*(\frac{1}{2}K_2\,\Theta_2^2) \tag{3.12}$$

The above two equations (3.11 and 3.12) were solved for the independent variables and the kinematic coefficients. Because segment 2 is considered rigid in this case, substituting $\Theta_2{=}0$ is essential and results in:

$$-F.dx - \frac{\partial V}{\partial x}dx = 0 \tag{3.13}$$

$$\frac{\partial V}{\partial x} = K_1\,\Theta_1\frac{\partial\Theta_1}{\partial x} \tag{3.14}$$

$$\frac{\partial\Theta_1}{\partial x} = -\frac{cos(\theta_2)}{l_{12}sin(\Theta_1+\theta_1+\theta_2)} \tag{3.15}$$

The equations are made non-dimensional, in a way that allows for design flexibility, with the use of the following terms:

$$m = sin(\theta_1)/sin(\theta_{2i}) = L_2/L_1 \tag{3.16}$$

$$v = K_1/K_2 \tag{3.17}$$

$$f = \frac{F}{K_1} = F*\frac{L_1^2}{\gamma K_\Theta\,E\,I_1} \tag{3.18}$$

To non-dimensionalize the first case, equations (3.14 and 3.15) were substitute into equation (3.13) and then using equation (3.18) results in:

$$f + L_1\Theta_1\frac{\partial\Theta_1}{\partial x} = 0 \tag{3.19}$$

23

The final LBCCSM model's equations for the first case, which were solved numerically, are: equations (3.9, 3.10 and 3.19).

3.1.3 Second Case: The Deflection of Both Segments

In this case, both segments experience some deflection, and so the Pseudo-Rigid-Body Model looks like Figure 3.2 (b). The loop closure equations for this case are:

$$-x + l_{11}\cos(\theta_1) + l_{12}\cos(\theta_1 + \Theta_1) + l_{21}\cos(\theta_2 - \Theta_2) + l_{22}\cos(\theta_2) + l_{23}\cos(\theta_2 + \Theta_2) = 0 \quad (3.20)$$

$$l_{11}\sin(\theta_1) + l_{12}\sin(\theta_1 + \Theta_1) - l_{21}\sin(\theta_2 - \Theta_2) - l_{22}\sin(\theta_2) - l_{23}\sin(\theta_2 + \Theta_2) = 0 \quad (3.21)$$

Equations (3.11 and 3.12) were solved again for the independent variables result in:

$$-F.dx - \frac{\partial V}{\partial x}dx = 0 \tag{3.22}$$

$$F.\frac{\partial x}{\partial \theta_2}d\theta_2 - \frac{\partial V}{\partial \theta_2}d\theta_2 = 0 \tag{3.23}$$

Solving for the kinematic coefficients within δ*V*/δ*x* and δ*V*/δ*θ*₂ using equations (3.20) and (3.21) with δ*x*/δ*θ*₂ = 0 due to both (*x*) and (*θ*₂) are being chosen as independent variables results in:

$$\frac{\partial V}{\partial x} = K_1\,\Theta_1\,\frac{\partial \Theta_1}{\partial x} + 2\,K_2\,\Theta_2\,\frac{\partial \Theta_2}{\partial x} \tag{3.24}$$

$$\frac{\partial V}{\partial \theta_2} = K_1\,\Theta_1\,\frac{\partial \Theta_1}{\partial \theta_2} + 2\,K_2\,\Theta_2\,\frac{\partial \Theta_2}{\partial \theta_2} \tag{3.25}$$

$$\frac{\partial \Theta_1}{\partial x} = \frac{\sin(\theta_2)}{l_{12}\cos(\omega_3)} \tag{3.26}$$

$$\frac{\partial \Theta_1}{\partial \theta_2} = \frac{l_{22} + 2l_{21}\cos(\Theta_2)}{l_{12}\cos(\omega_3)} \tag{3.27}$$

$$\frac{\partial \Theta_2}{\partial x} = -\frac{\cos(\omega_1)}{2l_{21}\sin(\Theta_2)[\cos(\omega_1)\cos(\theta_2) - \sin(\omega_1)\sin(\theta_2)]} \tag{3.28}$$

$$\frac{\partial \Theta_2}{\partial \theta_2} = \frac{l_{21}\sin(\omega_2) + l_{22}\sin(\omega_3) + l_{23}\sin(\omega_4)}{l_{21}(\sin(\omega_4) - \sin(\omega_2))} \tag{3.29}$$

24

To non-dimensionalize the second case, equations (3.24 and 3.29) were substitute into equation (3.23) and using equations (3.16 to 3.18) results in:

$$f + \Theta_1 \frac{\partial \Theta_1}{\partial x} + 2 \frac{L_1}{v} \Theta_2 \frac{\partial \Theta_2}{\partial x} = 0 \tag{3.30}$$

$$\Theta_1 \frac{\partial \Theta_1}{\partial \theta_2} + 2 \frac{1}{v} \Theta_2 \frac{\partial \Theta_2}{\partial \theta_2} = 0 \tag{3.31}$$

The final LBCCSM model's equations for the second case, which were solved numerically, are: equations (3.20, 3.21, 3.30 and 3.31). The derivations of the above kinematic coefficients were done using the Mathcad software with the code shown in Appendix B. It is worth noting that the LBCCSM Matlab numerical simulation uses both cases' equations, i.e. equations (3.9, 3.10 and 3.19) from the first case and equations (3.20, 3.21, 3.30 and 3.31) from the second case. In addition, the numerical simulation uses the critical angle (θ_2) to switch between being solved using the first case assumptions, to using the second case assumptions. Based on the input parameters, the critical angle (θ_2) can be calculated using equations (3.8 and 3.10). The full Matlab code used in this simulation can be found in Appendix C. The next section discusses how the LBCCSM model is used to create step-by-step design guidelines.

3.2 Design Approaches

Two separate design approaches are presented, as different applications may have different input/output requirements. The first approach considers the maximum vertical deflection of the model, while the second approach considers the maximum force. The design parameters required by both approaches are maximum desired deflection, material selection, safety-factor, compliant segments' widths, maximum force required for actuator selection and maximum footprint (i.e. the maximum rectangular area the mechanism can fit inside and move freely without interfering with other components (X) and (b_{max}), as shown in Figure 3.2. In both

25

approaches, the maximum linear deflection is considered as an input, which is the main purpose of this mechanism.

Both approaches are illustrated using step-by-step guidelines along with flow charts and design plots. In the next section, some practical design examples are given to illustrate the process of using the design plots. The design plots are graphical representations of the numerical solution to the model using Matlab. They represent the solution with one of the parameters, (θ_1), preselected as shown in Table 3.1 for selected values. Plots for (θ_1) of 20, 40 and 60 can be found in Appendix D. The LBCCSM model can work for any value of the first segment's initial angle (θ_1), as long as it satisfies a design condition of, $5^o < \theta_1 < 85^o$.

Table 3.1 Selective value of θ_1.

Initial angle (θ_1) in [deg]	Footprint aspect ratio	Segments' stresses
20	Low	High
30		
40	Intermediate	Intermediate
50		
60	High	Low
70		

The following are descriptions of every design plot generated using the LBCCSM model:

Figure 3.5 (a-c): For the three selected values of (θ_1), the relationship between the different values of maximum footprint ratio (b_{max}/X) and the second segment's initial angles (θ_{2i}) is presented over a range of stiffness coefficient ratios (v). The Footprint ratio varies with the change of stiffness ratio (v). The plot illustrates three different types of qualitative solutions. The first type is represented by the right most black curve, and shows the footprint ratio when no buckling occurs on segment 2. The second group of solutions is the minimum limit represented by the left black curve and it occurs when segment 1 is rigid while segment 2 buckles. Finally,

26

between the two limits are the solutions that combine the buckling of segment 2 and the bending of segment 1.

Figure 3.6 (a-c): For the three selected values of (θ_1), the relationship between the different values of the first segment's Pseudo-Rigid-Body (PRB) angle (Θ_1) and the second segment's initial angle (θ_{2i}) is presented over a range of stiffness coefficient ratios (v). The plot illustrates two different types of qualitative solutions. The first type is represented by the black curve, and shows the (Θ_1) of segment 1 when segment 2 acts only as a load and displacement transmitter. The second type shows the solutions that combine the buckling of segment 2 and the bending of segment 1.

Figure 3.7 (a-c): For the three selected values of (θ_1), the relationship between the different values of the second segment's initial angle (θ_{2i}) and the non-dimensional force (f) is presented over a range of stiffness coefficient ratios (v). The plot illustrates two different types of qualitative solutions. The first type is represented by the black curve, and shows the (f) required to actuate the system when no buckling occurs on segment 2. The second type shows the solutions that combine the buckling of segment 2 and the bending of segment 1.

Figure 3.8, Figure 3.9, and Figure 3.10: Each of these plots consider different values of (θ_1), equal to 30°, 50° and 70° respectively. They are used to find the stiffness coefficient ratios (v) after calculating the non-dimensional force-flexibility coefficients (J). This coefficient is a dimensionless representation of the maximum force and a material flexibility index. Part (a) of the plots considers a low range of stiffness coefficient ratio values corresponding to a lower force range. Alternatively, Part (b) considers a higher range of both values.

Those plots were generated from the Matlab Code in Appendix C for the selected values of θ_1; for any other spesific θ_1 plots, the same code can be applied by modifying the values of θ_1.

a)

Figure 3.5 (b_{max}/X) vs (θ_{2i}) over range of (v), (a) $\theta_1=30^o$, (b) $\theta_1=50^o$ and (c) $\theta_1=70^o$.

28

b)

Figure 3.5 (Continued)

c)
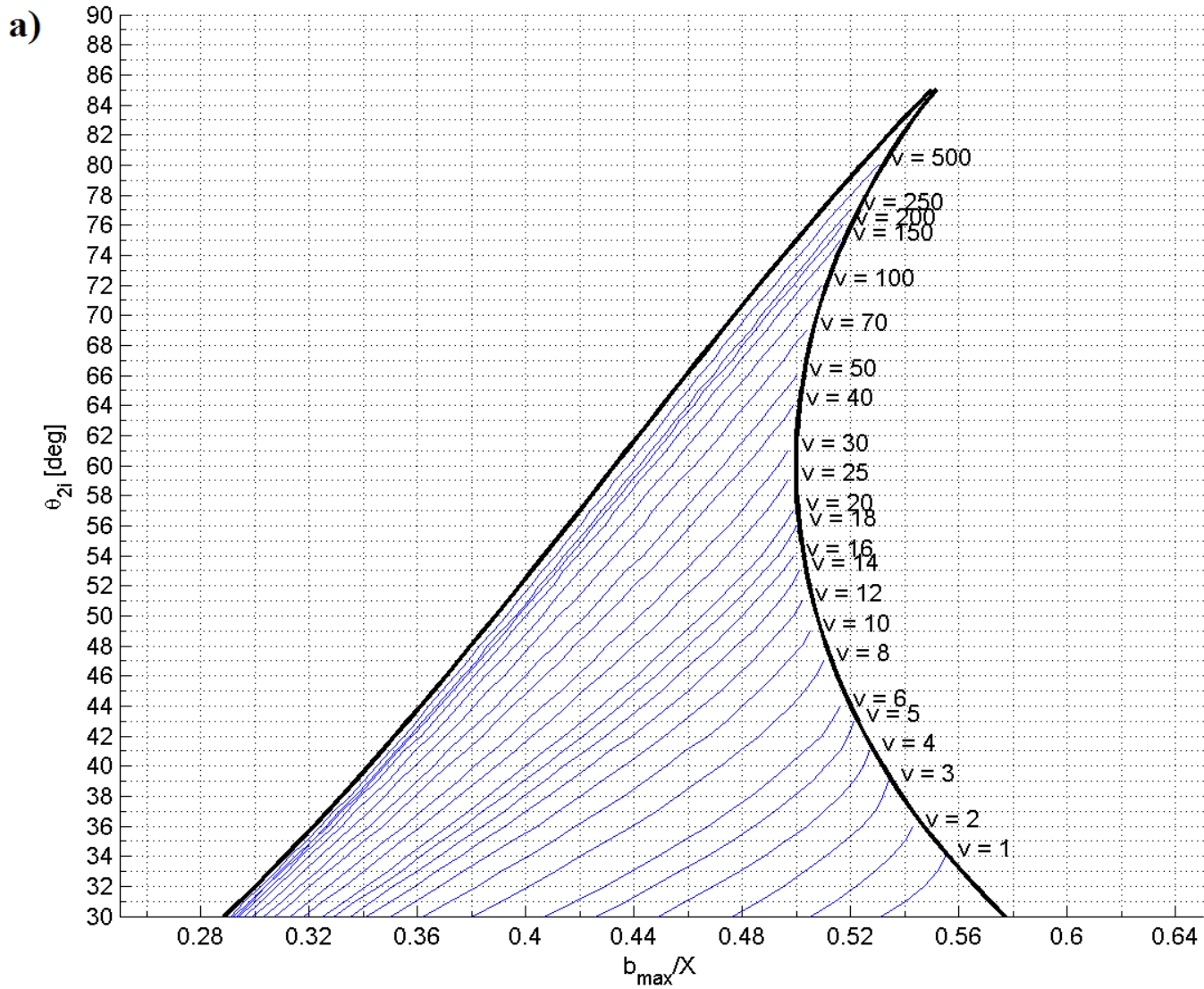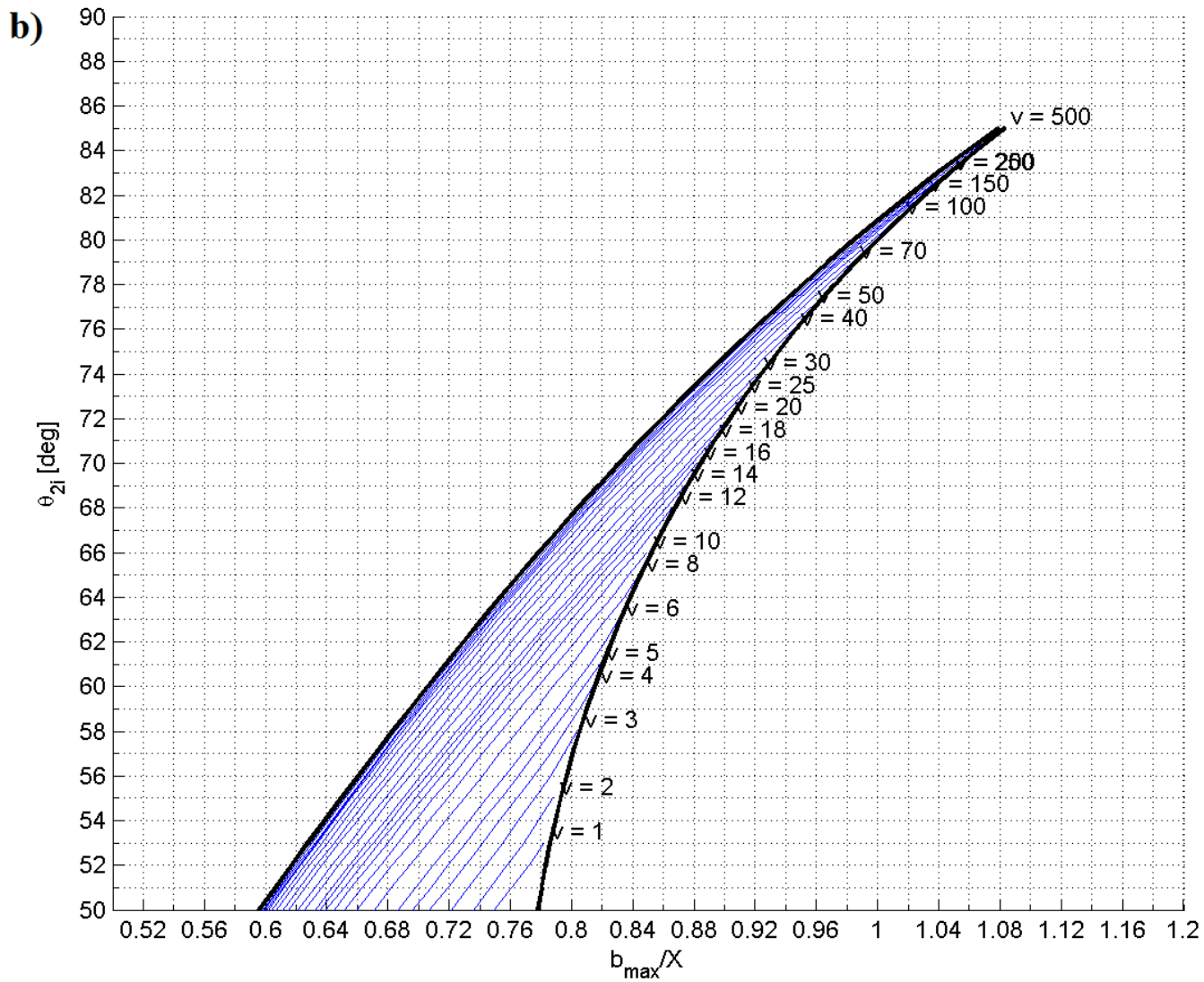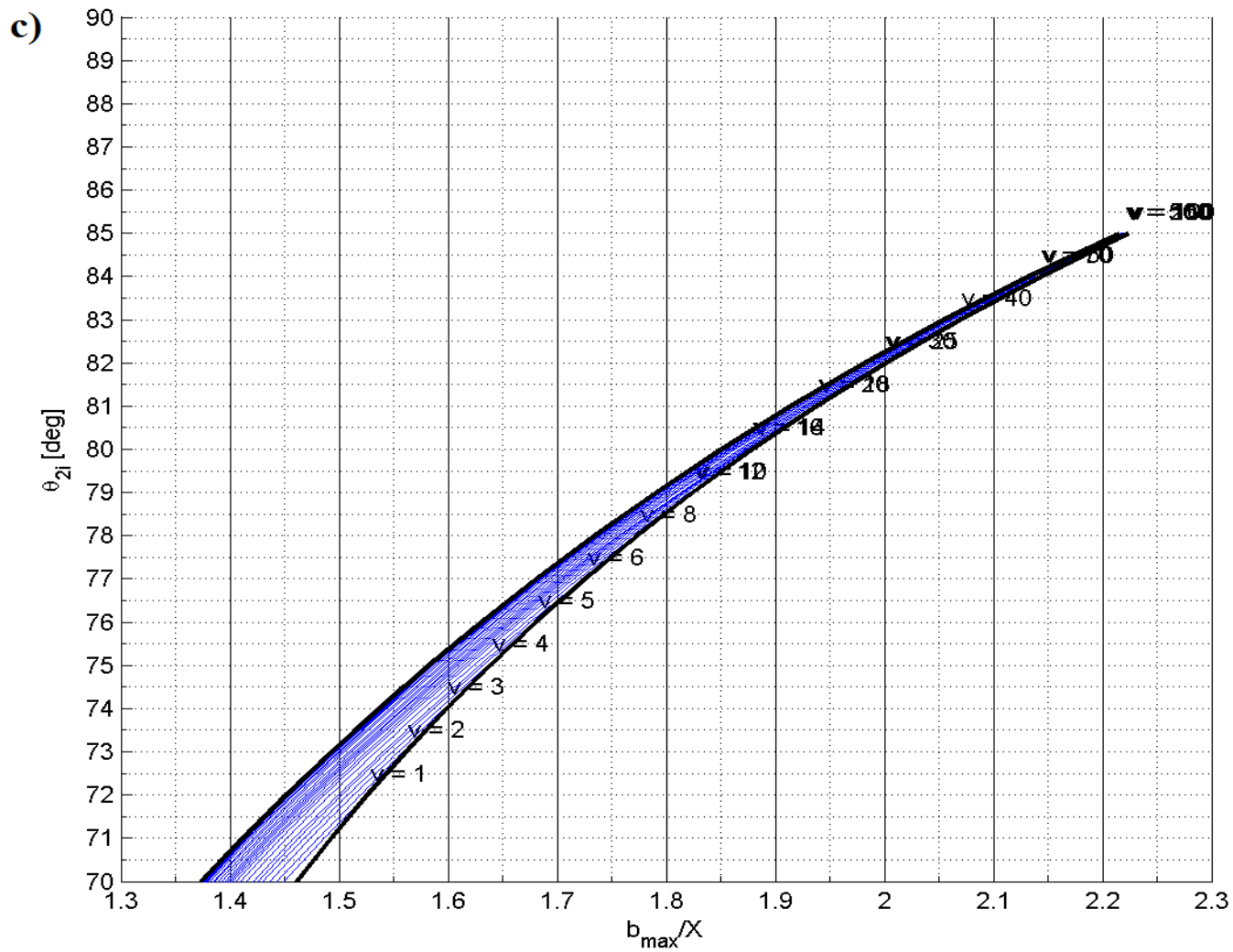
Figure 3.5 (Continued)

Figure 3.6 (Θ_1) vs (θ_{2i}) over range of (v), (a) $\theta_1=30^o$, (b) $\theta_1=50^o$ and (c) $\theta_1=70^o$.

Figure 3.6 (Continued)

32

c)
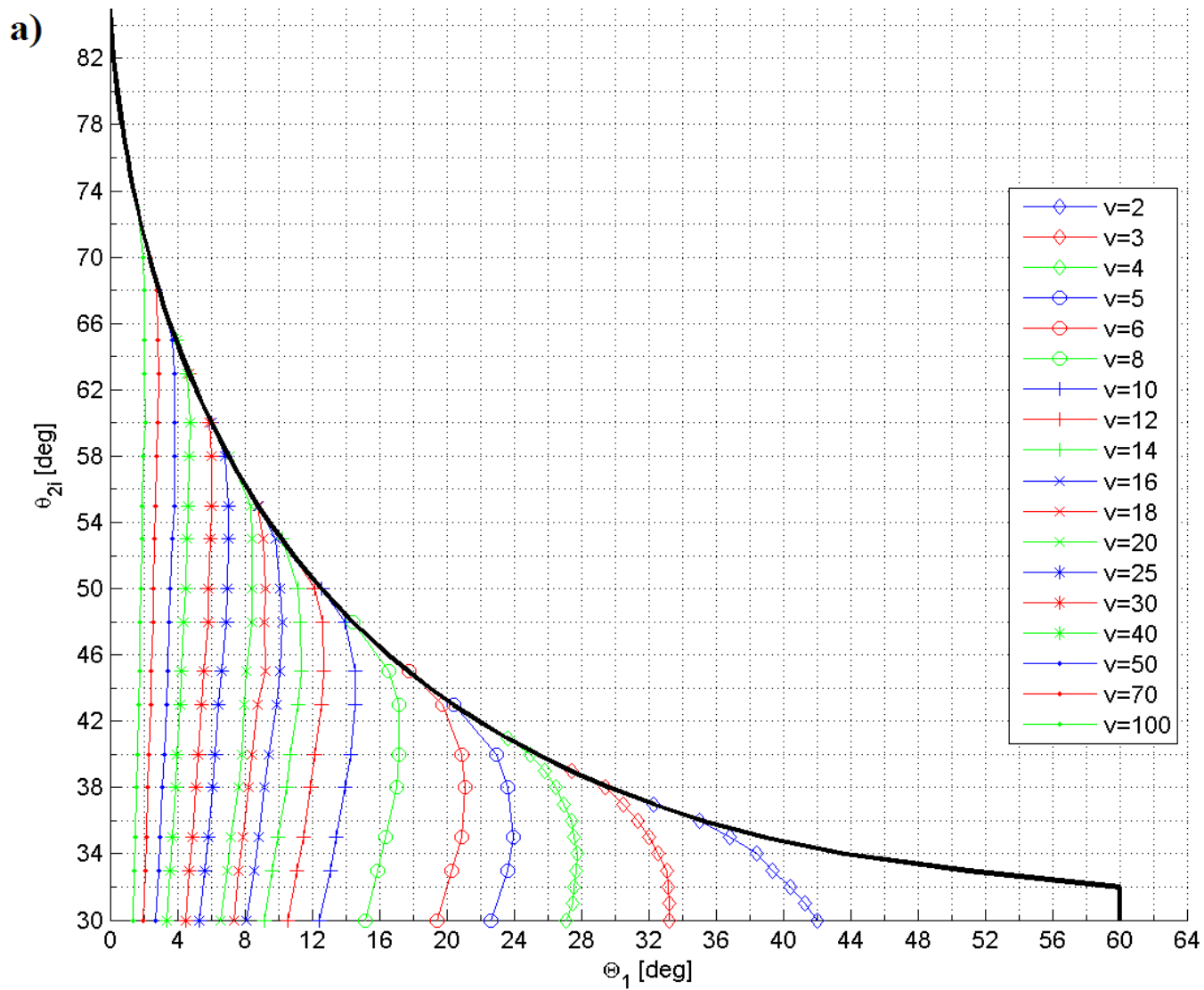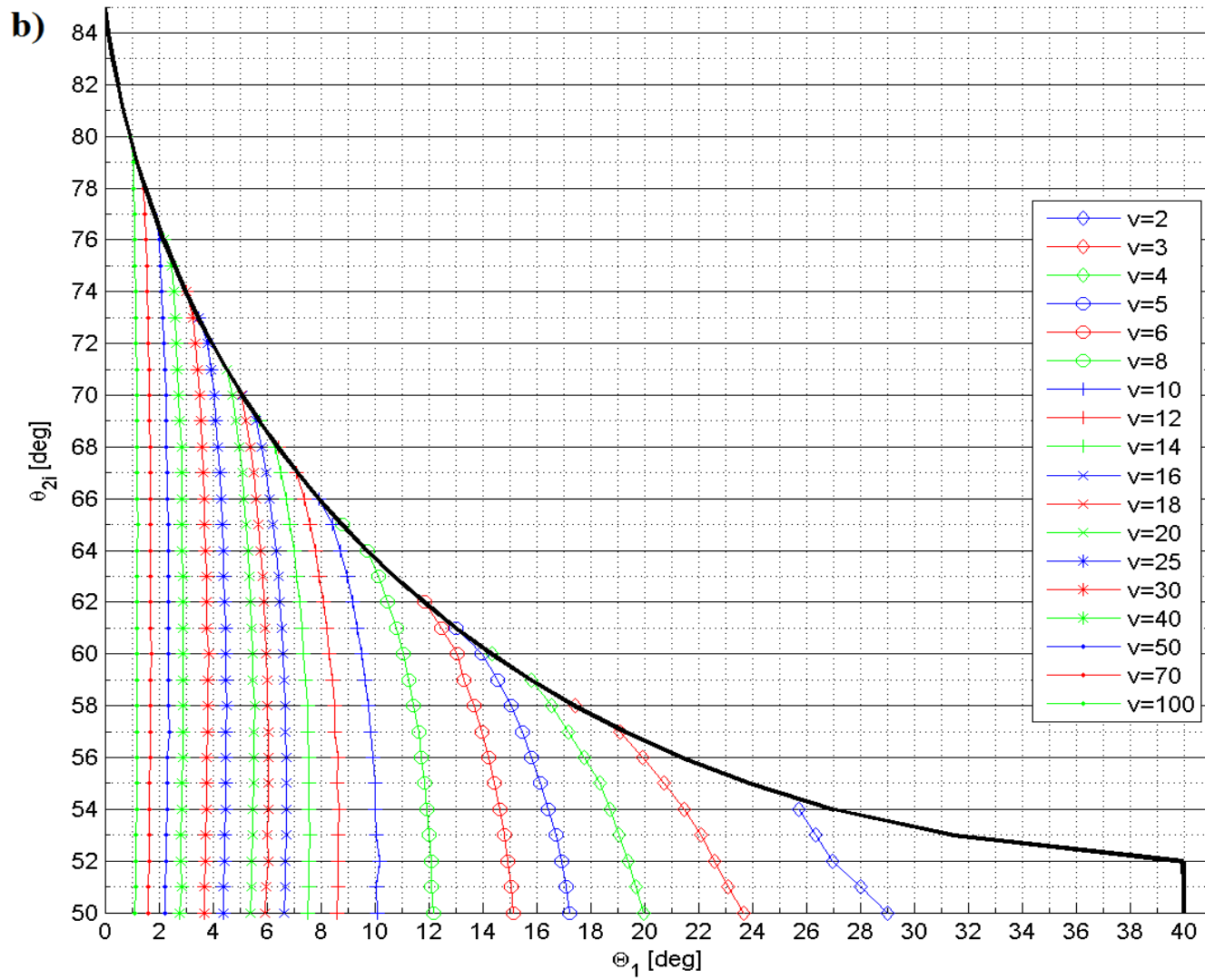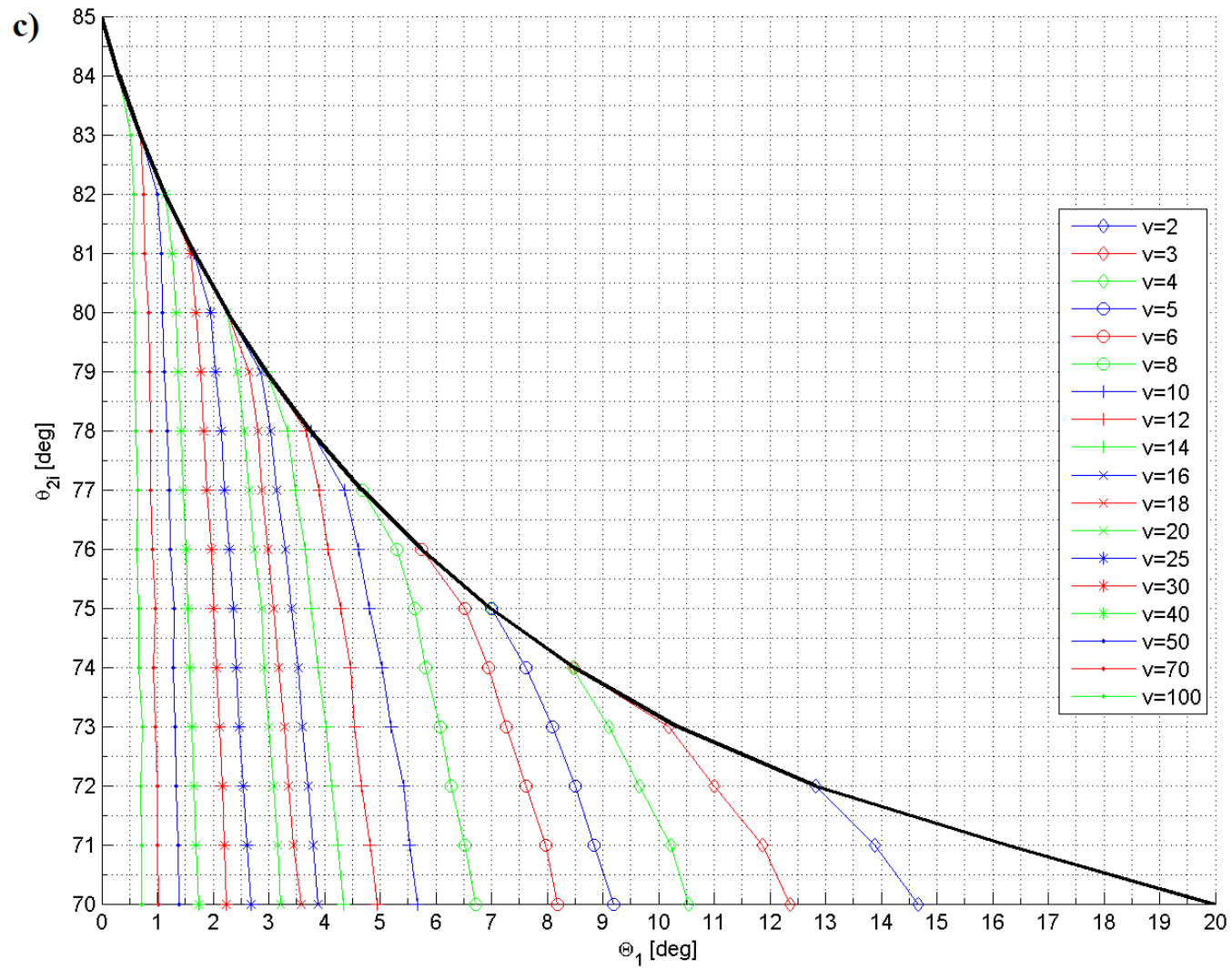
Figure 3.6 (Continued)

Figure 3.7 (f) vs (θ_{2i}) over range of (v), (a) $\theta_I=30^o$, (b) $\theta_I=50^o$ and (c) $\theta_I=70^o$.

b)
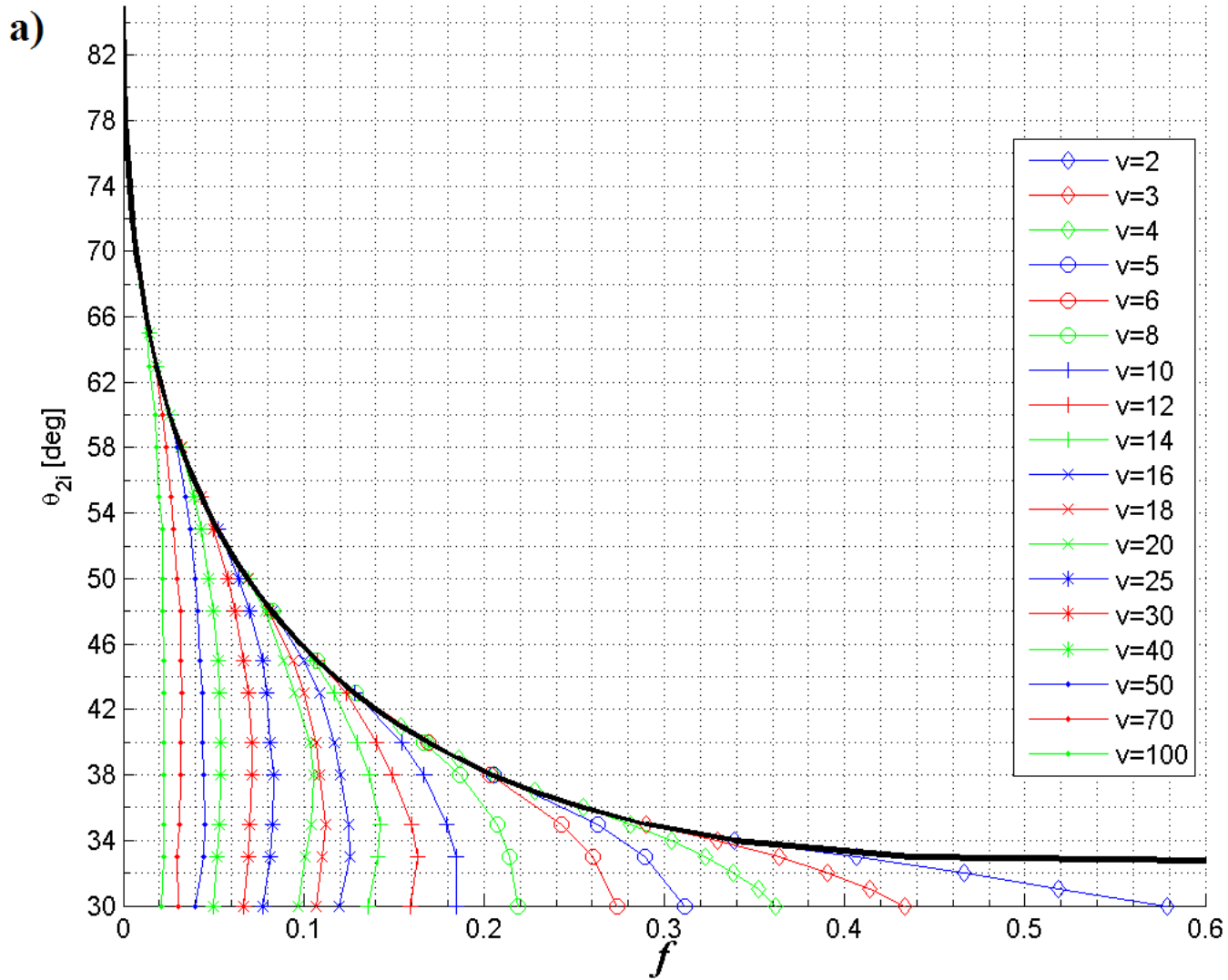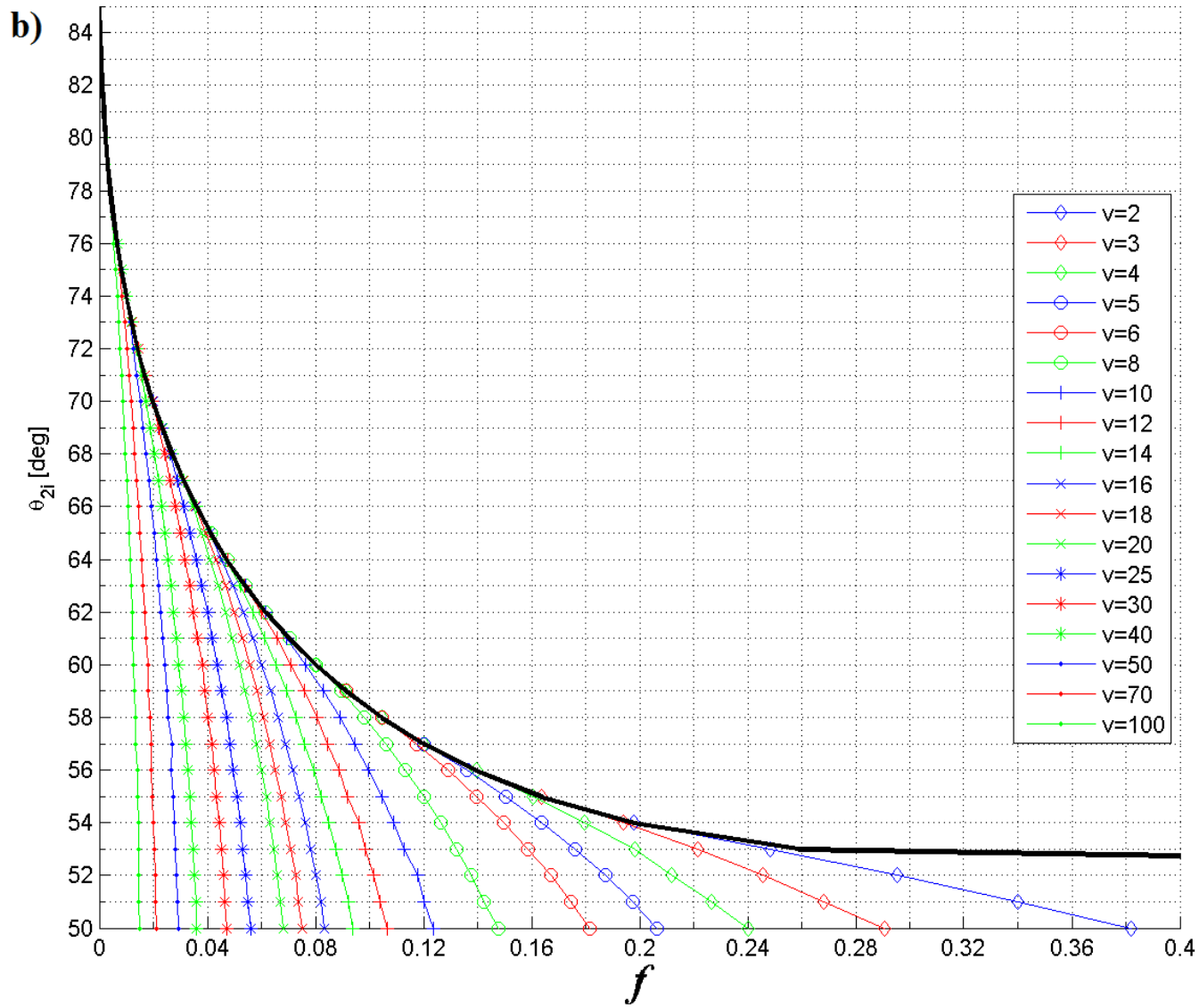
Figure 3.7 (Continued)
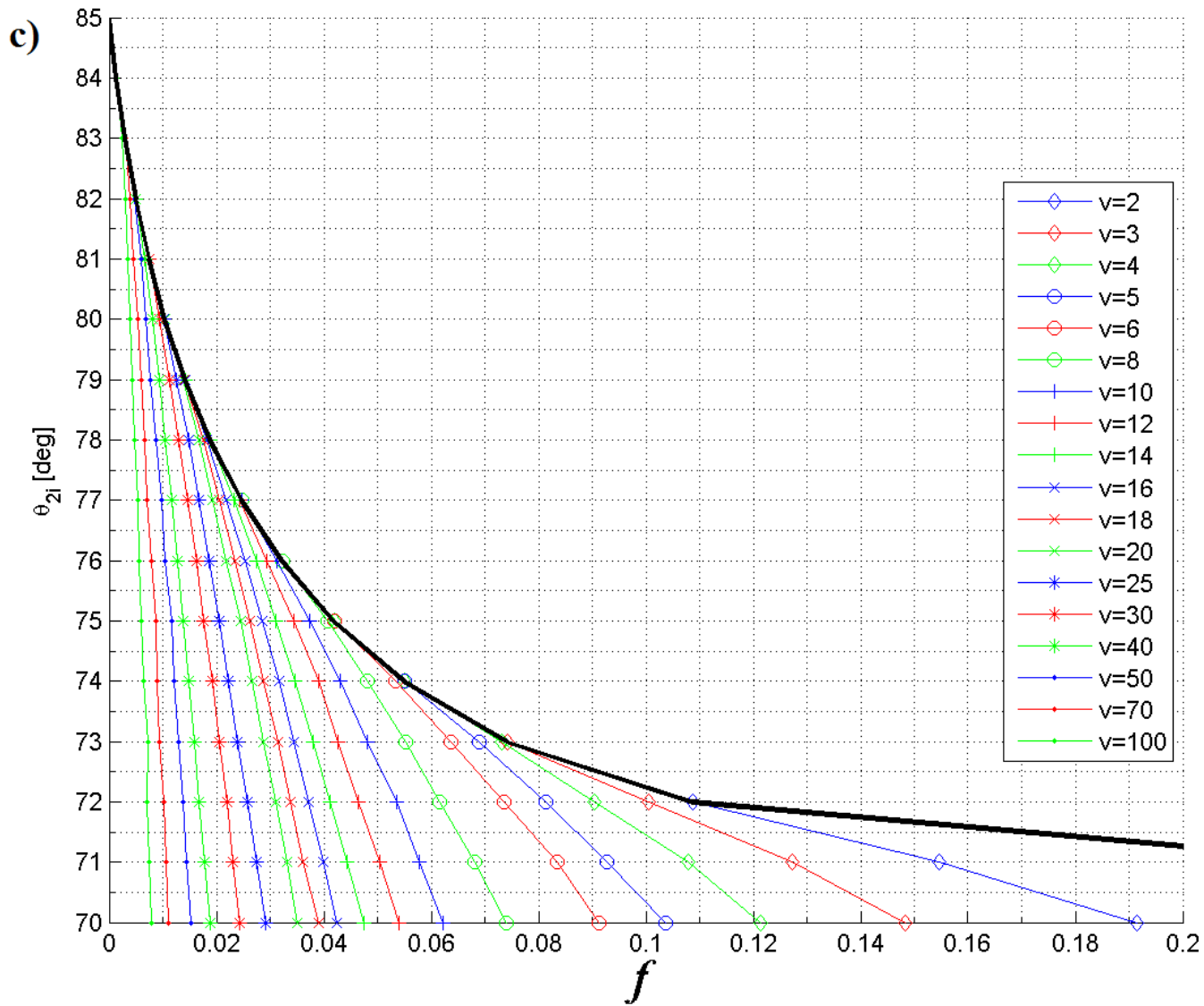
Figure 3.7 (Continued)
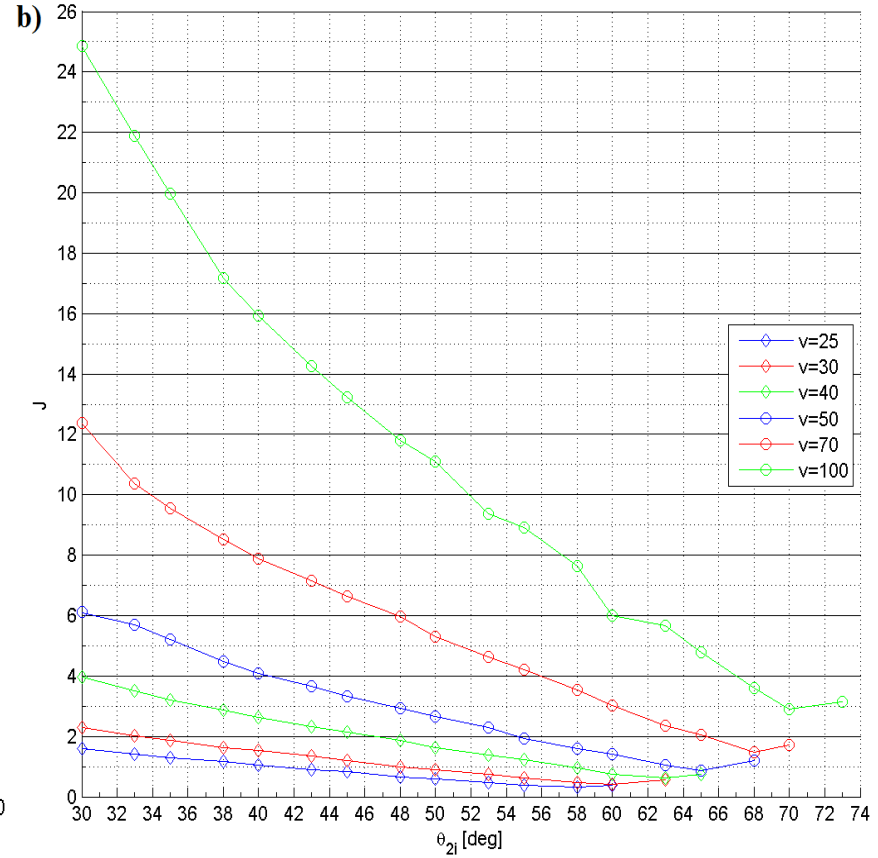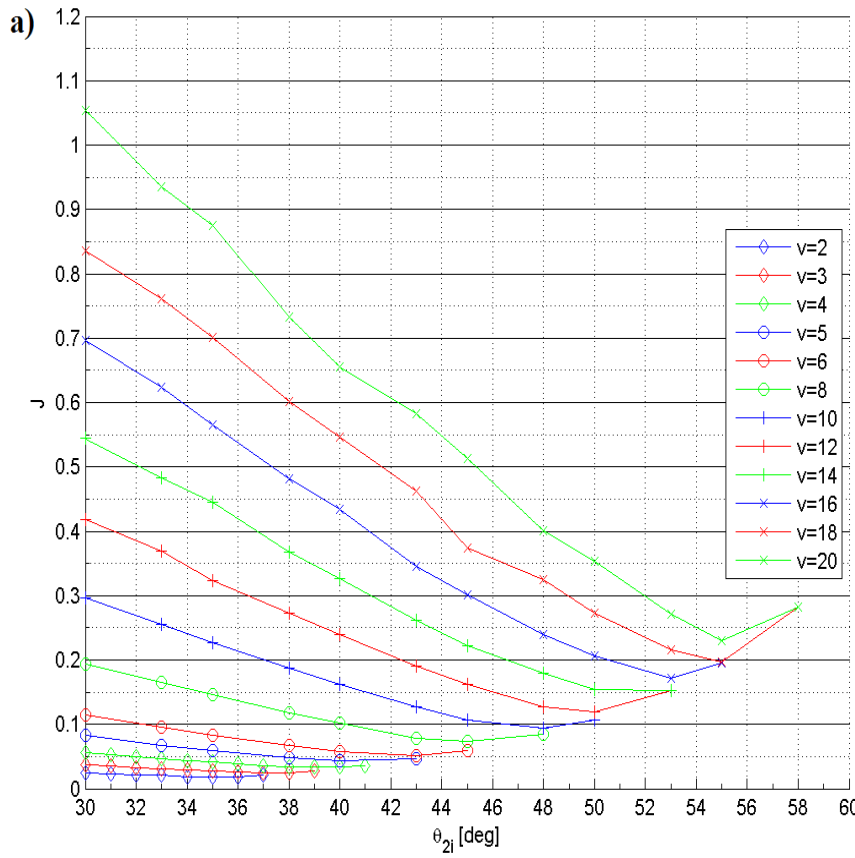
Figure 3.8 (J) vs (θ_{2i}) for $\theta_1=30^{\mathrm{o}}$ over range of (v), (a) Lower and (b) Higher force range.
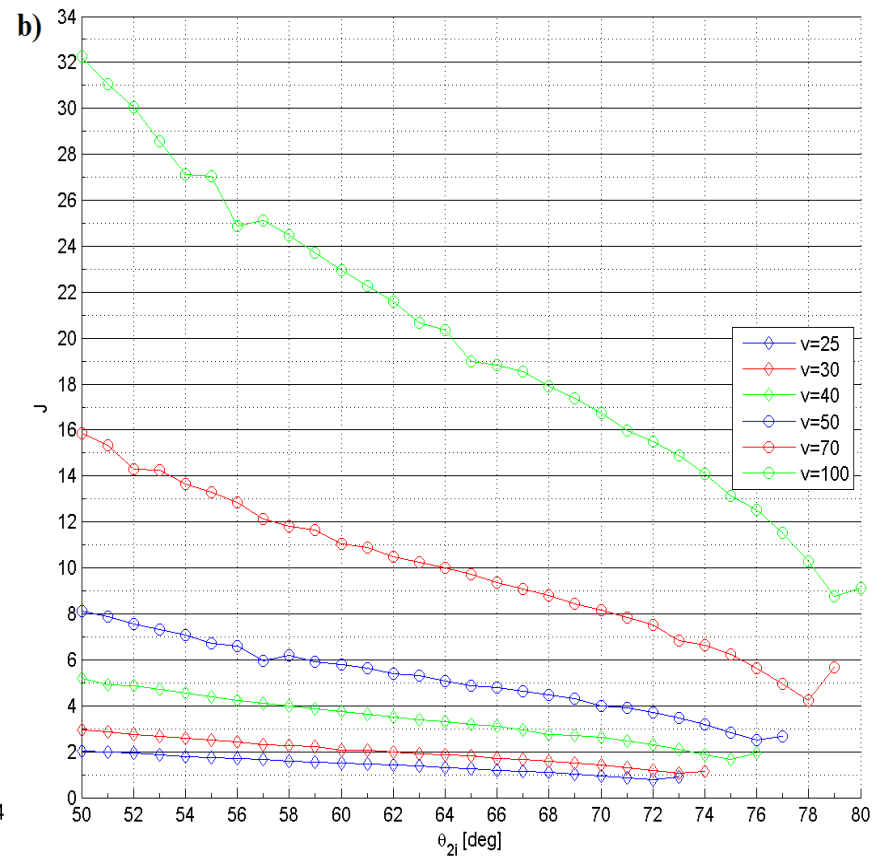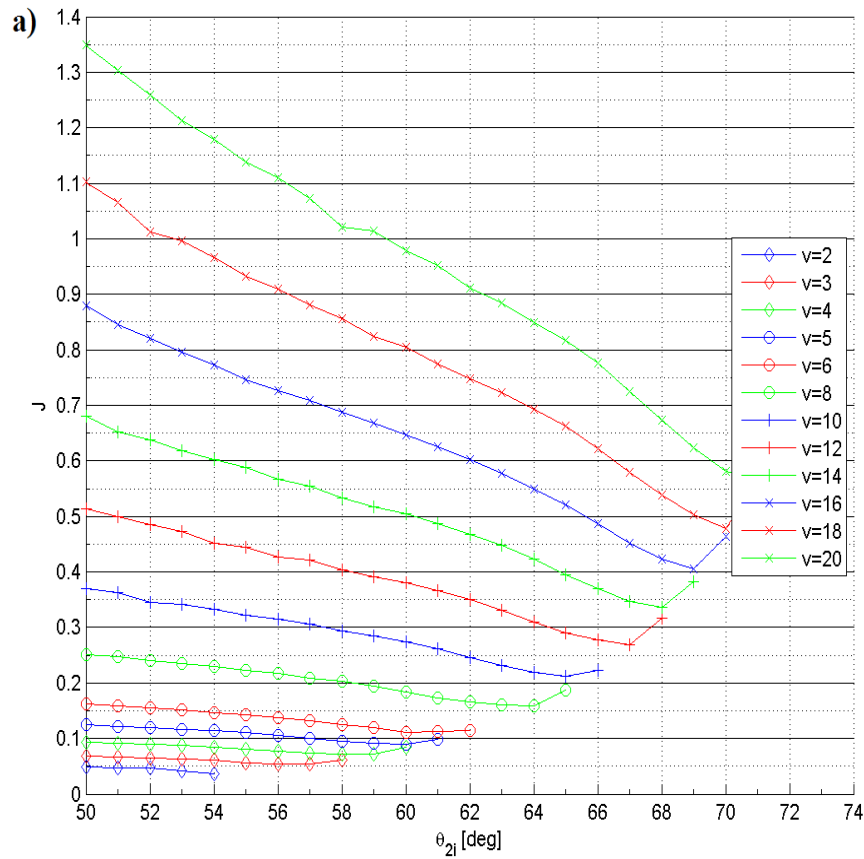
Figure 3.9 (J) vs (θ_{2i}) for $\theta_1=50^o$ over range of (v), (a) Lower and (b) Higher force range.
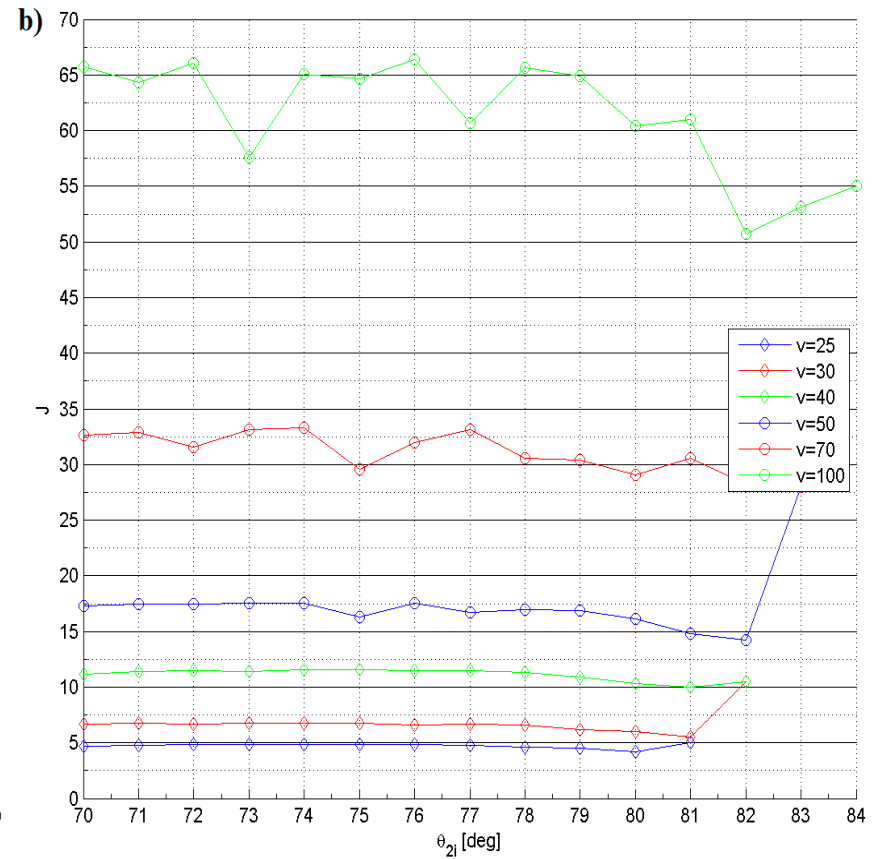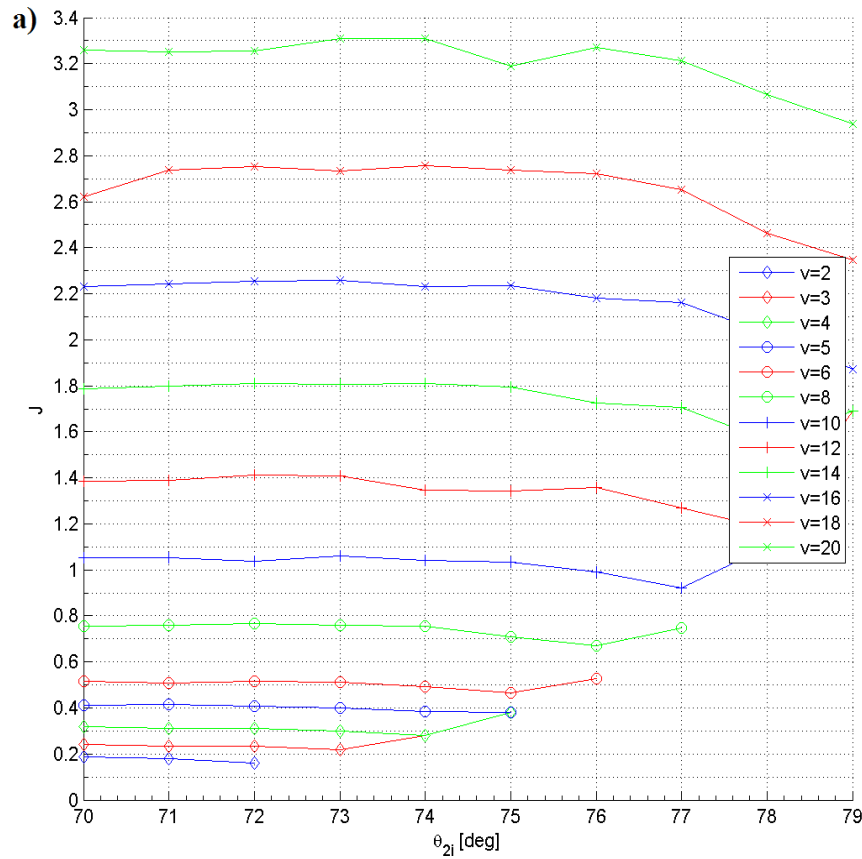
Figure 3.10 (*J*) vs (θ_{2i}) for θ_1=70$^\text{o}$ over range of (*v*), (a) Lower and (b) Higher force range.

3.3 First Design Approach

In this approach, if the design is only constrained by how much of an area, i.e. footprint, the mechanism will occupy, along with the maximum linear deflection, then the input design parameters are the maximum desired deflection, footprint, material selection, safety factor and material thickness. The output design parameters are the segments' initial angles, the force required to actuate the mechanism and the segments' widths.

3.3.1 Flow Chart

A flow chart was developed for this approach, seen in Figure 3.11. This shows the input parameters, plots and equations to use, intermediate outputs and the final outputs of the design.
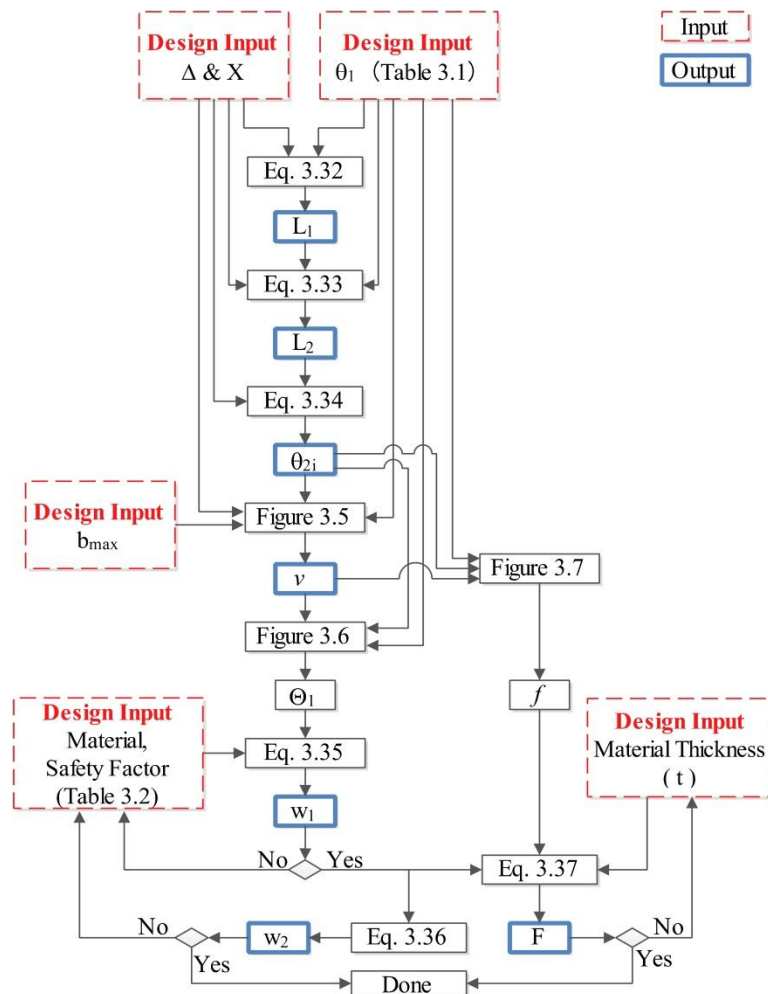
Figure 3.11 The design flow chart for the first approach.

3.3.2 Step-By-Step Design Guidelines

Here are the steps used with the aid of the flow chart in Figure 3.11 and the plots. The order in which inputs and outputs are used is as follows:

- Input design parameters:

    1- (Δ), the mechanism's maximum linear deflection [mm].

    2- (X), the maximum horizontal footprint [mm] shown in Figure 3.2.

    3- (θ_1), the initial angle of segment 1 [deg].

    4- (b_{max}), the maximum vertical footprint [mm] shown in Figure 3.2.

    5- The material's mechanical properties and safety factor.

    6- (t), the material thickness [mm].

- Output design parameters:

    1- (L_1 and L_2), the segments' length [mm].

    2- (θ_{2i}), the segments' initial angle [deg].

    3- (v), the stiffness coefficient.

    4- (w_1 and w_2), the segments' width [mm].

    5- (F_{max}), the maximum actuation force needed [N].

Step 1: Choose the linear deflection (Δ), which is the distance between the first stable point and the second stable point. Also, choose the maximum horizontal footprint (X).

Step 2: Choose a value of (θ_1), the initial angle of segment 1, from Table 3.1 based on the desired aspect ratio and stress level.

Step 3: Use equation (3.32), which is derived from the cosine law based on the segments' angles shown in Figure 3.2 (a), to calculate the first segment's length (L_1).

$$L_1 = \left(X - \frac{\Delta}{2}\right)\frac{1}{cos(\theta_1)} \tag{3.32}$$

41

Step 4: Use equation (3.33) to calculate the second segment's length (L_2).

$$L_2 = L_1 \sqrt{\left(\frac{\Delta}{2L_1}\right)^2 + (sin(\theta_1))^2} \qquad (3.33)$$

Step 5: Use equation (3.34) to calculate the second segment's initial angle (θ_{2i}).

$$\theta_{2i} = cos^{-1}\left(\frac{\Delta}{2L_2}\right) \qquad (3.34)$$

Step 6a: Choose the value of (b_{max}), which is the maximum vertical deflection that should satisfy the following condition: $(b_i = L_1 sin(\theta_1)) \leq b_{max} \leq L_2$

Step 6b: Calculate the non-dimensional value of the mechanism's maximum height (b_{max}/X). Use the part of plot in Figure 3.5 that is for the selected (θ_1) to find the stiffness coefficient ratio (v).

Step 7: Use the part of plot in Figure 3.6 that is for the selected (θ_1) to find the PRBM angle of segment 1 (Θ_1) at the maximum vertical deflection.

Step 8: Use equation (3.35), along with the material's properties (E, σ_y), shown in table 2 for selective material, and safety factor selection, to find (w_1) which was derived using equation (3.5) and the following equations:

$$\sigma_{max} = \frac{M*c}{I_1} \text{ and } SF = \frac{\sigma_y}{\sigma_{max}} \text{ where } c = \frac{w_1}{2}$$

$$W_1 = \frac{\sigma_y}{SF*E} * \frac{1}{\gamma K_\Theta} * \frac{L_1}{\Theta_1} \qquad (3.35)$$

Table 3.2 Example of material selection and their properties [1].

Material name	Young's modulus E [GPa]	Yield stress σ_y [MPa]
Polypropylene	1.35	35
HDPE	1.08	29.6
HMWPE	0.937	27

Step 9: Use equation (3.16) to find the ratio of the initial angles (m). Calculate (w_2) using equation (3.36), which is derived using equations (3.3, 3.4, 3.16 and 3.17). If the segments'

widths are not possible due to reasons such as manufacturing difficulties, repeat step 8 with a different material or safety factor.

$$w_2 = \sqrt[3]{m/(2v)} * w_1 \tag{3.36}$$

Step 10: Use the part of plot in Figure 3.7 that is for the chosen (θ_1) to find the non-dimensional force (f).

Step 11: The maximum actuation force (F_{max}) can be calculated using equation (3.37), which was derived from equation (3.18). The material thickness, (t), used to calculate the 2nd moment of area, is the same for both segments. If the calculated force is not possible due to actuator limitations, repeat this step with a different material thickness.

$$F_{max} = \frac{\gamma K_\Theta E\, I_1 f}{L_1^2} \tag{3.37}$$

3.3.3 Design Example

Using the flow chart as guidance, an example is given to illustrate the walk-through between the design plots and equations for this design approach using the LBCCSM model.

- Design statement:

    A linear bistable mechanism needs to be designed. The distance between the two stable points is 25.2 mm and the mechanism should fit in an area of 43.8 mm by 21 mm. The mechanism is laser cut from a 5 mm thick Polypropylene sheet with design safety factor of 1.

- Design inputs:

    $\Delta = 25.2$ mm, $X = 43.8$ mm, $b_{max} = 21$ mm, $t = 5$ mm and SF = 1.

    $\gamma = \rho = 0.85$ and $K_\Theta = 2.65$ from the PRBM [1].

- Design solution:

    Step 1: $\Delta = 25.2$ mm and $X = 43.8$ mm.

43

Step 2: From Table 3.1, $\theta_1 = 30^o$ for low footprint.

Step 3: Using equation (3.32), $L_1 = 36.03$ mm.

Step 4: Using equation (3.33), $L_2 = 22$ mm

Step 5: Using equation (3.34), $\theta_{2i} = 55^o$.

Step 6a: From inputs, $b_{max}/X = 0.48$, $b_i = 18$ mm.

Step 6b: Using Figure 3.5 (a), $v = 25$.

Step 7: Using Figure 3.6 (a), $\Theta_1 = 7^o$.

Step 8: Material: Polypropylene, $E = 1.35$ GPa, $\sigma_y = 35$ MPa.

Using equation (3.35), $w_1 = 3.39$ mm.

Step 9: Using equation (3.16), m = 0.61. Using equation (3.36), $w_1 = 0.78$ mm.

Step 10: Using Figure 3.7 (a), $f = 0.04$.

Step 11: Using equation (3.37), $F_{max} = 1.52$ N.

- Design conclusion:

    Following the steps of this approach and guided by the flow chart, the mechanism should be designed and cut with the first segment's length is 36.03 mm at 30° angle clockwise and its width is 3.39 mm. The second segment's length is 22 mm at 55° angle counter clockwise and 0.78 mm in width. The actuator must be able to provide a force of 1.52 N.

3.3.4 FEA Modeling Using ANSYS Workbench

The same example was modeled using the FEA software ANSYS. Table 3.3 compares results between the LBCCSM model and FEA showing relatively low error percentage giving the fact that the LBCCSM model did not include internal stress analysis nether the design of the

44

living hinges in which both considered future work for this topic. Figure 3.12 shows the results from FEA modeling for the maximum y-axis deflecting that correspond to $b_{max} - b_i$.

Table 3.3 Example 1: LBCCSM vs FEA results comparisons.

Type	Parameter	LBCCSM Model	FEA Model	Error (%)
Input	$b_{max} - b_i$	3 mm	2.81 mm	6.33 %
Output	F_{max}	1.52 N	1.48 N	2.70 %
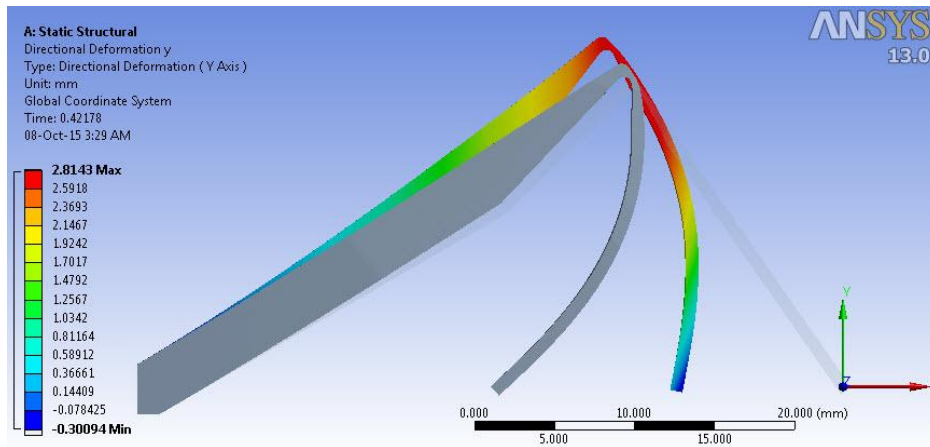
Figure 3.12 Example 1: FEA maximum vertical displacment.

Figure 3.13 shows the force-displacement and potential energy curves for the results from both the LBCCSM model and the FEA analysis. The x-axis represents the displacement (Δ) with respect to the coordinate system at the tip of the moving link shown in Figure 3.12. The force-displacement curves, shown in dotted lines, follow the left y-axis; whereas the potential energy (or work)-displacement curves, shown in dashed lines, follow the right y-axis. For all the curves, the bold lines are for the LBCCSM model where the light lines correspond to the FEA modeling.

From the background section on bistability, Figure 3.13 represent the typical behavior of bistable mechanism under the design loading conditions. When force represented in the plot, which is the horizontal applied force at the tip of the moving link (L_2), is equal to zero represents

45

an equilibrium state for the mechanism. The stable equilibrium positions of the mechanism occur at the local minimum of the potential energy curves where the unstable equilibrium position occurs at the local maximum of the same curves [20]. The C-arrow and D-arrow indicate the unstable position for the results from the FEA and LBCCSM models, respectively. The location difference is in the order of one millimeter apart, which considered acceptable for the design giving the fact that LBCCSM model requires less computational time by following the design guidelines. The first stable position for both models is the same because of zero applied force; the second stable position occurs at $\Delta \approx$ -23.8 mm for the FEA model, shown by the B-arrow, and at the end of the design input of Δ = 25.2 for the LBCCSM. The reason is that the LBCCSM model did not account for the elastic energy absorbed by the Polypropylene material at the living hinges, where the accurate FEA analysis showed that absorbed energy indicated by the A-arrow.
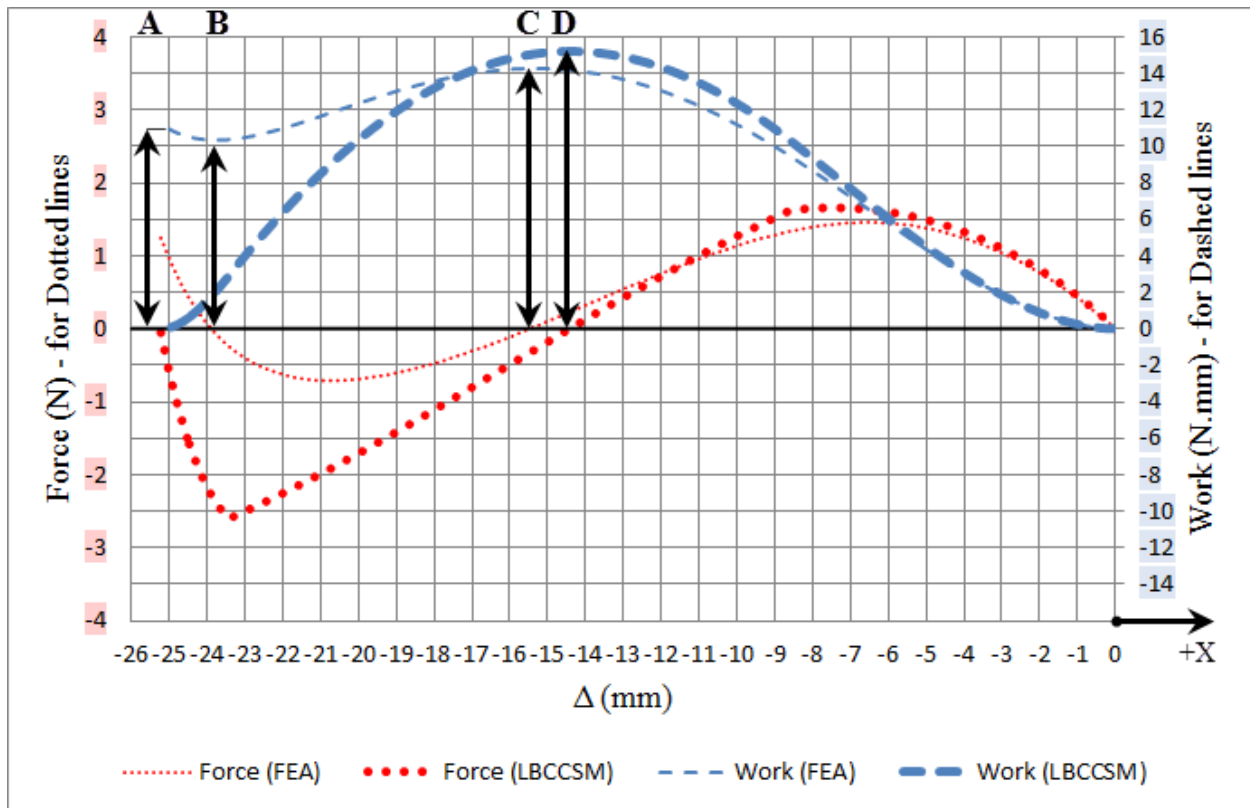
Figure 3.13 Example 1: Force-displacment and work-displacment curves.

3.4 Second Design Approach

In this approach, if the maximum force required to actuate the mechanism and the maximum deflection are the primary constraints, then the maximum deflection, actuating force, material selection, safety factor and material thickness are considered to be the input parameters while the segments' widths, footprint and the segments' initial angles are considered as the design outputs.

3.4.1 Flow Chart

A flow chart was developed for this approach, as seen in Figure 3.14. This shows the input parameters, plots and equations to use, intermediate outputs and final outputs of the design.
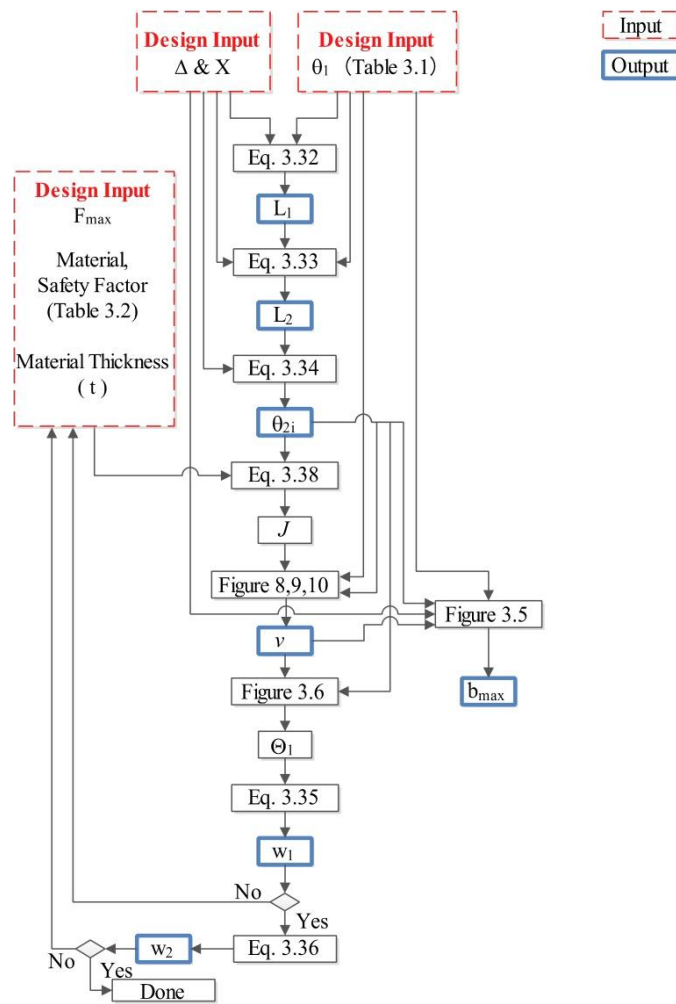
Figure 3.14 The design flow chart for the second approach.

3.4.2 Step-By-Step Design Guidelines

Here are the steps used with the aid of the flow chart in Figure 3.14 and the plots. The order in which the inputs and outputs are used is as follows:

- Input design parameters:

    1- (Δ), the mechanism's maximum linear deflection [mm].

    2- (X), the maximum horizontal footprint [mm] shown in Figure 3.2.

    3- (θ_1), the initial angle of segment 1 [deg].

    4- (F_{max}), the maximum actuation forces required [N].

    5- The material's mechanical properties and safety factor.

    6- (t), the material thickness [mm].

- Output design parameters:

    1- (L_1 and L_2), the segments' length [mm].

    2- (θ_{2i}), the segments' initial angle [deg].

    3- (v), the stiffness coefficient ratio.

    4- (b_{max}), the maximum vertical footprint [mm] shown in Figure 3.2.

    5- (w_1 and w_2), the segments' width [mm].

Step 1 through Step 5 is the same as in the first approach.

Step 6a: Specify the maximum force (F_{max}) limited by the design, i.e. actuator force limit along with the material used to manufacture the mechanism and its properties, safety factor and material thickness (t). Knowing those inputs, calculate the non-dimensional coefficient (J) using equation (3.38). This equation was derived from combining both equations (3.35 and 3.37).

48

$$J = \frac{f}{12\,(\gamma K_\Theta)^2\,\Theta_1^3} = \underbrace{\frac{F_{max}}{E\,L_1\,t}}_{\text{Unitless Force}} * \underbrace{\left(\frac{SF\,E}{\sigma_y}\right)^3}_{\text{Material Flexibility Index}} \qquad (3.38)$$

Step 7 through Step 9 is the same as in the first approach.

Step 10: Use the part of Figure 3.5 that is for the selected (θ_1) along with the stiffness coefficient ratio (v) and (θ_{2i}) to find the value of the mechanism's maximum height (b_{max}).

3.4.3 Design Example

Using the flow chart as guidance, an example is given to illustrate the walk-through between the design plots and equations for this design approach using the LBCCSM model.

- Design statement:

    A linear bistable mechanism needs to be designed. The distance between the two stable points is 55 mm and the mechanism should fit in a length of 70 mm. The actuator used has a maximum force output of 2 N. The mechanism is laser cut from a 7 mm thick Polypropylene sheet with design safety factor of 1.5.

- Design inputs:

    $\Delta = 55$ mm, $X = 70$ mm, $F_{max} = 2$ N, $t = 7$ mm and SF = 1.5

    $\gamma = \rho = 0.85$ and $K_\Theta = 2.65$ from the PRBM [1].

- Design solution:

    Step 1: $\Delta = 55$ mm and $X = 70$ mm.

    Step 2:   From Table 3.1, $\theta_1 = 50^o$ for intermediate footprint.

    Step 3:   Using equation (3.32), $L_1 = 66.12$ mm.

    Step 4:   Using equation (3.33), $L_2 = 57.63$ mm

    Step 5:   Using equation (3.34), $\theta_{2i} = 61.5^o$.

    Step 6a: Using equation (3.38), $J = 0.62$.

49

Step 6b: Using Figure 3.9 (a), $v = 16$.

Step 7: Using Figure 3.6 (b), $\Theta_1 = 6.52^o$.

Step 8: Material: Polypropylene, $E = 1.35$ GPa, $\sigma_y = 35$ MPa,

Using equation (3.35), $w_1 = 4.45$ mm.

Step 9: Using equation (3.16), m = 0.87. Using equation (3.36), $w_1 = 1.34$ mm.

Step 10: Using Figure 3.5 (b), $b_{max}/X = 0.78$, $b_{max} = 54.6$ mm and, $b_i = 50.65$ mm.

- Design conclusion:

  Following the steps of this approach and guided by the flow chart, the mechanism should be designed and cut with the first segment's length is 66.12 mm at 50° angle clockwise and its width is 4.45 mm. The second segment's length is 57.63 mm at 61.5^o angle counter and 1.34 mm in width. The mechanism should fit in an area of 54.6 mm by 70 mm.

3.4.4 FEA Modeling Using ANSYS Workbench

The same example was modeled using FEA. The following Table 3.4 compares results between the LBCCSM model and FEA. Errors in the model's force estimate are relatively high because the LBCCSM model uses pin joints instead of short-length flexural pivots as in the FEA model. The results show that our model predicts a lower stiffness than the FEA model does, means that the use of flexural pivots at hinges B and C, from Figure 3.1, may add flexibility and lower stresses. Figure 3.15 shows the FEA results for the maximum y-axis deflecting ($b_{max} - b_i$); whereas Figure 3.16 shows the force-displacment and work-displacment curves for LBCCSM and FEA model. The LBCCSM model predection in this example was more accurate in terms of the forces due to the use of equation 3.38, whereas in the first example equation 3.37 was used.

Table 3.4 Example 2: LBCCSM vs FEA results comparisons.

Type	Parameter	LBCCSM Model	FEA Model	Error (%)
Input	F_{max}	2 N	2.19 N	8.67 %
Output	b_{max} - b_i	3.95 mm	4.23 mm	6.62 %
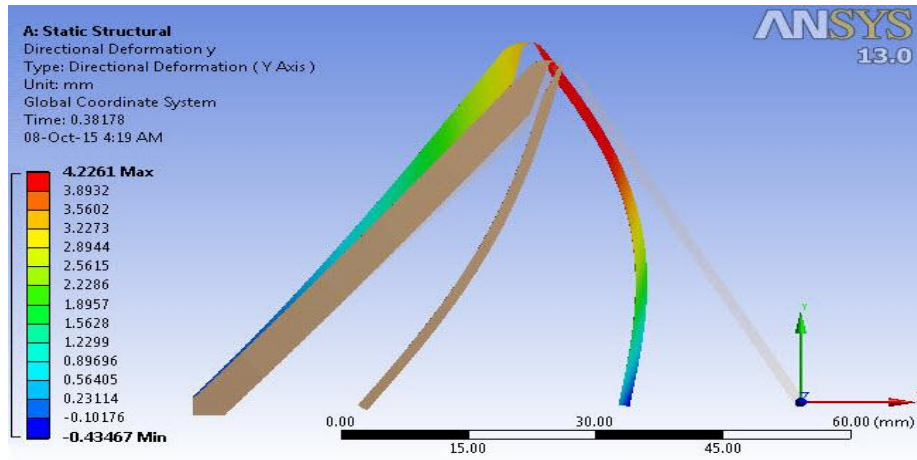
Figure 3.15 Example 2: FEA maximum vertical displacment.
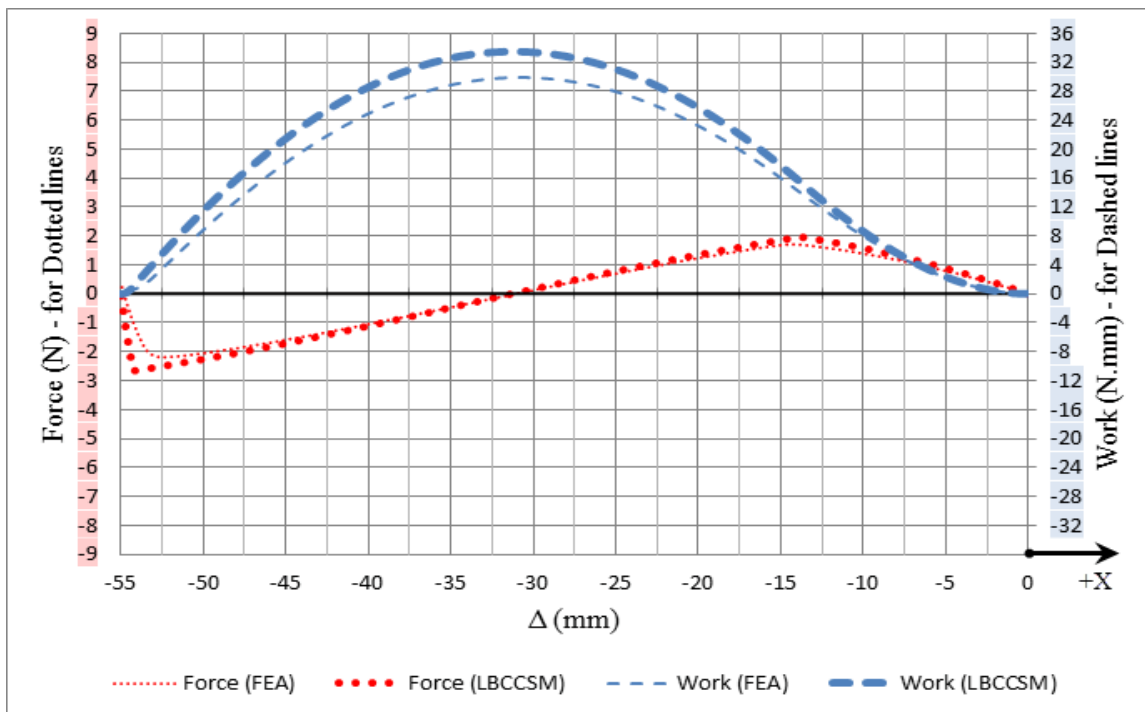
Figure 3.16 Example 2: Force-displacment and work-displacment curves.

51

CHAPTER 4: SMSF USING LINEAR BISTABLE LINK ELEMENTS [*]

This section presents a new concept of a Shape-Morphing Space-frame (SMSF), which is a novel application utilizing the Linear Bistable Compliant Crank-Slider Mechanism (LBCCSM). The frame's initial shape is constructed from a single-layer grid of flexures, rigid links and LBCCSMs. The grid is bent into the space-frame's initial cylindrical shape, which can morph because of the inclusion of LBCCSMs in its structure. The design parameters consist of the frame's initial height, its tessellation pattern (including bistable elements' placement), its initial diameter, and the final desired shape. The method used in placing the bistable elements is a novel contribution to this work as it considers the principal stress trajectories. Two different examples of Shape-Morphing Space-frames will be presented, each starting from a cylindrical-shell space-frame and morphing, one to a hyperbolic-shell space-frame and the other to a spherical-shell space-frame, both morphing by applying moments, which shear the cylindrical shell, and forces, which change the cylinder's radius using Poisson's effect. Space-frames are widely used in structures (roof structure for example) with complex geometries that involve heavy computations and optimization using genetic algorithm [25].

The bistability can be achieved by storing and releasing strain energy in its compliant segments within the designed range of motion. Such an example of bistable mechanism is the Linear Bi-stable Compliant Crank-Slider-Mechanism (LBCCSM), shown in Figure 4.1that can produce predictable and controllable length change in mechanical systems, allowing the

---

[*] This chapter was published previously in [11]. Permission is included in Appendix H.

morphing of its length from one specific length into a different specific length. The analysis done in Chapter 3 was on the upper half of the element across the horizontal symmetry line; mirroring the design can produce this type of element and it can be design to any specific application.

Figure 4.1 LBCCSM elements, (a) Normally open and (b) Normally closed.

It is good to mention, as we modify the shape of a structure; one important subject that needs to be consider is the Poisson effete from the classical mechanics of material theorem. This phenomenon describes the change in geometry under the applied load; a positive Poisson would be a negative ratio of axial to transvers strain (cylinder under tension would elongate and decrease its radius), were the negative Poisson is the vice versa [26]. Describing the vertices within a space-frame is done by taking the advantages of the torus geometry. When the product of the principal curvature at a vertex is negative, that vertex is on hyperbolic profile where the positive product indicates spherical profile as shown in Figure 4.2.
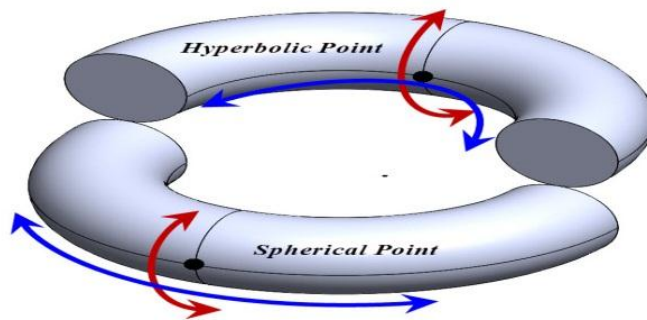
Figure 4.2 Hyperbolic and spherical point on Torus geometry.

53

This chapter is organized as follows: First, the modeling of the SMSF considering a companion of theory from 2-D tessellation, design algorithms and morphing strategies; second, two different design examples are shown highlighting the different design approaches if the desired final space-frame is a Hyperbolic-Shell or Spherical-Shell; third, results discussion and data comparison between the mathematical model and the different prototype constructed; finally, some concluding remarks regarding the design of the prototype, in addition to some future work that needed to enhance the design model.

4.1 Methods of SMSF Modeling

The methods followed in the SMSF modeling are explained starting with the tessellation of the single-layer grid into sub-grid elements, followed by description of the mathematical algorithm used accounting for designs inputs, the functionality of types of elements used and a model possibility check to ensure the geometry before and after morphing is valid. Design strategies are carried out in order to build a prototype of the SMSF. The parameters and nomenclatures used in this chapter and their definitions can be found in Appendix A.

4.1.1 SMSF Tessellation

The frame's initial shape is constructed from a single-layer grid of flexures, rigid links and LBCCSMs. To simplify the tessellation of this single-layer grid, a square sub-grid (k x s) is considered where single elements of rigid links and LBCCSMs form it. Figure 4.3 shows that a single –layer grid (a) is formed by arrays of square sub-grid (b) which consist of 8 different elements that could be split in two different way, as shown in (c-1) and (c-2); and in order to minimize the number of connection/joint between elements, (c-1) of element arrangement is preferred over the (c-2) arrangement. The (c-2) arrangement can be considered as a miniature sub-grid of (b) as shown in (d). Because the LBCCSMs are going to be used as the bi-stable

54

elements in the chosen configuration, a study of each single combination between the rigid links and the LBCCSMs forming the six elements in Figure 4.3 is carried out considering minimum variable links that produce high degrees-of-freedom of the square element.
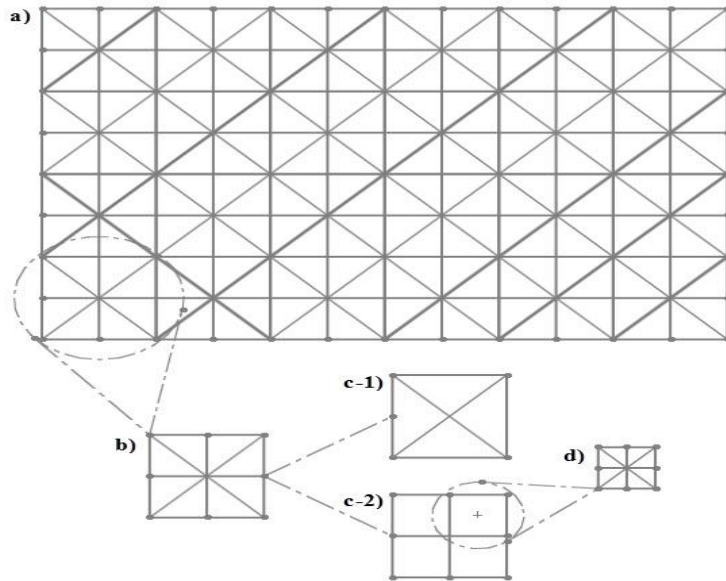
Figure 4.3 The square tessellations of the single-layer grid.

In order for a selected square frame made of six elements to be stable, only five elements need to be constrained, thus a and novel method is used in this research to determine which of the elements needs to be rigid link and which needs to be bi-stable by using the LBCCSM. For any square element, two degrees-of-freedom are located at each corner totaling eight DOF and by subtracting two DOF for the position (local origin of the square) and one DOF for orientation leaves five total DOF that describe deformation of the square, four DOF for side deformations and one DOF for shear deformation. The novel method $\binom{5}{n}$ of concept is carried out where (5) is the total number of elements that can be selected, four sides and one diagonal, and (n) is the number of elements with variable length. In order to choose which of the five elements can be selected as a rigid link or considered to be LBCCSM, the different combination between the $\binom{5}{n}$

is shown in Figure 4.4 .Table 4.1 illustrates each combination by identifying which element is being selected as LBCCSM and its type of being a side or a diagonal. Moreover, it indicate if the selected LBCCSMs location would move independently from each other, the ability to be arrayed vertically and horizontally, the number of shapes it can form and the possibility to morph from its initial square form to a trapezoidal and parallelogram as a final shape. The ability of the sub-grid square being arrayable in certain way is important, for example; in order for two sub-grid squares to be horizontally arrayable, the right side of the left square should behave the same way as the left side of the right square.

In order to identify which of the $\binom{5}{n}$ would best fit the design needs; the proceeding sections will explain the design algorithm used and the morph strategies followed to guide this selection. In Figure 4.4, Black line (Rigid links), Dashed-Red line (LBCCSM), Solid-blue line (Rigid links after morphing the square element), Dashed-blue line (LBCCSM after morphing).

Figure 4.4 The different combination of $\binom{5}{n}$.

Table 4.1 Reference to Figure 4.4, the different combination of $\binom{5}{n}$ and their criteria.

(adj. for adjacent) (opp. for opposite) (Y for Yes and N for No) ref. Figure 4.4	$\binom{5}{n}$	LBCCSM location		Independent movment of LBCCSM	Arrayable configuration		Number of shapes formed	Morphing to Trapezoid	Morphing to Parallelogram
		Side	Diagonal		Vertical	Horizontal			
A1	$\binom{5}{0}$	0	0	N/A	Y	Y	1	N	N
B1	$\binom{5}{1}$	1	0	Y	Y	Y	2	N	Y
B2		0	1	Y	N	Y	2	N	N
C1	$\binom{5}{2}$	2 adj	0	N	N	N	4	N	N
C2		2 opp	0	Y	Y	Y	4	Y	Y
C3		1	1	Y	N	Y	4	Y	Y
D1	$\binom{5}{3}$	2 adj	1	Y	N	N	8	Y	Y
D2		2 opp	1	Y	Y	Y	8	Y	Y
D3		3 adj	0	Y	N	Y	8	Y	Y
D4		2 adj	1	Y	N	N	8	Y	Y
E1	$\binom{5}{4}$	4	0	Y	Y	Y	16	Y	Y
E2		3	1	Y	N	Y	16	Y	Y
F1	$\binom{5}{5}$	4	1	Y	Y	Y	32	Y	Y

4.1.2 Design Algorithm

Because the start of the design is a single-layer grid formed by (k x s) chain of sub-grid square element that would bend into the space-frame's initial cylindrical shape, it is important to identify the design space and limitation to minimize the design possibilities and yet achieve the desired outcome. For the purpose of this work and to demonstrate one of the applications of the LBCCSMs, the ability to morph a cylindrical-shell to either hyperbolic-shell or spherical-shell are considered that shows a change of the shell's diameter across its height. The space-frame's initial cylindrical shape circumference will be approximated by a polygon, which the number of sides (s) is considered as a design input, and because considering the initial and final morph of the space-frame to have its two ends identical without morphing, the top and bottom of the s-sided polygon will be constructed out of individual rigid links joined by its end. The initial

57

height (h_o) of the cylinder will be divided into (k) slices with vertical elements that are of rigid links to provide stability to the space-frame and to act as force transmitter. The height of each slice will be equal to the length of the polygon's side (l_s) because a square sub-grid was the chosen shape.

Moreover, the three other inputs of the design are the initial radius of the circumscribed circle (ρ_o), the change in radius ($\Delta\mu$) and the two ends of the space-frame plane's relative rotation ($\Delta\tau$) as shown in Figure 4.5for the hyperbolic-shell morph and Figure 4.6 for the spherical-shell morph. This relative rotation of the planes is the main control in morphing the space-frame and it's carried out using the applied rotation at the ends.
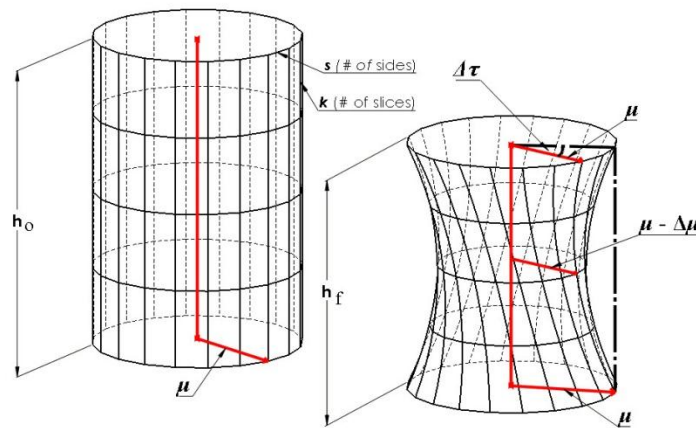
Figure 4.5 The parameters used to define the SMSF in the hyperbolic-shell morphing.
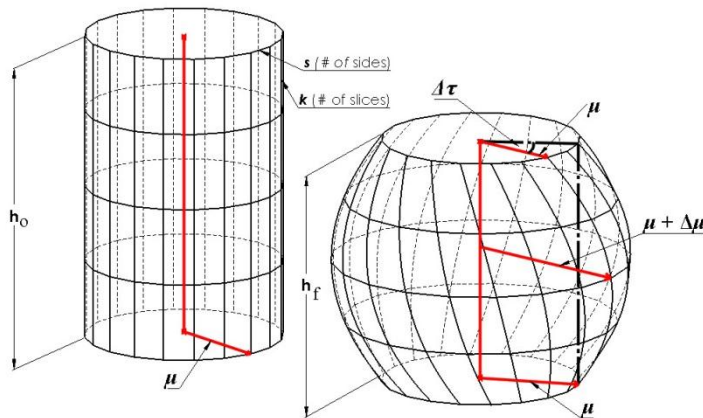
Figure 4.6 The parameters used to define the SMSF in the spherical-shell morphing.

58

The mathematical modeling was done using Matlab utilizing the polygon's geometry to locate each point on the initial space-frame and the corresponding location for that point on the space-frame's final shape. Lines then connects those points and its lengths are compared to calculate the change in length that then would be used in designing the specific LBCCSM for that element. Force analysis was not included in this study as this research addresses the kinematic use of the LBCCSMs only. The full Matlab code used in this simulation can be found in Appendix C.8.

The following are the main Matlab code equations from the polygon's geometry:

$$l_s = 2 * \rho_o * \sin(\pi/s) \tag{4.1}$$

$$h_o = k * l_s \tag{4.2}$$

The equation used to describe the profile of the space-frame as a function of (μ) along the height to achieve the desired morph:

$$\mu(h) = \rho_o + \Delta\mu * \left(1 - \left(\frac{2}{h_o}\right)^2 * \left(h - \frac{h_o}{2}\right)^2\right) \tag{4.3}$$

Substituting equation 4.2 into equation 4.3 results in:

$$\mu(h) = \rho_o + \Delta\mu * \left(\frac{4*(k-1)}{k^2}\right) \tag{4.4}$$

The sign of the change of radius ($\Delta\mu$) is important as it determine the final morph shape; negative sign will produce a hyperbolic profile where positive sign will produce a spherical profile. A Model Possibility Check (*MPC*) was put into place within the algorithm to check if the desired morph would be possible considering (*s*), (*k*), ($\Delta\mu$) and the restriction of the polygons' sides and the vertical elements being a rigid link.

$$(MPC) \quad \rightarrow \quad l_s \geq \Delta\mu * \left(\frac{4*(k-1)}{k^2}\right) \quad \text{If false, then:} \tag{4.5}$$

Decrease (*s*) or/and Decrease ($\Delta\mu$) or/and Increase (*k*)

59

Because the sub-grid is chosen to be square, the initial height of each segment is equal to the side length (l_s) and the MPC equation ensures that if the vertical rigid elements would lie horizontally after morphing the space-frame does not change in length due to the large value of ($\Delta\mu$) of that slice (k). Decreasing (s) will increase the value of (l_s) to maintain the initial radius of the circumscribed circle (ρ_o), decreasing ($\Delta\mu$) will decrease the change in radius at each slice insuring the vertical elements remains rigid even if they would lie horizontally. Increasing the number of slice (k) will decrease the ($\Delta\mu$) at each slice insuring vertical links remains rigid.

4.2 Morphing Strategies

The strategy followed in designing the specific SMSFs were purely done from the geometrical aspect of the design as this chapter illustrates one of the novel uses of the linear bi-stable elements LBCCSM. Placing those LBCCSM determine the final shape of the space-frame, choosing the appropriate elements configuration within the sub-grade square tessellation is carried out in reference to Figure 4.4and Table 4.1. Navigation through this figure and table would require some initial design inputs, and the one considered are:

1- The two ends of the space-frame are considered fixed shape, thus its links are rigid.

2- The vertical elements are considered rigid as a mean for load transmission and structural support, thus all diagonal elements need to be LBCCSMs.

3- Symmetrical geometry across the plane of mid height, thus an even number of slice (k).

4- Within the square elements, the diagonal and side LBCCSM elements should move independently from each other.

5- The ability for the sub-grid square to be able to morph to both trapezoid and parallelogram shapes.

6- The end slices are arrayable horizontally only.

7- The intermediate slices are arrayable both vertically and horizontally.

8- If more than one arrangement is found, the arrangement that have the higher number of shape formed is considered for more DOF.

Referring to Table 4.1 and Figure 4.4 along with the initial design input, the end slices are chosen to be C3 from $\binom{5}{n}$ where only one side and the diagonal are LBCCSM. On the other hand, the choice of D2 from $\binom{5}{n}$ best fits the inputs where two opposite side and the diagonal are LBCCSM and its ability to have joint side with the end slices. As shown in Figure 4.1, the LBCCSM have two stable positions (normally open and normally closed) with a delta change in length, and depending on the initial state of its stable position and location. Four different design configurations can be produced out of the LBCCSMs' two initial stable positions and their two locations (diagonal or radial element). The characterization of each design was based on element location within the sub-grid square, its initial bi-stable state, directionality after loading, Poisson effect and morphed shape as shown in Table 4.2 (a-d).

Table 4.2 Design configurations for the LBCCSM placement within the square sub-grid.
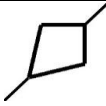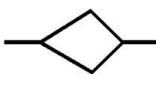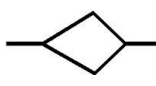
(a) Configuration Design 1		SMSF's Directionality after loading
Element Location and State		
Name	Symbol	
Diagonal element initially open (δeio)		Shorter
Radial element initially open (ρeio)		Necking
Poisson Effect: Negative ($-\nu$)		
Morphed shape fits Hyperbolic profile		

(b) Configuration Design 2		SMSF's Directionality after loading
Element Location and State		
Name	Symbol	
Diagonal element initially closed (δeic)		Longer
Radial element initially open (ρeio)		Necking
Poisson Effect: Positive ($+\nu$)		
Morphed shape fits Hyperbolic profile		

61

Table 4.2 (Continued)

(c) Configuration Design 3			(d) Configuration Design 4		
Element Location and State		SMSF's Directionality after loading	Element Location and State		SMSF's Directionality after loading
Name	Symbol		Name	Symbol	
Diagonal element initially open (δeio)		Shorter	Diagonal element initially closed (δeic)		Longer
Radial element initially closed (ρeic)		Bulging	Radial element initially closed (ρeic)		Bulging
Poisson Effect: Positive (+ν)			Poisson Effect: Negative (-ν)		
Morphed shape fits Spherical profile			Design best fits Spherical profile		

Figure 4.7 illustrates the type of applied loads for each design to morph the space-frame from its initial shape to its final shape; those loads can be applied simultaneously or individually depending on the application. The LBCCSM elements are represented as well showing the bi-stability transformation between the two states of the space-frame. The following section will demonstrate two design examples showing the results from the mathematical model and the actual prototype.
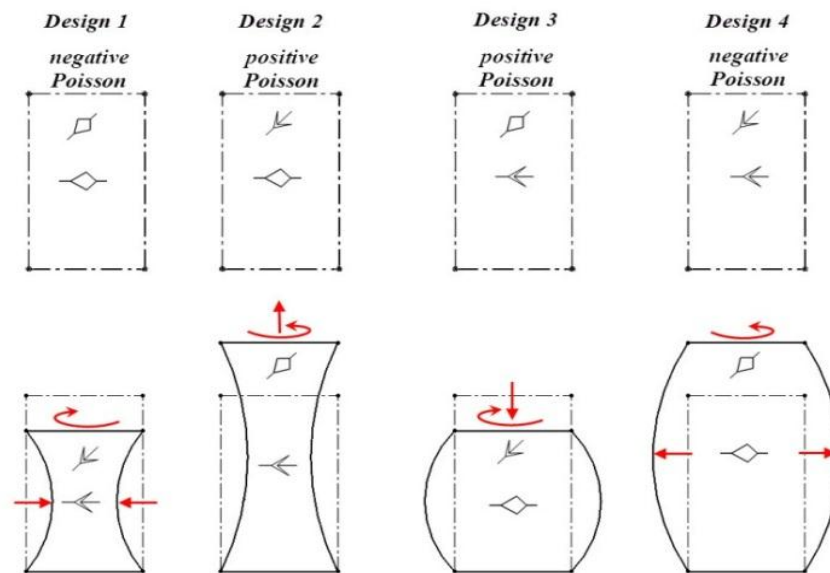
Figure 4.7 Loading conditions for each of the four design configuration from Table 4.2.

4.3 Design Examples

In this section, two designs were chosen one having a hyperbolic space-frame and a spherical space-frame for the other one. Because there are two design of each space-frame, the hyperbolic example was taken with negative Poisson effect where the spherical example addresses the positive Poisson effect. Initial design parameter where for both example are chosen to be similar with minor different as followed:

- Number of sides of the polygon (s) = 10.

- Number of slices (k) = 4.

- Initial cylinder diameter (ρ_o) = 300 mm.

- The change in space-frame diameter at mid height:

    ($\Delta\mu$) = -140 mm for the hyperbolic space-frame, and

    ($\Delta\mu$) = +140 mm for the spherical space-frame.

- The change in angle between the end plans ($\Delta\tau$) = 80$^\text{o}$.

    Clockwise for the hyperbolic space-frame, and

    Counter clockwise for the spherical space-frame.

The LBCCSM elements were laser cut from a 1/8 inch thick Polypropylene co-polymer material where the rigid links were laser cut from a 1/8 inch thick acrylic sheet. Each LBCCSM is secured with pin and guide type slider across its length to prevent the out of plane deformation. The added guiders do not affect the links' bi-stability nor translate any force. Individual elements are then connected together using fasteners and H-shape joint to give the space-frame the enough degrees-of-freedom as spherical joint. The joints are made of Polypropylene material laser cut from a 1/16 inch thick sheet and they are flexible that each end can bend and twist independently as shown in Figure 4.18. Because the design is symmetrical across the mid-plane, the number of

63

different LBCCSM required is reduced by half. Each end of the cylindrical space-frame is secured by decagon plate connected by a low friction shaft to ensure that the two planes remain parallel.

4.3.1 Example 1: Hyperbolic-Shell SMSF

The hyperbolic SMSF was chosen to be modeled using the design 1 from Table 4.2 (a). The diagonal and radial elements are LBCCSM and vertical elements are rigid link. Because the desired applied torque is in the clockwise direction, the LBCCSM elements were placed along the diagonal line that shears the square sub-grid the most in order for the actuation can take place. Figure 4.8 shows the results of the mathematical algorithm from Matlab, the calculated change in length of each element is then tabulated and was used to design the LBCCSM. Figure 4.9 shows the constructed single-layer grid in its two dimensional form showing the sub-grid arraying pattern. The grid is then bent into the space-frame's initial cylindrical shape as shown in Figure 4.10. The torque was applied first to deform the diagonal elements followed by radial force to deform the radial element forming the hyperbolic SMSF as shown in Figure 4.11 and Figure 4.12 respectively.
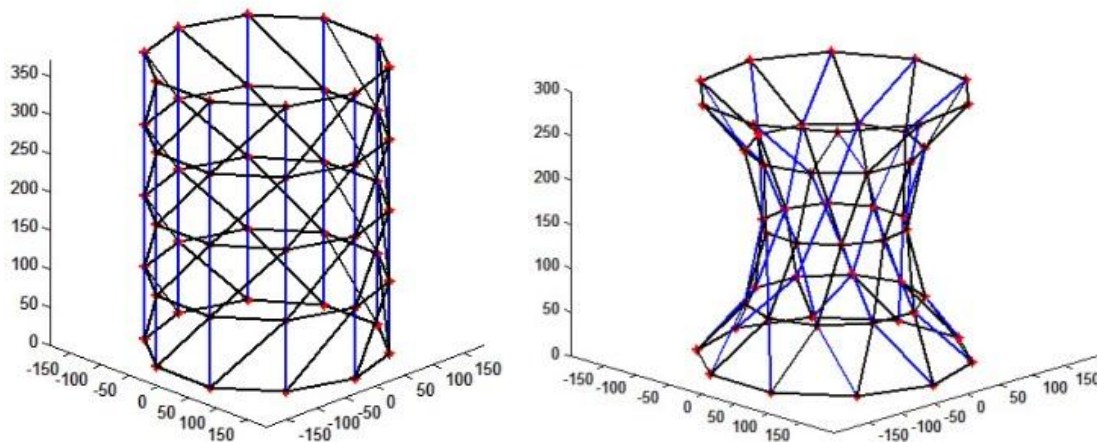
Figure 4.8 Hyperbolic SMSF using Matlab, Initial state (left) and final state (right).

64
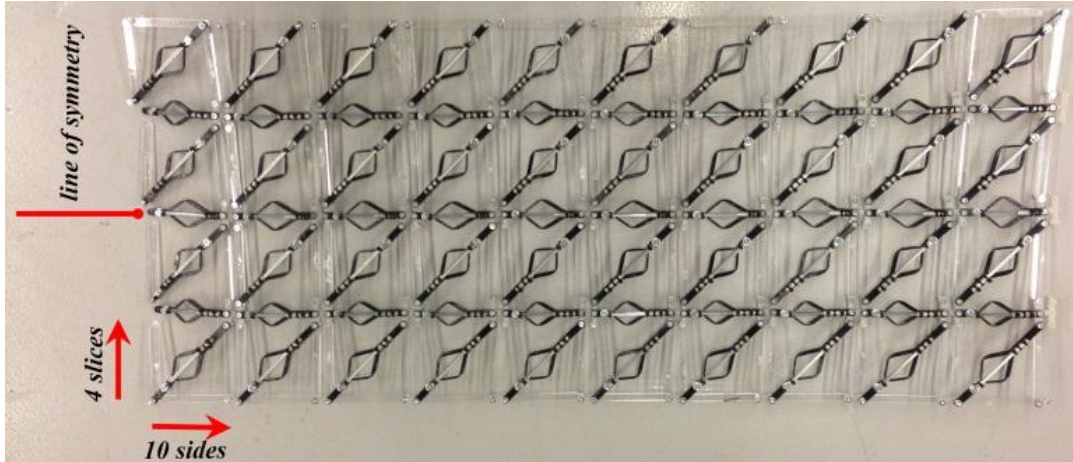
Figure 4.9 The single-layer grid tessellation pattern for the hyperbolic SMSF.

Figure 4.10 The hyperbolic SMSF at its initial cylindrical shape before morphing.

Figure 4.11 The hyperbolic SMSF after applying clockwise torque loading.
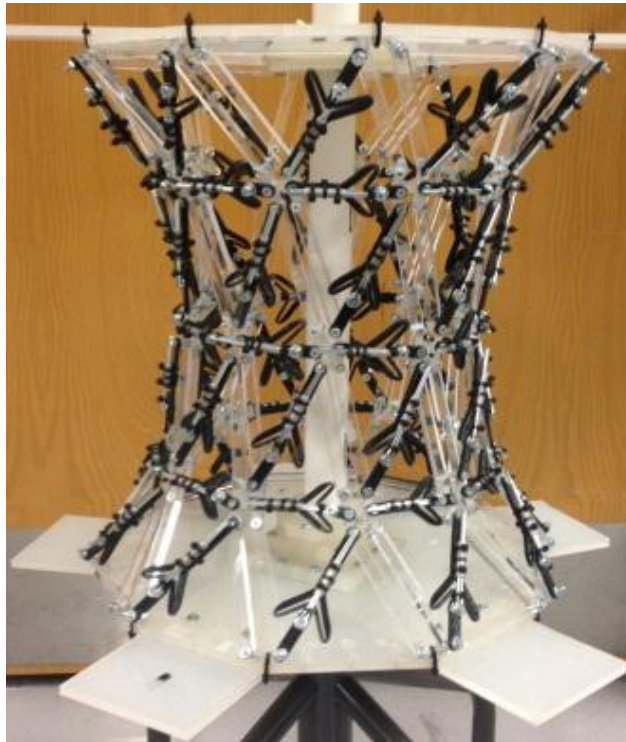
Figure 4.12 The hyperbolic SMSF after applying radial loading.

4.3.2 Example 2: Spherical-Shell SMSF

The spherical SMSF was chosen to be modeled using the design 3 from Table 4.2 (c). The diagonal and radial elements are LBCCSM and vertical elements are rigid link. Because the desired applied torque is in the counter clockwise direction, the LBCCSM elements were placed along the diagonal line that shears the square sub-grid the most in order for the actuation can take place. The same procedure as the previous example was followed here; Figure 4.13 shows the results of the mathematical algorithm from Matlab, the calculated change in length of each element is then tabulated and was used to design the LBCCSM. Figure 4.14 shows the constructed single-layer grid in its two dimensional form showing the sub-grid arraying pattern. The grid is then bent into the space-frame's initial cylindrical shape as shown in Figure 4.15. The torque load was applied first to deform the diagonal elements followed by axial force to deform the radial element forming the spherical SMSF as shown in Figure 4.16 and Figure 4.17 respectively.
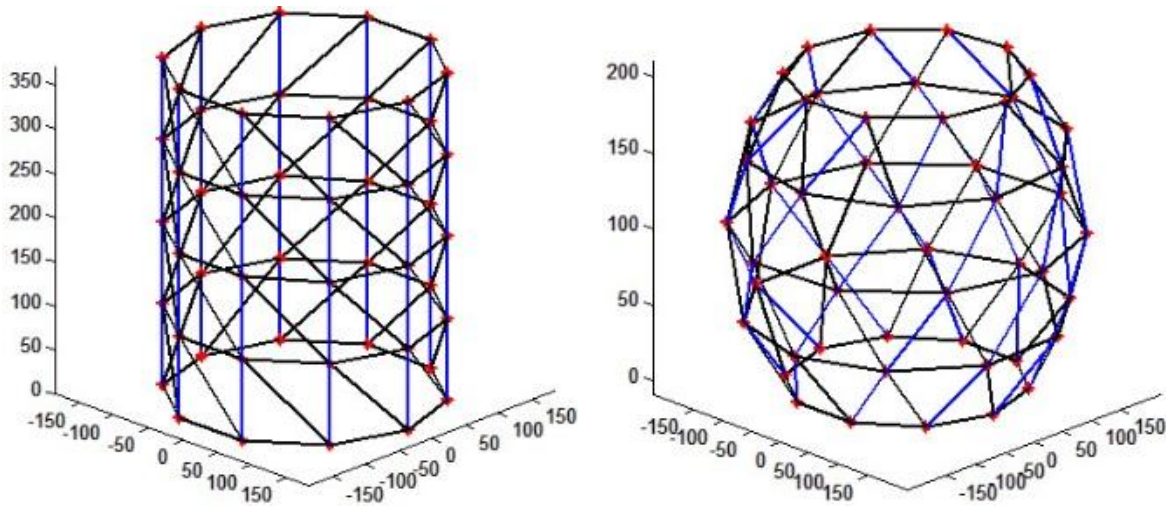
Figure 4.13 Spherical SMSF using Matlab, Initial state (left) and final state (right).

Figure 4.14 The single-layer grid tessellation pattern for the spherical SMSF.

Figure 4.15 The spherical SMSF at its initial cylindrical shape before morphing.

Figure 4.16 The spherical SMSF after applying counter-clockwise torque loading.

Figure 4.17 The spherical SMSF after applying vertical loading.

4.4 Results and Discussion

The results between the mathematical model and the prototype are addressed from a geometrical point of view. The results were expected to be different between both methods; the mathematical model takes into account that links are lines and connected to each other by a vertex and act as a spherical joint. Where the prototype is constructed using H-shaped, which we think it's the source of most of the error, joints that are not optimized or included in the mathematical model which is not the purpose of this research and might be consider as a future work. Moreover, the prototype gains extra height due to those H-joins along with its effect on the change in radii; thus the comparison between the two methods of each example is done using the percentage error of the relative change between the geometrical values of the SMSF as shown in Table 4.3.

Table 4.3 Measurements comparison between the mathematical model and the prototype.

Hyperbolic SMSF	Geometrical Measurements	h_o	h_f	h_f/h_o	ρ_o	ρ_f	ρ_f/ρ_o	$\rho_f-\rho_o$
	Matlab	370.82	299.09	0.81	150	80	0.53	-70
	Prototype	445	380	0.85	185	120	0.65	-65
	% error			5.55			17.78	

Spherical SMSF	Geometrical Measurements	h_o	h_f	h_f/h_o	ρ_o	ρ_f	ρ_f/ρ_o	$\rho_f-\rho_o$
	Matlab	370.82	201.23	0.54	150	220	1.47	70
	Prototype	455	300	0.66	185	250	1.35	65
	% error			17.70			8.53	

(Dimensions are in millimeter)
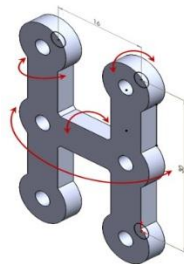
Figure 4.18 H-shape joint used in space-frame and its DOFs.

70

CHAPTER 5: SMSF USING QUADRILATERAL BISTABLE UNITCELL ELEMENTS

In this chapter, using the knowledge gained from the previous chapters in dealing with the space-frame shape morphing (SMSF); a new concept of shape morphing is advanced.

5.1 Proof of Concept: Designing and Modeling

The problem description for this chapter is to design a disk like structure with the ability to morph into a sphere. Or specifically, the circumference of a disk structure is approximated by a ten-sided polygon that would then morph into a hollow sphere structure that is approximated by 60-sided polyhedron. The disk-to-sphere structure is tessellated into ten sides for the latitudes circles and 12 sides for the longitude circles; the disk's thickness and radius are chosen at the design stage. The strategy in morphing the initial shape of the structure (disk) into its final shape (sphere) is that the radial lines on the surface of the disk bend but do not stretch, whereas the circumferential lines compress. Moreover, the radial lines on the disk become longitude lines on the sphere and the circumferential lines become latitude lines on the sphere. The disk's thickness splits in half, the upper half becomes the thickness of the upper hemisphere and the lower half becomes the thickness of the lower hemisphere. The proceeding sub-sections discuss the steps used in disk tessellation and the detailed morphing strategies. The nomenclature used in this chapter can be found in the Appendix A.

5.1.1 Disk Tessellation

Because the disk has a given thickness, the projection of it, which is a circle, is tessellated. To better understand the topology involved in morphing the disk into a hemisphere,

geometrical analysis was carried out using the known equations of circles and spheres by correlating them to each other using their parameters shown in Figure 5.1 (a).
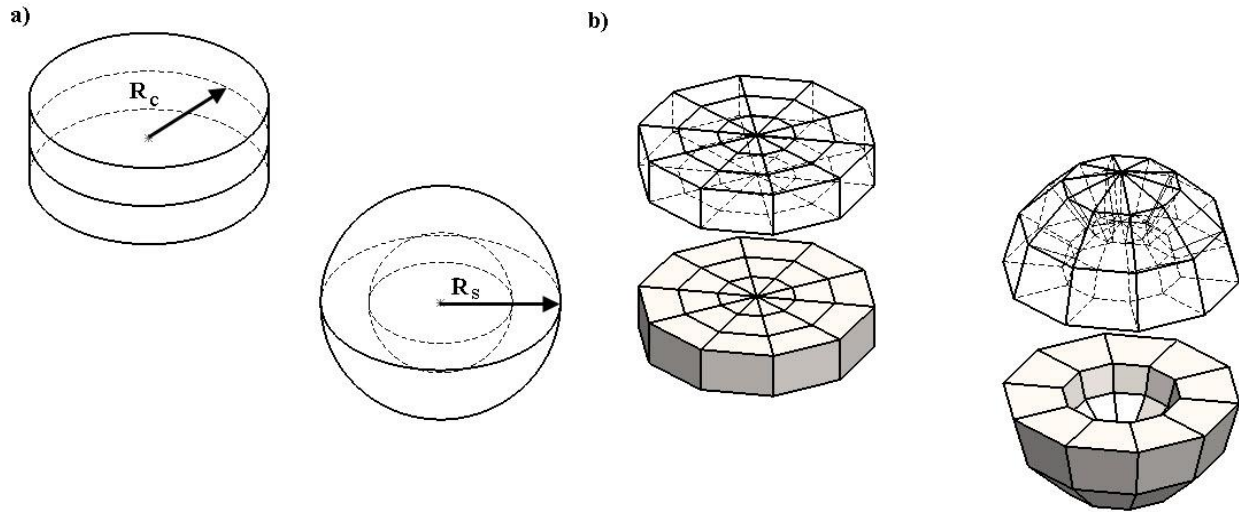
Figure 5.1 Disk-to-Sphere's, (a) original and (b) approximated geometry.

As it was stated before and to avoid using curved link mechanisms, polygons will be used to approximate the circles that construct the disk as shown in Figure 5.1 (b). The advantages of using polygons for circle approximation are not only limited to the use of straight link mechanism but also a measure of refine the design and knowing its limitations. Increasing the number of sides will refine the circle approximation and will also increase the number of unit-cells and increase the complexity of the design, vice-versa. The following are the steps used to construct the disk tessellation using the computer aided design software Solidworks; dimensions used are also noted along with the explanation of how those parameters affect the final design.

Step 1: A regular ten-sided polygon is used with a circumscribed circle radius (R_c) of 150 mm was chosen (the same size as was chosen for the shell SMSF in Chapter 4).

Step 2: In order to make the polygon's structure manageable, two smaller ten-sided polygons were constructed inside one another with a difference of 50 mm, as shown in Figure 5.2. Increasing the number of intermediate polygons will refine the hemisphere's outer curvature.

72
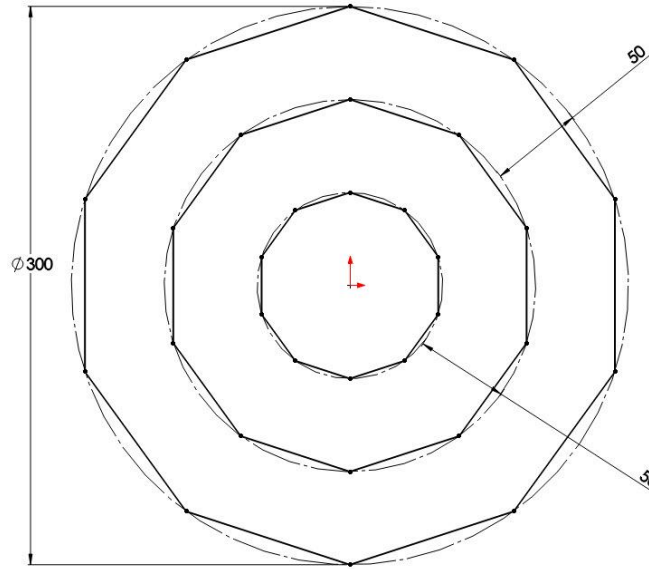
Figure 5.2 Top view of the three ten-sided polygons, lengths are in mm.

Step 3: A design choice of 50 mm was given to the disk's half thickness (to be consistent with the three polygons' offset dimension) and, by connecting the nodes (the vertices of the polygons) by straight lines; a polygon sector can be constructed as shown in Figure 5.3. The polygon will have ten identical sectors and, for clarity, only one is shown along with lines notation.
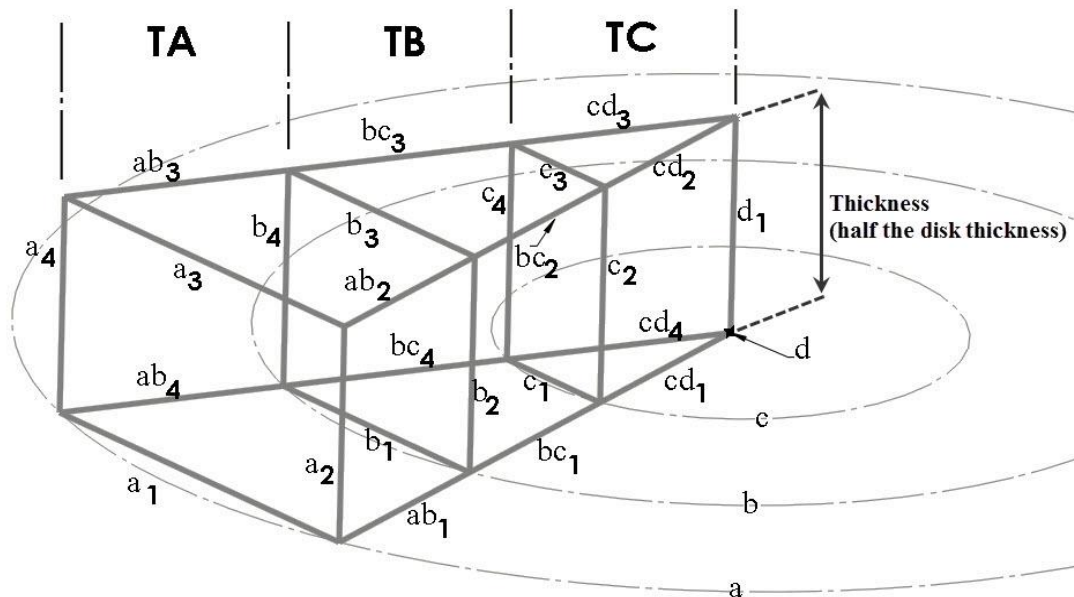
Figure 5.3 The constructed wireframe for the polygon's sector with notations.

73

Step 4: A design choice at this stage should be made as in which of the lines should be variable and which should be fixed in length. The thickness of the disk-to-sphere structure is considered to be fixed in this design example; thus, the lines (a, b and d) $_{2\ and\ 4}$ and d_1, shown in Figure 5.3, are equal 50 mm. Figure 5.4 shows the side view of the sector's backside wireframe after morphing; the radius of the hemisphere (R_s) can be determined geometrically. As mentioned before (the radial lines on the surface of the disk bend and do not stretch), the lines (ab, bc and cd) $_3$, shown in Figure 5.3, would bend to approximate half arc and similarly for lines (ab, bc and cd) $_2$. Because those three lines are considered equal to one another and fixed in length (50 mm), the outside radius of the hemisphere will be 96.59 mm.
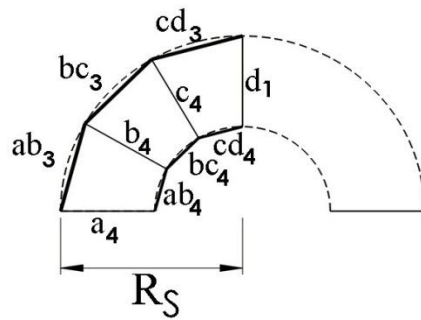
Figure 5.4 The sector's wireframe back surface shown from the side view.

Step 5: After the determination of the hemisphere radius, another ten-sided polygon is drawn on the top view that is in Figure 5.4 with a circumscribed circle radius (R_s) of 95.49 mm. The nodes are then connected together forming the morphed sector as shown in Figure 5.5.
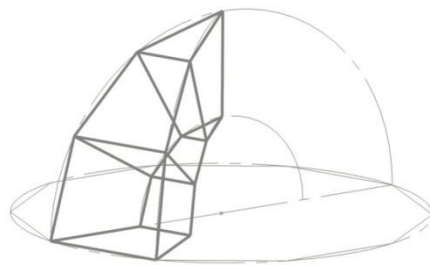
Figure 5.5 The morphed sector's wireframe to wedge.

74

Step 6: Having the wireframe's sector in its two positions (before and after morphing), Table 5.1 is constructed showing the dimensions different of each link between the initial and final shape. Moreover, given this data, we can analyze how TA and TB can morph from a trapezoidal prism to a quadrilateral-base pyramid; similarly the morphing of TC from the triangular prism to the triangular-base pyramid. The following section will discuss the morphing strategies involved.

Table 5.1 The wireframe dimensions in the initial and final state of the sector.

Segment	Link Name	Length (mm)	
		@ Disk	@ Hemisphere
TA	a_1	92.71	28.12
	a_2	50	50
	a_3	92.71	59.02
	a_4	50	50
	ab_1	50	23.55
	ab_2	50	50
	ab_3	50	50
	ab_4	50	23.55
TA / TB	b_1	61.8	24.35
	b_2	50	50
	b_3	61.8	51.11
	b_4	50	50
TB	bc_1	50	23.55
	bc_2	50	50
	bc_3	50	50
	bc_4	50	23.55
TB / TC	c_1	30.9	14.06
	c_2	50	50
	c_3	30.9	29.51
	c_4	50	50
TC	cd_1	50	23.55
	cd_2	50	50
	cd_3	50	50
	cd_4	50	23.55
	d_1	50	50

5.1.2 Morphing Strategies

In this section, analysis will be carried out on how a trapezoidal prism can be morphed into a quadrilateral-base pyramid and a triangular prism into a triangular-base pyramid. To understand the problem with clarity, working with a regular three-dimensional wireframe, such as a cube instead of the trapezoidal prism, will provide a general insight on the degrees-of-freedom and what are the parameters involved to control the movements of each link within the wireframe. Section 4.1.1 explained that a quadrilateral two-dimensional frame made of six links (four sides and two diagonal) will have (-1) degree-of-freedom; thus, only five links are needed to fully define the frame making it a structure with zero degrees-of-freedom and leading to the method of $\binom{5}{n}$, which was discussed in depth. Following the similar method, the same five links are used (four sides and a diagonal) but in this case it extends to the third dimension by giving it a depth as shown in Figure 5.6.
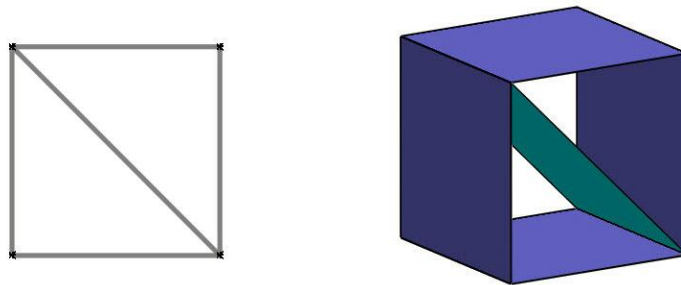
Figure 5.6 Quadrilateral structure in its 2D and 3D form.

The mobility equations will remain the same as the planar case because all the pin joints and links are collinear. The method of $\binom{5}{n}$ is also applicable in this situation, where *n* is the number of surfaces that need to change length. The analysis of the cube can be extended to the trapezoidal prism because it is a special case from where two opposite surfaces are inclined inward or outward from one another.

In the case of the triangular prism, the two-dimensional aspect shows that if three links were connected in a loop with three pin joints between each link, it will result in a structure with zero degrees-of-freedom. Adding a third dimension by giving it a thickness will result in three surfaces connected in a loop with three hinges; it is also a structure as shown in Figure 5.7.
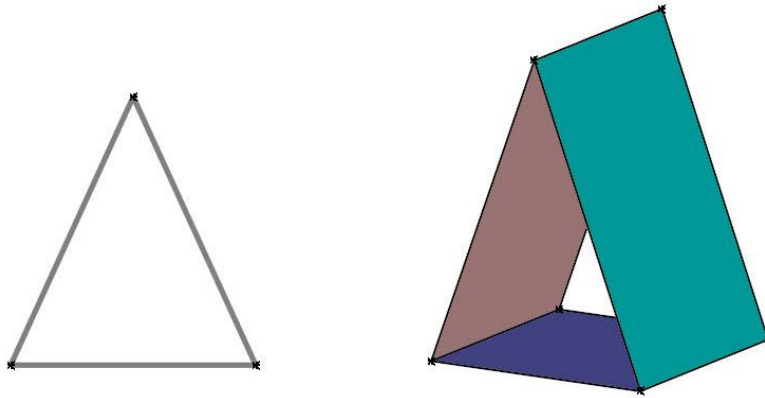
Figure 5.7 Triangular structure in its 2D and 3D form.

From Figure 5.3, the chosen sector consists of three segments in which TA and TB is a trapezoidal prism sharing a surface, and TC is a triangular prism sharing one surface with the TB. Figure 5.8 shows the 11 different surfaces needed to construct the one out of ten sectors.
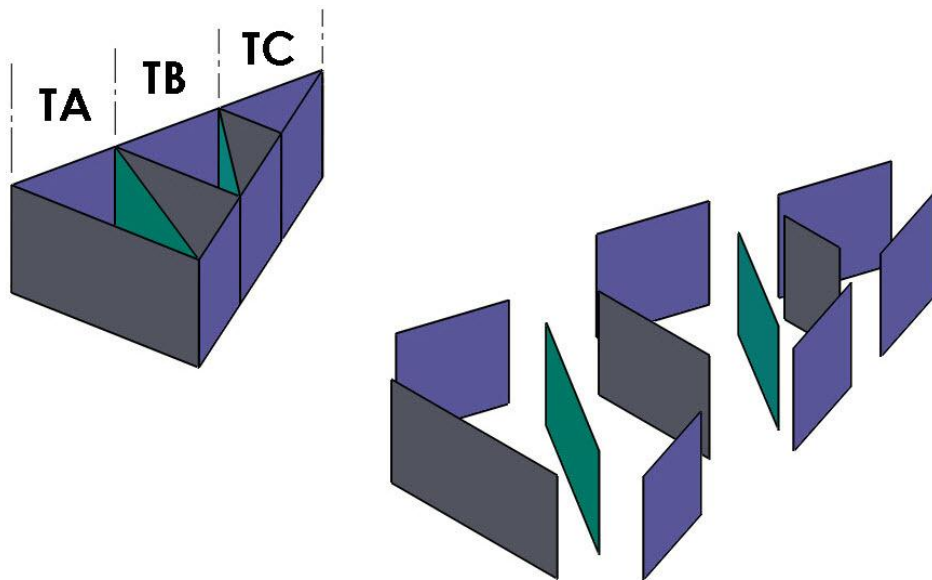
Figure 5.8 Shows the 11 planes needed to construct the sector's structure.

Analyzing the sector in general, it can be considered as one large triangular prism in which only three surfaces can be used to construct it, eliminating the need for the intermediate surfaces and reducing it from 11 to three. Regardless if the surfaces are curved or planer, the triangular prism sector will remain a structure before and after the morph, as shown in Figure 5.9. The kinematics involved in constructing the surface on one hand and its compliancy on the other hand, will be analyzed based on each segment's individual morph behavior.
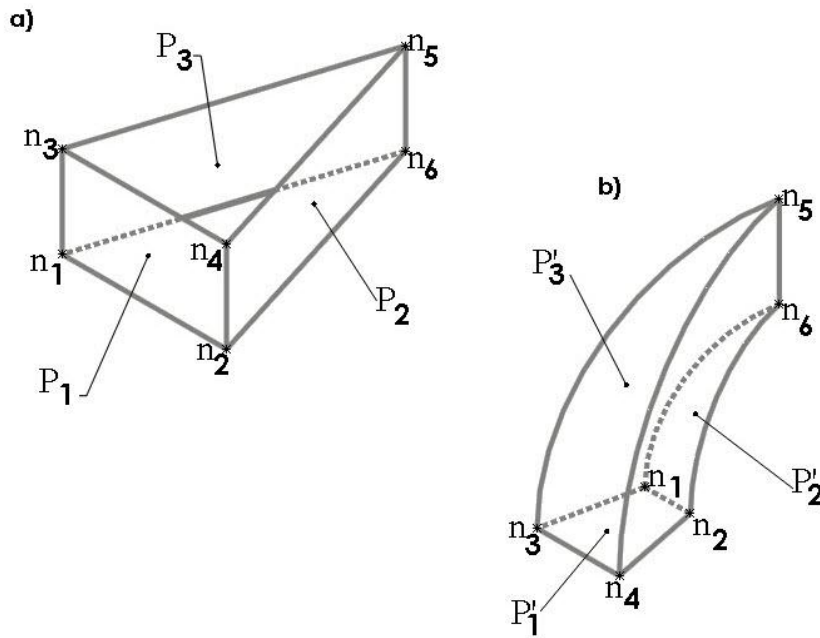
Figure 5.9 Shows the nodes and planes in (a) sector, (b) wedge.

5.2 Mechanism Synthesis

The mechanism synthesis involved in morphing the planes is investigated using kinematic graphic design. Because the sector in Figure 5.9 is composed of three surfaces (P_1, P_2 and P_3), where P_2 and P_3 are similar in design and behavior, controlling the nodes (n_1 to n_6) via a compliant mechanism will allow the required relative displacement between the nodes, as in Table 5.1 in the form of length change for each link. It is possible to solve this problem using the linear bistable link elements (LBCCSM) introduced in Chapter 3, which results in a much more

complicated spatial mechanism with its associated degrees-of-freedom and will increase the number of elements needed to assemble a prototype. Using the concept of a cell element reduces the number elements needed for the design and assembly. Figure 5.10 illustrates the area of the unit-cell in which a mechanism connecting the nodes (vertices) should fi, morphing P_1 from a rectangular to a trapezoidal cell element P'_1 and P_2 from a rectangular to an arched rectangular cell element P'_2. Four extra intermediate nodes are added for P_2 and P_3 corresponding to the disk tessellation described in section 5.1.1.
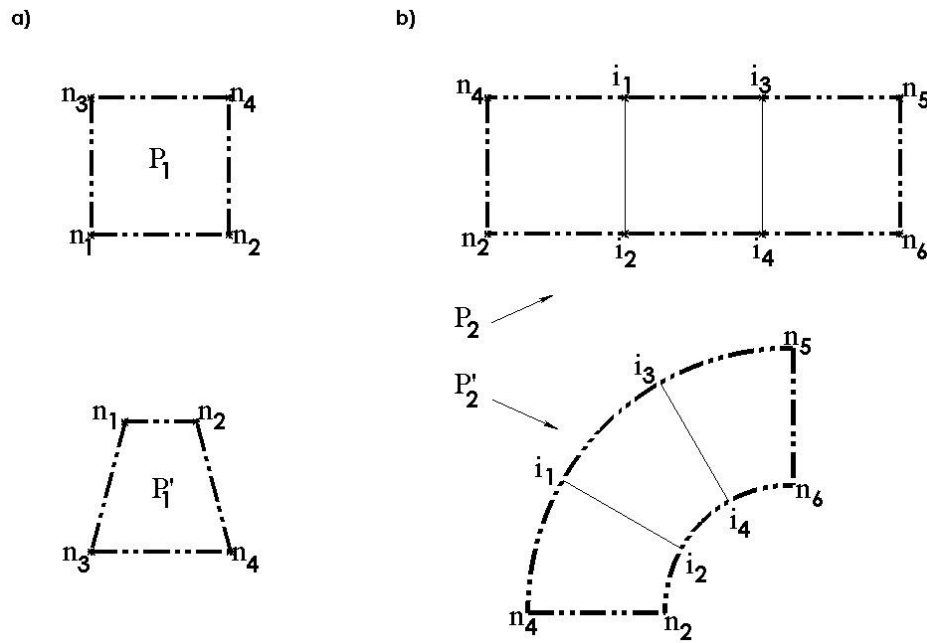
Figure 5.10 The initial and final state of plans (a) P_1, (b) P_2.

5.3 Type and Dimension Synthesis

Identifying the unit-cell's initial and final state was a key step in the mechanism type selection process. Summarizing the information from Figure 5.3, Figure 5.9 and Figure 5.10 along with Table 5.1 into Table 5.2, guided the mechanism type selection in terms of design choices and constraints.

79

Table 5.2 The dimensions involved in Figure 5.10.

Plane	Connectoin between Nodes		Link name	Length (mm)		Δ Length (mm)
				Initial	Final	
Figure 5.9	Figure 5.10		Figure 5.3	Table 5.1		
P_1	n_1	n_2	a_1	92.71	28.12	64.59
	n_2	n_4	a_2	50	50	0
	n_4	n_3	a_3	92.71	59.02	33.69
	n_3	n_1	a_4	50	50	0
P_2	n_2	n_4	a_2	50	50	0
	n_4	i_1	ab_2	50	50	0
	i_1	i_3	bc_2	50	50	0
	i_3	n_5	cd_2	50	50	0
	n_5	n_6	d_1	50	50	0
	n_6	i_4	cd_1	50	23.55	26.45
	i_4	i_2	bc_1	50	23.55	26.45
	i_2	n_2	ab_1	50	23.55	26.45
	i_1	i_2	b_2	50	50	0
	i_3	i_4	c_2	50	50	0

The mechanisms' parameters from Table 5.2 are written in the form of constraints:

- Constraint #1 for P_1: The relative displacement between nodes (n_1, n_3) and (n_2, n_4) should be zero.

- Constraint #2 for P_1: The relative displacement between nodes (n_1, n_2) and (n_3, n_4) should be collinear and toward each other.

- Constraint #3 for P_2 and P_3: The relative displacement between each consecutive node should be zero except between nodes (n_2, i_2), (i_2, i_4) and (i_4, n_6) which should be collinear and toward each other.

- Constraint #4 for all the nodes: If the relative displacement between two nodes is zero (no length change), then a single rigid link can be used to connect both nodes. Two or more rigid links can be used to link between the nodes that have collinear relative displacement (collinear length change between nodes); therefore, a minimum of one extra node should be introduced between the original two nodes. Figure 5.11 shows the rigid links and

80

identifies the minimum number of external nodes for each mechanism within P_1 and P_2. A minimum of six external nodes for P_1 and five external nodes for P_2 must be used in the prospective mechanism; those nodes are translated to be living hinges connecting the compliant links.
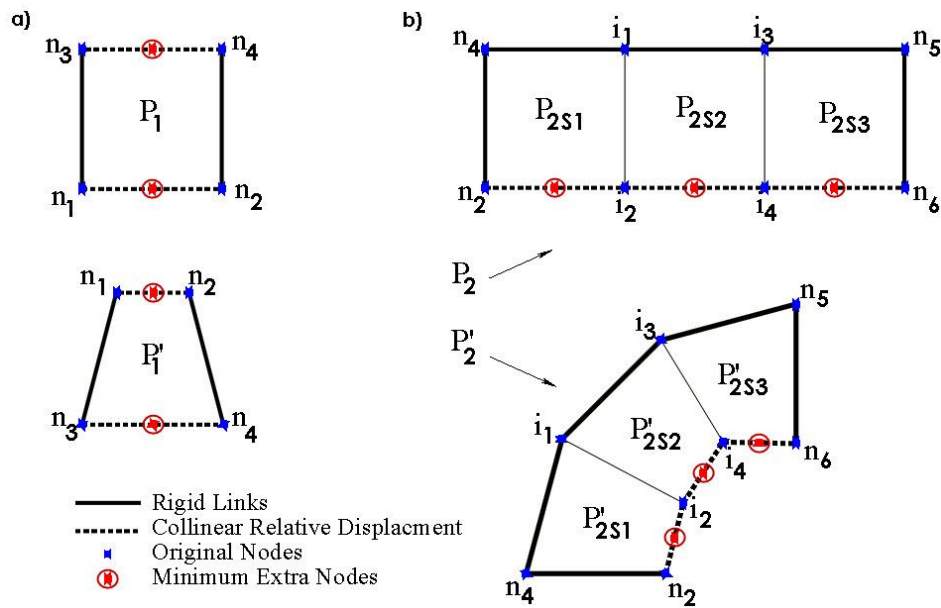
Figure 5.11 Rigid links and nodes in (a) P_1, (b) P_2.

- Constraint #5: The mechanism should be contained within the assigned surfaces (P_1, P_2 and P_3) and its links should not interfere with each other, i.e. links should not cross to enable single plane fully compliant manufacture.

Furthermore, a one-degree-of-freedom mechanism should be considered because the mechanism is the unit-cell, and to reduce the number of actuators required to control the overall design. The most important constraint is the ability to laser cut the mechanism from a single sheet of polymer; this requires the mechanism to be planar and single layer. Solving the kinematic equations for an unknown mechanism, where only the initial and final state of four of its nodes is given, turns the problem into a mechanism synthesis. Furthermore, solving for the

links' shape, interferences, overlapping, and the containment of the mechanism within a specific footprint requires extensive formulation and coding.

5.3.1 The Synthesis of P_1

For proof of concept, the approach followed in solving this design problem for P_1 was simplified by the use of existing mechanisms and the use of Solidworks CAD software. From the Design of Machinery [60], the number of single-degree-of-freedom mechanism and its valid isomers possible for the four-bar, six-bar, eight-bar, ten-bar, and twelve-bar linkages are, respectively: 1,2,16,230 and 6856. Analyzing each isomer as a potential solution was done both deductively and via Solidworks. Figure 5.12 shows the four-bar and six-bar isomers for one degree-of-freedom mechanism.
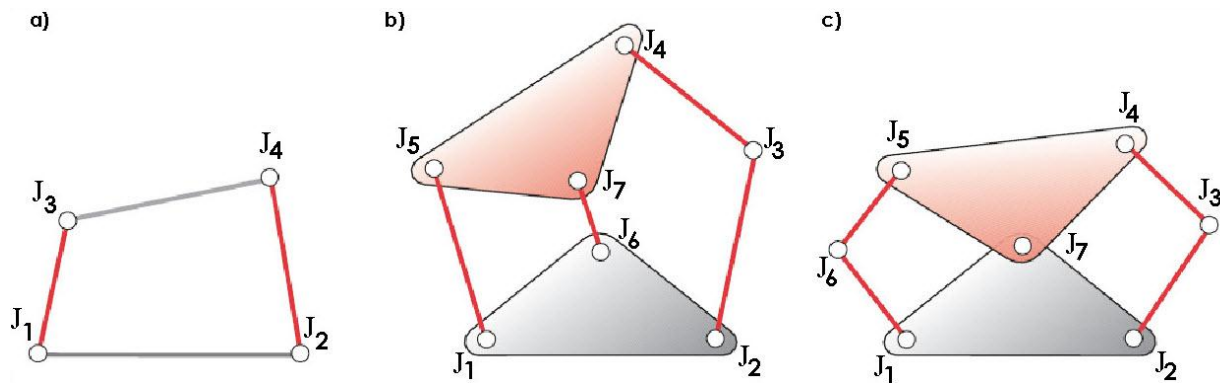
Figure 5.12 The four-bar and six-bar isomers for one DOF mechanism, adapted from [60].

If four of the outside pin joints of the mechanism are considered to be the nodes of P_1, then the four-bar mechanism cannot be utilized because its fixed length sides do not allow the change from rectangle to trapezoid. In the Stephenson's six-bar isomer, Figure 5.12 (b), there are five outer nodes, which violate constraint #4, which calls for a minimum of six outer nodes for it to satisfy P_1 design, as shown in Figure 5.11. In Watt's six-bar isomer in Figure 5.12 (c), there

are six outer nodes, which satisfy the minimum nodes requirement in constraint #4 and there are three ways to arrange those nodes.

The first arrangement involves taking nodes (J_2, J_1), shown in Figure 5.12, as (n_1, n_3), shown in Figure 5.10, and (J_4, J_5) as (n_2, n_4) which does not satisfy constraint #2 due to its scissor type motion between (J_1, J_5) and (J_2, J_4) where one moves inward forcing the other to move outward. The second arrangement involves taking nodes (J_1, J_6) as (n_1, n_3) and (J_3, J_4) as (n_2, n_4), which satisfies constraint #1, #2 and #4. The satisfaction of the 5th constraint can be verified graphically by means of the CAD software using the following steps:

Step 1: The initial and final state of the mechanism is drawn using the dimensions provided in Table 5.2, as shown in Figure 5.13 (a). The solid lines represent rigid links and the dashed lines are drawn to represent the area where the mechanism should be contained.

Step 2: Drawing the rest of the links' schematic according to Figure 5.12 (c) without any dimensions or constraints on both P_1 and P'_1, as shown in Figure 5.13 (b).

Step 3: Using a feature in Solidworks that allows the selection of two lines and constrain them to be equal is carried out between each link in P_1 and the corresponding link in P'_1, as shown in Figure 5.13 (c). This is an effective way to figure out the dimensions associated with each link without solving for the kinematic equation.

Step 4: The constructed mechanism is then manipulated in Solidworks to it fit within the assigned area in both states.

The result of this second arrangement violates constraint #5, as shown in Figure 5.13 (c); the length of the dotted link is not the same between P_1 and the corresponding link in P'_1. At the current length, the mechanism is contained within the assigned area but once the final equal link constrain is added, the mechanism is driven out of bound. The third arrangement is a mirror of

the second and also violates constraint #5; thus, both isomers of the six-bar mechanism with one degree-of-freedom cannot be used in the required design.
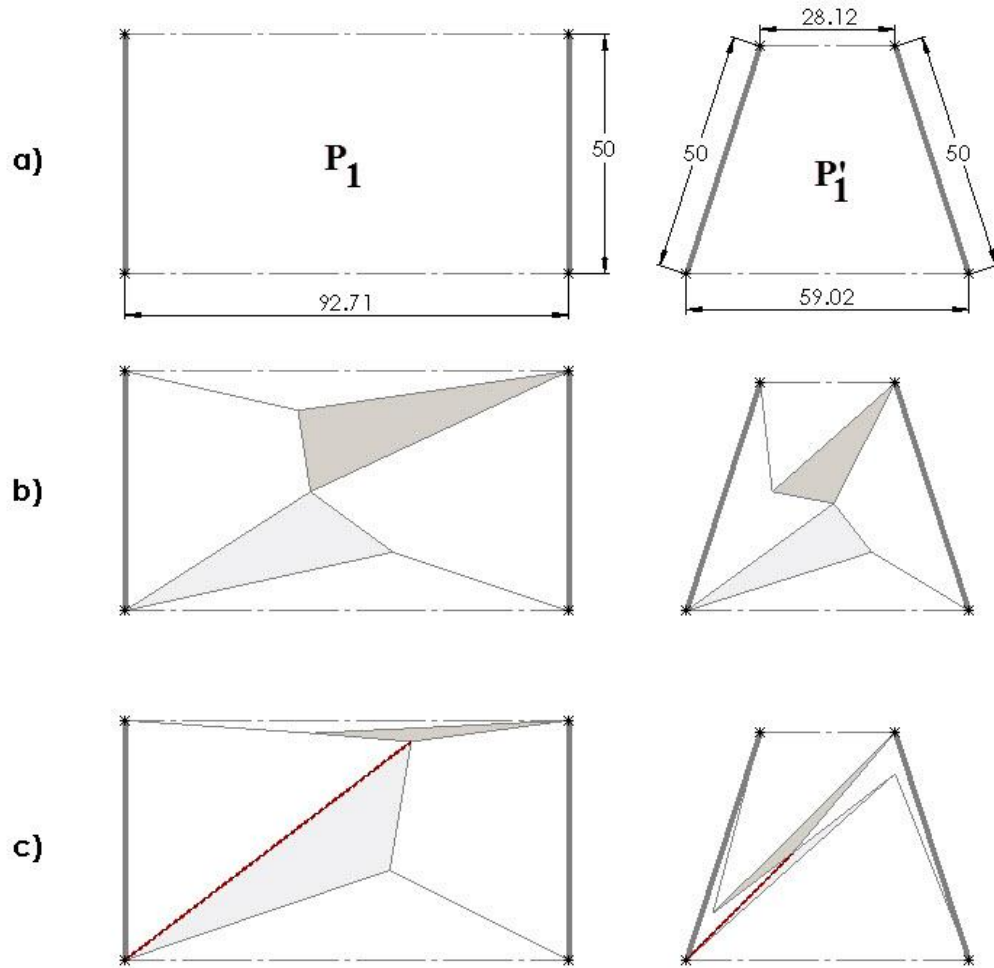
Figure 5.13 P_1 mechanism, (a) boundary, (b) without constraints, (c) constrained.

For the reason that neither the four-bar nor the six-bar mechanisms satisfied the required constraints, the eight-bar mechanism with its 16 isomers, shown in Figure 5.14 (a-p), are analyzed individually using the same methodology and reduced according to the following two observations:

1- Isomers with less than five outer nodes are eliminated, shown in Figure 5.14 (e, g and p).

2- Isomers with quaternary link, which is the link that connects to other links at four nodes, are eliminated, shown in Figure 5.14 (f, h, i, j, k, l and m), due to the extra constraints needed in Solidworks to match the initial and final state of the mechanism. Unlike the ternary link where fixing its three sides fixes the link.

After studying the remaining isomers shown in Figure 5.14 (a, b, c, d, n and o), it was concluded that isomer (a) can provide the solution to the given problem satisfying all the constraint and dimensions required by the design. This solution will be discussed thoroughly.
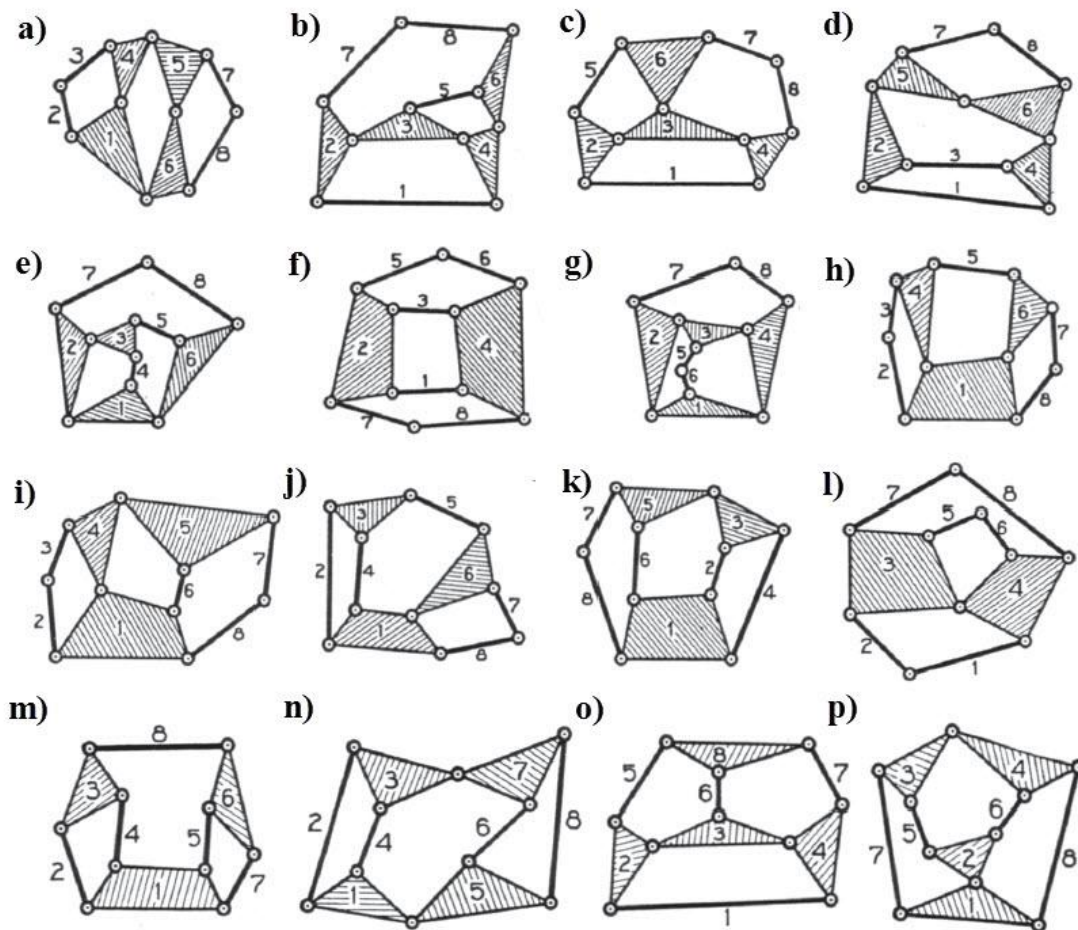
Figure 5.14 The eight-bar mechanism with its 16 isomers, adapted from [60].

Figure 5.15, with reference to Figure 5.14 (a) , shows the results after following the four steps involved in the 2nd arrangement of Watt's six-bar isomer where the five constrains are verified and met in this design arrangement.
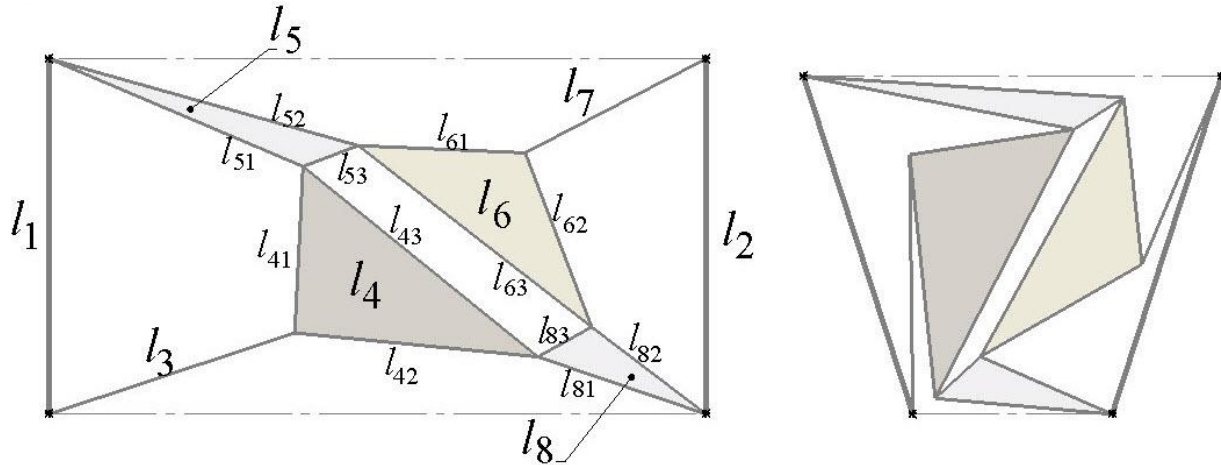
Figure 5.15 P$_1$ schematics with eight-bar mechanism and links' notation.

To fully define the sketch in Solidworks, Table 5.3 illustrates the additional constraints added to the lines in both P$_1$ and P'$_1$.

Table 5.3 P$_1$ with eight-bar mechanism constraints.

Plane Location	Constraint Type	Between Entities	
P$_1$	Collinear	l_4	l_7
	Collinear	l_{81}	l_{43}
	Angle = 60°	l_1	l_{51}
	Vertical	l_1	
	Vertical	l_2	
	Equal	l_{53}	l_{84}
	Equal	l_{43}	l_{63}
P'$_1$	Horizontal	l_{52}	
	Horizontal	l_{81}	
	Angle = 60°	l_1	l_{51}
	Collinear	l_{43}	l_{63}
	Collinear	l_{84}	l_{43}
	Collinear	l_{53}	l_{63}

86

Figure 5.16 shows the fully defined mechanism's arrangement, and at this stage of the design, all the lines are considered rigid links and all the nodes are pin joints. On that note, Figure 5.17 illustrate the mechanism's movement using five different translational positions from its initial state in P_1 to its final state in P'_1.
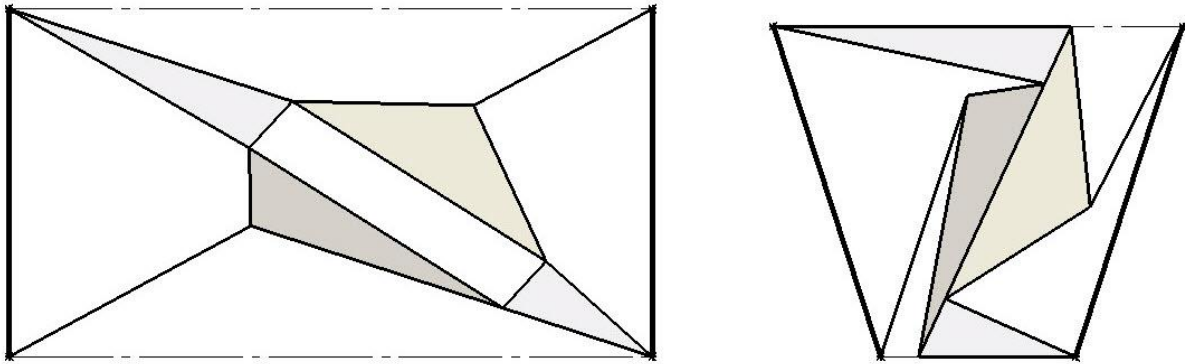
Figure 5.16 P_1 final mechanism in its initial and final state.
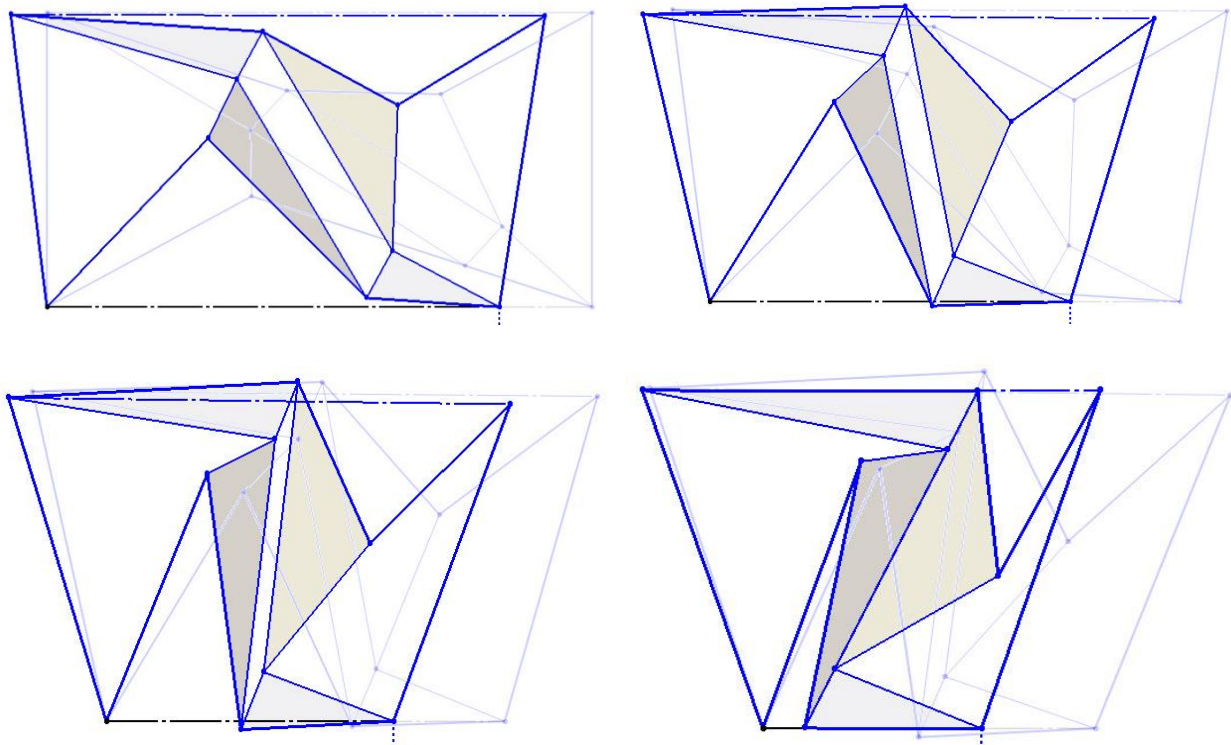
Figure 5.17 P_1 mechanism's movement using five different translational positions.

The final stage of the design involves converting the mechanism's linkages to compliant segments where the pin joints are replaced with flexural pivots. The design of those flexural pivots is done in Solidworks to meet the laser cutter's limitations. Stress concentration, fatigue and durability analysis are not included in this design and will be considered in future work on this topic. Figure 5.18 (a-c) shows the development of the design from the concluded outline of the mechanism in (a) to the complete design in a compliant form in (c); the full dimension of this design is shown in Appendix E.1.
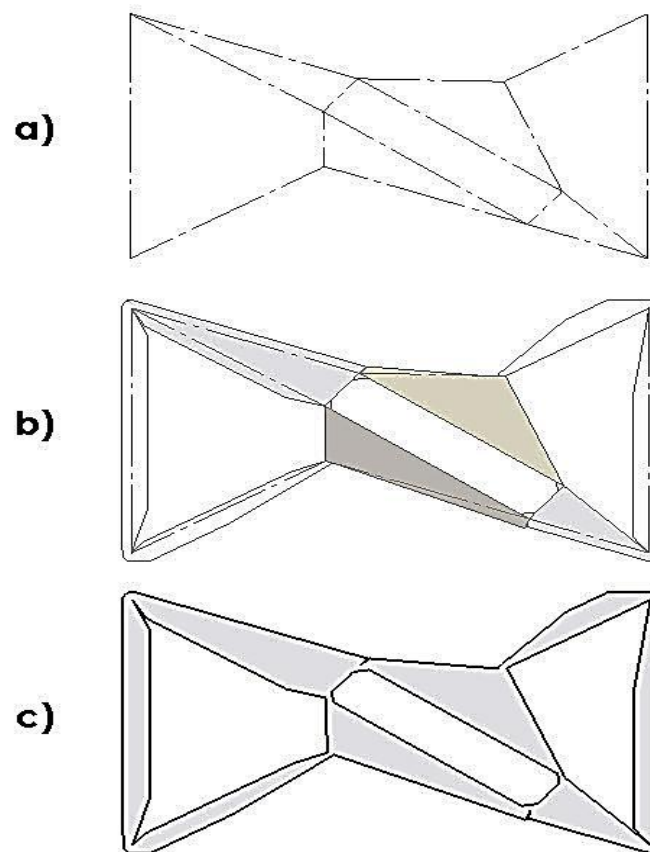
Figure 5.18 P_1 mechanism from outline to a fully compliant mechanism.

It is good to mention that some of the disqualified isomers can work for small length change between nodes (n_1, n_2) and (n_3, n_4). The proposed design procedures can guide the mechanism selection, which for proof of concept is faster than solving for it. Involving the

kinematic, kinetic and stress analysis is possible if solving for a specific application. The bistability analysis for this design is discussed in the next chapter.

5.3.2 The Synthesis of P_2 and P_3

The synthesis of the remaining two planes P_2 and P_3 of the sector in Figure 5.9 is described in this section. Because the planes are identical, the analysis of one plane can be applied to the other without any modification. In order for P_2 to change its initial state from rectangular to an arched rectangular cell element P'_2, it was divided into three equal parts as per the disk tessellation described in section 5.1.1. Referring to Table 5.2 and constraint #3 for P_2 and P_3 from section 5.3 that state "the relative displacement between each consecutive node should be zero except between nodes (n_2, i_2), (i_2, i_4) and (i_4, n_6) should be collinear and toward each other", requires that a minimum of one extra node should be placed between the nodes with collinear displacement. The analysis of P_{2S1} section, shown in Figure 5.19, is carried as an individual unit-cell and applied to the rest of the two sections P_{2S2} and P_{2S3}.
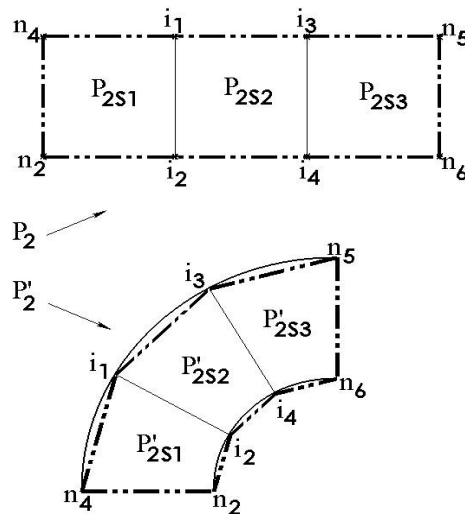
Figure 5.19 Shows the sub-section of P_2 for synthesis.

The four-bar mechanism cannot be applied due to its four sides being rigid; where in section P_{2S1} one side should have the ability to displace inward. On the other hand, Stephenson's

six-bar isomer Figure 5.12 (b) satisfies the minimum requirement of five outer nodes along with the constraint #3. Figure 5.20 shows the mechanism in Solidworks in the initial and final state with the inner links constrained to be equal; thus satisfying constraint #5.
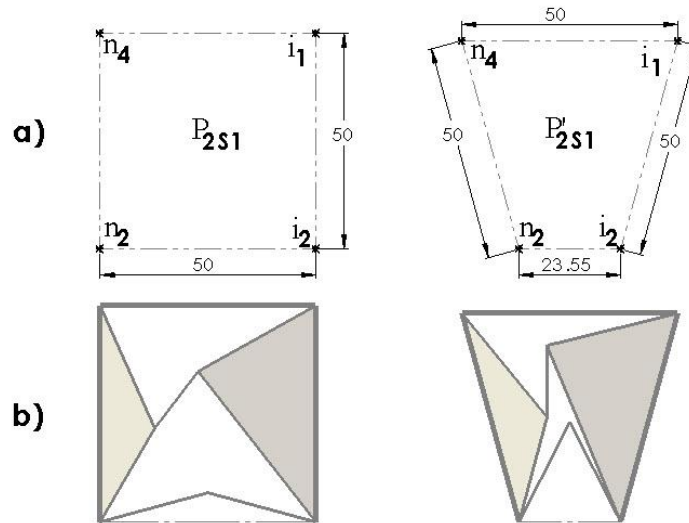
Figure 5.20 Shows P_{2S1}, (a) its boundary, (b) fitted Stephenson's six-bar isomer.

This mechanism has one degree-of-freedom through its six links and seven joints; and because the design requires the unit-cells to be bistable, the mechanism should be a structure with zero degree-of-freedom in its initial and final state. Analyzing the mechanism using the graph theory where links and joints are represented by points and lines respectively [70], gives an alternative way to develop mechanisms undergoing certain constraints. Figure 5.21 illustrates the example of Stephenson's six-bar isomer using the graph theory.
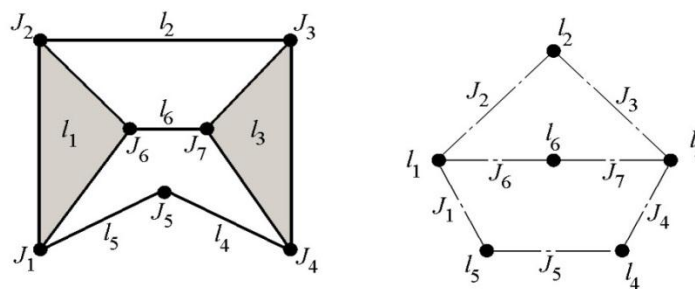
Figure 5.21 Stephenson's six-bar isomer in graph theory, adapted from [70].

90

A mechanism with five links connected in loop satisfies the minimum of five outer nodes (or joints) but would have two degrees-of-freedom, as shown in Figure 5.22 (a). Adding two links and four joints to the mechanism will reduce the mobility to zero, which in graph theory means two points and four lines respectively need to be added. Considering the symmetry in the design, those two points (or links) can be placed either inside the loop or outside, as shown in Figure 5.22 (b). Similarly for the four lines (or joints), two lines should be added in either side of the symmetry line and should avoid a three line loop when connecting otherwise, it will result in three links connected in a loop turning it into a single link. Figure 5.22 (c) shows the two possibilities of the mechanism which in fact are identical to one another, where Figure 5.22 (d) shows the final mechanism schematics in reference to its graph theory representation.
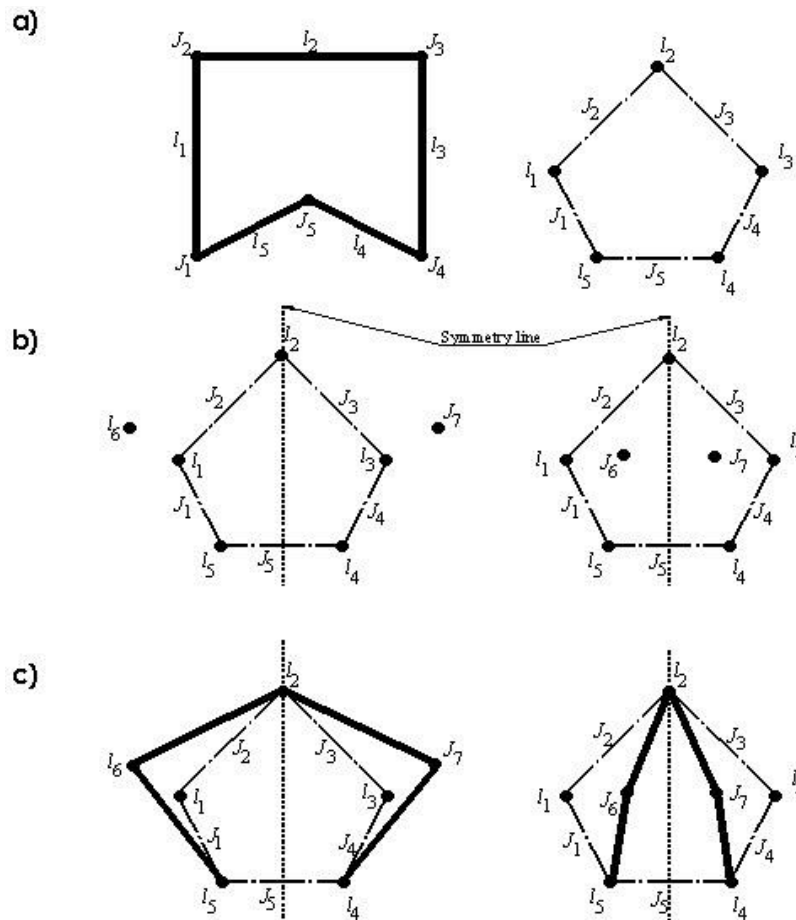
Figure 5.22 Converting five-bar mechanism into a zero-mobility mechanism.

91

d)
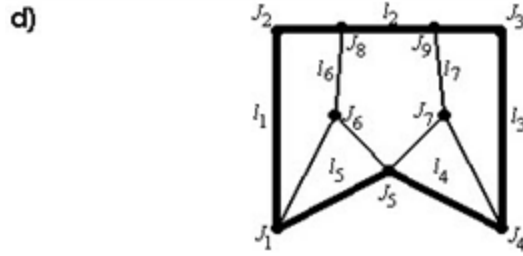
Figure 5.22 (Continued)

The new mechanism will have seven links and nine joints resulting in zero degree-of-freedom, as shown in Figure 5.23. The stress concentration, fatigue and durability analysis of this mechanism is considered a future work for this topic. To fully define the sketch in Solidworks, Table 5.4 illustrates the additional constraints added to the lines in both P_{2S1} and P'_{2S1}; the dashed lines are not those of the mechanism but for constraints purposes.

The final stage of the design involves converting the mechanism's linkages to compliant segments. Figure 5.24 (a-c) shows the development of the design from the outline of the mechanism in (a) to the complete design in a compliant form in (c); the full dimension of this design is referenced in Appendix E.2.
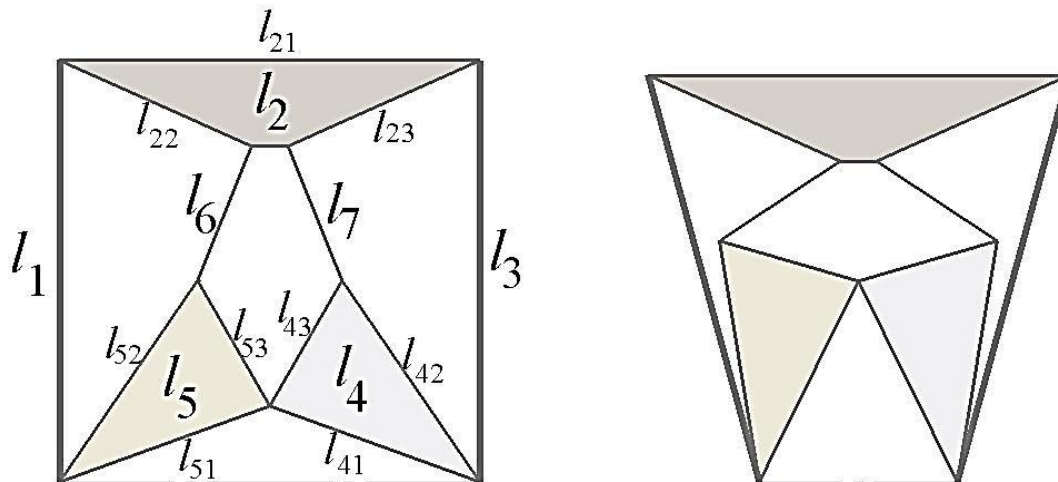
Figure 5.23 P_{2S1} schematics with seven-bar mechanism and links' notation.

Table 5.4 P$_{2S1}$ with seven-bar mechanism constraints.

Plane Location	Constraint Type	Between Entities	
P$_{1S1}$	Equal	l_{42}	l_{52}
	Equal	l_{41}	l_{51}
	Equal	l_6 l_7 l_{43} l_{53}	
	Equal	l_{22}	l_{23}
	Vertical	l_1	
	Vertical	l_3	
	Horizontal	l_{21}	
	Angle $= 24^O$	l_{22}	l_{21}
	Angle $= 24^O$	l_{23}	l_{21}
	Angle $= 43.96^O$	l_6	l_7
	Length $= 25$ mm	l_{22}	l_{23}
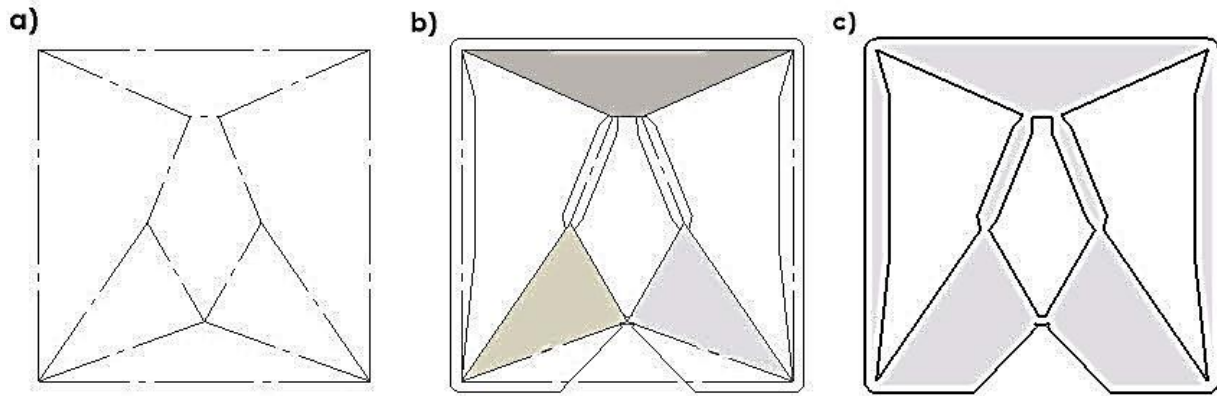
Figure 5.24 P$_{2S1}$ mechanism construction from outline to a fully compliant mechanism.

5.4 Design Prototypes and Fabrication

Building the shape-shifting space-frame prototype was the next step after it was designed; this section illustrates the fabrication procedures involved. The process involves laser cutting the bistable unit-cells from the sheet of material in two-dimensional and then construct the three-dimensional SMSF. Material selection is important for this type of design; the compliant mechanism is based on replacing mechanical joints with living hinges that should endure

93

material deformation and fatigue during actuation. Therefore, Polypropylene Copolymer was chosen due to its high flexural modulus of 145,000 psi and that is can withstand up to 10% of elongation before break; the full data sheet and physical properties from the manufacturer can be found in Appendix F. The unit-cells are modeled in Solidworks and saved in DXF format then imported to the laser machine for cutting. For illustration purposes, each of the mechanisms forming the planes P_1, P_2 and P_3, as shown in Figure 5.9, are introduced separately with the actual bistable unit-cell.

Figure 5.10 (a) and Figure 5.18 (c), reference the mechanism required to morph the unit cell within P_1 from a rectangular to a trapezoidal cell element; Figure 5.25 shows the actual prototype in its two states. There are two additional links added to the actual prototype to provide the bistability feature; the placement of those two links will be discussed in the next chapter.

Figure 5.25 P_1 mechanism cut from Polypropylene Copolymer sheet.

For the plane P_2, in reference to Figure 5.10 (b) and Figure 5.24 (c), the analysis of P_{2S1} section is patterned into the other two sections P_{2S2} and P_{2S3} as shown in Figure 5.26. The prototype demonstrates the mechanism's ability to morph the unit-cell from a rectangular to an arched rectangular cell element with a 90-degree angle. The mechanism design and prototype for P_2 is duplicated for the third surface P_3.

94
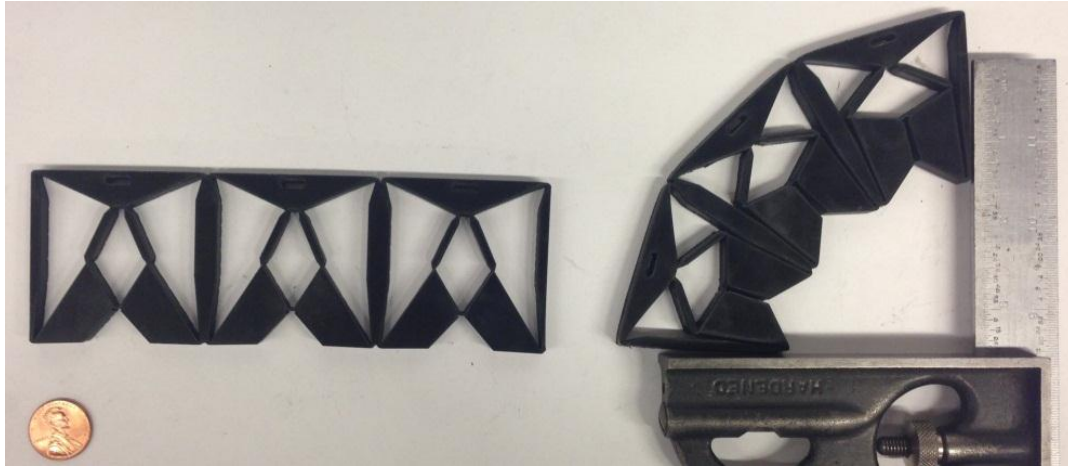
Figure 5.26 P_2 mechanism cut from Polypropylene Copolymer sheet.

The next step is constructing the sector shown in Figure 5.9 and, because the disk tessellation requires ten identical sectors, minimizing the number of connections between sectors is important. For this reason, each sector is flattened where the mechanism of P_1 is in the middle and the other two mechanisms of P_2 and P_3 are in either side as shown in Figure 5.27. Joining the two ends of the final mechanism forms the sector shown from the top view in Figure 5.28.
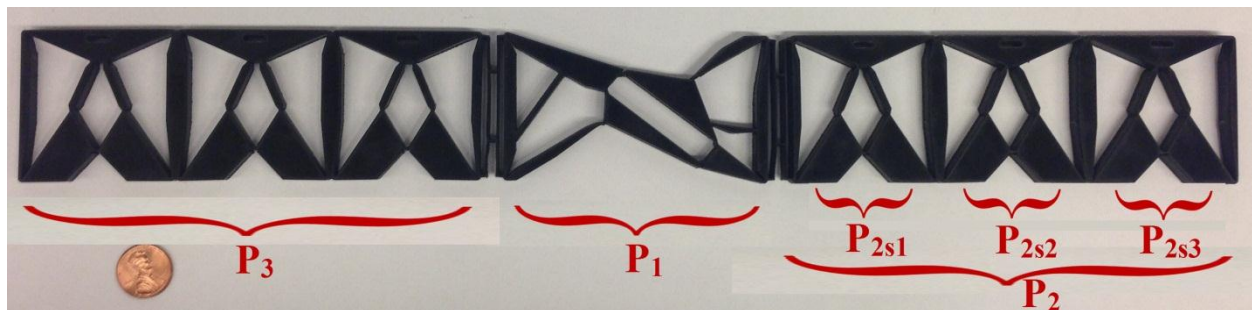
Figure 5.27 The flattened mechanism of the sector.

Figure 5.29 shows the isometric view of the final mechanism in its initial state as a sector to its final morphed state as a wedge with a 90-degree arc. The designs of the bistable elements within the mechanisms are introduced in next chapter.

95
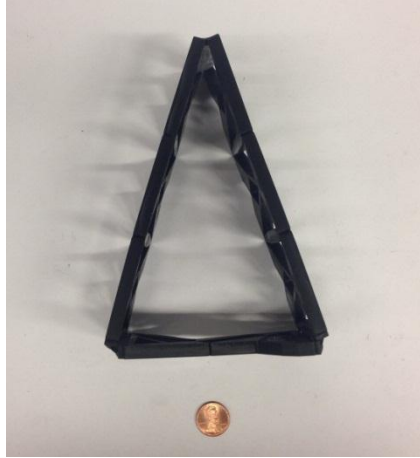
Figure 5.28 The connected mechanism of the sector from top view.
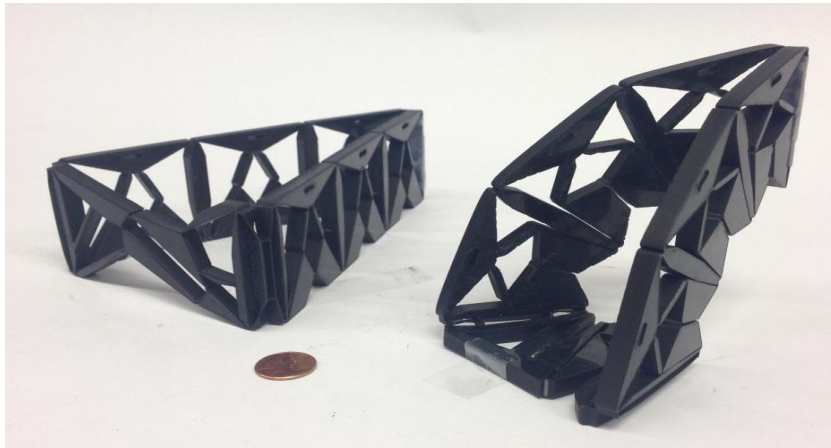
Figure 5.29 The sector's mechanism in initial and final state.
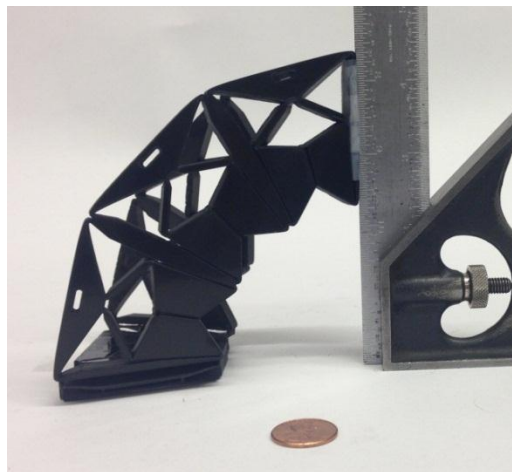
Figure 5.30 The sector's mechanism in the final showing the 90-degree bend.

It becomes clear that if the sectors where to be arranged in a circular pattern, they will form a disk and the wedges will form a spherical shape. Two prototypes were made with two different sectors' arrangement; the following sub-sections will discuss each arrangement individually with figure illustrations. Figure 5.31 shows the process of laser cutting the ten sectors from the Polypropylene Copolymer sheets.

Figure 5.31 Laser cutting the mechanisms from Polypropylene Copolymer sheets.

5.4.1 One Disk to Hemisphere SMSF

The sectors' arrangement in this prototype involves connecting all ten together in a circular pattern as one single layer to form a disk that can morph to a hemisphere. The connections between sectors are done using zip ties through three circular cuts made at the top of each sector. Figure 5.32 shows the assembled prototype in its initial disk state from isometric and top view, while Figure 5.33 shows the prototype in its final hemisphere shape after morph.

The actuation of this prototype is done manually; an inward radial force is applied to the sector from nodes n_1 and n_2, as shown in Figure 5.9, via a connected cable that runs to the center of the mechanism. An animated motion of a simplified sector frame is done using Solidworks, as shown in Figure 5.34, illustrating the directions of force and displacement involved. The

97

horizontal support is the table where the prototype is laying on and the vertical support with groove represents the other nine sectors that are a connected circular pattern. The center point of the disk will translate vertically due to the symmetry in both design and applied forces around the disk's vertical axis. The ten cables connected from the disk's bottom vertices are joined at the center and passed through an opening in the table; applying a tension downward will translate to an inward radial force at the bottom vertices which can slide along the table's surface.
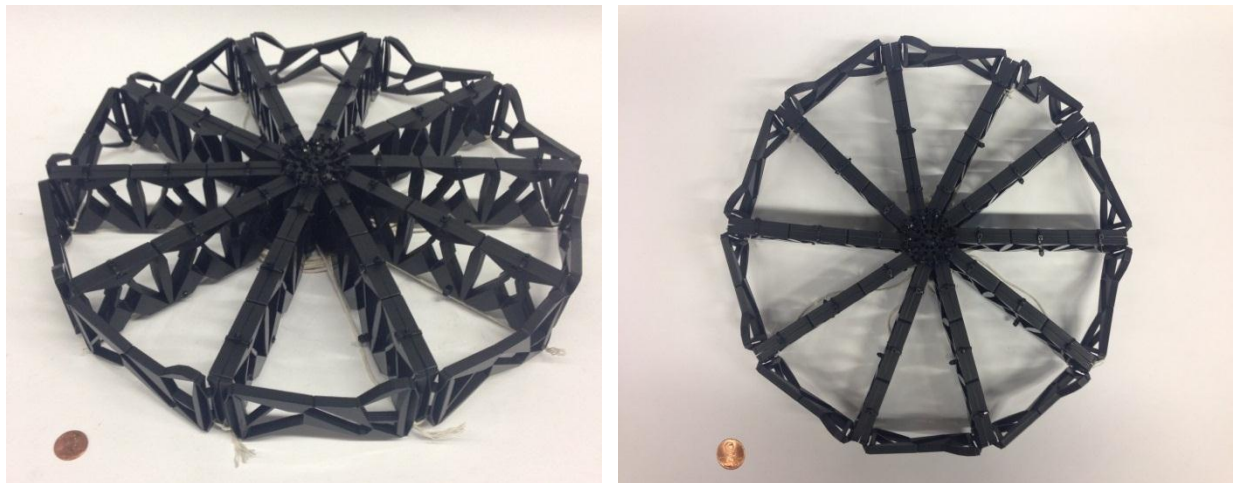
Figure 5.32 One-Disk SMSF initial state (left) isometric view, (right) top view.
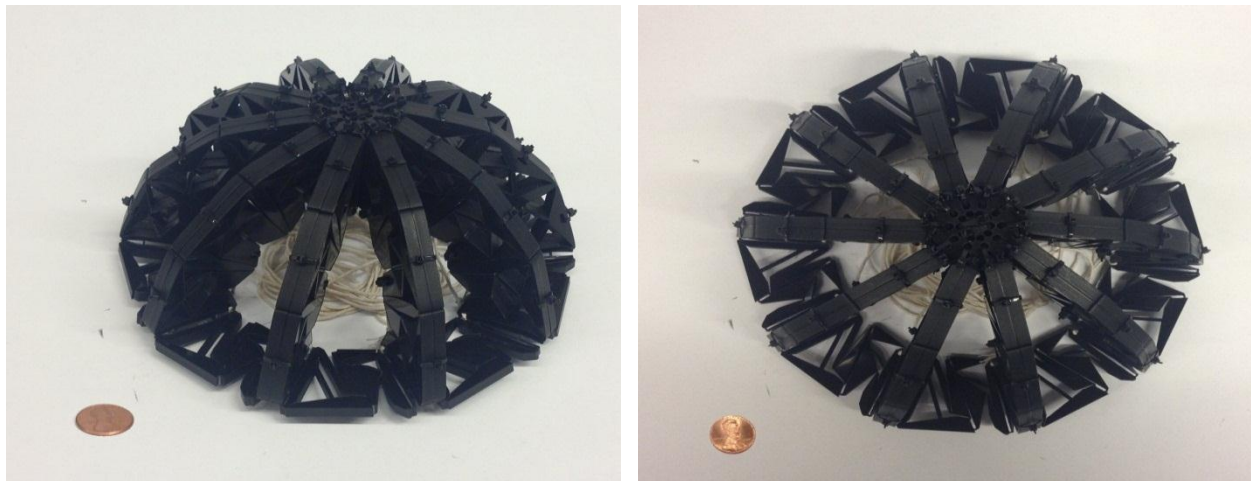
Figure 5.33 One-Disk SMSF final state (left) isometric view, (right) top view.
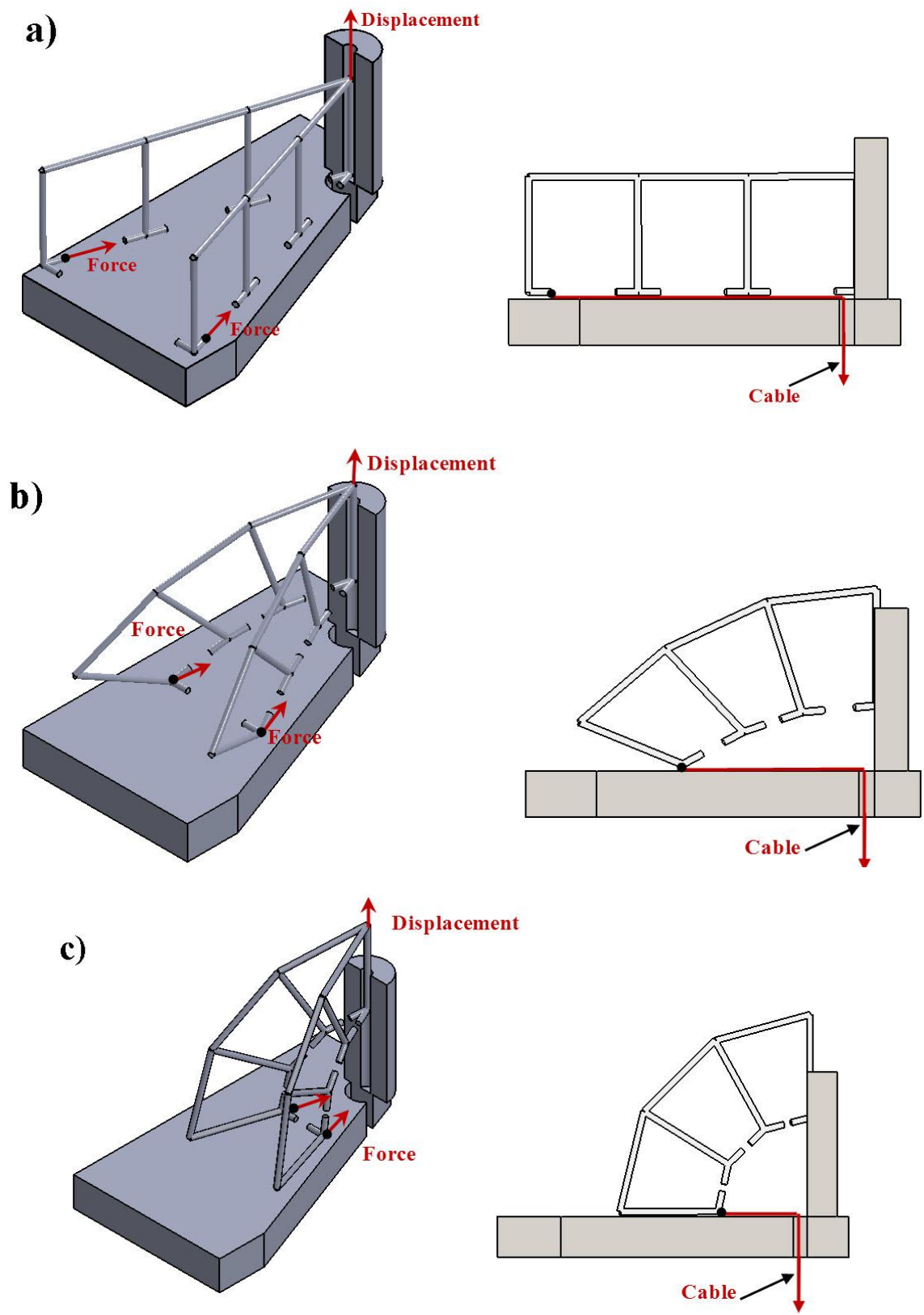
Figure 5.34 Solidworks simulation of the sector's wireframe actuation.

Figure 5.35 is taken from the actual prototype's actuation, at different time frames, showing the disk SMSF morph into a hemisphere. In black is the prototype and the white lines are the actual cables connected at the bottom vertices which runs into the center down through the table with maximum applied tension of 40 lbf, measured via load scale.

Figure 5.35 One-Disk SMSF prototype actuation.

5.4.2 Two Disks to Sphere SMSF

The other possible arrangement involves constructing a set of two disks; where each disk is composed of five sectors arranged in a circular pattern with equal spacing. Both disks are placed on top of each other as two layers with one sector rotational offset. Therefore, for each disk with five sectors equally spaced, a gap will form between every two sectors and by placing

another five sectors disk in such a way that should cover the gaps in the first disk, as shown in Figure 5.36 via isometric and top view. This arrangement gives the prototype the possibility to morph the structure a from two-layer disks to a sphere, as shown in Figure 5.37. The actuation for this prototype will be discussed in the following section in details along with experimental testing.
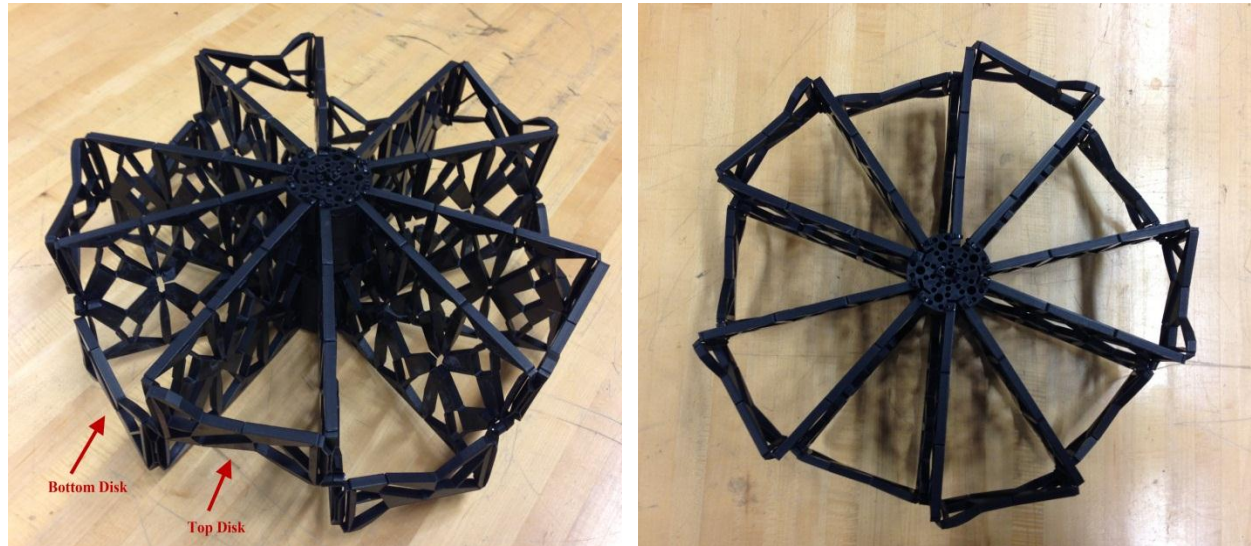
Figure 5.36 Two-Disk SMSF initial state (left) isometric view, (right) top view.
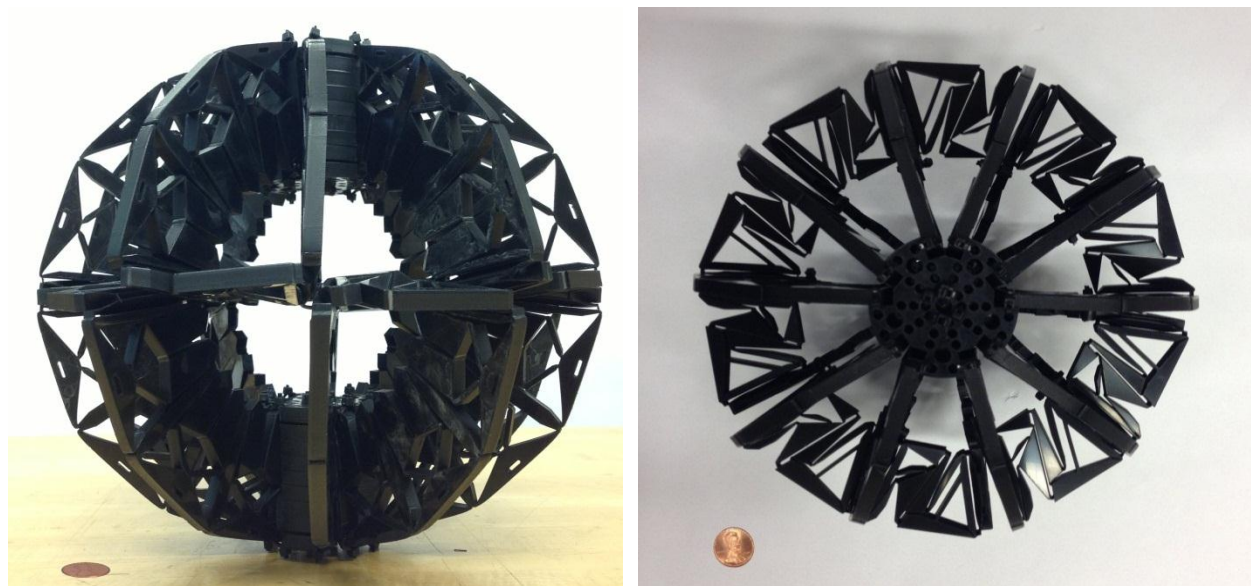
Figure 5.37 Two-Disk SMSF final state (left) isometric view, (right) top view.

101

5.5 Spherical SMSF: Force-Displacement Analysis

Actuating the spherical SMSF is similar to the hemisphere's actuation but in this case, two hemispheres are connected together symmetrically across the plane. The two disks are connected together using the sectors' vertices located mid-plane; to do that, two simple alterations were done on the original sector's mechanism without affecting the mechanisms dynamics. The first alteration, shown in Figure 5.38, is adding small material extension at the vertices with a circular cutout inside it to act as a hinge between the two disks and a connection point for the cables. The second alteration is extending the adjacent mechanisms' bottom section as a support and protection for the hinges.
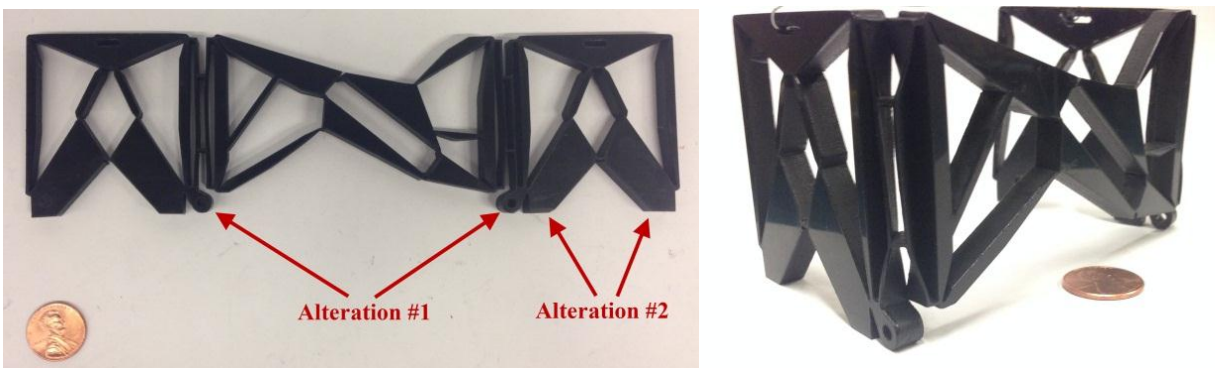
Figure 5.38 Modified sector's mechanism (left) top view, (right) isometric view.

Figure 5.39 shows the connection between both disks utilizing the first alteration as hinges when the cables are secured and passed through the center using an aluminum disk as a ground support. The cables from each vertex are passed in an alternating manner from above and below the support through an opening within it. As a result, five cables will be pulled upward that actuate half of the sectors and the other five cables are pulled downward to actuate the remaining sectors.
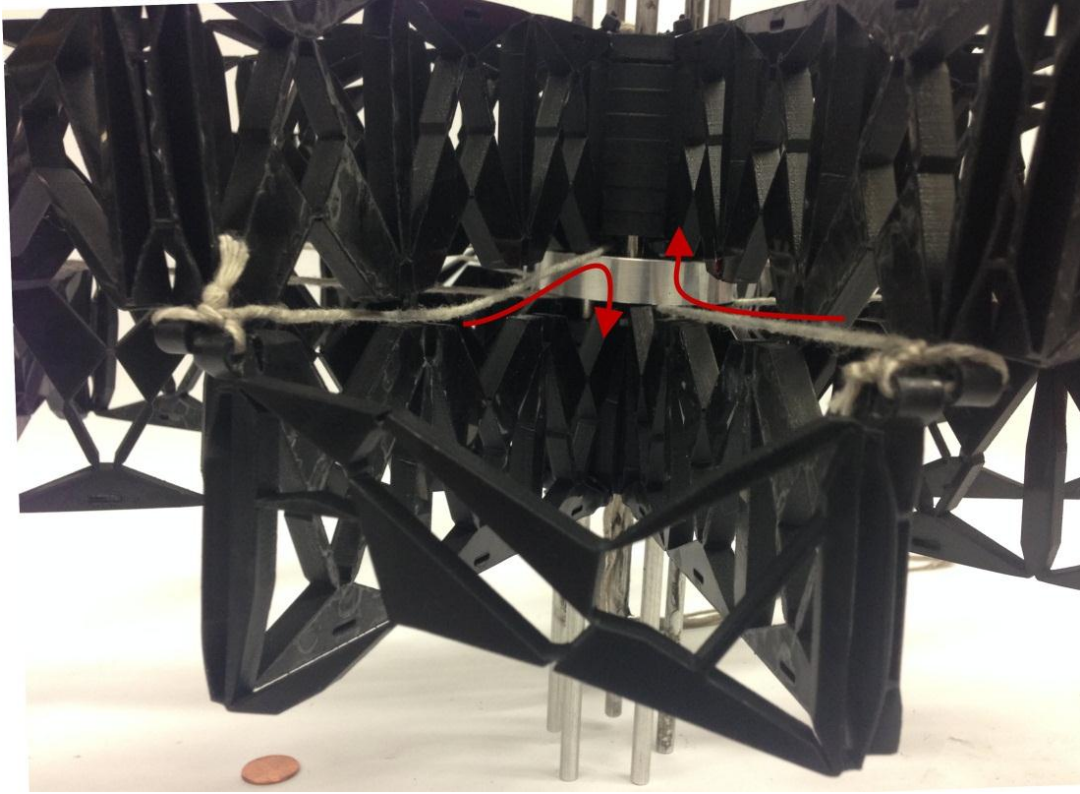
Figure 5.39 The cables' path within the mechanisms.

Assembling the spherical SMSF in this manner allows the use of a tensile machine to provide tension at both ends of the cables for the prototype's actuation. The experimental setups involved securing the SMSF's cables from both ends to the tensile machine and apply the vertical displacement. Figure 5.40 was taken while the test was in progress showing the SMSF when in its initial state as a disk and then in its final state as a sphere.

In the experiment, the actuation was carried out at four different rates of applied displacement to observe the force behavior at each rate. Figure 5.41 shows the force-displacement results at each rate combined into one plot for compression; the actual experimental data is tabulated and can be found in Appendix G.

103
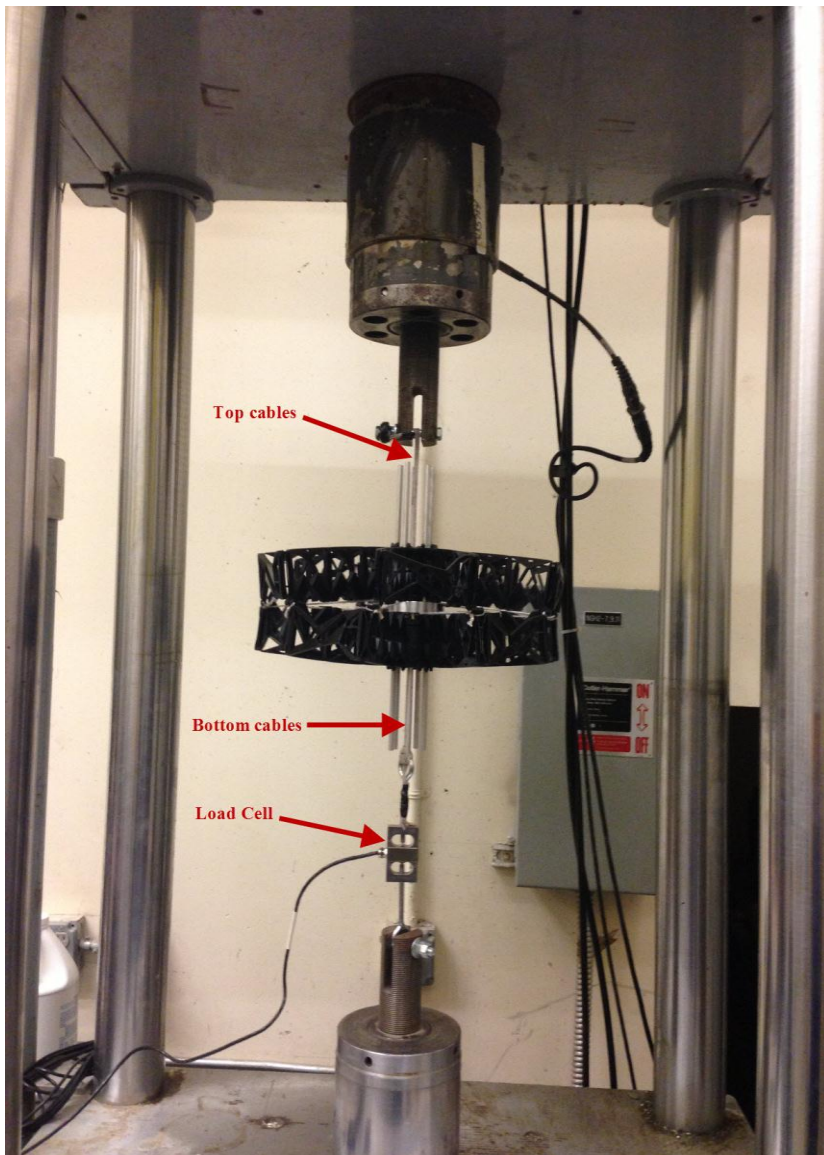
Figure 5.40 Spherical SMSF tensile test at the (left) initial, (right) final states.

The plot can be divided into four main different zones in terms of behavior; those behaviors correspond to the prototype's intermediate actuation. Figure 5.42 illustrates those actuations at different zones, the arrow points to the part of the mechanism that has been actuated to its second stable position where the circled section points to the ones in the first stable position and yet to be actuated. The followings are the description of each zone in reference to the Figure 5.42 and Figure 5.27:

Zone 1: As the experiment begins, the tension applied is translated into radial forces that increase gradually storing strain energy within the compliant mechanism. Due to the mechanism's bistability feature and after it reaches the unstable equilibrium position, the energy stored will be released in the form of negative force applied within the mechanism causing the sudden drop. This corresponds to P_{2S3} mechanism being actuated to its second stable position in all sectors.

Zone 2: Corresponds to P_{2S2} mechanisms being actuated to their second stable. The force required for those mechanisms is less due to some energy stored within them during the loading accorded in zone 1.

Zone 3: Corresponds to P_{2S1} mechanisms being actuated to their second stable.

Zone 4: Corresponds to P_1 mechanisms being actuated to their second stable.

After morphing the SMSF prototype to its second stable position as a sphere, the increasing load beyond zone 4 is converted to strain energy stored within the compliant mechanisms in which the tests were stopped at that point not to damage the SMSF prototype. Because the tests were done using displacement loading, it can be observed that the reaction forces throughout the curves are inversely proportional to the displacement rate. At low displacement rate, the potential energy gradually builds up within the compliant links showing more identifying features on its the curve than that of higher displacement rate result curve.

105
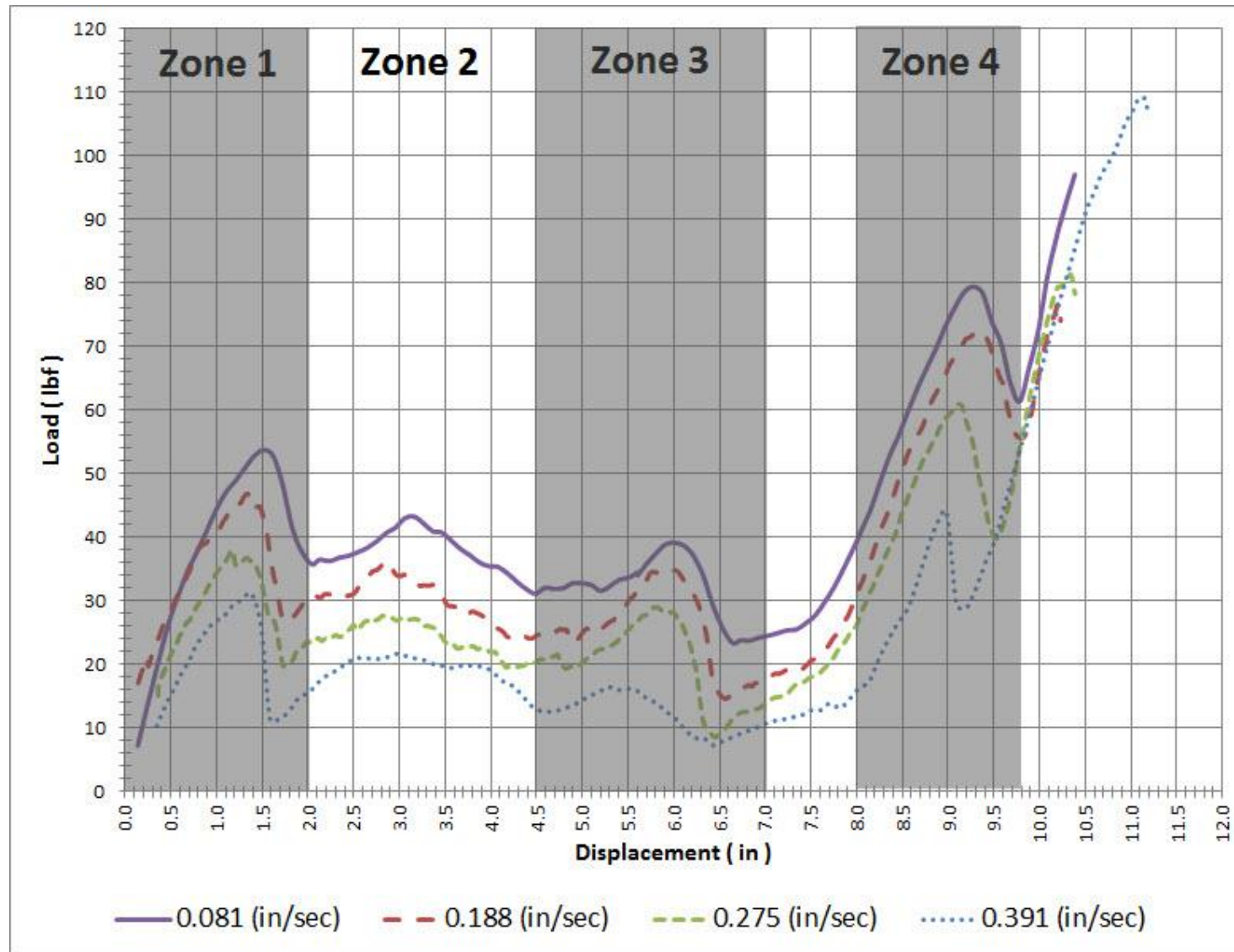
Figure 5.41 Force-displacement curves and zones identification.

106
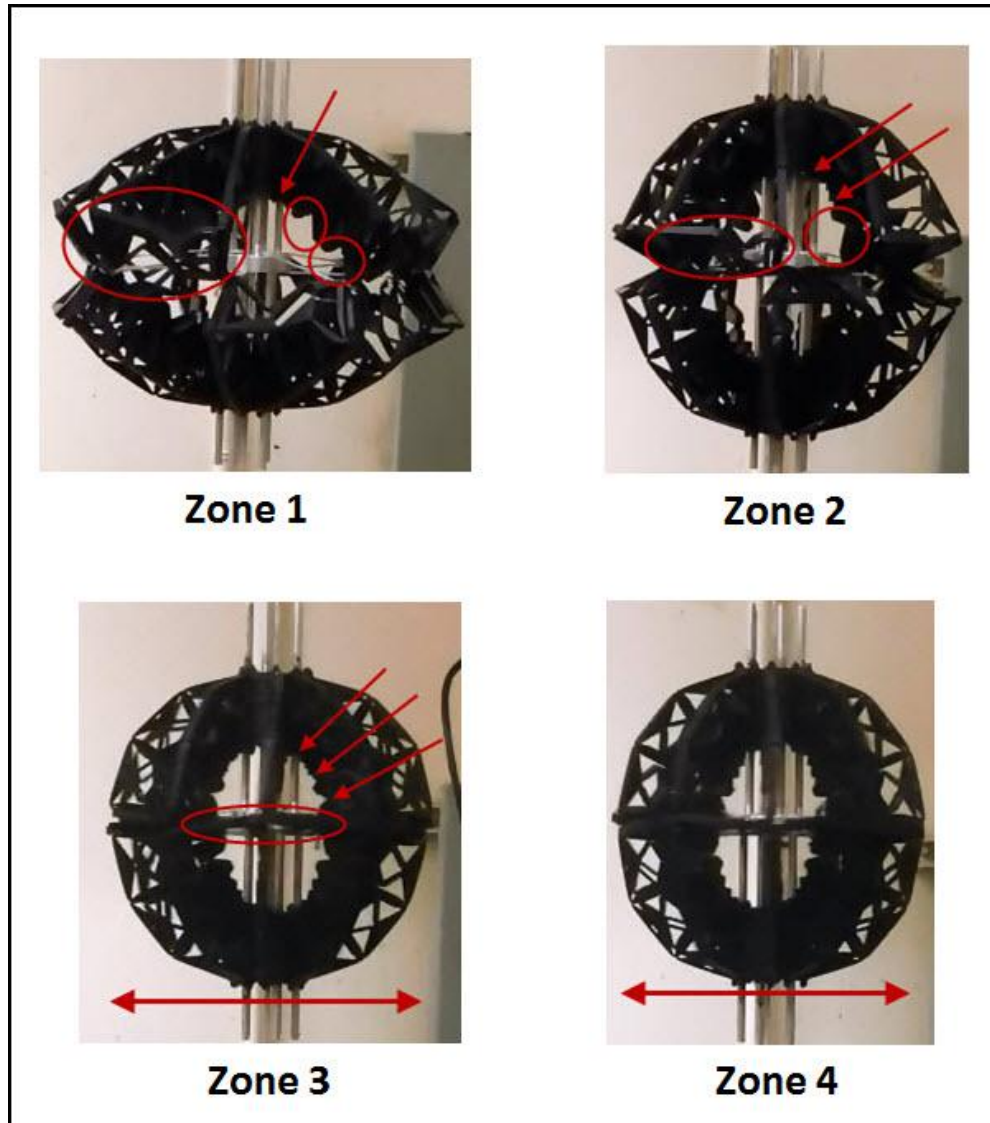
Figure 5.42 Spherical SMSF actuations at different zones.

The following chapter will describe the kinematic analysis involved in transforming regular mechanisms into bistable mechanisms using compliant segments. To aid this transformation, Solidworks will be used to graphically represent the relation between links' rotation and coupler curves at a point on the m mechanism. The methods followed are effective only if the initial and final states of the mechanism are given.

107

CHAPTER 6: DESIGN OF MECHANISM STABILITY USING OVER-CONSTRAINT

An extensive analysis, identifying bistability behavior in four-bar compliant mechanisms, was done by Howell [28]. His studies resulted in calculating the required torsional stiffness in each joint and the modification of the links' geometry to achieve the bistability behavior. The toggle positions are also set by the configuration of the mechanism links i.e. elbow up or down; the only way to have a specific intermediate stable position along the movement of the linkages is by designing a hard-stop. Another different approach to achieve this behavior was done in [30] by utilizing translational joints and springs in the studied models. All those approaches require extensive formulation by solving the kinematic and energy equations for each specific design. With advanced software solutions like Solidworks, simulating the kinematics can be used to design bistable behavior in a compliant mechanism with four-bar PRBM.

The following section presents the steps involved using Solidworks to synthesize a mechanism's geometry in order to achieve a design's specific bistability requirement. This method will ensure a stable position without the need of a hard-stop as in [28]. There are two main initial design considerations that need to be met before considering this analysis. First, both (first and second) state of the mechanism should be chosen and should represent the mechanism's desired stable positions. The first state is the position that the mechanism was manufactured or assembled at, whereas the second state is the position at which the mechanism is toggled to. The second consideration is the assumption that the magnitude of the joints' torsional spring stiffness is small i.e. living hinges [1].

6.1 Bistability In a Four-bar Compliant Mechanism Using Solidworks

This section introduces a novel use of the Solidworks software following a step-by-step procedure to construct a four-bar compliant mechanism with any two desired stable positions. The bistability is found by utilizing the perpendicular bisector from Burmester's theory [31, 32] along with the coupler curve concept in a graphical representation. Those steps can be applied to any two positions of four-bar mechanism to find a solution to its bistability; further design constraints might be implemented to ensure the ability to fabricate the mechanism. The extra possible design constraints are discussed at the end of the procedure to fine-tune the final mechanism's solution.

The main idea is to be able to attach a Potential Energy Element (PEE), such as a spring or a compliant link to the mechanism, thus generating the energy curve shown in Figure 2.3upon actuation. This new element has two points of attachment; one of those points needs to be attached on the mechanism itself whereas the other point could be attached to the ground link or, in special cases, to the mechanism itself. The design steps are shown with an illustrative example, which was chosen arbitrarily, to support the generality of this method. The design produced is split into two stages; the first stage describes the construction of the kinematic layout of the bistable mechanism, whereas the second stage examines the change in potential energy between the two equilibrium positions.

6.1.1 Design Stage One: Kinematic Analysis Using Solidworks

At this stage of the design, the kinematic requirements to achieve the bistability behavior in the mechanism are established using Solidworks rather than the traditional methods by solving for the kinematic coefficient through a system of equations analysis. This use of Solidworks reduces the computational time needed and gives the designer more visual understanding of the

problem as well as the ability to verify the mechanism's behavior real time. For comparison, if the four-bar linkages shown in Figure 6.1 were to be analyzed for bistability using the method in [28], the second stable position will be predefined by the mechanism itself, as shown depending on the location of the torsional spring (K).
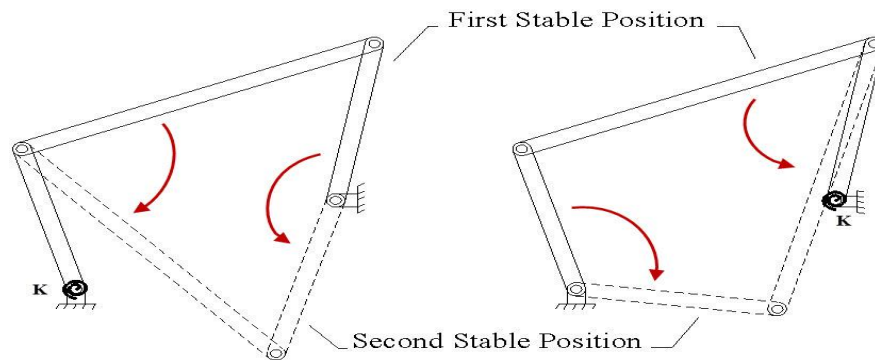
Figure 6.1 The second stable position depends on spring location and first position.

The previous figure is an example where the unique second stable position for the given four-bar depends on the mechanism's first position and the spring location. Below are the steps to follow to specify an intermediate stable position without the use of hard-stop:

Step 1: Identify the two desired stable states of the mechanism and sketch the links as lines connecting pin joints in both states, as shown in Figure 6.2 (b). The lengths of the links do not change between its initial and final position, in Solidworks this is implemented with equality constraints. The links are numbered clockwise with the ground being link (l_4).
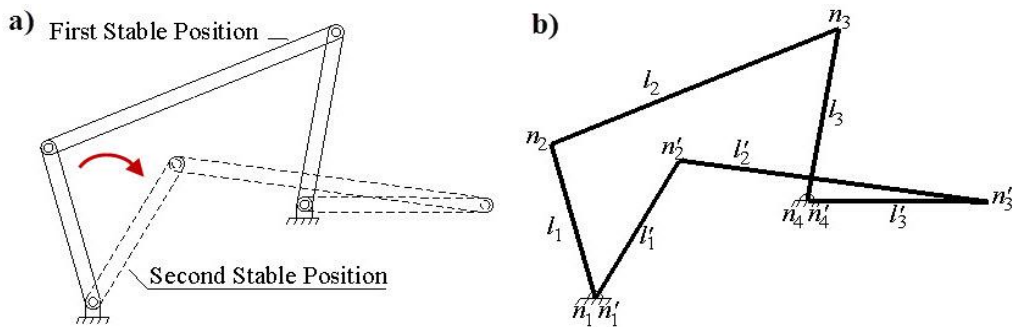
Figure 6.2 The mechanism's two stable position as design input.

The center points (fixed ground pivots) of the mechanism are identified as (n_1) and (n_4) where the circle points (moving pivots) are (n_2) and (n_3); this leads to (l_2) being the targeted link for the analysis.

Step 2: Construct the perpendicular bisectors of lines (n_2 and n'_2) and (n_3 and n'_3) segments. The intersection of these perpendicular bisectors is pole point (P), as shown in Figure 6.3.
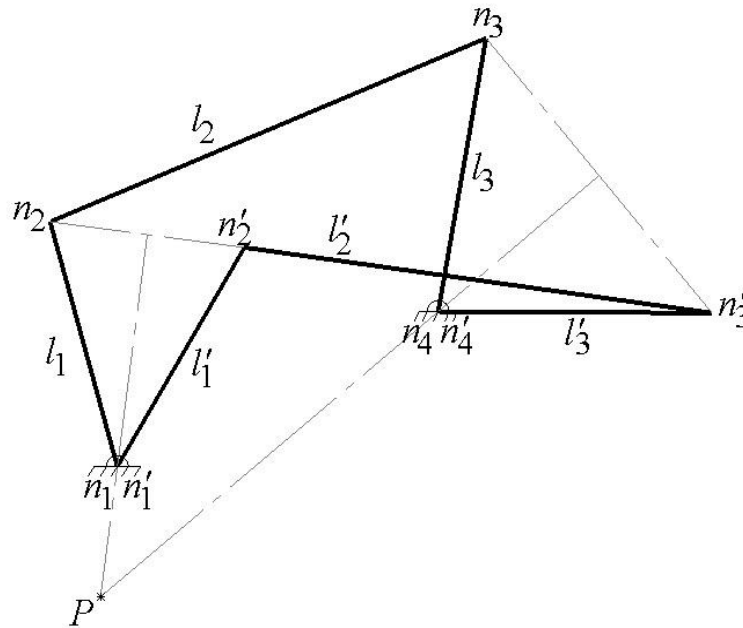
Figure 6.3 The mechanism's pole point for (l_2).

The second link need not necessarily be a straight link connecting between joints (n_2) and (n_3); it could be in any geometrical shape as long as it is rigid and it contains points (n_2 and n_3). Therefore, a point on the second link, which connects to one end of the potential energy element, needs to be selected.

Step 3: To give an extra degree-of-freedom for the potential energy element (PEE) placement point, a ternary link representation of (l_2) is sketched out, as shown in Figure 6.4. The lines (l_{21}) and (l_{22}) do not change length and so $|l_{21}| = |l'_{21}|$ and $|l_{22}| = |l'_{22}|$. The points (m_Q) and

111

(m'_Q) are on the mechanism itself and represent the one attachment point of the PEE at its initial and final state, respectively.
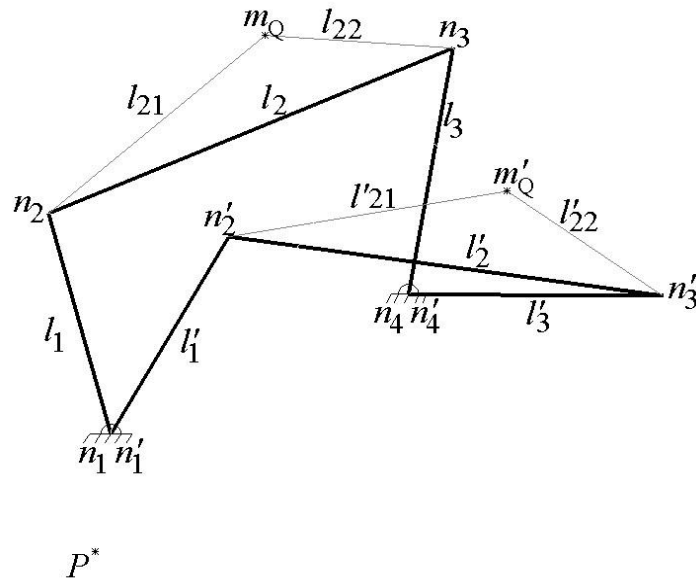
Figure 6.4 Ternary link representation of the coupler link to place the point (m_Q).

Step 4: As shown in Figure 6.5, two individual lines (l_Q) and (l'_Q) from the points (m_Q) and (m'_Q) are drawn to a point (Q); those lines represent the PEE at its initial and final state, respectively. Considering those two lines as a source for potential energy requires them to be un-deformed at both states (initial and final), thus an equality constraint is added to them. Both lines are attached to a single point (Q) that represents the second attachment point for the PEE. Additional constraints on the location of this point are described at later design stage.

Knowing that the point (P) represents the finite rotation pole of the second link between initial and final states, every point on that link would have the same pole while the mechanism moves between the predefined initial and final position. Thus;

Step 5: Construct the perpendicular bisector line between the points (m_Q) and (m'_Q) where it must pass through point (P), and every point on that line is a possible location for point (Q) generated in step 2, as shown in Figure 6.6.

112
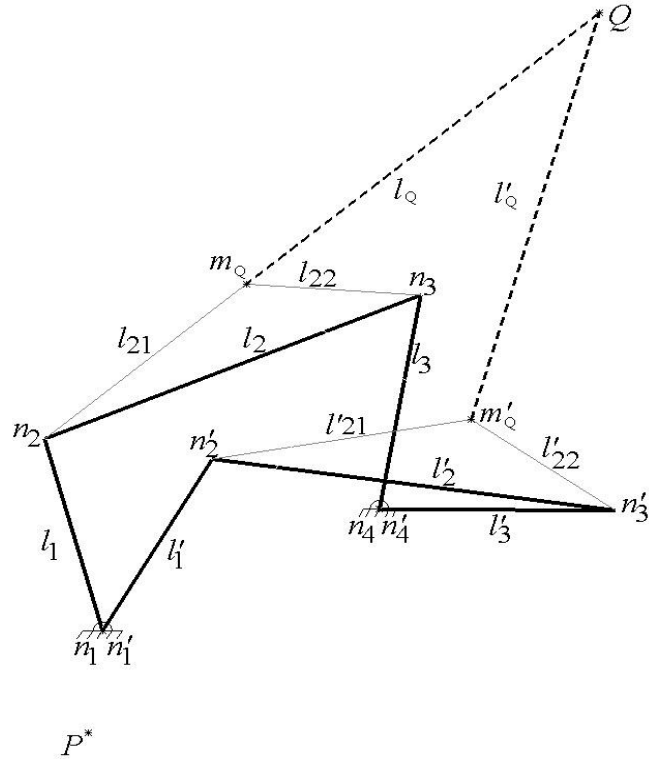
Figure 6.5 Shows the PEE representation as (l_Q) with the point (Q).
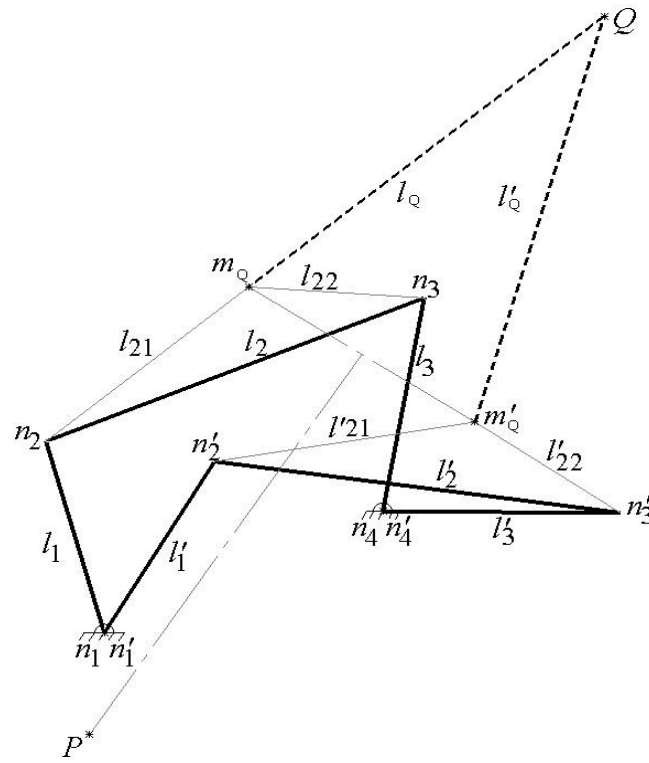
Figure 6.6 The perpendicular bisector of point (m_Q) connected to the pole point (P).

6.1.2 Design Stage Two: Potential Energy Analysis Using Solidworks

After establishing the mechanism's kinematics, this stage will analyze potential energy aspect to the design in order to achieve bistability through the PEE. Referencing Figure 6.6, the extra constraint imposed on the mechanism is adding the PEE, with points (Q) and (m_Q) being its center point and circle point respectively. The effect of that is the point (m_Q) has two incompatible zero-stress paths while the mechanism is in motion. The first path is defined by the coupler curve generated from the mechanism's original center points (n_1) and (n_2), while the second path is a circular arc centered at (Q). The actual path the point (m_Q) follows is a stressed path which depends on the relative flexibility (or stiffness) of the four-bar versus the PEE.

Using Solidworks, the following sequence of steps identify the two paths, providing an in-depth analysis of the PEE. For steps 6 and 7, either step can be followed first before the other, those two steps are about defining the location of the two points (Q) and (m_Q). This is an under-specify problem and leaves room to add constraints specific to the mechanism's application such as the force required to toggle the mechanism and the stiffness of the links required by design.

Step 6: The placement of the attachment point (Q) should be decided; different designs require different locations depending on the space limitation of the mechanism. The only condition is that point (Q) cannot be placed on a moving link; consequently, it can be only placed on the ground link. Moreover, fixing the point (Q) first partially restrict the location of the point (m_Q) by only allowing it to move at an equal distance apart; meaning only the angle between the lines (l_Q) and (l'_Q) will vary but the lines have to remains equal in length. For the purpose of illustration, the center point (Q) is placed above the mechanism, as shown in Figure 6.6. Its position can be fine-tuned in a later stage of the design to satisfy the stress limits of the PEE.

Step 7: Next, the location of the point (m_Q) is selected by the second link's geometrical design and limitation. In the case of this step precedes step 6, the fixing of point (m_Q) defines the pole line between points (P) and (Q) which consequently makes point (Q) only valid across that line. Because this section presents a general step-by-step design procedure, let the location of this point be selected as shown in Figure 6.6; the exact location can be considered as design input for a specific application. The proceeding steps remain the same regardless of the position chosen.

Step 8: The first zero-stress path for point (m_Q) is found using the coupler curve generated from the mechanism's original center points. Using the motion analysis within Solidworks, the path of point (m_Q) is traced throughout the rotational cycle of the mechanism. Figure 6.7 (a) and (b) shows the traced path in links display as well as in line representation, respectively.
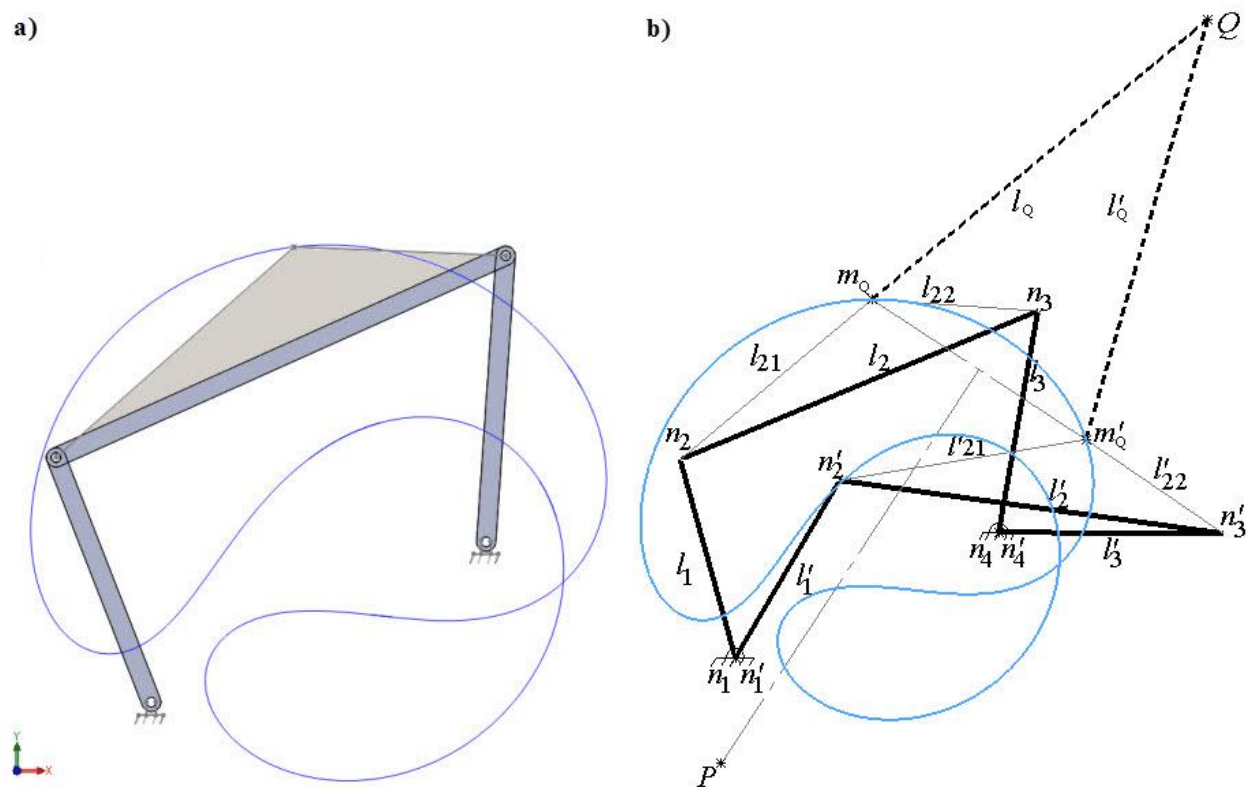
Figure 6.7 The first zero-stress path of the point (m_Q) following the coupler curve.

Step 9: Finding the second path that point (m_Q) follows by being a circle point for the center point (Q). This path is a circular arc connecting both the points' two stable positions with a radius of (l_Q) and its center being point (Q), as shown in Figure 6.8.

Step 10: Super imposing both paths of the point (m_Q) reveals the type of deformation that the PEE experiences. In this example, and assuming the four-bar mechanism's links ($l_1 - l_4$) are rigid, the link (l_Q) should be compressed to be able to toggle between both stable positions, as shown in Figure 6.9.
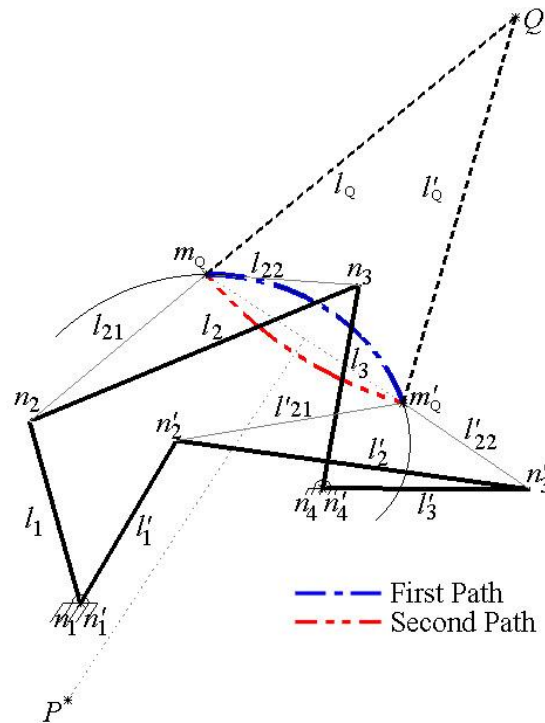
Figure 6.8 The second path of the point (m_Q) as an arc.

Knowing that a stable equilibrium point is a minimum potential energy and an unstable equilibrium point is a maximum potential energy is the key idea behind that bistability of such mechanism. The points of intersection between the two curves (first and second) are going to be a minimum potential energy, the link (l_Q) is not being compressed or stretched when the two curves intersects. Everywhere else, the difference between these two curves results in tension or

116

compression and the unstable equilibrium point occurs when the difference between the two curves become the maximum. The whole reason this idea works is because the path generated by the point (Q) and the path generated by the coupler curves are different.
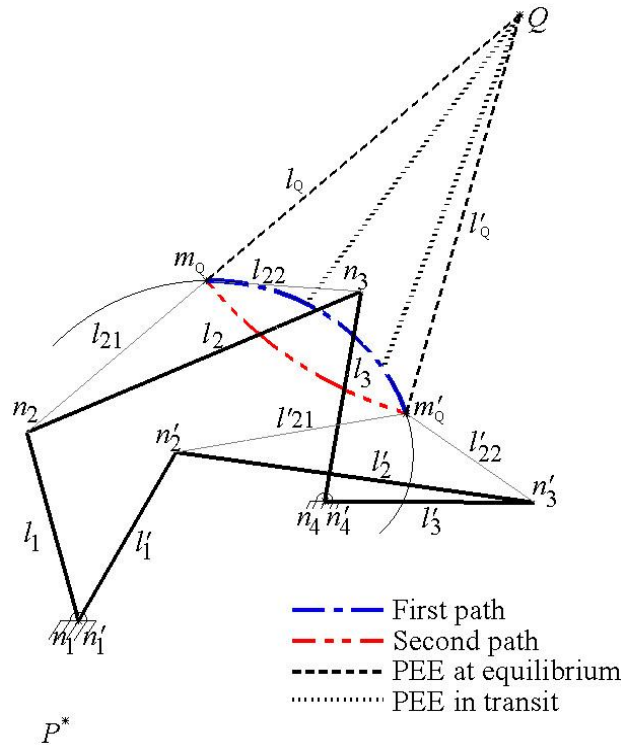
Figure 6.9 The PEE in a compressed deformation.

This concludes the general step-by-step design procedures to establish a bistability behavior in a four-bar mechanism with any two desired positions. The analysis of the two paths is specific to each design; from the example used, the PEE will experience a compressive load to follow the coupler curve path. The same example can be re-designed if a tensional load on the PEE is required; the position of the point (Q) can act as a knob to control the magnitude and direction of deflection on the element. Figure 6.10 shows if the center point (Q) was placed at the opposite side from what is in Figure 6.6; the coupler curve remains the same because the mechanism did not change but the path of the circle point (m_Q) changes. The result is that the PEE experiences elongation along the path between the two stable positions.
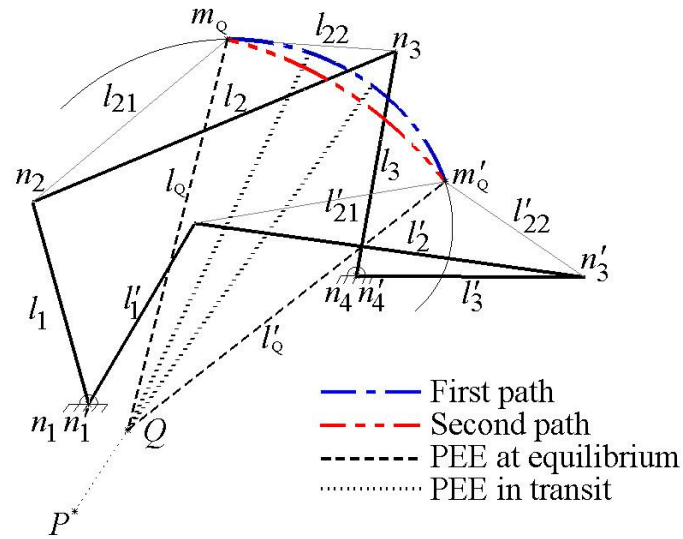
Figure 6.10 The PEE in an elongated deformation.

The specific analysis of the PEE and the two paths will be discussed further for a specific problem in this research. The general approach to the problem will be the same for any mechanism but differ in the actual data.

6.2 Bistability by Over-Constraint

The idea behind bistability by over-constraining the mechanism is introducing a compliant link that represents the PEE in the previous section. Because this research is targeting one degree-of-freedom mechanisms, adding an extra link with two joints would result in zero degree-of-freedom transforming the mechanism into a structure. At each stable position the mechanism will remain a structure; however, while it is in actuation, the flexibility of the compliant link permits the mechanism to toggle between its stable positions.

In this section, a detailed analysis is presented in converting the unit-cell element in P_1 SMSF, from Chapter 5, into bistable element using the step-by-step design procedure. Followed by a demonstration in how to transform parallel four-bar linkages, which a special case of linkages, into a mechanism with two stable positions using the over-constraint by compliant link.

118

6.2.1 SMSF: Unit-Cell Bistability Synthesis

The unit-cell element used in Chapter 5 for P_1 design was based on an eight bar mechanism with one degree-of-freedom; because one of the design's requirements is bistability, the unit-cell should behave like a structure at each stable position. Further observation on that selected design, shown in Figure 5.15, reveals that the mechanism can be split into two four-bar mechanisms attached at the center, as shown in Figure 6.11.
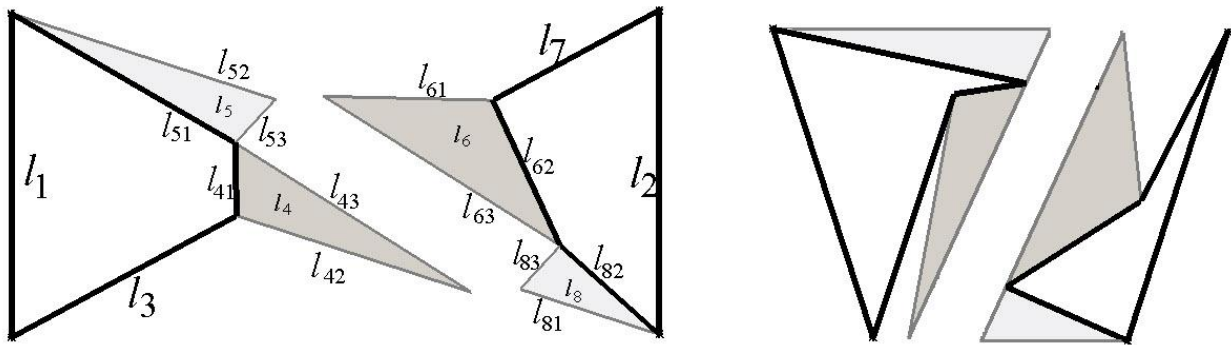
Figure 6.11 P_1's mechanism splits into two four-bar mechanism.

For the left half of the mechanism, the angle between links (l_1) and (l_{52}) remains constant at 60 degrees from the design constraints in Table 5.3. Thus, the bistability of the left part can be achieved by following the methods proposed by Howell in [28], by increasing the magnitude of the torsional spring constant at the joint between the two links. This was done be connecting a rigid link between links (l_1) and (l_5); essentially eliminating the joint between them. This reduces the mechanism into three links and three joints, converting to a structure with zero degree-of-freedom. As a result, the mechanism, shown in Figure 6.12, will toggle between the two stable positions by bucking link (l_3) due to being thinner than (l_4); making it sufficiently flexible to toggle.

119
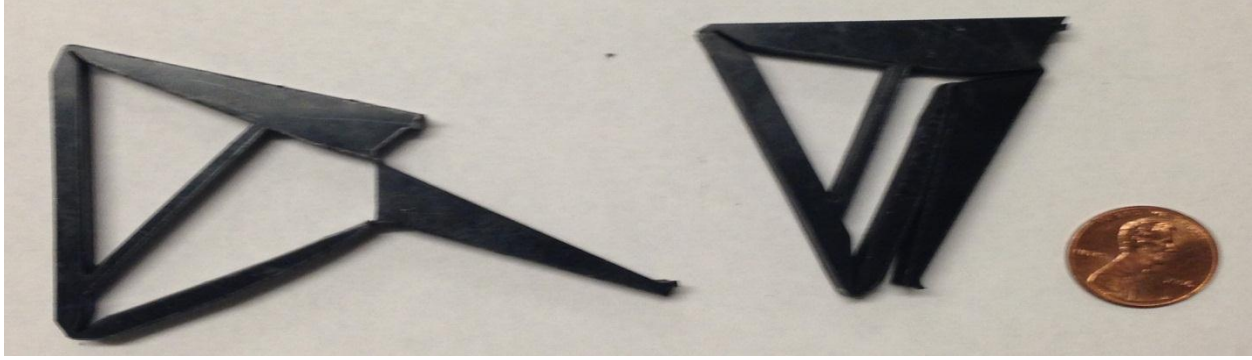
Figure 6.12 The prototype of P_1's left half at both stable positions.

In the right half of the mechanism, the angle between links (l_8) and (l_2) increases when the mechanism is in actuation to produce the final trapezoidal shape. Consequently, the joint between both links needs to be small and act as a living hinge with very low stiffness, eliminating the possibility to use the method utilized in the left half. The alternative solution is introducing a compliant link (PEE) following the method proposed in section 6.1; adding a link and two joints normally turns the mechanism into a structure with zero degrees-of-freedom. Specifically, the compliance of the PEE permits the toggling of the mechanism, thus the placement of the compliant link is important.

The steps in Section 6.1 were used to design a solution that satisfies the following specific design constraints:

1- The mechanism should be contained within a specified area without interference;

2- The ability to laser cut the design from a thin sheet of polymer;

3- The stresses on the compliant link or PEE should be within the material's limits; and

4- The PEE's ability to generate enough potential energy to overcome the (small but non-zero) restoring torques within the mechanism's living hinge joints while moving from first to second position and back.

120

For steps 1 and 2: From the analysis of P_1 in Section 5.3.1, the initial and final state of the mechanism is known with its dimensions. Figure 6.13 shows both states with the perpendicular bisectors drawn for the end points of (l_{62}) to identify its pole point (P).

For steps 3 to 7: Given the geometrical constraint of the mechanism, the attachment point (m_Q) of the compliant link (PEE) has to be on link (l_{62}). The lines (l_Q) and (l'_Q) are sketched out representing the PEE at its initial and final state respectively, along with its perpendicular bisector connecting its point (Q) to the pole point (P). Point (Q) is attached to link (l_2) to satisfy the constraint of the mechanism being contained within the specified area, as shown in Figure 6.14.

Given the fact that both attachment points (m_Q) and (Q) are on the mechanism's link (l_{62}) and (l_2) respectively limits their position in order to satisfy the non-interference within the mechanism. The restriction is caused by the PEE at its second stable position represented in link (l'_Q); both of its end points (m'_Q) and (Q) can only slide over the links (l'_{62}) and (l_2), respectively. Assuming point (Q) is the control, its position is limited to the distance between the joint (n_1) up to where the links (l'_2) and (l'_{62}) are parallel and collinear, as shown in Figure 6.15.
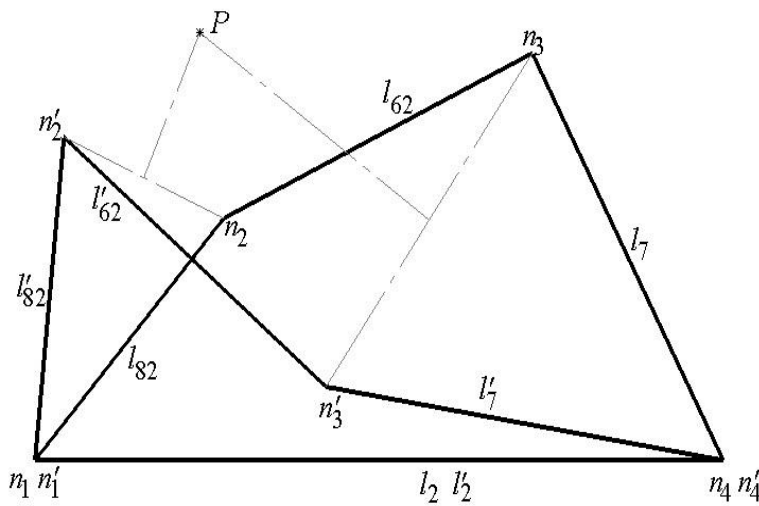
Figure 6.13 P_1's right half at both state with the pole point (P) identified.
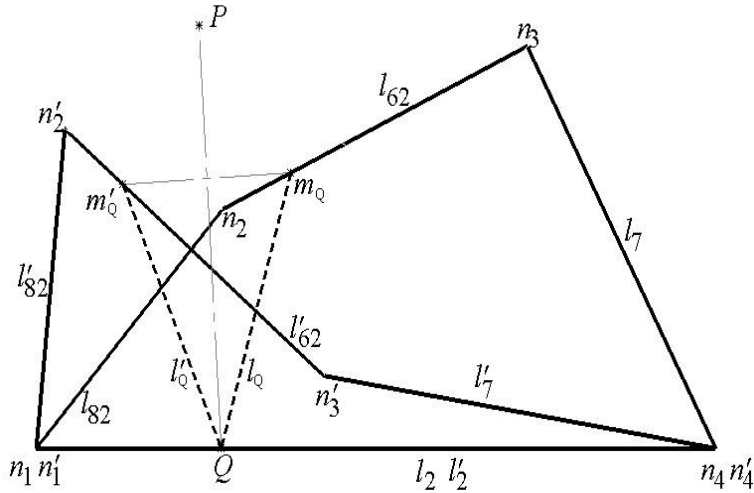
Figure 6.14 The PEE placement with its point (Q) placed on the ground link (l_2).
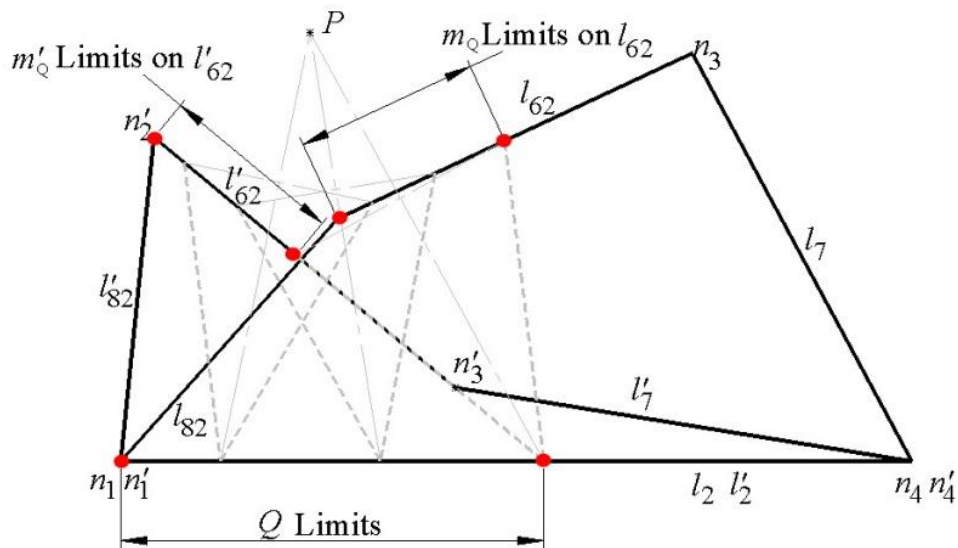
Figure 6.15 The limits of points (m_Q), (m'_Q) and (Q) on the mechanism.

For step 8: Knowing that the positions of the point (m_Q) along the limits within (l_{62}), shown in Figure 6.15 are infinite in theory, eight different coupler curves generated using Solidworks at different intervals across the link (l_{62}) to visualize the change in the curves' behavior, as shown in Figure 6.16. All of those curves and any intermediate ones represent different solutions to the bistability behavior and are considered to be the first path that point (m_Q) traces.
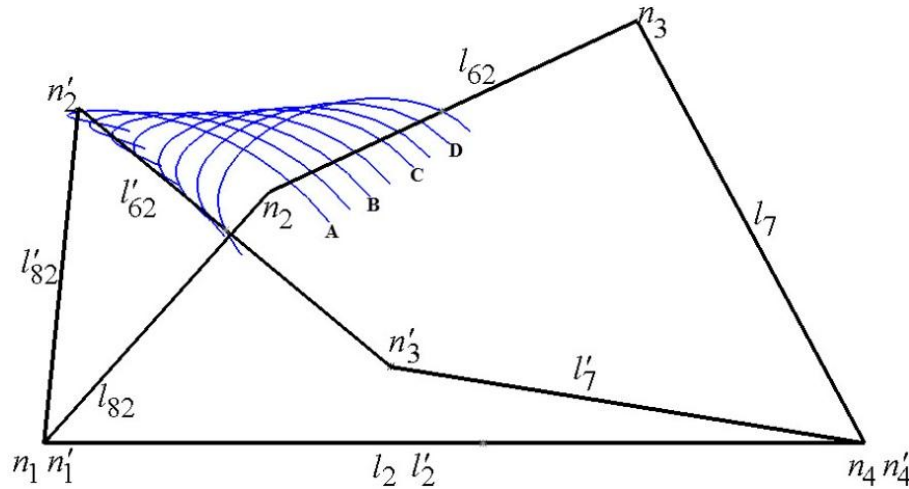
Figure 6.16 Eight different coupler curves generated for (m_Q) within its limits.

For steps 9 and 10: Four coupler curves of point (m_Q) are selected and superimposed on the second arc path associated with the position of the (m_Q) being the circle point to the center point (Q). Each coupler curve is considered a configuration and named (A, B, C and D) for later reference, as shown in Figure 6.16.

The selection process for the solution was done upon visual observation of each configuration, the satisfaction of the design constraints and the ability to produce the prototype as follows:

- Configuration A: It was disqualified due to the maximum distance between the two paths measured to be 0.8 mm compared to the PEE's length of 19.5 mm, which may not provide enough potential energy to overcome the shiftiness within the mechanism. Furthermore, the trace of point (m_Q) has to pass the second stable position to follow the coupler curve which might introduce unwanted intermediate position, as shown in Figure 6.17 (a);

- Configuration B: It was also disqualified due to the same reason as configuration A from the trace point of view, as shown in Figure 6.17 (b);

- Configuration C: It qualifies to be a solution due to there being enough paths suppuration and the absence of intermediate position caused by the associated coupler curve; the PEE would experience elongation to follow the coupler curve as shown in Figure 6.17 (c); and

- Configuration D: It was disqualified due to the large angle difference that the PEE undergoes between the initial and final state (about 107 degrees), which might cause high stress at the joints. Furthermore, the close proximity between the PEE and link (l_{62}) as the final state might cause issues in designing the PEE when thickness is added, as shown in Figure 6.17 (d).
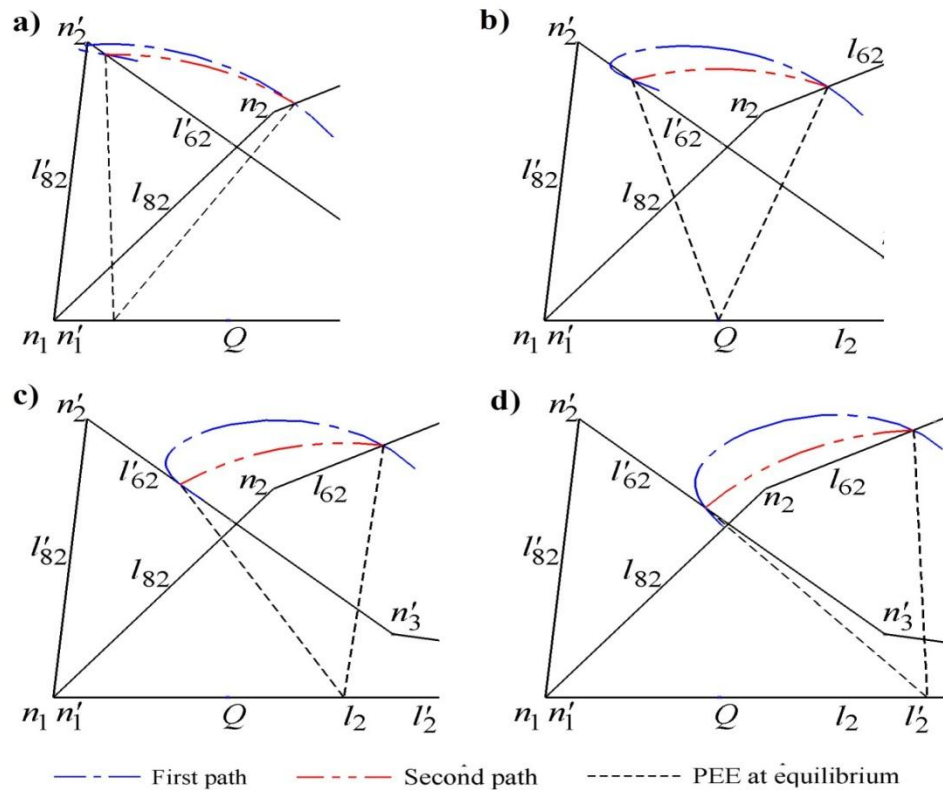
Figure 6.17 The superimposed two paths of (m_Q) for the selected coupler curves.

For a proof of concept in the SMSF design, the configuration C was selected to be the design choice without claiming it is the only solution to the mechanism's bistability. Locating the optimum position of the point (m_Q) may require optimization analysis of the mechanism,

which may be considered in future work. Figure 6.18 shows the right half of the mechanism's prototype, from section 5.3.1, with the compliant link added for bistability; the detailed dimensions of the PEE can be found in Appendix E.3. Adding the PEE elements equals to adding a link and two joints to the four-bar mechanism for a total of five links and six joints converting it to a structure with zero degree-of-freedom. As a result, the mechanism will toggle between two stable positions by elongating the PEE, allowing for one degree-of-freedom while actuation.
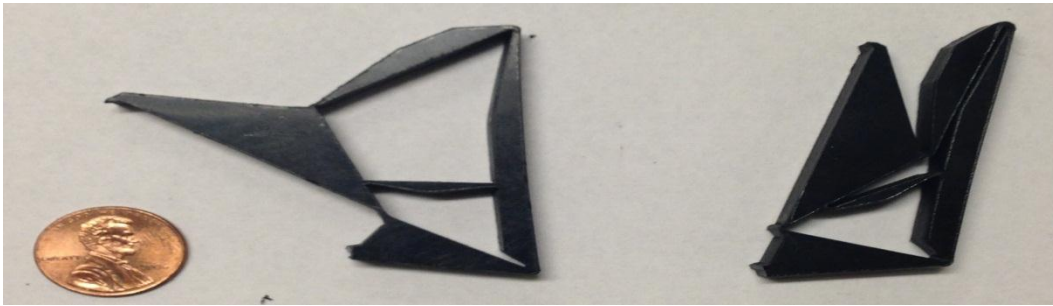
Figure 6.18 The prototype of P_1 right half at both stable positions.

Looking at the final P_1 mechanism, the left half combined two links as one eliminating one link and one joint where the right half added one link and two joints as shown in Figure 6.19 (b). The total mobility is (-1) using eight links and eleven joint; this over-constrained mechanism behaves as a structure in both stable positions with enough flexibility within its compliant links to toggle between them.
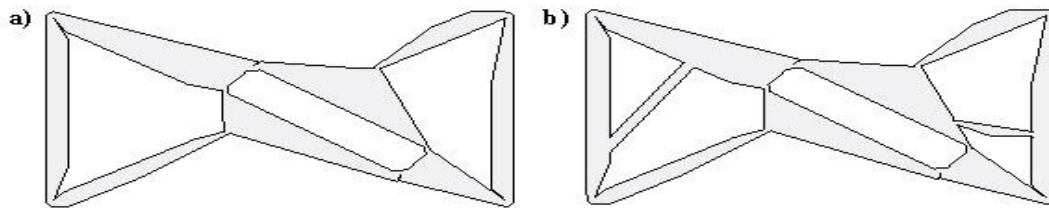
Figure 6.19 P_1 mechanism, (a) With mobility of one, (b) with mobility of (-1).

This conclude our first design example of using the over-constraint technique in the SMSF models, the following sub-section will introduce the second design example for this chapter.

6.2.2 Parallel Four-bar Compliant Mechanism Bistability

The parallelogram linkage is one of the classical four-bar mechanisms with one degree-of-freedom. It is considered to be a change point mechanism and, according to the work done in [28]; it can achieve bistability by placing the torsional spring at any joint location. The second stable position considered being predefined according to the mechanism's initial state and dimensions; any alternative second stable position can occur by a designed hard-stop. As an example, Figure 6.20 (a) and (b) shows the two stable positions in which the mechanism can toggle between by placing the spring (K) at the bottom left and right joints respectively taking the bottom link as the ground. The method proposed in this chapter allows the mechanism to have a second stable position by design via over-constraining it using compliant link as PEE. This sub-section illustrates with design example using the step-by-step procedure to convert a parallelogram linkage into a mechanism with two bistable positions as shown in Figure 6.20 (c), along with a produced working prototype for behavior demonstration.
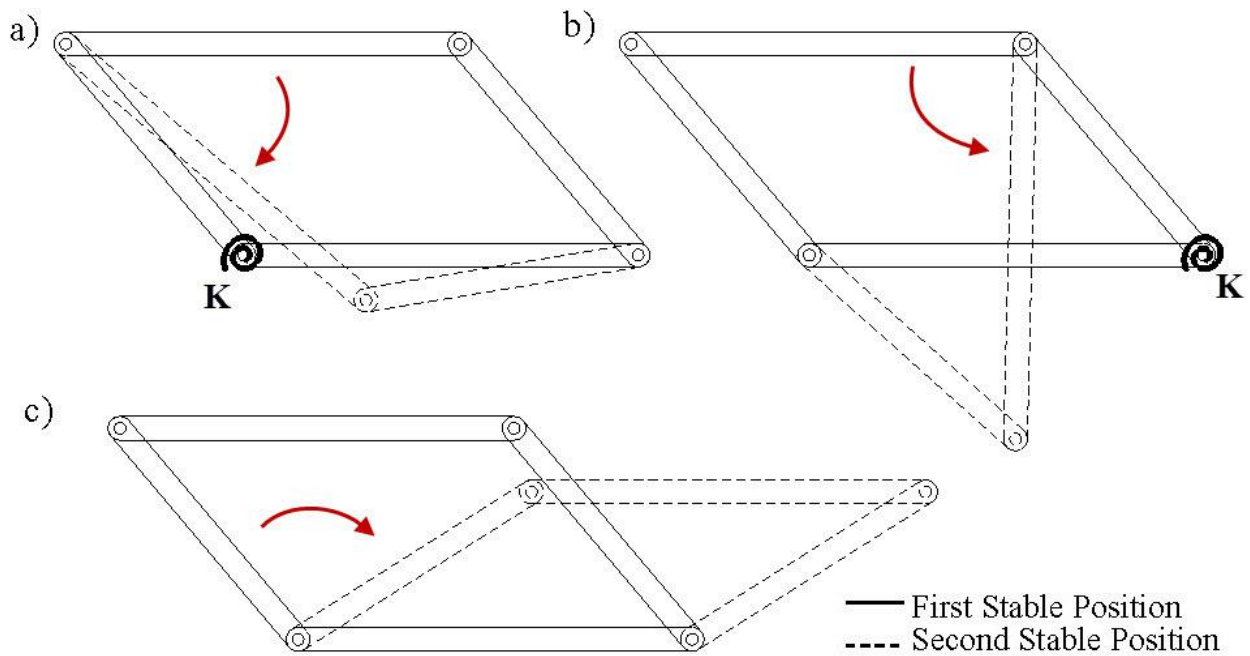
Figure 6.20 A parallelogram linkage at different toggled positions.

Considering the same P_1 SMSF's design constraint, Figure 6.21 illustrates the entire step-by-step procedure. The perpendicular bisectors of the link (l_2) at both ends are parallel unlike other mechanisms, where the intersection of the bisectors represents the pole point (P). For this reason, the pole of (l_2) is considered to be any line between both bisectors that is parallel to them. The two attachment points of the PEE (Q) and (m_Q) are placed on the pole line and link (l_2), respectively. The dimension (d_P) represents the distance of the pole line from the left bisector and (d_Q) controls the distance of point (Q) from (l_4) along the pole line in either direction. The first path of the point (m_Q) is along the coupler curve that is an arc in which its center is the intersection point between the link (l_4) and the pole line. The second path is also an arc with point (Q) as its center; depending on the location of (Q) being above or below the ground link (l_4) translates to what type of loading the PEE experiences (either compression or tension, respectively). Assuming the mechanism's links are rigid and with low torsional stiffness at the joints, Figure 6.21 (a) shows when the PEE experiences compression by being forced to follow the first path when absent the PEE, it would follow the second path instead. Furthermore, Figure 6.21 (b) shows the tension loading on the PEE when point (Q) is below (l_4).
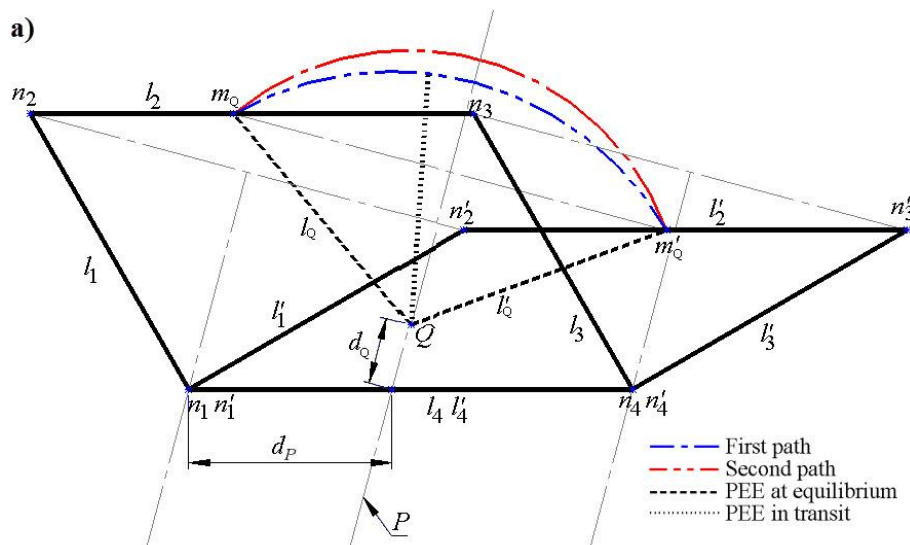
Figure 6.21 The mechanism where the PEE experiences (a) tension, (b) compression.
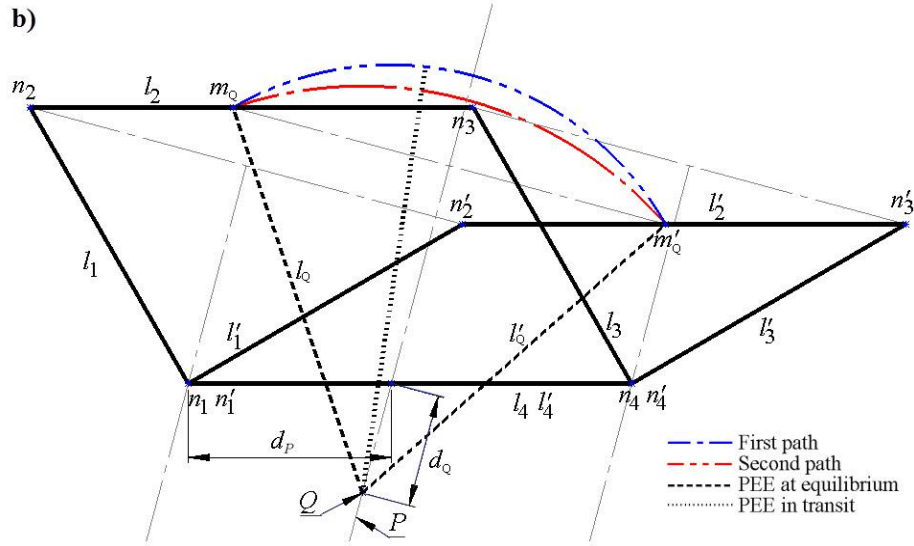
Figure 6.21 (Continued)

For prototype demonstration, the mechanism shown in Figure 6.21 (a) is considered where the PEE or (l_Q) undergo compressive loading. The mechanism was laser cut as a single piece from a Polypropylene Copolymer sheet, shown in Figure 6.22, and the detailed dimensions of the mechanism can be found in Appendix E.4. Because this research focuses on the mechanism's kinematics, therefore the joints and the PEE are cut as small as the laser cutter reliably can without detailed stress or fatigue analysis.
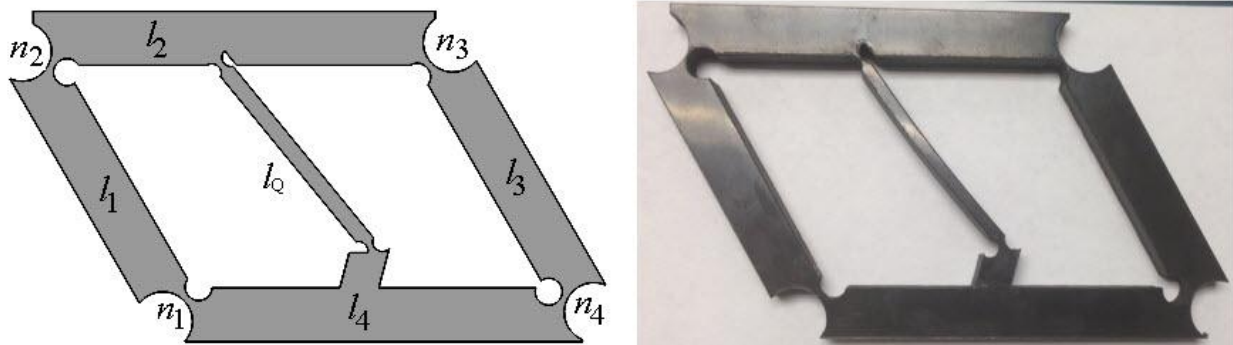
Figure 6.22 The final designed mechanism (Left) Solidworks, (Right) Prototype.

128

This mechanism was designed to toggle between two stable positions; the first stable position is when the angle between the two links (l_4) and (l_1) is at 120 degrees counter-clockwise and the second stable position at 30 degrees counter-clockwise for the same links. Figure 6.23 shows two identical prototypes placed on top of each other at the two stable positions without any external constraints to hold them at their perspective position.

Figure 6.23 Identical prototypes showing the two stable positions.

Figure 6.24 shows the individual stable positions on a polar grid to illustrate their perspective angles as well as the intermediate unstable position showing the bucking of the PEE due to the difference in the two paths that point (m_Q) traces, as shown in Figure 6.21 (a).

Figure 6.24 The prototype at its (a) initial, (b) intermediate and (c) final state.

129
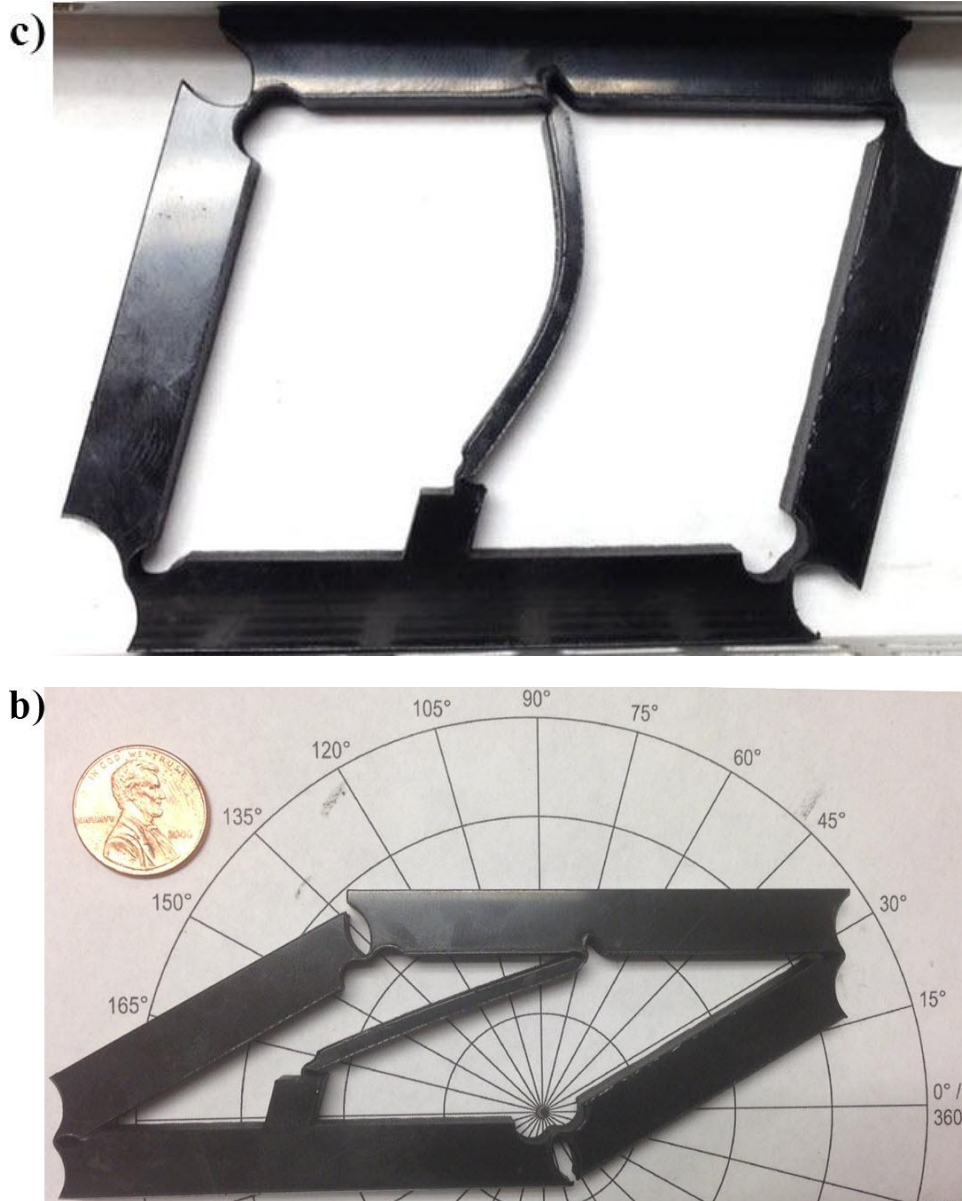
Figure 6.24 (Continued)

The FEA analysis preformed on the model shows high stress concentration at the joints exceeding the yield point of the material, which corresponds to the material deformation observed on the actual prototype. Figure 6.25 shows the stresses in the PEE when buckling at the mechanism unstable position, whereas Figure 6.26 shows the stress concentration at the joints

130

when the mechanism at the second stable position. Optimizing the stress-strain behavior at the joint and on the PEE element may be considered in future work on this topic.
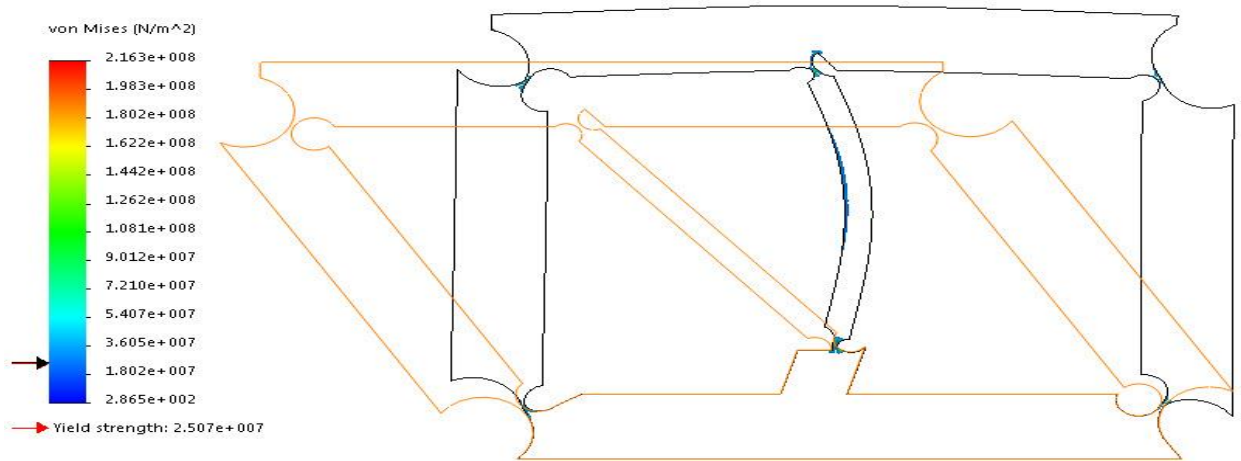
Figure 6.25 FEA analysis of the mechanism at the unstable position.
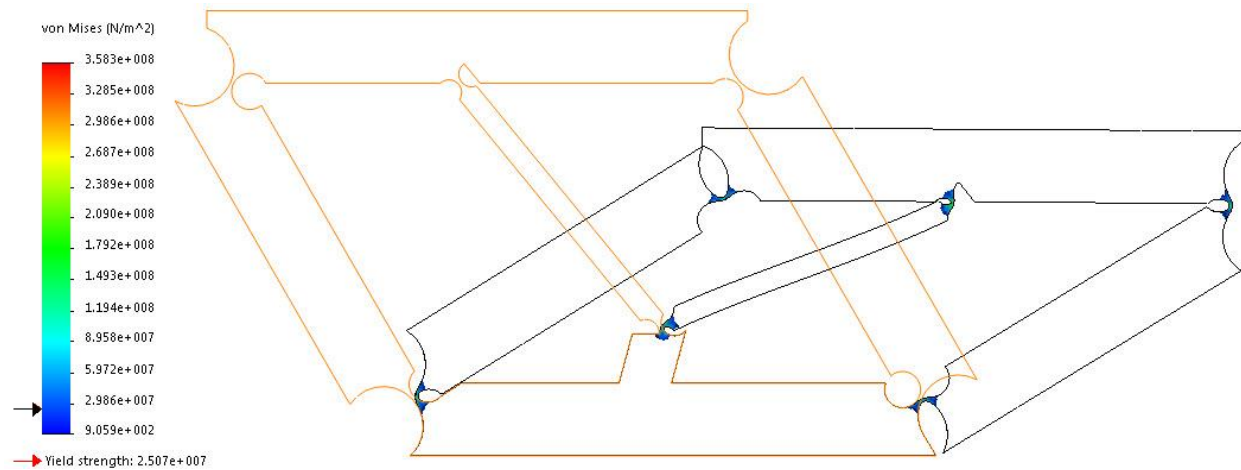
Figure 6.26 FEA analysis of the mechanism at the second stable position.

CHAPTER 7: CONCLUSION, RECOMMENDATIONS AND FUTURE WORK

7.1 Conclusion

The novel contributions in this Dissertation included:

1- The ability to design specific element for a specific length change by introducing the Linear Bi-stable Compliant Crank-Slider-Mechanism (LBCCSM). The model's theories were discussed along with introducing two different design approaches:

    a- The first approach considers the maximum vertical deflection of the model.

    b- The second approach considers the maximum force applied to the model.

These approaches are simplified using step-by-step design guidelines and flow charts identifying the equations and plots to use. An example for each approach also provided to simulate the walk through. Moreover, a novel use of the Linear Bi-stable Compliant Crank-Slider-Mechanism (LBCCSM) was also introduced by using the elements to do morphing space-frame.

    c- The modeling methods and strategies were discussed along with introducing a new concept of $\binom{5}{n}$ to guide the selection process of the LBCCSM placement within the sub-grid square that forms the single-layer grid. Two examples:

    d- The cylindrical to hyperbolic shell SMSF, and

    e- The cylindrical to spherical shell SMSF

were modeled geometrically and prototyped for result comparison and proving of concept.

2- Different variation of morphing space-frame using unit-cell bistable elements were also introduced with the methodology in mechanism synthesis involved. The example of morphing a disk like structure into a hemisphere was modeled and prototyped as a proof of concept for that topic.

3- The ability to transform a given one degree-of-freedom mechanism and turn it into bistable is also considered a novel contribution to this work. This new approach to design bistable mechanisms in general using the Computer-aided design (CAD) software reduces the complexity of the problem along with providing visual aspect of behaviors.

7.2 Recommendations and Future Work

This research lays the foundation for future work on shape morphing structures using compliant mechanism elements. The introduced methods allow the morphing of simple geometric forms; there are enormous amount of future work to customize this to specific problems and devices that are of practical importance and adapting the work to more complicated geometric forms.

The recommended future work on the LBCCSM, in Chapter 3, will be aimed at improving and enhance the design model to accommodate the stress concentration areas along with the design of the living hinges and incorporating the work done by Howell [27]. Additionally, more extensive comparisons should be considered between the presented mathematical model, the FEA and the actual prototype. For the hyperbolic and spherical SMSF, in Chapter 4, improving the design of the H-shaped living hinge will provide more accurate comparison between the Matlab algorithm and the actual prototype. There are different varieties of discipline that could be involved in the morphing strategy for better understanding such as topology optimization, origami theory, and design optimization. Instead of the single-layer grid,

133

double-layer grid designs are also possible to introduce a thickness to the space-frame. Also, for morphing of complicated and non-axisymmetric surfaces; stress trajectories can be utilized in placing the bistable elements to be actuated by the applied loads. The shape-shifting-surfaces (SSSs) [9] can be modified and used as added attachments to the space-frame to give it its surface profile, or coating the SMSFs with water proof layer using origami based skins. Incorporating intermediate surfaces in the hemisphere and sphere SMSF structure, in Chapter 5, could provide extra structural support. Additionally, more refined flexural pivots design in terms of stress concentration, fatigue and durability analysis would provide better LBCCSM and SMSF models. Finally, further investigation on the new methodology, in Chapter 6, by optimizing the stress-strain behavior at the joint and on the PEE element for making mechanisms bistable could be more important for some applications such as bistable switches, sensitive sensors, vibration isolators or energy absorbers.

134

REFERENCES

[1]   Howell, L. L., 2001, "Compliant Mechanisms", Wiley, New York, ISBN 978-0471384786.

[2]   Salamon, B. A., 1989, "Mechanical Advantage Aspects in Compliant Mechanisms Design," M.S. Thesis, Purdue University.

[3]   Motsinger, R. N., 1964, "Flexural Devices in Measurement Systems," Chapter 11 in Measurement Engineering, by P. K. Stein, Stein Engineering Services, Phoenix, AZ.

[4]   Paros, J. M., and Weisbord, L., 1965, "How to Design Flexural Hinges," Machine Design, Nov. 25, pp. 151-156.

[5]   Chow, W. W., 1981, "Hinges and Straps," Chapter 12 in Plastics Products Design Handbook, Part B, E. Miller, ed., Marcel Dekker, New York.

[6]   Hoetmer, Karin, Herder, Just L and Kim, Charles. "A Building Block Approach for the Design of Statically Balanced Compliant Mechanisms". International Design Engineering Technical Conference San Diego, California, USA,2009. Vols. DETC2009 87451.

[7]   Howell, L. L., Midha A., and Norton, T. W., 1996, "Evaluation of Equivalent Spring Stiffness for Use in a Pseudo-Rigid-Body Model of Large-Deflection Compliant Mechanisms," ASME Journal of Mechanical Design, 118(1):126-131.

[8]   Lusk, C., 2011, "Quantifying Uncertainty For Planar Pseudo-Rigid Body Models" in Proceedings of the 2011 Design Engineering Technical Conferences & Computers and Information in Engineering Conference, Washington, DC, Aug 29-31, 2011. DETC2011-47456.

[9]   Lusk, C., and Montalbano, P., 2011, "Design Concepts For Shape-Shifting Surfaces" in Proceedings of the 2011 Design Engineering Technical Conferences & Computers and Information in Engineering Conference, Washington, DC, Aug 29-31, 2011. DETC2011-47402.

[10]   Alqasimi, A., Lusk, C., and Chimento, J., "Design of a Linear Bi-stable Compliant Crank-Slider-Mechanism (LBCCSM)" in Proceedings of the 2014 Design Engineering Technical Conferences & Computers and Information in Engineering Conference, Buffalo, NY, Aug 17-20, 2014. DETC2014-34285.

[11]   Alqasimi, A., and Lusk, C., "Shape-Morphing Space Frame (SMSF) Using Linear Bistable Elements" in Proceedings of the 2015 Design Engineering Technical Conferences & Computers and Information in Engineering Conference, Boston, MA, Aug 2-5, 2015. DETC2015-47526.

[12]   Howell, L. L. and Midha, A., "Parametric Deflection Approximations for End-Loaded, Large-Deflection Beams in Compliant Mechanisms", ASME, March 1995, Journal of Mechanical Design, Vol. 117, pp. 156-165.

[13]   Saxena, A. and Kramer, S.N., 1998, "A Simple and Accurate Method for Determining Large Deflections in Compliant Mechanisms Subjected to End Forces and Moments," Journal of Mechanical Design, Trans. ASME, Vol. 120, No.3, pp. 392-400, erratum, Vol. 121, No. 2, p.194.

[14]   Howell, L.L. and Midha, A., 1994b, "The Development of Force-Deflection Relationships for Compliant Mechanisms," Machine Elements and Machine Dynamics, DE-Vol. 71, 23rd ASME Biennial Mechanisms Conference, pp. 501-508.

[15]   Dado M. H, 2001 "Variable Parametric Pseudo-Rigid Body Model for Large Deflection Beams with End Loads" International Journal of Non-linear Mechanics, 2001.

[16]   Howell, L.L. and Midha, A., 1995b, "Determination of the Degrees of Freedom of Compliant Mechanisms Using the Pseudo-Rigid-Body Model Concept," Proceedings of the Ninth World Congress on the Theory of Machines and Mechanisms, Milano, Italy, Vol. 2, pp. 1537-1541.

[17]   Howell, L.L. and Midha, A., 1995b, "Determination of the Degrees of Freedom of Compliant Mechanisms Using the Pseudo-Rigid-Body Model Concept," Proceedings of the Ninth World Congress on the Theory of Machines and Mechanisms, Milano, Italy, Vol. 2, pp. 1537-1541.

[18]   Chimento, J., Lusk,C., and Alqasimi, A., "A 3-D Pseudo-Rigid Body Model for Rectangular Cantilever Beams With an Arbitrary Force End-Load" in Proceedings of the 2014 Design Engineering Technical Conferences & Computers and Information in Engineering Conference, Buffalo, NY, Aug 17-20, 2014. DETC2014-34292.

[19]   Logan, P., and Lusk, C., "Pseudo-Rigid-Body Models for End-Loaded Heavy Cantilever Beams" in Proceedings of the 2015 Design Engineering Technical Conferences & Computers and Information in Engineering Conference, Boston, MA, Aug 2-5, 2015. DETC2015-47526.

[20]   Kota, S., and Ananthasuresh, G. K., "Designing compliant mechanisms", Mechanical Engineering-CIME, vll7 (ll):93-96, 1995.

[21] Chen, G., Gou, Y. and Zhang, A., "Synthesis of Compliant Multistable Mechanisms through Use of a Single Bistable Mechanism", Journal of Mechanical Design, 133(8), 081007 (Aug 10, 2011) doi:10.1115/1.4004543.

[22] Ishii, H. and Ting, K. L., "SMA Actuated Compliant Bistable Mechanisms", Mechatronics, Volume 14, Issue 4, May 2004, Pages 421-437.

[23] Opdahl, P. G., Jensen, B. D., and Howell, L. L., 1998, "An Investigation Into Compliant Bistable Mechanisms," in Proc. 1998 ASME Design Engineering Technical Conferences, DETC98/MECH-5914,.

[24] Smith, C. and Lusk, C., 2011, "Modeling and Parameter Study Of Bistable Spherical Compliant Mechanisms" in Proceedings of the 2011 Design Engineering Technical Conferences & Computers and Information in Engineering Conference, Washington, DC, Aug 29-31, 2011. DETC2011-47397.

[25] Kociecki, M., Adeli, H., "Shape optimization of free-form steel space-frame roof structures with complex geometries using evolutionary computing" Engineering Application of Artificial Intelligence, Volume 38, February 2015, Pages 168-182.

[26] Schodek, D., Structures, Prentice-Hall, New Jersey, 1980.

[27] Chen, G. and Howell, L. L., "Two General Solutions of Torsional Compliance for Variable Rectangular Cross-Section Hinges in Compliant Mechanisms", Journal of the International Societies for Precision Engineering and Nanotechnology, Vol. 33, Issue 3, pp. 268-274, DOI:10.1016/j.precisioneng.2008.08.001.

[28] Jensen, B. D. and Howell, L. L., "Identification of Compliant Pseudo-Rigid-Body Four-Link Mechanism Configurations Resulting in Bistable Behavior", ASME. J. Mech. Des. 2004; 125(4):701-708. doi:10.1115/1.1625399.

[29] Schulze, E.F., 1955, "Designing Snap-Action Toggles", Product Engineering, November 1955, pp. 168-170.

[30] Jensen, B. and Howell, L. L., "Bistable Configurations of Compliant Mechanisms Modeled Using Four Link and Translational Joints" Journal of Mechanical Design, Vol. 126, Issue 4, pp. 657-666.

[31] Ceccarelli M, Koetsier T. Burmester and Allievi A., "Theory and Its Application for Mechanism Design at the End of 19th Century", ASME. J. Mech. Des.2008; 130(7): 072301-072301-16. doi:10.1115/1.2918911.

[32] Waldron, K. J. and Kinzel, G. L., "Kinematics, Dynamics, and Design of Machinery", Wiley, New York, 2 ed. 2003, ISBN 978-0471244172.

[33] Jensen, B. D, Howell, L. L. and Salmon, L. G., "Design of Two-Link, In-Plane, Bistable Compliant Micro-Mechanisms", Proceedings of DETC' 1998 ASME Design Engineering Technical Conferences, Sept 13-16, 1998, Atlanta, GA, DETC98/MECH-5837.

[34]   Luharuka, R. and Hesketh, P. J., "Design of fully compliant, in-plane rotary, bistable micromechanisms for MEMS applications", Sensors and Actuators A: Physical, Vol. 134, Issue 1, pp. 231-238 DOI:10.1016/j.sna.2006.04.030.

[35]   Masters, N. D. and Howell, L. L., "A self-retracting fully compliant bistable micromechanism", Journal of Microelectromechanical Systems, Vol. 12, Issue 3, pp. 273-280, DOI: 10.1109/JMEMS.2003.811751.

[36]   Lusk, C. and Howell, L. L., "Spherical Bistable Micromechanism", ASME. J. Mech. Des. 2008;130(4):045001-045001-6. doi:10.1115/1.2885079.

[37]   Sönmez, Ü. and Tutum, C. C., "A Compliant Bistable Mechanism Design Incorporating Elastica Buckling Beam Theory and Pseudo-Rigid-Body Model", ASME. J. Mech. Des. 2008;130(4):042304-042304-14. doi:10.1115/1.2839009.

[38]   "Bistable Buckled Beam: Elastica Modeling and Analysis of Static Actuation", International Journal of Solids and Structures, Vol. 50, Issue 19, pp. 2881-2893, DOI: 10.1016/j.ijsolstr.2013.05.005.

[39]   Vaz, M. A. and Silva, D., "Post-Buckling Analysis of Slender Elastic Rods Subjected to Terminal Forces", International Journal of Non-Linear Mechanics, Vol. 38, Issue 4, pp. 483-492, PII S0020-7462(01)00072-5, DOI: 10.1016/S0020-7462(01)00072-5.

[40]   Vaz, M. A. and Mascaro, G., "Post-Buckling Analysis of Slender Elastic Vertical Rods Subjected to Terminal Forces and Self-Weight", International Journal of Non-Linear Mechanics, Vol. 40, Issue 7, pp. 1049-1056, DOI: 10.1016/j.ijnonlinmec.2004.12.002.

[41]   Vaz, M. A., and Patel, M. H., "Post-Buckling Behaviour of Slender Structures with a Bi-linear Bending Moment-Curvature Relationship", International Journal of Non-Linear Mechanics.

[42]   Mazzilli, C., "Buckling and Post-Buckling of Extensible Sods Sevisited: A Sultiple-Scale Solution", International Journal of Non-Linear Mechanics, Vol. 44, Issue 2. pp. 200-208, DOI:10.1016/j.ijnonlinmec.2008.11.005

[43]   Khatait, J. P., Mukherjee, S., and Seth, B., "Compliant design for flapping mechanism: A minimum torque approach", Mechanism and Machine Theory, Vol. 41, Issue 1, pp. 3-16, DOI: 10.1016/j.mechmachtheory.2005.06.002.

[44]   Ishii, H. and Ting, K. L., "SMA actuated compliant bistable mechanisms", Mechatronics, Vol. 14, Issue 4, pp. 421-437, DOI: 10.1016/S0957-4158(03)00068-0.

[45]   Chanthasopeephan, T., Jarakorn, A., Polchankajorn, P. and Maneewarn, T., "Impact reduction mobile robot and the design of the compliant legs", Robotics and Autonomous Systems, Vol. 62, Issue 1, pp. 38-45, SI, DOI: 10.1016/j.robot.2012.07.017.

138

[46]   Dunning, A. G., Tolou, N. and Herder, J. L., "A compact low-stiffness six degrees of freedom compliant precision stage", Journal of the International Societies for Precision Engineering and Nanotechnology, Vol. 37, Issue 2, pp. 380-388, DOI: 10.1016/j.precisioneng.2012.10.007.

[47]   Du, Y. X., Chen, L. P. and Luo, Z., "Topology synthesis of geometrically nonlinear compliant mechanisms using meshless methods", Acta Mechanica Solida Sinica, Vol. 21, Issue 1, pp. 51-61,DOI: 10.1007/s10338-008-0808-3.

[48]   Deepak, S., Sahu, D., Dinesh, M., Jalan, S. and Ananthasuresh, G. K., "A Comparative Study of the Formulations and Benchmark Problems for the Topology Optimization of Compliant Mechanisms", Proceedings of the 2008 Design Engineering Technical Conferences & Computers and Information in Engineering Conference, New York, NY, AUG 03-06, 2008.

[49]   Su, H. and McCarthy J., "Synthesis of Bistable Compliant Four-Bar Mechanisms Using Polynomial Homotopy", ASME. J. Mech. Des. 2006;129(10):1094-1098, Doi:10.1115/1.2757192.

[50]   Limaye, P., Ramu, G., Pamulapati, S. and Ananthasuresh, G. K., "A compliant mechanism kit with flexible beams and connectors along with analysis and optimal synthesis rocedures", Mechanism and Machine Theory, Vol. 49, pp. 21-39, DOI: 10.1016/j.mechmachtheory.2011.07.008.

[51]   Meng, Q. L., Li, Y. M. and Xu, J., "A novel analytical model for flexure-based proportion compliant mechanisms", Journal of the International Societies for Precision Engineering and Nanotechnology, Vol. 38, Issue 3, pp. 449-457, DOI: 10.1016/j.precisioneng.2013.12.001.

[52]   Ahuett-Garza, H., Chaides, O., Garcia, P. N. and Urbina, P., "Studies about the use of semicircular beams as hinges in large deflection planar compliant mechanisms", Journal of the International Societies for Precision Engineering and Nanotechnology, Vol. 38, Issue 4, pp. 711-727, DOI: 10.1016/j.precisioneng.2014.03.008.

[53]   Guo, J. J. and Lee, K. M., "Compliant joint design and flexure finger dynamic analysis using an equivalent pin model", Mechanism and Machine Theory, Vol. 70, pp. 338-353,DOI:10.1016/j.mechmachtheory.2013.08.001.

[54]   Chen, G. M., Aten, Q. T. and Zirbel, S., "A Tristable Mechanism Configuration Employing Orthogonal Compliant Mechanisms", Journal of Mechanisms and Robotics, Vol. 2, Issue 1, 014501, DOI: 10.1115/1.4000529.

[55]   Ohsaki, M. and Nishiwaki, S., "Shape design of pin-jointed multistable compliant mechanisms using snapthrough behavior", Structural and Multidisciplinary Optimization, Vol. 30, Issue 4, pp. 327-334, DOI: 10.1007/s00158-005-0532-2.

[56]   Chen G. and Du, Y., "Double-Young Tristable Mechanisms", ASME. J. Mechanisms Robotics, 2012;5(1):011007-011007-7. doi:10.1115/1.4007941.

[57] Chen, G. M., Wilcox, D. L. and Howell, L. L., "Fully compliant double tensural tristable micromechanisms (DTTM)", Journal of Micromechanics and Microengineering, Vol. 19, Issue 2, 025011, DOI: 10.1088/0960-1317/19/2/025011.

[58] Kinzel, E. C., Schmiedeler, J. P. and Pennock, G. R., "Kinematic Synthesis for Finitely Separated Positions Using Geometric Constraint Programming", ASME. J. Mech. Des. 2005;128(5):1070-1079. doi:10.1115/1.2216735.

[59] Schmiedeler, J. P., Clark, B. C. and Kinzel, E. C., "Pennock GR. Kinematic Synthesis for Infinitesimally and Multiply Separated Positions Using Geometric Constraint Programming", ASME. J. Mech. Des. 2014;136(3):034503-034503-7. doi: 10.1115 /1.4026152.

[60] Norton, R. , "Design of Machinery", McGraw-Hill Education Material, 5 ed. 2011, ISBN 9780077421717.

[61] Murray, A. P., Schmiedeler, J. P. and Korte, B. M., "Kinematic Synthesis of Planar, Shape-Changing Rigid-Body Mechanisms", ASME. J. Mech. Des. 2008;130(3):032302-032302-10, doi:10.1115/1.2829892.

[62] Santer, M., Pellegrino, S., "Concept and Design of a Multistable Plate Structure", ASME. J. Mech. Des. 2011;133(8):081001-081001-7. doi:10.1115/1.4004459.

[63] Cooper, J. E. , Chekkal, I., Cheung, R. C. M., Wales, C., Allen, N. J., Lawson, S., Peace, A. J., Cook, R., Standen, P., Hancock, S. D. and Carossa, G. M., "Design of a Morphing Wingtip", Journal of Aircraft, Vol. 52, No. 5 (2015), pp. 1394-1403, doi: 10.2514 /1.C032861

[64] Saito, K., Tsukahara, A. and Okabe, Y., "New Deployable Structures Based on an Elastic Origami Model", ASME. J. Mech. Des. 2015;137(2):021402-021402-5. doi:10.1115/ 1.4029228.

[65] Santer, M. and Pellegrino, S., "Compliant multistable structural elements", International Journal of Solids and Structures, Vol. 45, Issue 24, pp. 6190-6204, DOI: 10.1016/j.ijsolstr 2008.07.014.

[66] Shaw, L. A. and Hoplins, J. B., "A Shape-controlled Compliant Microarchitecture Material", in Proceedings of the 2015 Design Engineering Technical Conferences & Computers and Information in Engineering Conference, Boston, MA, Aug 2-5, 2015. DETC2015-46643.

[67] Kociecki, M. and Adeli, H., "Shape optimization of free-form steel space-frame roof structures with complex geometries using evolutionary computing", Engineering Applications of Artificial Intelligence, Vol. 38, pp. 168-182, DOI: 10.1016/ j.engappai. 2014.10.012.

[68]   GANDHI, U. N., "Two-dimensional morphing structure for aircraft wing, has shape-memory alloy elements that extend from anchor to hinge, springs extend from anchor to another hinge, and rigid elements extend between hinges", Toyota Motor Engineering & Manufacturing North America Inc. (TOYT-C), Patent Numbers: US2015047337-A1 ; US8991769-B2.

[69]   Henry, C. P., Mcknight, G. P., Smith, S. P., Henry, C., Mcknight, G. and Smit S., "Adaptive structural core for morphing panel structures of an e.g. aircraft has actuator attachment points that are provided on the core bodies arranged in a repeating manner", Boeing Co. (BOEI-C), Patent Numbers: WO2011059571-A1 ; EP2470422-A1 ; CN102686478-A ; JP2013510763-W ; US8746626-B1.

[70]   Tsai, L., "Mechanism Design: Enumeration of Kinematic Structures According to Function", CRC Press, Florida, 1st ed, 2000, ISBN 978-0849309014.

[71]   Gallego, J. A. and Herder, J., "classifications For Literature on Compliant Mechanisms: A Design Methodology Based Approach", ASME International Design Engineering Technical Conferences/Computers and Information in Engineering Conference Location: San Diego, CA Date: AUG 30-SEP 02, 2009, DETC2009-87334.

APPENDIX A: NOMENCLATURE

L_1, L_2 Length of segment 1 and segment 2, respectively [mm].

θ_1 Angle at which segment 1 lies (CW) [deg].

θ_{2i} Initial angle at which segment 2 lies (CCW) [deg].

θ_2 Changing angle of segment 2 (CCW) [deg].

Θ_1 The PRBM angle of segment 1 [deg].

Θ_2 The PRBM angle of segment 2 [deg].

γ Characteristic radius (Fixed-Pinned) = 0.85 [1].

ρ Characteristic radius (Pinned-Pinned) = 0.85 [1].

K_Θ Stiffness coefficient = 2.65 [1].

ω_1 $= \Theta_1 + \theta_1$

ω_2 $= \Theta_1 + \Theta_2 + \theta_1 + \theta_2$

ω_3 $= \Theta_1 + \theta_1 + \theta_2$

ω_4 $= \Theta_1 - \Theta_2 + \theta_1 + \theta_2$

K_1 Characteristic pivot stiffness of segment 1 [N.mm].

K_2 Characteristic pivot stiffness of segment 2 [N.mm].

X, x	Changing distance between point A and point C [mm].
Δ	Output displacement from point C to point C``.
F, M	Applied force [N] and moment [N.m] respectively.
V	Total spring energy of the characteristic pivots.
E	Young's modulus [N/ mm^2].
σ_y	The yield stress [MPa].
SF	The safety factor.
m	Initial angles ratio.
v	Stiffness coefficient ratio.
f	Non-dimensional force.
I_1	2nd moment of area of segment 1 [mm^4].
I_2	2nd moment of area of segment 2 [mm^4].
t	Material thickness [mm].
w_1	First segment's width [mm].
w_2	Second segment's width [mm].
F_t	Tangential force at the tip of segment 1 [N].
F_B	The buckling force of segment 2 [N].
F_p	The passive force from the F_B component [N].
J	Non-dimensional force-flexibility coefficient.

s	Number of the polygon sides.
k	Number of the total slices forming a cylindrical shape.
n	Number of the bi-stable elements LBCCSM.
h_o	Space-frame's initial height before morphing [mm].
h_f	Space-frame's morphed height [mm].
h	Space-frame's heights at each slice [mm].
ρ_o	Space-frame's initial circumscribed radius [mm].
ρ_f	Space-frame's morphed circumscribed radius [mm].
μ	Space-frame radius across the height [mm].
$\Delta\mu$	SMSF change in radius [mm].
l_s	Length of each polygon's side [mm].
$\Delta\tau$	Relative rotation between two parallel planes [deg].

144

APPENDIX B: MATHCAD CODE

$$A := L12\sin(\theta1 + \Theta1) \qquad a1 := L11\cdot\sin(\theta1)$$

$$B := L21\cdot\cos(\theta2)\cdot\sin(\Theta2) \qquad a2 := L11\cdot\cos(\theta1)$$

$$C := L12\cos(\theta1 + \Theta1) \qquad a3 := L22\sin(\theta2)$$

$$D := L21\cdot\sin(\theta2)\cdot\sin(\Theta2) \qquad a4 := L22\cos(\theta2)$$

$$z1 := \begin{pmatrix} -A & -2\cdot B & 0 & 0 & 0 & 0 \\ C & 2\cdot D & 0 & 0 & 0 & 0 \\ 0 & 0 & -A & -2\cdot B & 0 & 0 \\ 0 & 0 & C & 2\cdot D & 0 & 0 \\ 0 & 0 & 0 & 0 & -A & -2\cdot B \\ 0 & 0 & 0 & 0 & C & 2\cdot D \end{pmatrix} \qquad z2 := \begin{pmatrix} \Theta1x \\ \Theta2x \\ \Theta1\theta1 \\ \Theta2\theta1 \\ \Theta1\theta2 \\ \Theta2\theta2 \end{pmatrix} \qquad z3 := \begin{pmatrix} 1 \\ 0 \\ a1 + A \\ -a2 - C \\ a3 + 2\cdot L21\cdot\sin(\theta2)\cdot\cos(\Theta2) \\ a4 + 2\cdot L21\cdot\cos(\theta2)\cdot\cos(\Theta2) \end{pmatrix}$$

$$z \rightarrow \begin{bmatrix} \dfrac{\sin(\theta2)}{L12\cos(\Theta1 + \theta1)\cdot\cos(\theta2) - L12\sin(\Theta1 + \theta1)\cdot\sin(\theta2)} \\[2ex] -\dfrac{\cos(\Theta1 + \theta1)}{2\cdot L21\cdot\cos(\Theta1 + \theta1)\cdot\cos(\theta2)\cdot\sin(\Theta2) - 2\cdot L21\cdot\sin(\Theta1 + \theta1)\cdot\sin(\theta2)\cdot\sin(\Theta2)} \\[2ex] \dfrac{\sin(\theta2)\cdot(L12\sin(\Theta1 + \theta1) + L11\cdot\sin(\theta1))}{L12\cos(\Theta1 + \theta1)\cdot\cos(\theta2) - L12\sin(\Theta1 + \theta1)\cdot\sin(\theta2)} - \dfrac{\cos(\theta2)\cdot(L12\cos(\Theta1 + \theta1) + L11\cdot\cos(\theta1))}{L12\cos(\Theta1 + \theta1)\cdot\cos(\theta2) - L12\sin(\Theta1 + \theta1)\cdot\sin(\theta2)} \\[2ex] \dfrac{\sin(\Theta1 + \theta1)\cdot(L12\cos(\Theta1 + \theta1) + L11\cdot\cos(\theta1))}{2\cdot L21\cdot\cos(\Theta1 + \theta1)\cdot\cos(\theta2)\cdot\sin(\Theta2) - 2\cdot L21\cdot\sin(\Theta1 + \theta1)\cdot\sin(\theta2)\cdot\sin(\Theta2)} - \dfrac{\cos(\Theta1 + \theta1)\cdot(L12\sin(\Theta1 + \theta1) + L11\cdot\sin(\theta1))}{2\cdot L21\cdot\cos(\Theta1 + \theta1)\cdot\cos(\theta2)\cdot\sin(\Theta2) - 2\cdot L21\cdot\sin(\Theta1 + \theta1)\cdot\sin(\theta2)\cdot\sin(\Theta2)} \\[2ex] \dfrac{\cos(\theta2)\cdot(L22\cos(\theta2) + 2\cdot L21\cdot\cos(\theta2)\cdot\cos(\theta2))}{L12\cos(\Theta1 + \theta1)\cdot\cos(\theta2) - L12\sin(\Theta1 + \theta1)\cdot\sin(\theta2)} + \dfrac{\sin(\theta2)\cdot(L22\sin(\theta2) + 2\cdot L21\cdot\cos(\theta2)\cdot\sin(\theta2))}{L12\cos(\Theta1 + \theta1)\cdot\cos(\theta2) - L12\sin(\Theta1 + \theta1)\cdot\sin(\theta2)} \\[2ex] -\dfrac{\sin(\Theta1 + \theta1)\cdot(L22\cos(\theta2) + 2\cdot L21\cdot\cos(\theta2)\cdot\cos(\theta2))}{2\cdot L21\cdot\cos(\Theta1 + \theta1)\cdot\cos(\theta2)\cdot\sin(\Theta2) - 2\cdot L21\cdot\sin(\Theta1 + \theta1)\cdot\sin(\theta2)\cdot\sin(\theta2)} - \dfrac{\cos(\Theta1 + \theta1)\cdot(L22\sin(\theta2) + 2\cdot L21\cdot\cos(\theta2)\cdot\sin(\theta2))}{2\cdot L21\cdot\cos(\Theta1 + \theta1)\cdot\cos(\theta2)\cdot\sin(\Theta2) - 2\cdot L21\cdot\sin(\Theta1 + \theta1)\cdot\sin(\theta2)\cdot\sin(\theta2)} \end{bmatrix}$$

$$z2 := z \text{ simplify} \rightarrow \begin{bmatrix} \dfrac{\sin(\theta 2)}{L12\cos(\Theta 1 + \theta 1 + \theta 2)} \\[2em] -\dfrac{\cos(\Theta 1 + \theta 1)}{2 \cdot L21 \cdot \cos(\Theta 1 + \theta 1) \cdot \cos(\theta 2) \cdot \sin(\theta 2) - 2 \cdot L21 \cdot \sin(\Theta 1 + \theta 1) \cdot \sin(\theta 2) \cdot \sin(\theta 2)} \\[2em] -\dfrac{L12\cos(\Theta 1 + \theta 1 + \theta 2) + L11 \cdot \cos(\theta 1 + \theta 2)}{L12\cos(\Theta 1 + \theta 1 + \theta 2)} \\[2em] -\dfrac{L11 \cdot \sin(\Theta 1)}{L21 \cdot (\sin(\Theta 1 - \Theta 2 + \theta 1 + \theta 2) - \sin(\Theta 1 + \Theta 2 + \theta 1 + \theta 2))} \\[2em] \dfrac{L22 + 2 \cdot L21 \cdot \cos(\Theta 2)}{L12\cos(\Theta 1 + \theta 1 + \theta 2)} \\[2em] \dfrac{L22\sin(\Theta 1 + \theta 1 + \theta 2) + L21 \cdot \sin(\Theta 1 + \Theta 2 + \theta 1 + \theta 2) + L21 \cdot \sin(\Theta 1 - \Theta 2 + \theta 1 + \theta 2)}{L21 \cdot (\sin(\Theta 1 - \Theta 2 + \theta 1 + \theta 2) - \sin(\Theta 1 + \Theta 2 + \theta 1 + \theta 2))} \end{bmatrix}$$

$$\Theta 1 x := z2_0 \qquad \Theta 1\theta 1 := z2_2 \qquad \Theta 1\theta 2 := z2_4$$

$$\Theta 2 x := z2_1 \qquad \Theta 2\theta 1 := z2_3 \qquad \Theta 2\theta 2 := z2_5$$

$$\Theta 1 x \rightarrow \frac{\sin(\theta 2)}{L12\cos(\Theta 1 + \theta 1 + \theta 2)}$$

$$\Theta 2 x \rightarrow -\frac{\cos(\Theta 1 + \theta 1)}{2 \cdot L21 \cdot \cos(\Theta 1 + \theta 1) \cdot \cos(\theta 2) \cdot \sin(\theta 2) - 2 \cdot L21 \cdot \sin(\Theta 1 + \theta 1) \cdot \sin(\theta 2) \cdot \sin(\theta 2)}$$

$$\Theta 1\theta 1 \rightarrow -\frac{L12\cos(\Theta 1 + \theta 1 + \theta 2) + L11 \cdot \cos(\theta 1 + \theta 2)}{L12\cos(\Theta 1 + \theta 1 + \theta 2)}$$

$$\Theta 2\theta 1 \rightarrow -\frac{L11 \cdot \sin(\Theta 1)}{L21 \cdot (\sin(\Theta 1 - \Theta 2 + \theta 1 + \theta 2) - \sin(\Theta 1 + \Theta 2 + \theta 1 + \theta 2))}$$

$$\Theta 1\theta 2 \rightarrow \frac{L22 + 2 \cdot L21 \cdot \cos(\Theta 2)}{L12\cos(\Theta 1 + \theta 1 + \theta 2)}$$

$$\Theta 2\theta 2 \rightarrow \frac{L22\sin(\Theta 1 + \theta 1 + \theta 2) + L21 \cdot \sin(\Theta 1 + \Theta 2 + \theta 1 + \theta 2) + L21 \cdot \sin(\Theta 1 - \Theta 2 + \theta 1 + \theta 2)}{L21 \cdot (\sin(\Theta 1 - \Theta 2 + \theta 1 + \theta 2) - \sin(\Theta 1 + \Theta 2 + \theta 1 + \theta 2))}$$

APPENDIX C: MATLAB CODES

C.1 Solving for the Buckling of Segment 2

```matlab
function PRBSM08b

clc
clear all
format shortG

%-----------------
%  Input Parameters
%-----------------

Theta_1_start = 20; %in Degrees!
Theta_1_stp = 10; %in Degrees!
Theta_1_end = 80; %in Degrees!

Theta_2i_stp = 1; %in Degrees!
Theta_2i_end = 85; %in Degrees!

% x0=[ oX ; oCap_Theta_1 ; oCap_Theta_2 ; oDf];

count=0;
for ii= [1 2 3 4 5 6 8 10 12 14 16 18 20 25 30 40 50 70 100]
%v_start:v_stp:v_end;
    for jj=Theta_1_start:Theta_1_stp:Theta_1_end;
        for kk=jj:Theta_2i_stp:Theta_2i_end;
            count=count+1;
        end
    end
end

Sol_mat=[];
bx_mat=[];
bx_max_mat=[];
b_over_x_maxL=0;

counter=count;
for Theta_1 = deg2rad([ Theta_1_start : Theta_1_stp :
Theta_1_end ]);
```

147

```matlab
for v = [1 2 3 4 5 6 8 10 12 14 16 18 20 25 30 40 50 70 100 150
200 250 500] %v_start : v_stp : v_end;

    b_over_x_n=0;
                            %Theta_2i_start
for Theta_2i = deg2rad([ rad2deg(Theta_1) : Theta_2i_stp :
Theta_2i_end]);

    iter=[ counter rad2deg(Theta_1) v rad2deg(Theta_2i) ]
    rad2deg(Theta_2i);
    m = sin(Theta_1)/sin(Theta_2i);

    L1 = 1;
    L2 = L1*m;
    gama = 0.85;

    L11= (1-gama)*L1;
    L12= gama*L1;

    L21= gama*L2/2;
    L22= (1-gama)*L2;
    L23= gama*L2/2;

    oX = L1*cos(Theta_1)+L2*cos(Theta_2i);    %z(1)
    oCap_Theta_1 = deg2rad(1e-3);             %z(2)
    oCap_Theta_2 = deg2rad(1e-3);             %z(3)
    oDf = 1e-3 ;                              %z(4)

    % x2=[ oX ; oCap_Theta_1 ; oCap_Theta_2 ; oDf]; %new one in
line 76

    Sol_mat_s=[];
    bx_mat_s=[];
    X_max = oX;

%----------------------------------
%  Solving at what angle L2 Buckls
%----------------------------------

    x0= [ deg2rad(44) ; deg2rad(44) ]; %that is initial guess of
Cap_Theta_1, Theta_2 resp.

    opts0=optimset('MaxFunEvals',5e6, 'MaxIter',5e6,
'TolFun',1e-6);

    [z0,fval0] = fsolve(@Equ0 ,x0 ,opts0);
```

```matlab
        Cap_Theta_1 = abs(rad2deg(z0(1)));
        Theta_2 = abs(rad2deg(z0(2)));
        %Theta_2_end = Theta_2_start + 0;
        fval0;

        b = gama*L1*sin(Theta_1+deg2rad(Cap_Theta_1))+(1-
gama)*L1*sin(Theta_1);

        Sol_mat=[Sol_mat;
rad2deg(Theta_1),v,rad2deg(Theta_2i),Theta_2,oX,Cap_Theta_1,oCap
_Theta_2,oDf];
        Sol_mat_s=[Sol_mat_s;
rad2deg(Theta_1),v,rad2deg(Theta_2i),Theta_2,oX,Cap_Theta_1,oCap
_Theta_2,oDf];

        bx_mat=[bx_mat;
rad2deg(Theta_1),v,rad2deg(Theta_2i),Theta_2,b,oX];
        bx_mat_s=[bx_mat_s;
rad2deg(Theta_1),v,rad2deg(Theta_2i),Theta_2,b,oX];
        b_max=max(bx_mat_s(:,5));

        b_over_x= ceil((b_max/X_max)*1000)/1000;

        b_over_x_maxL=
floor((m/(cos(Theta_1)+cos(Theta_2i)*m))*1000)/1000;

        if b_over_x >= b_over_x_maxL ;, break, end
        if b_over_x_n > b_over_x ;, break, end
        %if abs(b_over_x - b_over_x_maxL) < 1e-4;, break, end
        %if b_over_x == b_over_x_maxL;, break, end

        b_over_x_n = b_over_x;

save('PRBSM08b')

% fprintf('          v          Theta_1      Theta_2i
Theta_2       X      Cap_Theta_1    Cap_Theta_2     Df')
Sol_mat_s;
% fprintf('          v          Theta_1      Theta_2i
Theta_2       b        X')
bx_mat_s;
b_max;
X_max;

bx_max_mat= [bx_max_mat;
rad2deg(Theta_1),v,rad2deg(Theta_2i),b_max,X_max,b_over_x];
```

```matlab
% Cap_Theta_1_max_mat= [Cap_Theta_1_max_mat;
rad2deg(Theta_1),v,rad2deg(Theta_2i),Cap_Theta_1];

counter=counter-1;
end %for Theta_2i
save('PRBSM08b')
end %for v
save('PRBSM08b')
end %for Theta_1
save('PRBSM08b')

fprintf('         Theta_1        v        Theta_2i   Theta_2
X       Cap_Theta_1  Cap_Theta_2       Df')
Sol_mat
fprintf('         Theta_1        v        Theta_2i   Theta_2
b           X')
bx_mat
fprintf('         Theta_1        v        Theta_2i      b
X         b/X')
bx_max_mat
fprintf('         Theta_1        v        Theta_2i
Cap_Theta_1')
Cap_Theta_1_max_mat

%-------------------------------
%  Defining Equations 3.8 and 3.18
%-------------------------------

function Fun0 = Equ0(z0)
%    Fun0=[2.65*Cap_Theta_1-
(pi^2)*(1/(2*v*m))*sin(Theta_1+Cap_Theta_1+Theta_2);
%    L11*sin(Theta_1)+L12*sin(Theta_1+Cap_Theta_1)-
L2*sin(Theta_2)
%    ]

Fun0=[
    2.65*z0(1)-(pi^2)*(1/(2*v*m))*sin(Theta_1+z0(1)+z0(2));
    L11*sin(Theta_1)+L12*sin(Theta_1+z0(1))-L2*sin(z0(2))
    ];
end

save('PRBSM08b')
load('PRBSM08b')
end
```

C.2 The LBCCSM Model

```matlab
function PRBSM09

%--------------------------------------------------------
%  NOTE:
%  This part of the code takes long computational time,
%  it is advised to solve for individual Theta_1 and
%  then combine the data into one .mat file to be use
%  in the plotting code.
%--------------------------------------------------------

clc
clear all
format shortG

%------------------
%  Input Parameters
%------------------

% v_start = 5;
% v_stp = 2;
% v_end = 5;

Theta_1_start = 20 ; %in Degrees!
Theta_1_stp = 10;    %in Degrees!
Theta_1_end = 80;    %in Degrees!

%Theta_2i_start = Theta_1_start
%Theta_2i_start = #; %in Degrees!
Theta_2i_stp = 1;    %in Degrees!
Theta_2i_end = 85;   %in Degrees!

%Theta_2_start = Theta_2i_start;  %and could be bigger than
Theta_1_start!
%Theta_2_start = #;  %in Degrees!
Theta_2_stp = 0.05;  %in Degrees! 0.1  1 0.05  0.01(50 60)
0.005(70) 0.005(80)
Theta_2_end = 85;    %in Degrees! %180-Theta_2i_start;

% x0=[ oX ; oCap_Theta_1 ; oCap_Theta_2 ; oDf];
% v less than 4 can be done using 1 -- 0.05 -- L=10

count=0;
for ii= [5 6 8 10 12 14 16 18 20 25 30 40 50 70 100]
%v_start:v_stp:v_end;
    for jj=Theta_1_start:Theta_1_stp:Theta_1_end;
```

151

```matlab
        for kk=jj:Theta_2i_stp:Theta_2i_end;
            for ll=kk:Theta_2_stp:Theta_2_end;
                count=count+1;
            end
        end
    end
end


Sol_mat=[];
%%bx_mat=[];
%%bx_max_mat=[];
Cap_Theta_1_max_mat=[];
%--Cap_Theta_1_Limit_mat=[];

counter=count;
for Theta_1 = deg2rad([ round(Theta_1_start : Theta_1_stp :
Theta_1_end) ]);

for v = [5 6 8 10 12 14 16 18 20 25 30 40 50 70 100];
%round(v_start : v_stp : v_end);

for Theta_2i = deg2rad([ (rad2deg(Theta_1) : Theta_2i_stp :
Theta_2i_end)]);

    %rad2deg(Theta_2i)
    m = sin(Theta_1)/sin(Theta_2i);

    L1 = 1;                            % Using unit element
    L2 = L1*m;
    gama = 0.85;

    L11= (1-gama)*L1;
    L12= gama*L1;

    L21= gama*L2/2;
    L22= (1-gama)*L2;
    L23= gama*L2/2;

    oX = L1*cos(Theta_1)+L2*cos(Theta_2i);   %z(1)
    oCap_Theta_1 = deg2rad(11);              %z(2)
    oCap_Theta_2 = deg2rad(1e-2);            %z(3)
    oDf = 1e-3 ;                             %z(4)

    x0=[ oX ; oCap_Theta_1 ; oCap_Theta_2 ; oDf];

Sol_mat_s=[];
```

```matlab
bx_mat_s=[];
Cap_Theta_1_mat_s=[];
Cap_Theta_1_Limit_mat_s=[];


Theta_2_start = rad2deg(Theta_2i);

for Theta_2 = deg2rad([ Theta_2_start : Theta_2_stp :
Theta_2_end ]);

    iter= [counter
rad2deg(Theta_1),v,rad2deg(Theta_2i),rad2deg(Theta_2)]
    %rad2deg(Theta_2)
    %options =optimset('fsolve');
    opts2=optimset('MaxFunEvals',5e6, 'MaxIter',5e6,
'TolFun',5e-5);


    [z2,fval2] = fsolve(@Equ2 ,x0 ,opts2);

    X = z2(1);
    Cap_Theta_1 = rad2deg(z2(2));
    Cap_Theta_2 = rad2deg(z2(3));
    Df = z2(4);
    fval2;

    if Cap_Theta_2 > 90
        Cap_Theta_2 = oCap_Theta_2;
    else
        Cap_Theta_2;
    end

% % %      Cap_Theta_2=0;
    x1=[ x0(1,1) ; x0(2,1) ; x0(4,1)];

        if  Cap_Theta_2 < 0.1
            %rad2deg(Theta_2)
            opts1=optimset('MaxFunEvals',5e6, 'MaxIter',5e6,
'TolFun',5e-6);
            %x1=[ x0(1,1) ; x0(2,1) ; x0(4,1)]
            [z1,fval1] = fsolve(@Equ1 ,x1 ,opts1);

            X = z1(1);
            Cap_Theta_1 = rad2deg(z1(2));
            Cap_Theta_2 = 1e-7;
            Df = z1(3);
            fval1;
```

```matlab
        end

        opts1=optimset('MaxFunEvals',5e6, 'MaxIter',5e6,
'TolFun',5e-6);
        [z1L] = fsolve(@Equ1 ,x1 ,opts1);
        Cap_Theta_1_Limit = rad2deg(z1L(2));



    x0=[ X ; abs(deg2rad(Cap_Theta_1)) ;
abs(deg2rad(Cap_Theta_2)) ; Df];

% X2=roundn([x0(1,1);rad2deg(x0(2:3,1));x0(4,1)],-4);

    if abs(X) < 0.0001
        X = 0;
    end
    if abs(Cap_Theta_1) < 0.001
        Cap_Theta_1 = 0;
    end
    if abs(Cap_Theta_2) < 0.00001
        Cap_Theta_2 = 0;
    end
    if or(abs(Df) < 0.0001, abs(Df) > 1)
        Df = 0;
    end

    %%b = gama*L1*sin(Theta_1+deg2rad(Cap_Theta_1))+(1-
gama)*L1*sin(Theta_1);

    Sol_mat=[Sol_mat;
rad2deg(Theta_1),v,rad2deg(Theta_2i),rad2deg(Theta_2),X,Cap_Thet
a_1,Cap_Theta_2,Df];
    Sol_mat_s=[Sol_mat_s;
rad2deg(Theta_1),v,rad2deg(Theta_2i),rad2deg(Theta_2),X,Cap_Thet
a_1,Cap_Theta_2,Df];

    %%bx_mat=[bx_mat;
rad2deg(Theta_1),v,rad2deg(Theta_2i),rad2deg(Theta_2),b,X];
    %%bx_mat_s=[bx_mat_s;
rad2deg(Theta_1),v,rad2deg(Theta_2i),rad2deg(Theta_2),b,X];
    %%b_max=max(bx_mat_s(:,5));
    %%X_max=max(Sol_mat_s(:,5));

    %%b_over_x= b_max/X_max;
```

```matlab
    Cap_Theta_1_mat_s=[Cap_Theta_1_mat_s;
rad2deg(Theta_1),v,rad2deg(Theta_2i),Theta_2,Cap_Theta_1];
    Cap_Theta_1_Limit_mat_s=[Cap_Theta_1_Limit_mat_s;
rad2deg(Theta_1),rad2deg(Theta_2i),Theta_2,Cap_Theta_1_Limit];

%     if round(Cap_Theta_2) > 0
%         Cap_Theta_1_max = Cap_Theta_1;
%         Cap_Theta_1_max_mat=[ Cap_Theta_1_max_mat;
rad2deg(Theta_1),v,rad2deg(Theta_2i),Cap_Theta_1_max];
%         break
%     end
counter=counter-1;
save('PRBSM09')
end %for Theta_2
save('PRBSM09')


    Cap_Theta_1_max=max(Cap_Theta_1_mat_s(:,5));
    Cap_Theta_1_max_mat=[ Cap_Theta_1_max_mat;
rad2deg(Theta_1),v,rad2deg(Theta_2i),Cap_Theta_1_max];

    Cap_Theta_1_Limit_max=max(Cap_Theta_1_Limit_mat_s(:,4));

%Cap_Theta_1_Limit_mat=[Cap_Theta_1_Limit_mat;
rad2deg(Theta_1),rad2deg(Theta_2i),Cap_Theta_1_Limit_max];
%bx_max_mat=[bx_max_mat;
rad2deg(Theta_1),v,rad2deg(Theta_2i),b_max,X_max,b_over_x];

    if round(Cap_Theta_1_max*100)/100 >=
round(Cap_Theta_1_Limit_max*100)/100;,break, end



end %for Theta_2i
save('PRBSM09')
end %for Theta_1
save('PRBSM09')
end %for v
save('PRBSM09')

fprintf('        Theta_1          v       Theta_2i      Theta_2
X      Cap_Theta_1     Cap_Theta_2      Df')
Sol_mat
%%fprintf('        Theta_1         v       Theta_2i
Theta_2      b             X')
%%bx_mat
```

```matlab
%%fprintf('         Theta_1        v        Theta_2i     b
X          b/X')
%%bx_max_mat
fprintf('         Theta_1        v        Theta_2i
Cap_Theta_1_max')
Cap_Theta_1_max_mat
%--Cap_Theta_1_Limit_mat


%----------------------------------------
%  Defining Equations 3.9, 3.10 and 3.19
%----------------------------------------

function Fun1=Equ1(z1)
%     Fun=[-
X+L11*cos(Theta_1)+L12*cos(Theta_1+Cap_Theta_1)+L2*cos(Theta_2);
%     L11*sin(Theta_1)+L12*sin(Theta_1+Cap_Theta_1)-
L2*sin(Theta_2);
%     Df+Cap_Theta_1*(-
1)*(L1*cos(Theta_2))/(L12*sin(Cap_Theta_1+Theta_1+Theta_2)
%     ]

Fun1=[-
z1(1)+L11*cos(Theta_1)+L12*cos(Theta_1+z1(2))+L2*cos(Theta_2);
    L11*sin(Theta_1)+L12*sin(Theta_1+z1(2))-L2*sin(Theta_2);
    z1(3)-
z1(2)*(L1*cos(Theta_2))/(L12*sin(z1(2)+Theta_1+Theta_2))
    ];
end

%-----------------------------------------------
%  Defining Equations 3.20, 3.21, 3.30 and 3.31
%-----------------------------------------------

function Fun2=Equ2(z2)
% Fun=[-
X+L11*cos(Theta_1)+L12*cos(Theta_1+Cap_Theta_1)+L21*cos(Theta_2-
Cap_Theta_2)+L22*cos(Theta_2)+L23*cos(Theta_2+Cap_Theta_2);
%     L11*sin(Theta_1)+L12*sin(Theta_1+Cap_Theta_1)-
L21*sin(Theta_2-Cap_Theta_2)-L22*sin(Theta_2)-
L23*sin(Theta_2+Cap_Theta_2);
%
Df+Cap_Theta_1*(L1*sin(Theta_2))/(L12*cos(Cap_Theta_1+Theta_1+Th
eta_2))+2*(L1/v)*Cap_Theta_2*(-
1)*(cos(Cap_Theta_1+Theta_1))/(2*L21*cos(Cap_Theta_1+Theta_1)*co
s(Theta_2)*sin(Cap_Theta_2)-
2*L21*sin(Cap_Theta_1+Theta_1)*sin(Theta_2)*sin(Cap_Theta_2));
```

156

```matlab
%
Cap_Theta_1*(L22+2*L21*cos(Cap_Theta_2))/(L12*cos(Cap_Theta_1+Th
eta_1+Theta_2))+2*(1/v)*Cap_Theta_2*(L22*sin(Cap_Theta_1+Theta_1
+Theta_2)+L21*sin(Cap_Theta_1+Cap_Theta_2+Theta_1+Theta_2)+L21*s
in(Cap_Theta_1-
Cap_Theta_2+Theta_1+Theta_2))/(L21*(sin(Cap_Theta_1-
Cap_Theta_2+Theta_1+Theta_2)-
sin(Cap_Theta_1+Cap_Theta_2+Theta_1+Theta_2)))
%     ]

Fun2=[
    -
z2(1)+L11*cos(Theta_1)+L12*cos(Theta_1+z2(2))+L21*cos(Theta_2-
z2(3))+L22*cos(Theta_2)+L23*cos(Theta_2+z2(3));
    L11*sin(Theta_1)+L12*sin(Theta_1+z2(2))-L21*sin(Theta_2-
z2(3))-L22*sin(Theta_2)-L23*sin(Theta_2+z2(3));

z2(4)+z2(2)*(L1*sin(Theta_2))/(L12*cos(z2(2)+Theta_1+Theta_2))+2
*(L1/v)*z2(3)*(-
1)*(cos(z2(2)+Theta_1))/(2*L21*cos(z2(2)+Theta_1)*cos(Theta_2)*s
in(z2(3))-2*L21*sin(z2(2)+Theta_1)*sin(Theta_2)*sin(z2(3)));

z2(2)*(L22+2*L21*cos(z2(3)))/(L12*cos(z2(2)+Theta_1+Theta_2))+2*
(1/v)*z2(3)*(L22*sin(z2(2)+Theta_1+Theta_2)+L21*sin(z2(2)+z2(3)+
Theta_1+Theta_2)+L21*sin(z2(2)-
z2(3)+Theta_1+Theta_2))/(L21*(sin(z2(2)-z2(3)+Theta_1+Theta_2)-
sin(z2(2)+z2(3)+Theta_1+Theta_2)))
    ];
end


save('PRBSM09')
load('PRBSM09')
end
```

157

C.3 Grouping the Solution by the θ_1

```
%-----------------------------------------------------
%  NOTE:
%  The LBCCSM Model code PRBSM09.m used to solve for
%  the individual Theta_1. The resulting PRBSM09.mat
%  files were combined into one single file called
%  All_Sol_Mat.mat to be use in the plotting code.
%-----------------------------------------------------

clc
clear all
format shortG

load('All_Sol_Mat.mat')

% v_start = 5;
% v_stp = 2;
% v_end = 5;

Theta_1_start = 20 ; %in Degrees!
Theta_1_stp = 10; %in Degrees!
Theta_1_end = 80; %in Degrees!

%Theta_2i_start = Theta_1_start
%Theta_2i_start = 50; %in Degrees!
%Theta_2i_stp = 1; %in Degrees! 2.5  1 1.5  1(50 60) 1(70) 1(80)
Theta_2i_end = 85; %in Degrees! 50  85

%Theta_2_start = Theta_2i_start; %and could be bigger than
Theta_1_start!
%Theta_2_start = 20; %in Degrees!
%Theta_2_stp = 0.01; %in Degrees! 0.1  1 0.05  0.01(50 60)
0.005(70) 0.005(80)
%Theta_2_end = 85; %180-Theta_2i_start;
%Theta_2_end = 120; %in Degrees!


Sol_mat=[];
Sol_max_mat=[];


L= size(Cap_Theta_1_max_limit_mat);
row_start= 1;


% % L_start = 0;
```

```matlab
for Theta_1 = [20 30 40 50 60 70 80]; %round(Theta_1_start :
Theta_1_stp : Theta_1_end);
Theta_1;
ms= 1; me= 0;
ps= 1; pe=0;

    if Theta_1 == 20;, Sol_mat= Sol_mat_20;
        elseif Theta_1 == 30;, Sol_mat= Sol_mat_30;
            elseif Theta_1 == 40;, Sol_mat= Sol_mat_40;
                elseif Theta_1 == 50;, Sol_mat= Sol_mat_50;
                    elseif Theta_1 == 60;, Sol_mat= Sol_mat_60;
                        elseif Theta_1 == 70;, Sol_mat=
Sol_mat_70;
                            elseif Theta_1 == 80;, Sol_mat=
Sol_mat_80;, end

n= size(Sol_mat);

% % for LL = 1 : 1 : L(1,1);
% %     if Cap_Theta_1_max_limit_mat(LL,1)== z_Theta_1;
% %         L_start= LL;
% %          break
% %     end
% % end
% % L_end= LL + [(Theta_2i_end - z_Theta_1)];


for v = [2 3 4 5 6 8 10 12 14 16 18 20 25 30 40 50 70 100];
%round(v_start : v_stp : v_end);
v;
    if and( Theta_1 <= 40, v >= 5);
        Theta_2i_stp = 2.5;
    else
        Theta_2i_stp = 1;
    end
Theta_2i_stp;


    for k = row_start : 1 : n(1,1);
    if and( round(Sol_mat(k,1)) == round(Theta_1) , Sol_mat(k,2)
== v);
        pe=pe+1;
    end,end
    Theta_2i_max= max(Sol_mat(ps:pe,3));
    ps = pe +1;
```

```matlab
for Theta_2i = round(Theta_1 : Theta_2i_stp : Theta_2i_max);
Theta_2i;

iter= [ Theta_1 v Theta_2i ]

Sol_mat_s=[];


    for j = row_start : 1 : n(1,1);
    if and( round(Sol_mat(j,1)) == round(Theta_1) , Sol_mat(j,2)
== v);
        if Sol_mat(j,3) == Theta_2i;
        me=me+1;
%     else
%         break
    end,end,end

%count
%me = ms + count -1

Sol_mat_s = Sol_mat(ms:me,:);
Cap_Theta_1_max = max(Sol_mat_s(:,6));
Df_max = max(Sol_mat_s(:,8));

Sol_max_mat=[ Sol_max_mat; Theta_1, v, Theta_2i,
Cap_Theta_1_max, Df_max];

ms = me +1;

end %for Theta_2i
save('PRBSM10')
end %for v
save('PRBSM10')
end %for Theta_1
save('PRBSM10')

fprintf('      Theta_1      v      Theta_2i    THETA_1_max
Df_max')
Sol_max_mat

save('PRBSM10')
load('PRBSM10')
```

C.4 Plotting (b_{max}/X) vs. (θ_{2i}) Over Range of (v)

```matlab
%-------------------------------------------
%   PRBSM08b should be open also and RUN first
%-------------------------------------------

clc
clear all
clear figure

load('PRBSM08b.mat')
fprintf('        Theta_1        v        Theta_2i       b
X          b/X')
bx_max_mat
%fprintf('        Theta_1        v        Theta_2i
Cap_Theta_1')
%Cap_Theta_1_max_mat
n= size(bx_max_mat);
ms= 1;
me= 0;
row_start= 1;

Theta_2i_start = Theta_1_start;
Theta_2i_end = 85; %in Degrees!

bx_Limits_mat=[];

L_start = 1;
L_end = (Theta_2i_end - Theta_1_start)/Theta_2i_stp + 1;

for z_Theta_1 =Theta_1_start : Theta_1_stp : Theta_1_end
z_Theta_1;

for v = [1 2 3 4 5 6 8 10 12 14 16 18 20 25 30 40 50 70 100 150
200 250 500]
v;
for j = row_start : 1 : n(1,1);
j;
    if and(bx_max_mat(j,2) == v , round(bx_max_mat(j,1)) ==
round(z_Theta_1))
        me=me+1;
    else
        break
    end

end
```

```matlab
figure(z_Theta_1)   % b/x
hold on
grid on
plot3(bx_max_mat(ms:me,6),bx_max_mat(ms:me,3),repmat(z_Theta_1,s
ize(bx_max_mat(ms:me,6))))
text(bx_max_mat(me,6)+0.05,bx_max_mat(me,3)+0.5,['v =
',num2str(v)])
ylim([z_Theta_1 90])
xlabel('b_m_a_x/X')
ylabel('\theta_2_i [deg]')
set(gca,'xminortick','on')
set(gca,'Yminortick','on')
set(gca,'xminorgrid','on')
set(gca,'yminorgrid','on')
%title('b_m_a_x/X vs \theta_2_i for different (v) value')
hold off

row_start= me+1;
ms= me+1;

end

Theta_2i_start = z_Theta_1;

for Theta_2i = deg2rad([ Theta_2i_start : Theta_2i_stp :
Theta_2i_end]);

    m = sin(deg2rad(z_Theta_1))/sin(Theta_2i);
    b_over_x_maxL= m/(cos(deg2rad(z_Theta_1))+cos(Theta_2i)*m);
    b_over_x_minL=
sin(deg2rad(z_Theta_1))/(cos(deg2rad(z_Theta_1))+cos(Theta_2i)*m
);

    bx_Limits_mat= [bx_Limits_mat;
z_Theta_1,rad2deg(Theta_2i),b_over_x_maxL,b_over_x_minL];


end

figure(z_Theta_1)
%grid on
hold on
%plot(bx_Limits_mat(:,2),bx_Limits_mat(:,1))
%plot(bx_Limits_mat(:,3),bx_Limits_mat(:,1))
plot3(bx_Limits_mat(L_start:L_end,3),bx_Limits_mat(L_start:L_end
,2),repmat(z_Theta_1,size(bx_Limits_mat(L_start:L_end,3)))),'k','
LineWidth',2) %Max Limit  ,'k','LineWidth',2
```

```matlab
plot3(bx_Limits_mat(L_start:L_end,4),bx_Limits_mat(L_start:L_end
,2),repmat(z_Theta_1,size(bx_Limits_mat(L_start:L_end,4)))),'k','
LineWidth',2) %Min Limit
% set(gca,'XTick',0:0.02:bx_Limits_mat(1,3))
% set(gca,'YTick',Theta_1_start:5:90)
hold off

 L_start= L_end + 1;
 L_end= L_end +(Theta_2i_end/Theta_2i_stp) - (z_Theta_1 +
Theta_1_stp) + 1;

end

fprintf('         Theta_1    Theta_2i   b/x MaxL     b/x MinL')
bx_Limits_mat;

save('drawing08b')
```

C.5 Plotting (Θ_1) vs (θ_{2i}) Over Range of (v)

```matlab
%---------------------------------------------
%   PRBSM10 should be open also and RUN first
%---------------------------------------------

clc
clear all
clear figure

load('PRBSM10 - 2.mat')
fprintf('         Theta_1          v          Theta_2i
THETA_1_maxL')
Cap_Theta_1_max_limit_mat
fprintf('         Theta_1          v          Theta_2i  Df_maxL')
Df_max_limit_mat
fprintf('         Theta_1          v          Theta_2i    THETA_1_max
Df_max')
Sol_max_mat

n= size(Sol_max_mat);
L= size(Cap_Theta_1_max_limit_mat);
Y= size(Df_max_limit_mat);
ms= 1;
me= 0;
row_start= 1;

Theta_2i_end = 85; %in Degrees!


Lt_start = 0;

C_L={'bd-','rd-','gd-','bo-','ro-','go-', ...
    'b+-','r+-','g+-','bx-','rx-','gx-', ...
    'b*-','r*-','g*-','b.-','r.-','g.-'};


for z_Theta_1 = [20 30 40 50 60 70 80]
z_Theta_1;
i=0;
for LL = 1 : 1 : L(1,1);
    if Cap_Theta_1_max_limit_mat(LL,1)== z_Theta_1;
        Lt_start= LL;
         break
    end
end
Lt_end= LL + [(Theta_2i_end - z_Theta_1)];
```

164

www.manaraa.com

```matlab
for v = [2 3 4 5 6 8 10 12 14 16 18 20 25 30 40 50 70 100]
%v_start : v_stp : v_end; %[1 2 3 4 5 6 8 10 12 14 16 18 20 25
30 40 50 70 100 150 200 250 500] %v_start : v_stp : v_end;
%round(logspace(log10(5), log10(500),15))
v;
i=i+1;
for j = row_start : 1 : n(1,1);
j;
    if and(Sol_max_mat(j,2) == v , round(Sol_max_mat(j,1)) ==
round(z_Theta_1))
        me=me+1;
    else
        break
    end

end

figure(z_Theta_1)
hold on
grid on
plot3(Sol_max_mat(ms:me,4),Sol_max_mat(ms:me,3),repmat(z_Theta_1
,size(Sol_max_mat(ms:me,3))),C_L{i}) %  ,'LineSmoothing','on'
%text(Sol_max_mat(ms,3),Sol_max_mat(ms,4),num2str(v))
% ylim([z_Theta_1 85])
xlim([0 90]) % original ylim([0 90-z_Theta_1+5])
% set(gca,'YTick',[z_Theta_1 : 1 : 85])
% set(gca,'XTick',[0 : 1 : 20])
% set(gca,'xminortick','on')
% set(gca,'Yminortick','on')
% set(gca,'xminorgrid','on')
% set(gca,'yminorgrid','on')
ylabel('\theta_2_i [deg]')
xlabel('\Theta_1 [deg]')
%title('\Theta1 vs \theta2i for different (v) value')
mytitle=sprintf('(\\theta_1=%d^o)      \\Theta_1 vs \\theta_2_i
for different (v) values',z_Theta_1);
% title(mytitle)
%legend('2', '3', '4', '5', '6', '8', '10', '12', '14', '16',
'18', '20', '25', '30', '40', '50', '70',
'100','Location','East')
hold off

row_start= me+1;
ms= me+1;
```

```matlab
end

figure(z_Theta_1)
hold on
plot3(Cap_Theta_1_max_limit_mat(Lt_start:Lt_end,4),Cap_Theta_1_m
ax_limit_mat(Lt_start:Lt_end,3),repmat(z_Theta_1,size(Cap_Theta_
1_max_limit_mat(Lt_start:Lt_end,3))),'k','LineWidth',2) %Max
Limit  ,'k','LineWidth',2  ,'LineSmoothing','on'
legend('v=2', 'v=3', 'v=4', 'v=5', 'v=6', 'v=8', 'v=10', 'v=12',
'v=14', 'v=16', 'v=18', 'v=20', 'v=25', 'v=30', 'v=40', 'v=50',
'v=70', 'v=100','location','East')
% set(gca,'XTick',z_Theta_1:2:Theta_2i_end)
% set(gca,'YTick',Theta_1_start:5:90)
hold off

 %print figure(z_Theta_1) -dtiff -r600

end

save('drawing10Theta')
```

C.6 Plotting (f) vs (θ_{2i}) Over Range of (v) for the First Approach

```matlab
%-----------------------------------------------
%   PRBSM10 should be open also and RUN first
%-----------------------------------------------
% The non-dimensional force for the first approach
%-----------------------------------------------

clc
clear all
clear figure

load('PRBSM10 - 2.mat')
fprintf('        Theta_1        v       Theta_2i
THETA_1_maxL')
Cap_Theta_1_max_limit_mat
fprintf('        Theta_1        v        Theta_2i  Df_maxL')
Df_max_limit_mat
fprintf('        Theta_1        v       Theta_2i   THETA_1_max
Df_max')
Sol_max_mat

n= size(Sol_max_mat);
L= size(Cap_Theta_1_max_limit_mat);
Y= size(Df_max_limit_mat);
ms= 1;
me= 0;
row_start= 1;

Theta_2i_end = 85; %in Degrees!

Lf_start = 0;

C_L={'bd-','rd-','gd-','bo-','ro-','go-', ...
     'b+-','r+-','g+-','bx-','rx-','gx-', ...
     'b*-','r*-','g*-','b.-','r.-','g.-'};

for z_Theta_1 = [20 30 40 50 60 70 80]
z_Theta_1;
i=0;
for YY = 1 : 1 : Y(1,1);
    if Df_max_limit_mat(YY,1)== z_Theta_1;
        Lf_start= YY;
         break
    end
end
Lf_end= YY + [(Theta_2i_end - z_Theta_1)];
```

```matlab
for v = [2 3 4 5 6 8 10 12 14 16 18 20 25 30 40 50 70 100]
v;
i=i+1;
for j = row_start : 1 : n(1,1);
j;
    if and(Sol_max_mat(j,2) == v , round(Sol_max_mat(j,1)) ==
round(z_Theta_1))
        me=me+1;
    else
        break
    end

end

%%ys =
smooth(Cap_Theta_1_max_mat(ms:me,3),Cap_Theta_1_max_mat(ms:me,4)
,10,'rloess');

figure(z_Theta_1)
hold on
grid on
plot3(Sol_max_mat(ms:me,5),Sol_max_mat(ms:me,3),repmat(z_Theta_1
,size(Sol_max_mat(ms:me,5))),C_L{i}) %  ,'LineSmoothing','on'
% text(Sol_max_mat(me,5)+0.03,Sol_max_mat(me,3),['v=
',num2str(v)])
% xlim([0 0.4])
ylim([z_Theta_1 85]) % 90 original
% set(gca,'XTick',[0 : 0.04 : 0.4])
% set(gca,'YTick',[z_Theta_1 : 2 : 85])
% set(gca,'xminortick','on')
% set(gca,'Yminortick','on')
% set(gca,'xminorgrid','on')
% set(gca,'yminorgrid','on')
xlabel('Df')
ylabel('\theta_2_i [deg]')
%title('Df vs \theta2i for different (v) value')
mytitle=sprintf('(\\theta_1=%d^o)      Df vs \\theta_2_i for
different (v) values',z_Theta_1);
% % title(mytitle)
hold off

row_start= me+1;
ms= me+1;

end
```

```matlab
figure(z_Theta_1)
hold on
plot3(Df_max_limit_mat(Lf_start:Lf_end,4),Df_max_limit_mat(Lf_st
art:Lf_end,3),repmat(z_Theta_1,size(Df_max_limit_mat(Lf_start:Lf
_end,4))),'k','LineWidth',2) %Max Limit  ,'k','LineWidth',2
,'LineSmoothing','on'
legend('v=2', 'v=3', 'v=4', 'v=5', 'v=6', 'v=8', 'v=10', 'v=12',
'v=14', 'v=16', 'v=18', 'v=20', 'v=25', 'v=30', 'v=40', 'v=50',
'v=70', 'v=100','location','East')
% set(gca,'XTick',z_Theta_1:2:Theta_2i_end)
% set(gca,'YTick',Theta_1_start:5:90)
hold off

end
save('drawing10Df')
```

C.7 Plotting (J) vs (θ_{2i}) Over Range of (v) for the Second Approach

```matlab
%-----------------------------------------------
%   PRBSM10 should be open also and RUN first
%-----------------------------------------------
% The non-dimensional force for the second approach
%-----------------------------------------------

clc
clear all
clear figure

load('PRBSM10 - 2.mat')
fprintf('          Theta_1         v        Theta_2i
THETA_1_maxL')
Cap_Theta_1_max_limit_mat
fprintf('          Theta_1         v         Theta_2i  Df_maxL')
Df_max_limit_mat
fprintf('          Theta_1         v        Theta_2i   THETA_1_max
Df_max')
Sol_max_mat

C_L={'bd-','rd-','gd-','bo-','ro-','go-', ...
     'b+-','r+-','g+-','bx-','rx-','gx-', ...
     'b*-','r*-','g*-','b.-','r.-','g.-'};

rr = 1;             % =0 for LOW ,, =1 for HIGH

if rr == 0;
    vv=[2 3 4 5 6 8 10 12 14 16 18 20];
    else vv=[25 30 40 50 70 100]; end

for z_Theta_1 = [20 30 40 50 60 70] %Theta_1_start : Theta_1_stp
: Theta_1_end
z_Theta_1;
i=0;
row_start= 1;

if round(z_Theta_1) == round(20)
    if rr == 0;
    Sol_max_mat = J_20_low;
    figure(z_Theta_1)
    hold on
    xlim([20 46])
    ylim([0 0.9])
    set(gca,'XTick',[20 : 2 : 46])
    set(gca,'YTick',[0 : 0.1 : 0.9])
```

170

```
    hold off
    else
    Sol_max_mat = J_20_high;
    figure(z_Theta_1)
    hold on
    xlim([20 66])
    ylim([0 20])
    set(gca,'XTick',[20 : 2 : 66])
    set(gca,'YTick',[0 : 2 : 20])
    hold off
    end
end
if round(z_Theta_1) == round(30)
    if rr == 0;
    Sol_max_mat = J_30_low;
    figure(z_Theta_1)
    hold on
    xlim([30 60])
    ylim([0 1.2])
    set(gca,'XTick',[30 : 2 : 60])
    set(gca,'YTick',[0 : 0.1 : 1.2])
    hold off
    else
    Sol_max_mat = J_30_high;
    figure(z_Theta_1)
    hold on
    xlim([30 74])
    ylim([0 26])
    set(gca,'XTick',[30 : 2 : 74])
    set(gca,'YTick',[0 : 2 : 26])
    hold off
    end
end
if round(z_Theta_1) == round(40)
    if rr == 0;
    Sol_max_mat = J_40_low;
    figure(z_Theta_1)
    hold on
    xlim([40 66])
    ylim([0 1.3])
    set(gca,'XTick',[40 : 2 : 66])
    set(gca,'YTick',[0 : 0.1 : 1.3])
    hold off
    else
    Sol_max_mat = J_40_high;
    figure(z_Theta_1)
    hold on
```

```matlab
    xlim([40 80])
    ylim([0 30])
    set(gca,'XTick',[40 : 2 : 80])
    set(gca,'YTick',[0 : 2 : 30])
    hold off
    end
end
if round(z_Theta_1) == round(50)
    if rr == 0;
    Sol_max_mat = J_50_low;
    figure(z_Theta_1)
    hold on
    xlim([50 74])
    ylim([0 1.4])
    set(gca,'XTick',[50 : 2 : 74])
    set(gca,'YTick',[0 : 0.1 : 1.4])
    hold off
    else
    Sol_max_mat = J_50_high;
    figure(z_Theta_1)
    hold on
    xlim([50 80])
    ylim([0 34])
    set(gca,'XTick',[50 : 2 : 80])
    set(gca,'YTick',[0 : 2 : 34])
    hold off
    end
end
if round(z_Theta_1) == round(60)
    if rr == 0;
    Sol_max_mat = J_60_low;
    figure(z_Theta_1)
    hold on
    xlim([60 77])
    ylim([0 1.8])
    set(gca,'XTick',[60 : 1 : 77])
    set(gca,'YTick',[0 : 0.2 : 1.8])
    hold off
    else
    Sol_max_mat = J_60_high;
    figure(z_Theta_1)
    hold on
    xlim([60 83])
    ylim([0 40])
    set(gca,'XTick',[60: 1 : 83])
    set(gca,'YTick',[0 : 5 : 40])
    hold off
```

172

```matlab
        end
    end
    if round(z_Theta_1) == round(70)
        if rr == 0;
        Sol_max_mat = J_70_low;
        figure(z_Theta_1)
        hold on
        xlim([70 80])
        ylim([0 3.4])
        set(gca,'XTick',[70 : 1 : 80])
        set(gca,'YTick',[0 : 0.2 : 3.4])
        hold off
        else
        Sol_max_mat = J_70_high;
        figure(z_Theta_1)
        hold on
        xlim([70 84])
        ylim([0 70])
        set(gca,'XTick',[70 : 1 : 84])
        set(gca,'YTick',[0 : 5 : 70])
        hold off
        end
    end

    n= size(Sol_max_mat);
    ms= 1;
    me= 0;

    for v = vv ;
    v;
    i=i+1;
    for j = row_start : 1 : n(1,1);
    j;
        if and(round(Sol_max_mat(j,2)) == round(v) ,
    round(Sol_max_mat(j,1)) == round(z_Theta_1))
            me=me+1;
        else
            break
        end

    end

    figure(z_Theta_1)
    hold on
    grid on
    plot3(Sol_max_mat(ms:me,3),Sol_max_mat(ms:me,6),repmat(z_Theta_1
    ,size(Sol_max_mat(ms:me,3))),C_L{i}) %  ,'LineSmoothing','on'
```

173

```matlab
% text(Sol_max_mat(me,5)+0.03,Sol_max_mat(me,3),['v=
',num2str(v)])
% xlim([Sol_max_mat(ms,3) Sol_max_mat(me,3)])
% ylim([z_Theta_1 85]) % 90 original
% set(gca,'XTick',[Sol_max_mat(ms,3) : 1 : Sol_max_mat(me,3)])
% set(gca,'YTick',[z_Theta_1 : 2 : 85])
set(gca,'xminortick','on')
set(gca,'Yminortick','on')
set(gca,'xminorgrid','on')
set(gca,'yminorgrid','on')
xlabel('\theta_2_i [deg]')
ylabel('J')
%title('Df vs \theta2i for different (v) value')
mytitle=sprintf('(\\theta_1=%d^o)     Df vs \\theta_2_i for
different (v) values',z_Theta_1);
% % title(mytitle)
hold off

row_start= me+1;
ms= me+1;

end

figure(z_Theta_1)
hold on
%
plot3(Df_max_limit_mat(Lf_start:Lf_end,4),Df_max_limit_mat(Lf_st
art:Lf_end,3),repmat(z_Theta_1,size(Df_max_limit_mat(Lf_start:Lf
_end,4))),'k','LineWidth',2) %Max Limit  ,'k','LineWidth',2
,'LineSmoothing','on'
if rr == 0;
    legend('v=2', 'v=3', 'v=4', 'v=5', 'v=6', 'v=8', 'v=10',
'v=12', 'v=14', 'v=16', 'v=18', 'v=20','location','East')
else
    legend('v=25', 'v=30', 'v=40', 'v=50', 'v=70',
'v=100','location','East')
end
% set(gca,'XTick',z_Theta_1:2:Theta_2i_end)
% set(gca,'YTick',Theta_1_start:5:90)
hold off

end

save('drawing10Df2ndapp')
```

C.8 Cylindrical SMSF Morph Code

```matlab
clc, clear all
format short g

n=10;                          %number of sides "s"
m=4;                           %number of slice "k"

%--------------------
% 1st try: 10,4,150,70,-80, 11      Hyperbolic
% 2nd try: 10,4,150,-70,80, 22      Spherical
% 3rd try: 8,4,75,-35,-80
% 4th try:
%--------------------

ro_o= 150;                     %circumradius
a= 2*ro_o*sin(pi/n);           %side length   "ls"
h_o= m*a;                      %initial total height
h_f=000;                       % h_f should be > h_o
delta_ro= -70;                 %change in ro (minimum value along
the height)
Delta_theta= 80;               %total change in slice rotational
angle along the height
h_j=0;                         %the start height, first loop is
'zero' then changes

count=0;
error=0;
Sol_mat_p=[];    Sol_mat2_p=[];
Sol_mat_q=[];    Sol_mat2_q=[];
Sol_mat_q_r=[];  Sol_mat2_q_r=[];

L_p_mat=[]; L_q_mat=[]; L_q_r_mat=[];
Delta_mat=[];
rf= 100;                       %decimal rounding i.e. (100 ->
0.00)

bs_xb_p_mat=[];                %Points coordinates for Original
Shape j i=1,2
bs_xb_q_r_mat=[];              %Points coordinates for twist with
calculated height j i=1,2
Points_p_mat_f=[];             %Points coordinates for Original
Shape (vertical stripe) "FLAT"
Points_q_r_mat_f=[];           %Points coordinates for twist with
calculated height (vertical stripe) "FLAT"
Points_p_mat_t=[];             %Points coordinates for Original
Shape (original stripe) "TWIST"
```

175

```matlab
Points_q_r_mat_t=[];           %Points coordinates for twist with
calculated height (original stripe) "TWIST"



TAG=0;                         %adding Tag to points '[j i count]'
(Yes=1, No=0)
TAGc=1;                        %adding Tag to center of m (Yes=1,
No=0)
TAGs=1;                        %adding Tag to sids (Yes=1, No=0)
TAGd=0;                        %adding Tag to Diagonals (Yes=1,
No=0)
Diagonal=22;                   %showing Diagonal lines (Yes=11 to
the right, Yes=22 to the left, No=00)
Model_Check=1;                 %checking the model possibility!
(Yes=1, No=0)

[n m ro_o a h_o delta_ro Delta_theta];

for j= 1 : m+1;
    for i= 1 : n+1;
        [j i]; count=count+1;
        Theta_i_1= (2*pi/n)*(i-1);
        Theta_i= (2*pi/n)*(i);

        Delta_theta_j= (Delta_theta/m)*(j-1);
        Delta_Theta_j_1= (Delta_theta/m)*(j-2);
        Delta_theta_j_plus_1= (Delta_theta/m)*(j+1-1);

        h_o_j_1= (h_o/m)*(j-1);
        %%% h_j= (h_o/m)*(j);


        ro_factor_1= delta_ro * (1 - (2/h_o)^2 * (h_o/m)^2 * (j-
1-(m/2))^2);
        ro_factor_2= delta_ro * (1 - (2/h_o)^2 * (h_o/m)^2 *
(j+1-1-(m/2))^2);
        if abs(ro_factor_1)<0.0001, [j i];, ro_factor_1=0;, end
        if abs(ro_factor_2)<0.0001, [j i];, ro_factor_2=0;, end
        ro_j = ro_o - ro_factor_1;
        ro_j_plus_1 = ro_o - ro_factor_2;


        % Model possibility Check !!
        if Model_Check == 1
        ro_chk_1= 0;      %or same as -->   %delta_ro * (1 -
(2/h_o)^2 * (h_o/m)^2 * (1-1-(m/2))^2);
```

```matlab
        ro_chk_2=  delta_ro*(4*(m-1)/m^2);  %or same as -->
%delta_ro * (1 - (2/h_o)^2 * (h_o/m)^2 * (1+1-1-(m/2))^2);
        if or( ro_chk_1 > a, ro_chk_2 > a)
            error= 1, sprintf('Impossible Model !! decrease (n)
or increase (m) or decrease (delta_ro)'), break, end, end


        % original cylinder meshed
        p_i_1 =[ro_o * cos(Theta_i_1), ro_o * sin(Theta_i_1),
h_o_j_1];
        p_i =[ro_o * cos(Theta_i), ro_o * sin(Theta_i),
h_o_j_1];
        d_i = p_i - p_i_1;
        L_p=sqrt( d_i(1,1)^2 + d_i(1,2)^2 + d_i(1,3)^3);
        L_p_point=[(p_i(1,1)+p_i_1(1,1))/2,
(p_i(1,2)+p_i_1(1,2))/2, p_i_1(1,3)];


        % twisted cylinder with over all height = h_o
        q_i_1 =[ro_j * cos(Theta_i_1 + deg2rad(Delta_theta_j)),
ro_j * sin(Theta_i_1 + deg2rad(Delta_theta_j)),  h_o_j_1];
        q_i =[ro_j * cos(Theta_i + deg2rad(Delta_theta_j)), ro_j
* sin(Theta_i + deg2rad(Delta_theta_j)),  h_o_j_1];
        dd_i = q_i - q_i_1;
        L_q=sqrt( dd_i(1,1)^2 + dd_i(1,2)^2 + dd_i(1,3)^3);
        L_q_point=[(q_i(1,1)+q_i_1(1,1))/2,
(q_i(1,2)+q_i_1(1,2))/2, q_i_1(1,3)];


        % twisted cylinder with calculated height
        q_r_i_1 =[ro_j * cos(Theta_i_1 +
deg2rad(Delta_theta_j)), ro_j * sin(Theta_i_1 +
deg2rad(Delta_theta_j)),  h_j];
        q_r_i =[ro_j * cos(Theta_i + deg2rad(Delta_theta_j)),
ro_j * sin(Theta_i + deg2rad(Delta_theta_j)),  h_j];
        dd_r_i = q_r_i - q_r_i_1;
        L_q_r=sqrt( dd_r_i(1,1)^2 + dd_r_i(1,2)^2 +
dd_r_i(1,3)^3);
        L_q_r_point=[(q_r_i(1,1)+q_r_i_1(1,1))/2,
(q_r_i(1,2)+q_r_i_1(1,2))/2, q_r_i_1(1,3)];


        if i==1,
            L_p_mat=[L_p_mat; j 0 0 0 0 0];        L_p_mat(j,2)=
L_p;
            L_q_mat=[L_q_mat; j 0 0 0 0 0];        L_q_mat(j,2)=
L_q;
```

```matlab
                L_q_r_mat=[L_q_r_mat; j 0 0 0 0 0];
    L_q_r_mat(j,2)= L_q_r;
            end

        % replacing small number with "Zero"
        if abs(p_i_1(1,1))<0.0001, [j i];, p_i_1(1,1)=0;, end
        if abs(p_i_1(1,2))<0.0001, [j i];, p_i_1(1,2)=0;, end
        if abs(q_i_1(1,1))<0.0001, [j i];, q_i_1(1,1)=0;, end
        if abs(q_i_1(1,2))<0.0001, [j i];, q_i_1(1,2)=0;, end
        if abs(q_r_i_1(1,1))<0.0001, [j i];, q_r_i_1(1,1)=0;,
end
        if abs(q_r_i_1(1,2))<0.0001, [j i];, q_r_i_1(1,2)=0;,
end

        % Solution matrix
        Sol_mat_p=[Sol_mat_p; j i p_i_1 ro_o L_p count];
        Sol_mat_q=[Sol_mat_q; j i q_i_1 ro_j L_q count];
        Sol_mat_q_r=[Sol_mat_q_r; j i q_r_i_1 ro_j L_q_r count];

        Sol_mat2_p=[Sol_mat2_p; count j i ro_o 0 L_p];
        Sol_mat2_q=[Sol_mat2_q; count j i ro_j Delta_theta_j
L_q];
        Sol_mat2_q_r=[Sol_mat2_q_r; count j i ro_j Delta_theta_j
L_q_r];

        if or( i == 1, i ==2 )
            bs_xb_p_mat= [bs_xb_p_mat; j i p_i_1 ro_o 0 count];
            bs_xb_q_r_mat= [bs_xb_q_r_mat; j i q_r_i_1 ro_j
Delta_theta_j count];
        end


        figure(1)
        hold on
        %xlim([-100 100]), ylim([-100 100]), zlim([0
ceil(h_o/10)*10])
        set(gca,'XTick',[-150 : 50 : 150]), set(gca,'YTick',[-
150 : 50 : 150]), %set(gca,'ZTick',[0 : h_o])
        if and(i~=(n+1), TAG==1), text([p_i_1(1,1)],
[p_i_1(1,2)], [p_i_1(1,3)],['  ' num2str(j) ',' num2str(i) ','
num2str(count)]), end
        if and(i~=(n+1), TAGc==1), text([0], [0],
[p_i_1(1,3)],[num2str(p_i_1(1,3))]), end
                                 %, plot3([0], [0],
[p_i_1(1,3)],'b.','LineWidth',2), end
        % Drawing the links n
```

178

```matlab
        plot3([p_i(1,1)], [p_i(1,2)],
[p_i(1,3)],'r*','LineWidth',2)
        plot3([p_i_1(1,1) p_i(1,1)], [p_i_1(1,2) p_i(1,2)],
[p_i_1(1,3) p_i(1,3)],'k','LineWidth',2)
        if and(i==1, TAGs==1),
text([L_p_point(1,1)],[L_p_point(1,2)],[L_p_point(1,3)],['    '
num2str(L_p)]),
                                ,
plot3([L_p_point(1,1)],[L_p_point(1,2)],[L_p_point(1,3)],'b*','L
ineWidth',2), end
        hold off

        figure(2)
        hold on
        %xlim([-100 100]), ylim([-100 100]), zlim([0
ceil(h_o/10)*10])
        set(gca,'XTick',[-100 : 20 : 100]), set(gca,'YTick',[-
100 : 20 : 100]), %set(gca,'ZTick',[0 : h_o])
        if and(i~=(n+1), TAG==1), text([q_i_1(1,1)],
[q_i_1(1,2)], [q_i_1(1,3)],['  ' num2str(j) ',' num2str(i) ','
num2str(count)]), end
        if and(i~=(n+1), TAGc==1), text([0], [0],
[q_i_1(1,3)],[num2str(q_i_1(1,3))]), end
                                %, plot3([0], [0],
[q_i_1(1,3)],'b.','LineWidth',2), end
        % Drawing the links n
        plot3([q_i(1,1)], [q_i(1,2)],
[q_i(1,3)],'r*','LineWidth',2)
        plot3([q_i_1(1,1) q_i(1,1)], [q_i_1(1,2) q_i(1,2)],
[q_i_1(1,3) q_i(1,3)],'k','LineWidth',2)
        if and(i==1, TAGs==1),
text([L_q_point(1,1)],[L_q_point(1,2)],[L_q_point(1,3)],['    '
num2str(L_q)]),
                                ,
plot3([L_q_point(1,1)],[L_q_point(1,2)],[L_q_point(1,3)],'b*','L
ineWidth',2), end
        hold off

        figure(3)
        hold on
        %xlim([-100 100]), ylim([-100 100]), zlim([0
ceil(h_o/10)*10])
        set(gca,'XTick',[-150 : 50 : 150]), set(gca,'YTick',[-
150 : 50 : 150]), %set(gca,'ZTick',[0 : h_o])
        if and(i~=(n+1), TAG==1), text([q_r_i_1(1,1)],
[q_r_i_1(1,2)], [q_r_i_1(1,3)],['  ' num2str(j) ',' num2str(i)
',' num2str(count)]), end
```

```matlab
        if and(i~=(n+1), TAGc==1), text([0], [0],
[q_r_i_1(1,3)],[num2str(q_r_i_1(1,3))]), end
                                %, plot3([0], [0],
[q_r_i_1(1,3)],'b.','LineWidth',2), end
        % Drawing the links n
        plot3([q_r_i(1,1)], [q_r_i(1,2)],
[q_r_i(1,3)],'r*','LineWidth',2)
        plot3([q_r_i_1(1,1) q_r_i(1,1)], [q_r_i_1(1,2)
q_r_i(1,2)], [q_r_i_1(1,3) q_r_i(1,3)],'k','LineWidth',2)
        if and(i==1, TAGs==1),
text([L_q_r_point(1,1)],[L_q_r_point(1,2)],[L_q_r_point(1,3)],['
' num2str(L_q_r)]),
                                    ,
plot3([L_q_r_point(1,1)],[L_q_r_point(1,2)],[L_q_r_point(1,3)],'
b*','LineWidth',2), end
        hold off


    end


        % Model possibility Check !!
        if error== 1, sprintf('Impossible Model !! decrease (n)
or increase (m) or decrease (delta_ro)'), break, end

        % to find the height z with the twist
        if j < m+1
            i=1; j;
            qh_j_1 =[ro_j * cos(Theta_i_1 +
deg2rad(Delta_theta_j)), ro_j * sin(Theta_i_1 +
deg2rad(Delta_theta_j)),  h_j];
            qh_j =[ro_j_plus_1 * cos(Theta_i_1 +
deg2rad(Delta_theta_j_plus_1)), ro_j_plus_1 * sin(Theta_i_1 +
deg2rad(Delta_theta_j_plus_1))];
            if abs(qh_j_1(1,2))<0.001, [j i];, qh_j_1(1,2)=0;,
end
            if abs(qh_j(1,2))<0.001, [j i];, qh_j(1,2)=0;, end
            h_j =sqrt(a^2 - (qh_j(1,1) - qh_j_1(1,1))^2 -
(qh_j(1,2) - qh_j_1(1,2))^2 ) + h_j; % shorter
            %h_j =sqrt(a^2 + (qh_j(1,1) - qh_j_1(1,1))^2 +
(qh_j(1,2) - qh_j_1(1,2))^2 ) + h_j;  % longer
            h_j;
        end
```

180

```matlab
end


for j= 1 : m;

    % Model possibility Check !!
    if error== 1, sprintf('Impossible Model !! decrease (n) or
increase (m) or decrease (delta_ro)'), break, end

    for i= (1+(j-1)*(n+1)) : (j*(n+1));
        [j i (1+(j-1)*(n+1)) (j*(n+1))];


        if i~=(n+1)*j
            [j i n+1+i+1];

            L_p_m= sqrt( (Sol_mat_p(i,3)-Sol_mat_p(n+1+i,3))^2 +
(Sol_mat_p(i,4)-Sol_mat_p(n+1+i,4))^2 + (Sol_mat_p(i,5)-
Sol_mat_p(n+1+i,5))^2 );
            L_p_m_point= [
(Sol_mat_p(i,3)+Sol_mat_p(n+1+i,3))/2,
(Sol_mat_p(i,4)+Sol_mat_p(n+1+i,4))/2,
(Sol_mat_p(i,5)+Sol_mat_p(n+1+i,5))/2];
            L_p_d1= sqrt( (Sol_mat_p(i,3)-
Sol_mat_p(n+1+i+1,3))^2 + (Sol_mat_p(i,4)-
Sol_mat_p(n+1+i+1,4))^2 + (Sol_mat_p(i,5)-
Sol_mat_p(n+1+i+1,5))^2);
            L_p_d2= sqrt( (Sol_mat_p(i+1,3)-Sol_mat_p(n+1+i+1-
1,3))^2 + (Sol_mat_p(i+1,4)-Sol_mat_p(n+1+i+1-1,4))^2 +
(Sol_mat_p(i+1,5)-Sol_mat_p(n+1+i+1-1,5))^2);
            L_p_d1_point= [
(Sol_mat_p(i,3)+Sol_mat_p(n+1+i+1,3))/2,
(Sol_mat_p(i,4)+Sol_mat_p(n+1+i+1,4))/2,
(Sol_mat_p(i,5)+Sol_mat_p(n+1+i+1,5))/2];

            L_q_m= sqrt( (Sol_mat_q(i,3)-Sol_mat_q(n+1+i,3))^2 +
(Sol_mat_q(i,4)-Sol_mat_q(n+1+i,4))^2 + (Sol_mat_q(i,5)-
Sol_mat_q(n+1+i,5))^2 );
            L_q_m_point= [
(Sol_mat_q(i,3)+Sol_mat_q(n+1+i,3))/2,
(Sol_mat_q(i,4)+Sol_mat_q(n+1+i,4))/2,
(Sol_mat_q(i,5)+Sol_mat_q(n+1+i,5))/2];
            L_q_d1= sqrt( (Sol_mat_q(i,3)-
Sol_mat_q(n+1+i+1,3))^2 + (Sol_mat_q(i,4)-
Sol_mat_q(n+1+i+1,4))^2 + (Sol_mat_q(i,5)-
Sol_mat_q(n+1+i+1,5))^2);
```

```matlab
        L_q_d2= sqrt( (Sol_mat_q(i+1,3)-Sol_mat_q(n+1+i+1-
1,3))^2 + (Sol_mat_q(i+1,4)-Sol_mat_q(n+1+i+1-1,4))^2 +
(Sol_mat_q(i+1,5)-Sol_mat_q(n+1+i+1-1,5))^2);
        L_q_d1_point= [
(Sol_mat_q(i,3)+Sol_mat_q(n+1+i+1,3))/2,
(Sol_mat_q(i,4)+Sol_mat_q(n+1+i+1,4))/2,
(Sol_mat_q(i,5)+Sol_mat_q(n+1+i+1,5))/2];


        L_q_r_m= sqrt( (Sol_mat_q_r(i,3)-
Sol_mat_q_r(n+1+i,3))^2 + (Sol_mat_q_r(i,4)-
Sol_mat_q_r(n+1+i,4))^2 + (Sol_mat_q_r(i,5)-
Sol_mat_q_r(n+1+i,5))^2 );
        L_q_r_m_point= [
(Sol_mat_q_r(i,3)+Sol_mat_q_r(n+1+i,3))/2,
(Sol_mat_q_r(i,4)+Sol_mat_q_r(n+1+i,4))/2,
(Sol_mat_q_r(i,5)+Sol_mat_q_r(n+1+i,5))/2];
        L_q_r_d1= sqrt( (Sol_mat_q_r(i,3)-
Sol_mat_q_r(n+1+i+1,3))^2 + (Sol_mat_q_r(i,4)-
Sol_mat_q_r(n+1+i+1,4))^2 + (Sol_mat_q_r(i,5)-
Sol_mat_q_r(n+1+i+1,5))^2);
        L_q_r_d2= sqrt( (Sol_mat_q_r(i+1,3)-
Sol_mat_q_r(n+1+i+1-1,3))^2 + (Sol_mat_q_r(i+1,4)-
Sol_mat_q_r(n+1+i+1-1,4))^2 + (Sol_mat_q_r(i+1,5)-
Sol_mat_q_r(n+1+i+1-1,5))^2);
        L_q_r_d1_point= [
(Sol_mat_q_r(i,3)+Sol_mat_q_r(n+1+i+1,3))/2,
(Sol_mat_q_r(i,4)+Sol_mat_q_r(n+1+i+1,4))/2,
(Sol_mat_q_r(i,5)+Sol_mat_q_r(n+1+i+1,5))/2];


        if i==(1+(j-1)*(n+1)),
            L_p_mat(j,3)=L_p_mat(j+1,2);
L_p_mat(j,4)= L_p_m;       L_p_mat(j,5)= L_p_d1;
L_p_mat(j,6)= L_p_d2;
            L_q_mat(j,3)=L_q_mat(j+1,2);
L_q_mat(j,4)= L_q_m;       L_q_mat(j,5)= L_q_d1;
L_q_mat(j,6)= L_q_d2;
            L_q_r_mat(j,3)=L_q_r_mat(j+1,2);
L_q_r_mat(j,4)= L_q_r_m;    L_q_r_mat(j,5)= L_q_r_d1;
L_q_r_mat(j,6)= L_q_r_d2;
        end


        figure(1)
        hold on
        xlabel('X'),ylabel('Y'),zlabel('Z')
        % Drawing the links between m
```

```matlab
            plot3([Sol_mat_p(i,3) Sol_mat_p(n+1+i,3)],
[Sol_mat_p(i,4) Sol_mat_p(n+1+i,4)], [Sol_mat_p(i,5)
Sol_mat_p(n+1+i,5)],'b','LineWidth',2)
            if and(i==(1+(j-1)*(n+1)), TAGs==1),
text([L_p_m_point(1,1)],[L_p_m_point(1,2)],[L_p_m_point(1,3)],['
' num2str(L_p_m)]),
                , plot3([L_p_m_point(1,1)], [L_p_m_point(1,2)],
[L_p_m_point(1,3)],'b*','LineWidth',2), end
            % Drawing the Diagonal links
            if Diagonal==11, plot3([Sol_mat_p(i,3)
Sol_mat_p(n+1+i+1,3)], [Sol_mat_p(i,4) Sol_mat_p(n+1+i+1,4)],
[Sol_mat_p(i,5) Sol_mat_p(n+1+i+1,5)],'k','LineWidth',2), end
            if Diagonal==22, plot3([Sol_mat_p(i+1,3)
Sol_mat_p(n+1+i+1-1,3)], [Sol_mat_p(i+1,4) Sol_mat_p(n+1+i+1-
1,4)], [Sol_mat_p(i+1,5) Sol_mat_p(n+1+i+1-
1,5)],'k','LineWidth',2), end
            if and(i==(2+(j-1)*(n+1)), TAGd==1),
text([L_p_d1_point(1,1)],[L_p_d1_point(1,2)],[L_p_d1_point(1,3)]
,['    ' num2str(L_p_d1)]),
                , plot3([L_p_d1_point(1,1)], [L_p_d1_point(1,2)],
[L_p_d1_point(1,3)],'b*','LineWidth',2), end
            hold off


            figure(2)
            hold on
            xlabel('X'),ylabel('Y'),zlabel('Z')
            % Drawing the links between m
            plot3([Sol_mat_q(i,3) Sol_mat_q(n+1+i,3)],
[Sol_mat_q(i,4) Sol_mat_q(n+1+i,4)], [Sol_mat_q(i,5)
Sol_mat_q(n+1+i,5)],'b','LineWidth',1)
            if and(i==(1+(j-1)*(n+1)), TAGs==1),
text([L_q_m_point(1,1)],[L_q_m_point(1,2)],[L_q_m_point(1,3)],['
' num2str(L_q_m)]),
                , plot3([L_q_m_point(1,1)], [L_q_m_point(1,2)],
[L_q_m_point(1,3)],'b*','LineWidth',2), end
            % Drawing the Diagonal links
            if Diagonal==1, plot3([Sol_mat_q(i,3)
Sol_mat_q(n+1+i+1,3)], [Sol_mat_q(i,4) Sol_mat_q(n+1+i+1,4)],
[Sol_mat_q(i,5) Sol_mat_q(n+1+i+1,5)],'k','LineWidth',2), end
            if and(i==(2+(j-1)*(n+1)), TAGd==1),
text([L_q_d1_point(1,1)],[L_q_d1_point(1,2)],[L_q_d1_point(1,3)]
,['    ' num2str(L_q_d1)]),
                , plot3([L_q_d1_point(1,1)], [L_q_d1_point(1,2)],
[L_q_d1_point(1,3)],'b*','LineWidth',2), end
            hold off
```

```matlab
            figure(3)
            hold on
            xlabel('X'),ylabel('Y'),zlabel('Z')
            % Drawing the links between m
            plot3([Sol_mat_q_r(i,3) Sol_mat_q_r(n+1+i,3)],
[Sol_mat_q_r(i,4) Sol_mat_q_r(n+1+i,4)], [Sol_mat_q_r(i,5)
Sol_mat_q_r(n+1+i,5)],'b','LineWidth',2)
            if and(i==(1+(j-1)*(n+1)), TAGs==1),
text([L_q_r_m_point(1,1)],[L_q_r_m_point(1,2)],[L_q_r_m_point(1,
3)],['    ' num2str(L_q_r_m)]),
                , plot3([L_q_r_m_point(1,1)],
[L_q_r_m_point(1,2)], [L_q_r_m_point(1,3)],'b*','LineWidth',2),
end
            % Drawing the Diagonal links
            if Diagonal==11, plot3([Sol_mat_q_r(i,3)
Sol_mat_q_r(n+1+i+1,3)], [Sol_mat_q_r(i,4)
Sol_mat_q_r(n+1+i+1,4)], [Sol_mat_q_r(i,5)
Sol_mat_q_r(n+1+i+1,5)],'k','LineWidth',2), end
            if Diagonal==22, plot3([Sol_mat_q_r(i+1,3)
Sol_mat_q_r(n+1+i+1-1,3)], [Sol_mat_q_r(i+1,4)
Sol_mat_q_r(n+1+i+1-1,4)], [Sol_mat_q_r(i+1,5)
Sol_mat_q_r(n+1+i+1-1,5)],'k','LineWidth',2), end
            if and(i==(2+(j-1)*(n+1)), TAGd==1),
text([L_q_r_d1_point(1,1)],[L_q_r_d1_point(1,2)],[L_q_r_d1_point
(1,3)],['    ' num2str(L_q_r_d1)]),
                , plot3([L_q_r_d1_point(1,1)],
[L_q_r_d1_point(1,2)],
[L_q_r_d1_point(1,3)],'b*','LineWidth',2), end
            hold off


        end
    end
end

Sol_mat_p;
Sol_mat_q;
Sol_mat_q_r;

Sol_mat2_p;
Sol_mat2_q;
Sol_mat2_q_r;

Delta_mat(:,1)= L_q_r_mat(:,1);
Delta_mat(:,2)= L_q_r_mat(:,2)-L_p_mat(:,2);
Delta_mat(:,3)= L_q_r_mat(:,3)-L_p_mat(:,3);
```

```matlab
Delta_mat(:,4)= L_q_r_mat(:,4)-L_p_mat(:,4);
Delta_mat(:,5)= L_q_r_mat(:,5)-L_p_mat(:,5);
Delta_mat(:,6)= L_q_r_mat(:,6)-L_p_mat(:,6);


fprintf('            m        Bottom 2a    Top 3b        Side 4c
DiagonalR 5d  DiagonalL')
L_p_mat   = round(L_p_mat*rf)/rf
%fprintf('            m        Bottom 2a    Top 3b        Side 4c
DiagonalR 5d  DiagonalL')
%round(L_q_mat*rf)/rf
fprintf('            m        Bottom 2a    Top 3b        Side 4c
DiagonalR 5d  DiagonalL')
L_q_r_mat = round(L_q_r_mat*rf)/rf
Delta_mat = round(Delta_mat*rf)/rf


% Original Shape (vertical stripe)
xp1=0;                 yp1=0;                 yp3=0;
jump=0;
for j = 1 : m %ceil(m/2)

    xp2= xp1+ L_p_mat(j,2);
    yp2= yp1;
    xp3= (L_p_mat(j,5)^2 - L_p_mat(j,4)^2 +
L_p_mat(j,2)^2)/(2*L_p_mat(j,2)) + xp1;
    yp3= sqrt(abs(L_p_mat(j,4)^2 - (xp3 - L_p_mat(j,2))^2))
+yp3;
    %yp3= sqrt(L_p_mat(j,5)^2 - xp3^2) +yp3;
    xp4= xp3 - L_p_mat(j,3);
    yp4= yp3;

    if abs(xp4) < 0.1, xp4=0;, end

    [1 j; xp1 yp1; xp2 yp2; xp3 yp3; xp4 yp4];

    figure(4) % Figure 4 and initial 6 here are the same
    hold on
    %xlim([-10 a+10]), ylim([-10 ceil(m/2)*((h_o/m)+10)])
    plot([xp1 xp2], [yp1 yp2],'k:','LineWidth',1)
% Bottom
    plot([xp2 xp3], [yp2 yp3],'k:','LineWidth',1)
% Side Right
    plot([xp3 xp4], [yp3 yp4],'k:','LineWidth',1)
% Top
    plot([xp4 xp1], [yp4 yp1],'k:','LineWidth',1)
% Side Left
```

185

```matlab
    plot([xp1 xp3], [yp1 yp3],'k:','LineWidth',1)
% Diagonal
    hold off

    figure(6) % Figure 6 will be carried on
    hold on
    %xlim([-10 a+10]), ylim([-10 ceil(m/2)*((h_o/m)+10)])
    plot([xp1 xp2], [yp1 yp2],'k:','LineWidth',1)
% Bottom
    plot([xp2 xp3], [yp2 yp3],'k:','LineWidth',1)
% Side Right
    plot([xp3 xp4], [yp3 yp4],'k:','LineWidth',1)
% Top
    plot([xp4 xp1], [yp4 yp1],'k:','LineWidth',1)
% Side Left
    plot([xp1 xp3], [yp1 yp3],'k:','LineWidth',1)
% Diagonal
    hold off

    Points_p_mat_f(:,j)= [j; xp1; yp1; xp2; yp2; xp3; yp3; xp4;
yp4];

    xp1= xp4;           yp1= yp4;

    j=j+jump;
    figure(7)
    hold on
    plot3([bs_xb_p_mat(j,3) bs_xb_p_mat(j+1,3)],
[bs_xb_p_mat(j,4) bs_xb_p_mat(j+1,4)], [bs_xb_p_mat(j,5)
bs_xb_p_mat(j+1,5)],'k:','LineWidth',1)
    plot3([bs_xb_p_mat(j+1,3) bs_xb_p_mat(j+3,3)],
[bs_xb_p_mat(j+1,4) bs_xb_p_mat(j+3,4)], [bs_xb_p_mat(j+1,5)
bs_xb_p_mat(j+3,5)],'k:','LineWidth',1)
    plot3([bs_xb_p_mat(j+3,3) bs_xb_p_mat(j+2,3)],
[bs_xb_p_mat(j+3,4) bs_xb_p_mat(j+2,4)], [bs_xb_p_mat(j+3,5)
bs_xb_p_mat(j+2,5)],'k:','LineWidth',1)
    plot3([bs_xb_p_mat(j+2,3) bs_xb_p_mat(j,3)],
[bs_xb_p_mat(j+2,4) bs_xb_p_mat(j,4)], [bs_xb_p_mat(j+2,5)
bs_xb_p_mat(j,5)],'k:','LineWidth',1)
    plot3([bs_xb_p_mat(j,3) bs_xb_p_mat(j+3,3)],
[bs_xb_p_mat(j,4) bs_xb_p_mat(j+3,4)], [bs_xb_p_mat(j,5)
bs_xb_p_mat(j+3,5)],'k:','LineWidth',1)
    hold off

    Points_p_mat_t(:,j-jump)= [j-jump;
bs_xb_p_mat(j+0,3);bs_xb_p_mat(j+0,4);bs_xb_p_mat(j+0,5)...
```

186

```matlab
                                    ;
bs_xb_p_mat(j+1,3);bs_xb_p_mat(j+1,4);bs_xb_p_mat(j+1,5)...
                                    ;
bs_xb_p_mat(j+3,3);bs_xb_p_mat(j+3,4);bs_xb_p_mat(j+3,5)...
                                    ;
bs_xb_p_mat(j+2,3);bs_xb_p_mat(j+2,4);bs_xb_p_mat(j+2,5)];

    jump = jump+1;
end

% twisted cylinder with over all height = h_o (vertical stripe)
% for j = 1 %: ceil(m/2)
%
%     xq1=0;                  yq1=0;
%     xq2=L_q_mat(j,2);       yq2=0;
%     xq3=(L_q_mat(j,5)^2 + L_q_mat(j,2)^2 -
L_q_mat(j,4)^2)/(2*L_q_mat(j,2));
%     yq3=sqrt(L_q_mat(j,5)^2 - xq3^2);
%     xq4=xq3-L_q_mat(j,3); yq4=yq3;
%
%     figure(4)
%     hold on
%     xlim([-10 a+10]), ylim([-10 (h_o/m)+10])
%     plot([xq1 xq2], [yq1 yq2],'b','LineWidth',2)
% Bottom
%     plot([xq2 xq3], [yq2 yq3],'b','LineWidth',2)
% Side Right
%     plot([xq3 xq4], [yq3 yq4],'b','LineWidth',2)
% Top
%     plot([xq4 xq1], [yq4 yq1],'b','LineWidth',2)
% Side Left
%     plot([xq1 xq3], [yq1 yq3],'b','LineWidth',2)
% Diagonal
%     hold off
%
% end


% twisted cylinder with calculated height (vertical stripe)
x1=0;              y1=0;              y3=0;              x4=0;
jump=0;            %y3_2=0;
for j = 1 : m %ceil(m/2)

    x2= x1+ L_q_r_mat(j,2);
    y2= y1;
    x3= (L_q_r_mat(j,5)^2 - L_q_r_mat(j,4)^2 +
L_q_r_mat(j,2)^2)/(2*L_q_r_mat(j,2)) + x1;
```

187

```matlab
    if Delta_theta ==0,
        y3= sqrt(L_q_r_mat(j,4)^2 - (L_q_r_mat(j,2) - (x3 -
x4))^2) +y3;
    else
        y3= sqrt(L_q_r_mat(j,4)^2 - ((x3 - x4) -
L_q_r_mat(j,2))^2) +y3;
    end
    %y3_2 = sqrt(L_q_r_mat(j,5)^2 - (x3 - x4)^2) +y3_2;
    x4= x3 - L_q_r_mat(j,3);
    y4= y3;

    [2 j; x1 y1; x2 y2; x3 y3; x4 y4];

    figure(5) % Figure 5 and initial 6 here are the same
    hold on
    xlim([-10 a+10]), ylim([-10 ceil(m/2)*((h_o/m)+10)])
    plot([x1 x2], [y1 y2],'r','LineWidth',2)                    %
Bottom
    plot([x2 x3], [y2 y3],'r','LineWidth',2)                    %
Side Right
    plot([x3 x4], [y3 y4],'r','LineWidth',2)                    %
Top
    plot([x4 x1], [y4 y1],'r','LineWidth',2)                    %
Side Left
    plot([x1 x3], [y1 y3],'r','LineWidth',2)                    %
Diagonal
    hold off

    figure(6) % Figure 6 is carried on
    hold on
    %xlim([-10 a+10]), ylim([-10 ceil(m/2)*((h_o/m)+10)])
    plot([x1 x2], [y1 y2],'r','LineWidth',2)                    %
Bottom
    plot([x2 x3], [y2 y3],'r','LineWidth',2)                    %
Side Right
    plot([x3 x4], [y3 y4],'r','LineWidth',2)                    %
Top
    plot([x4 x1], [y4 y1],'r','LineWidth',2)                    %
Side Left
    plot([x1 x3], [y1 y3],'r','LineWidth',2)                    %
Diagonal
    hold off

    Points_q_r_mat_f(:,j)= [j; x1; y1; x2; y2; x3; y3; x4; y4];

    x1= x4;              y1= y4;
```

188

```matlab
    j=j+jump;
    figure(7)
    hold on
    plot3([bs_xb_q_r_mat(j,3) bs_xb_q_r_mat(j+1,3)],
[bs_xb_q_r_mat(j,4) bs_xb_q_r_mat(j+1,4)], [bs_xb_q_r_mat(j,5)
bs_xb_q_r_mat(j+1,5)],'r','LineWidth',2)
    plot3([bs_xb_q_r_mat(j+1,3) bs_xb_q_r_mat(j+3,3)],
[bs_xb_q_r_mat(j+1,4) bs_xb_q_r_mat(j+3,4)],
[bs_xb_q_r_mat(j+1,5) bs_xb_q_r_mat(j+3,5)],'r','LineWidth',2)
    plot3([bs_xb_q_r_mat(j+3,3) bs_xb_q_r_mat(j+2,3)],
[bs_xb_q_r_mat(j+3,4) bs_xb_q_r_mat(j+2,4)],
[bs_xb_q_r_mat(j+3,5) bs_xb_q_r_mat(j+2,5)],'r','LineWidth',2)
    plot3([bs_xb_q_r_mat(j+2,3) bs_xb_q_r_mat(j,3)],
[bs_xb_q_r_mat(j+2,4) bs_xb_q_r_mat(j,4)], [bs_xb_q_r_mat(j+2,5)
bs_xb_q_r_mat(j,5)],'r','LineWidth',2)
    plot3([bs_xb_q_r_mat(j,3) bs_xb_q_r_mat(j+3,3)],
[bs_xb_q_r_mat(j,4) bs_xb_q_r_mat(j+3,4)], [bs_xb_q_r_mat(j,5)
bs_xb_q_r_mat(j+3,5)],'r','LineWidth',2)
    hold off

    Points_q_r_mat_t(:,j-jump)= [j-jump;
bs_xb_q_r_mat(j+0,3);bs_xb_q_r_mat(j+0,4);bs_xb_q_r_mat(j+0,5)..
.
                                ;bs_xb_q_r_mat(j+1,3);bs_xb_q_r_mat(j+1,4);bs_xb_q_r_mat(j+1,5)..
.
                                ;bs_xb_q_r_mat(j+3,3);bs_xb_q_r_mat(j+3,4);bs_xb_q_r_mat(j+3,5)..
.
                                ;bs_xb_q_r_mat(j+2,3);bs_xb_q_r_mat(j+2,4);bs_xb_q_r_mat(j+2,5)];

    jump = jump+1;

end

bs_xb_p_mat
bs_xb_q_r_mat

Points_p_mat_f   =    round(Points_p_mat_f*rf)/rf
Points_q_r_mat_f =    round(Points_q_r_mat_f*rf)/rf
Points_p_mat_t   =    round(Points_p_mat_t*rf)/rf
Points_q_r_mat_t =    round(Points_q_r_mat_t*rf)/rf


bs_Delta_mat=[];
```

189

```matlab
for j = 1 : m

    if j == 1,
        bs_Delta_mat= [bs_Delta_mat; Delta_mat(j,5)];
    else
        bs_Delta_mat= [bs_Delta_mat; Delta_mat(j,2);
Delta_mat(j,5)];
    end

end

bs_Delta_mat


bs_mat=[]; xb_box=[];
x = abs(bs_Delta_mat)+5;
Theta_1 = [30;30;30;30;30;30;30];          % Degrees
w1 = 5.5;   %7
v = 7;      %7

for n = 1 : (2*m - 1)

    L1 = (x(n,1) -
abs(bs_Delta_mat(n,1))/2)*(1/cos(deg2rad(Theta_1(n,1))));
    L2 = L1 * sqrt((abs(bs_Delta_mat(n,1))/(2*L1))^2 +
(sin(deg2rad(Theta_1(n,1))))^2);
    Theta_2i = rad2deg(acos(abs(bs_Delta_mat(n,1))/(2*L2)));
    bi = L1 * sin(deg2rad(Theta_1(n,1)));

    m_bs = L2/L1;
    w2 = w1 * (m_bs/(2*v))^(1/3);

    bs_mat= [bs_mat; x(n,1) bi bs_Delta_mat(n,1) Theta_1(n,1)
Theta_2i L1 L2 w2];

    xb_box= [xb_box; x(n,1) L1*cos(deg2rad(Theta_1(n,1))) bi*2];

end

fprintf('         x          bi          Delta          Theta_1
Theta_2i        L1              L2              w2')
bs_mat
fprintf('         xi          xf          2bi')
xb_box

save('LineProject10')
```

APPENDIX D: LBCCSM MODEL'S PLOTS

D.1 LBCCSM Model's Plots for $\theta_1 = 20$

Figure A (b_{max}/X) vs (θ_{2i}) over range of (v) for $\theta_1 = 20^\circ$.
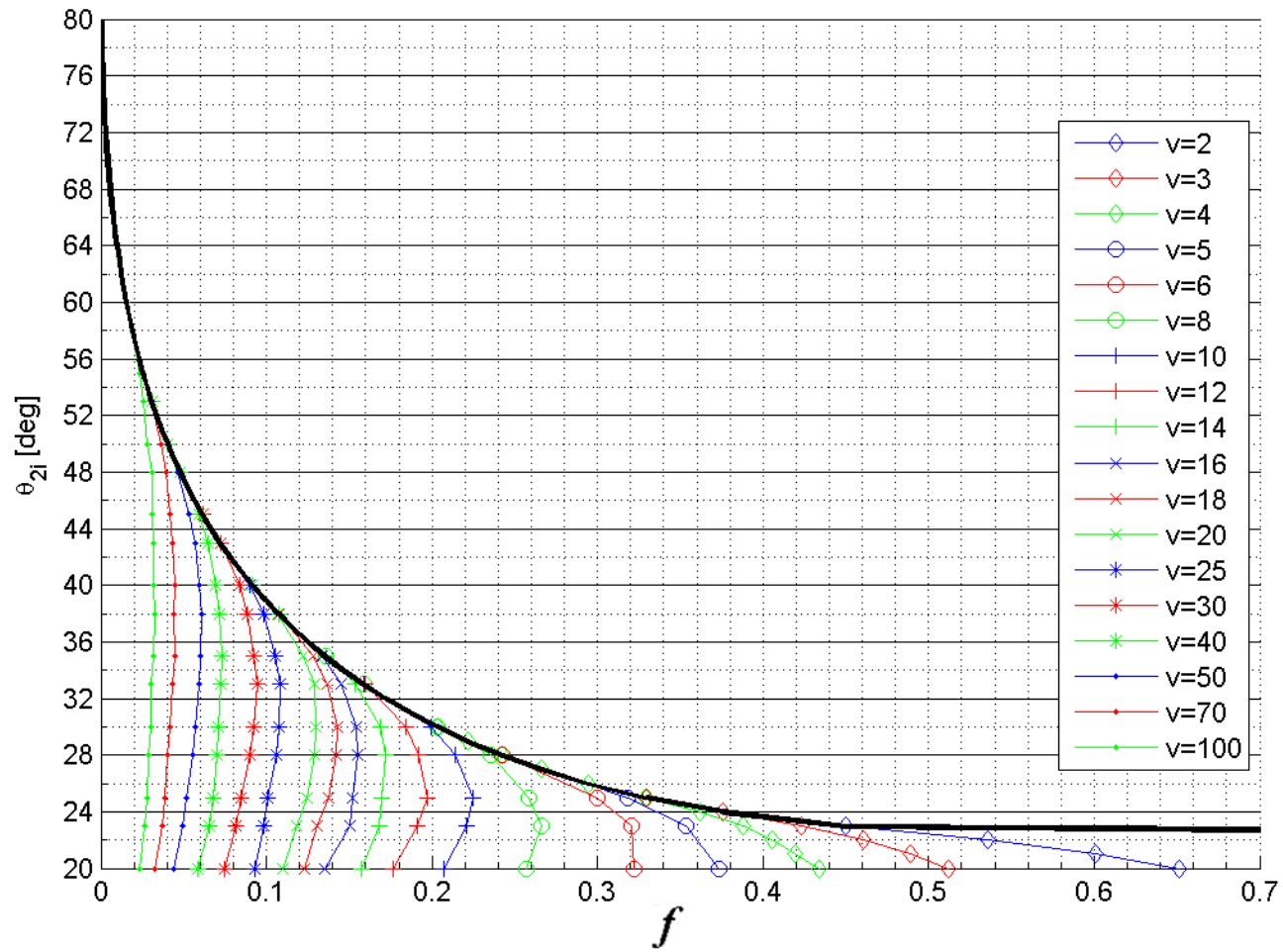
Figure B (Θ_1) vs (θ_{2i}) over range of (v) for $\theta_1=20^o$.

Figure C (f) vs (θ_{2i}) over range of (v) for θ_1=20°.

Figure D (J) vs (θ_{2i}) for θ_1=20° over range of (v), (a) Lower and (b) Higher force range.

195
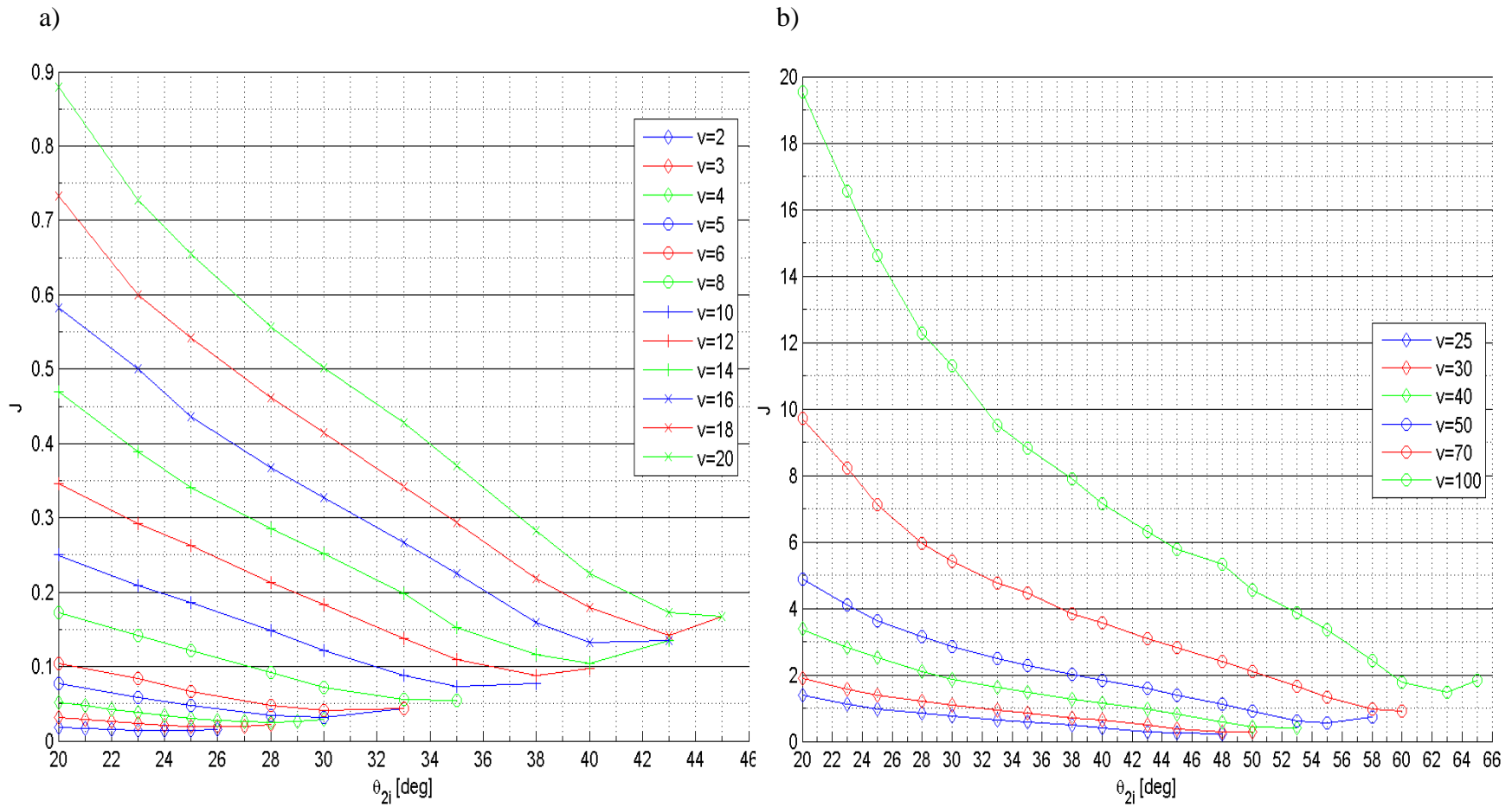
D.2 LBCCSM Model's Plots for $\theta_1 = 40$
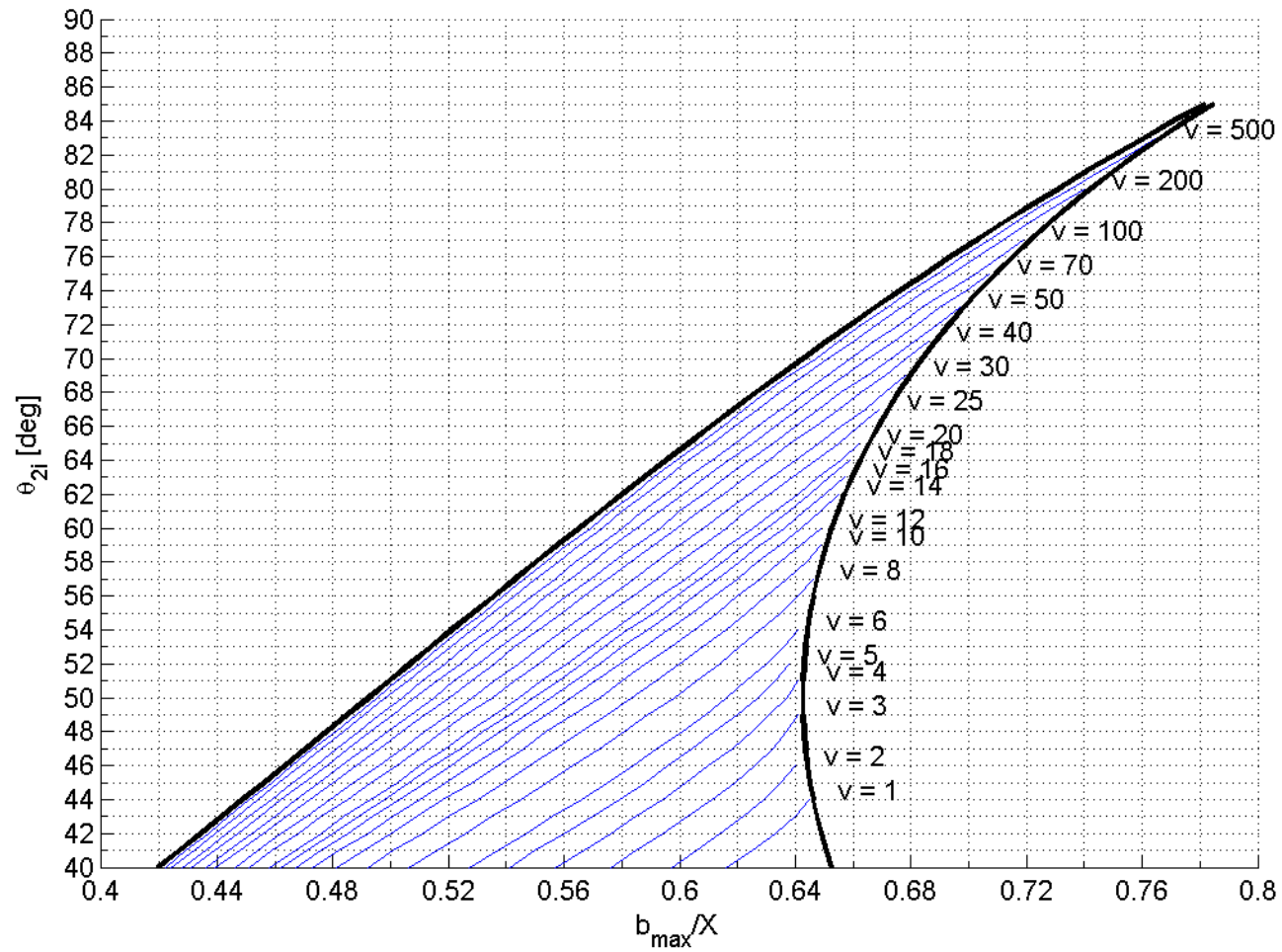
Figure E (b_{max}/X) vs (θ_{2i}) over range of (v) for $\theta_1 = 40^o$.
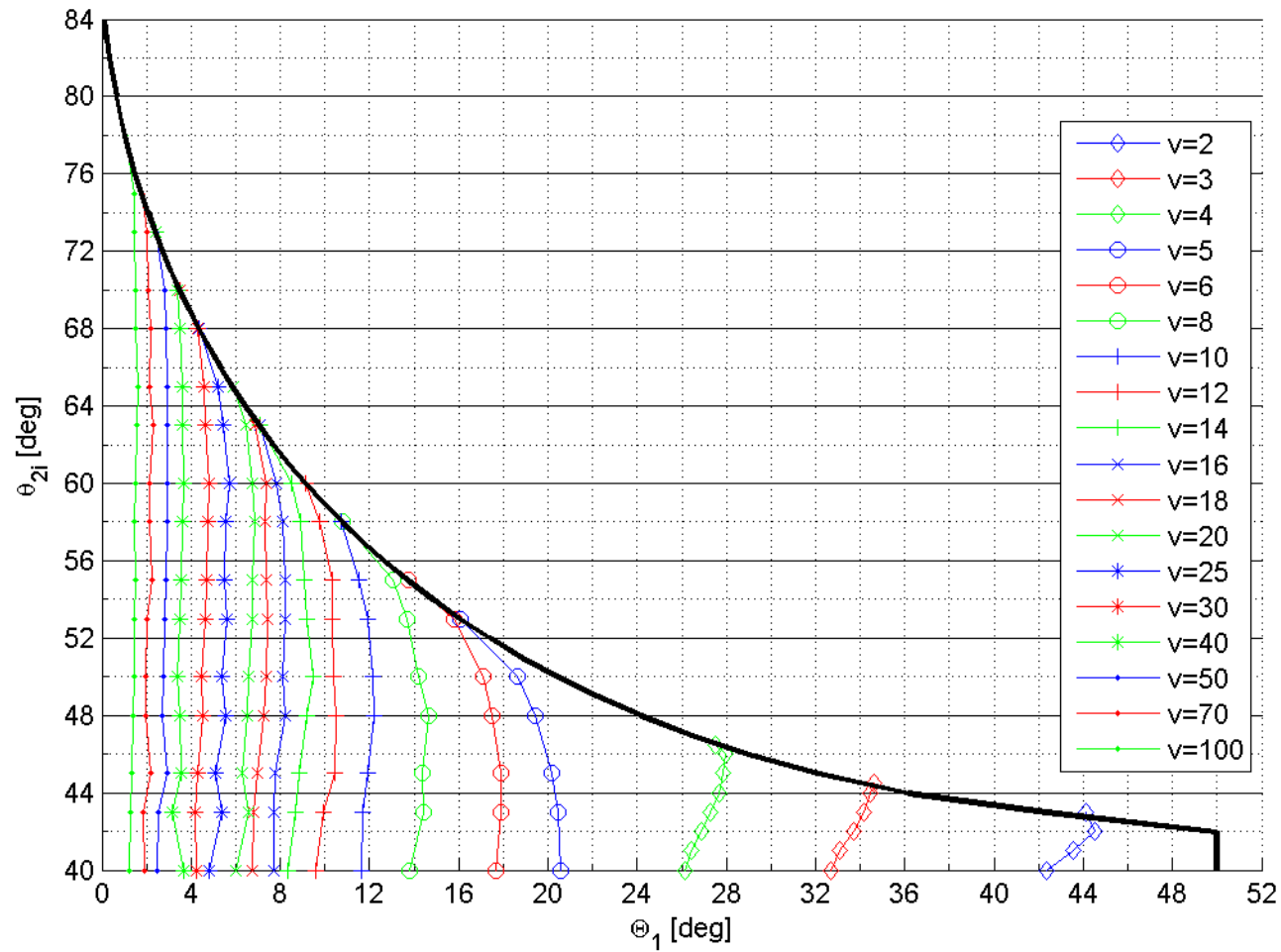
Figure F (Θ_1) vs (θ_{2i}) over range of (v) for θ_1=40$^\text{o}$.

197

Figure G (f) vs (θ_{2i}) over range of (v) for θ_1=40$^\text{o}$.

Figure H (*J*) vs (θ_{2i}) for θ_1=40° over range of (*v*), (a) Lower and (b) Higher force range.

D.3 LBCCSM Model's Plots for $\theta_1 = 60$
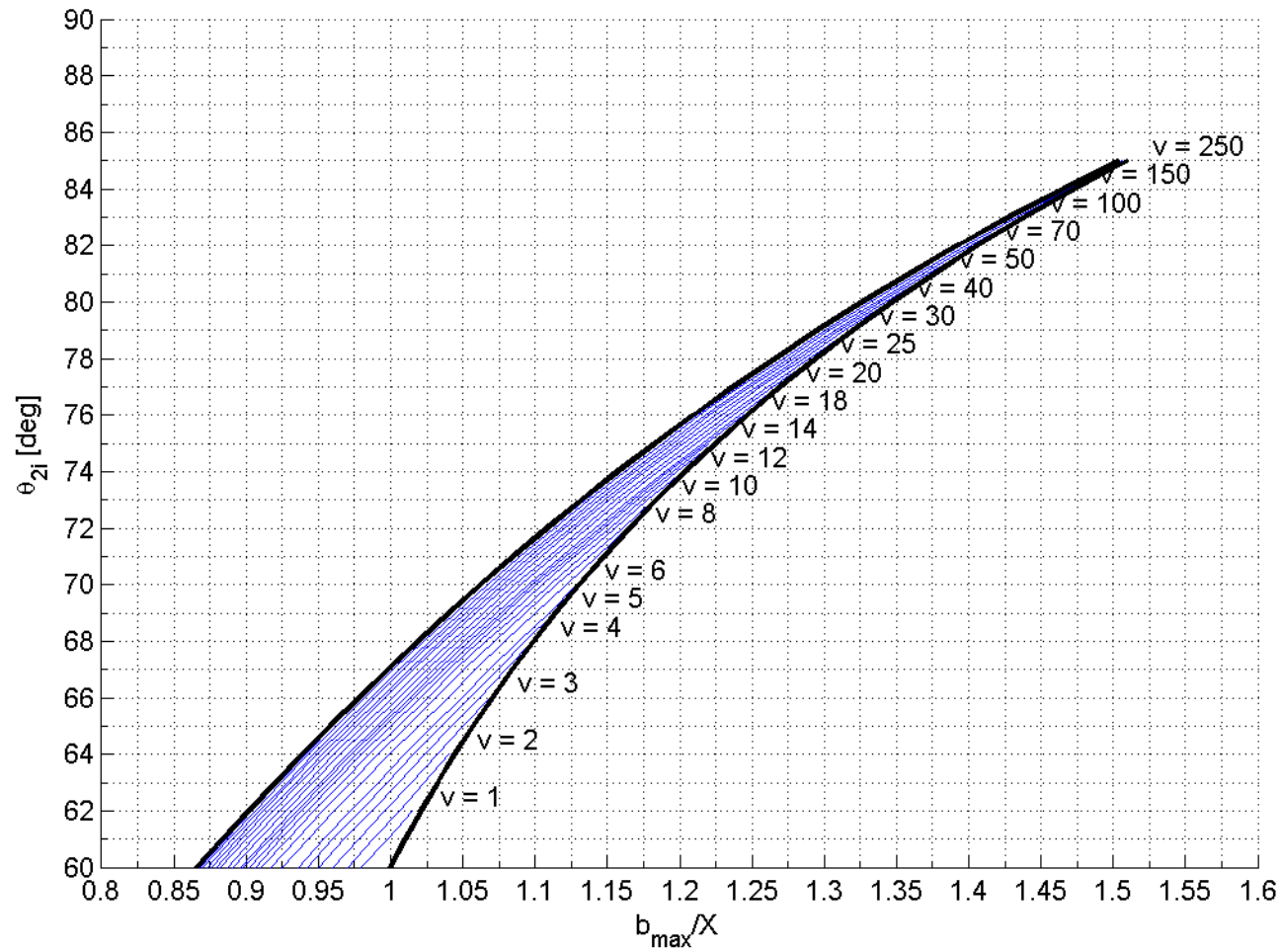
Figure I (b_{max}/X) vs (θ_{2i}) over range of (v) for $\theta_1=60^\circ$.
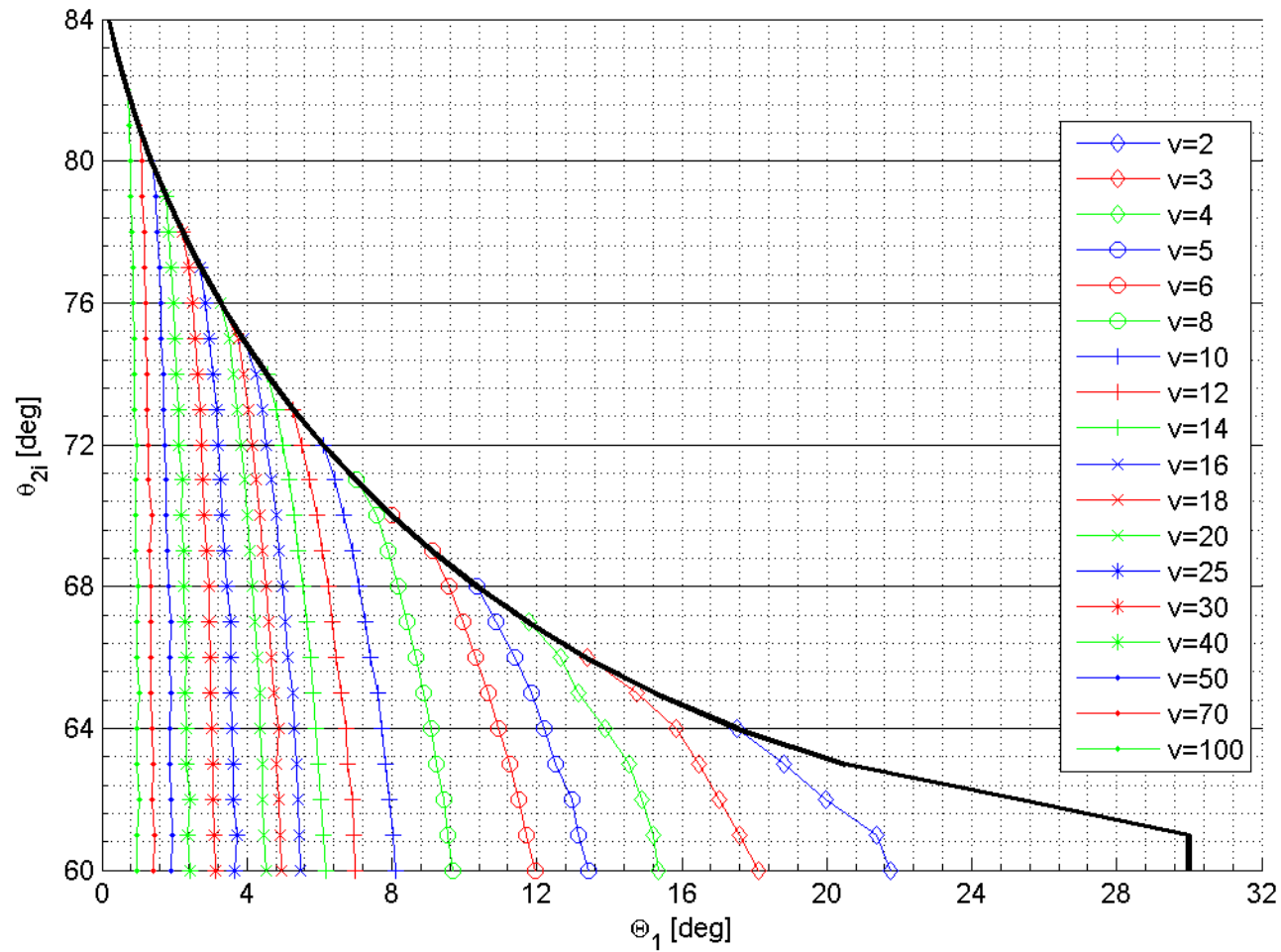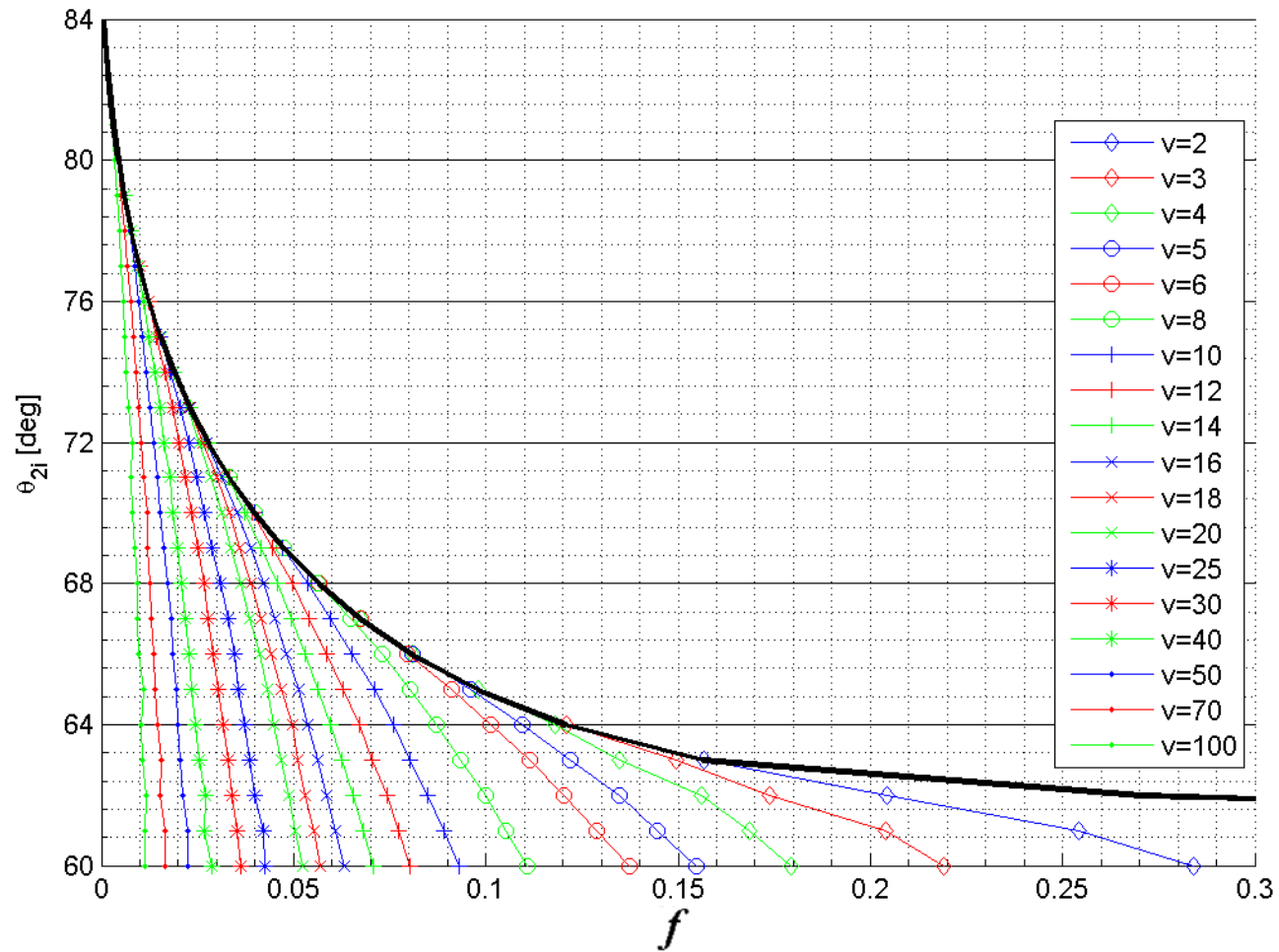
Figure J (Θ_1) vs (θ_{2i}) over range of (v) for θ_1=60$^\text{o}$.

Figure K (f) vs (θ_{2i}) over range of (v) for $\theta_1=60^o$.

Figure L (*J*) vs (θ_{2i}) for θ_1=60° over range of (*v*), (a) Lower and (b) Higher force range.

APPENDIX E: DESIGN DIMENSION (IN MILLIMETERS)

E.1 P₁ SMSF's Design Dimensions

Figure M P₁ SMSF: Initial state mechanism's constraints.

Figure N P₁ SMSF: Final state mechanism's constraints.

Figure O P$_1$ SMSF: Mechanism's design dimensions (without bistability).
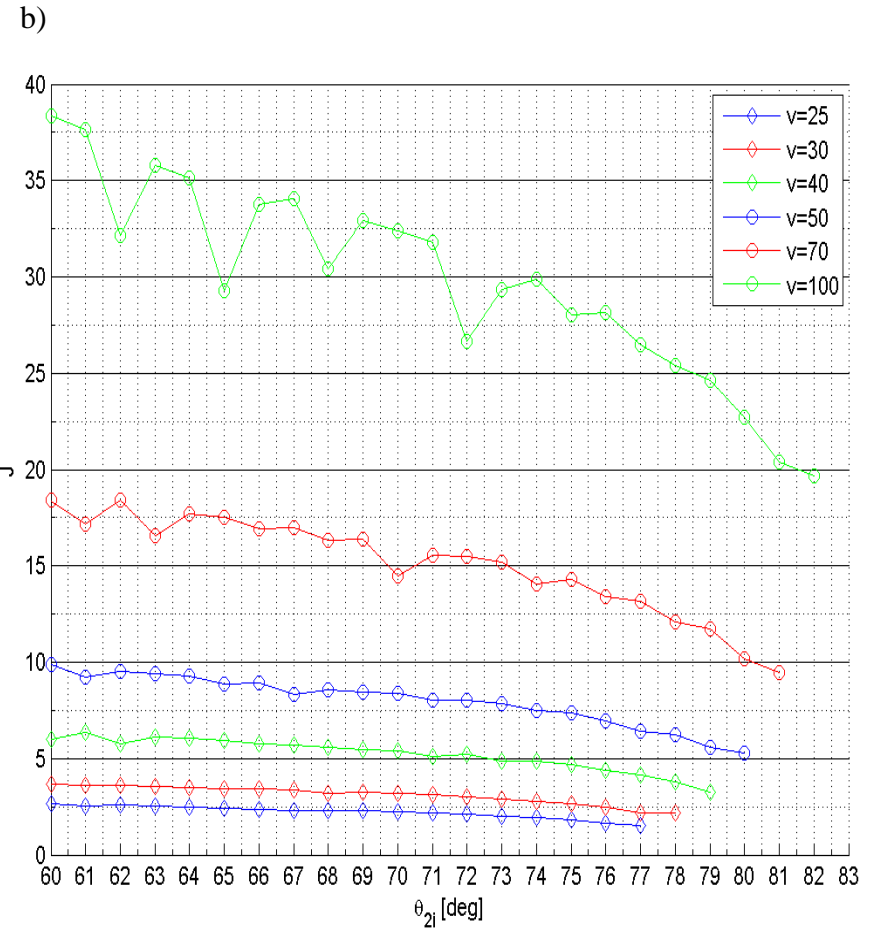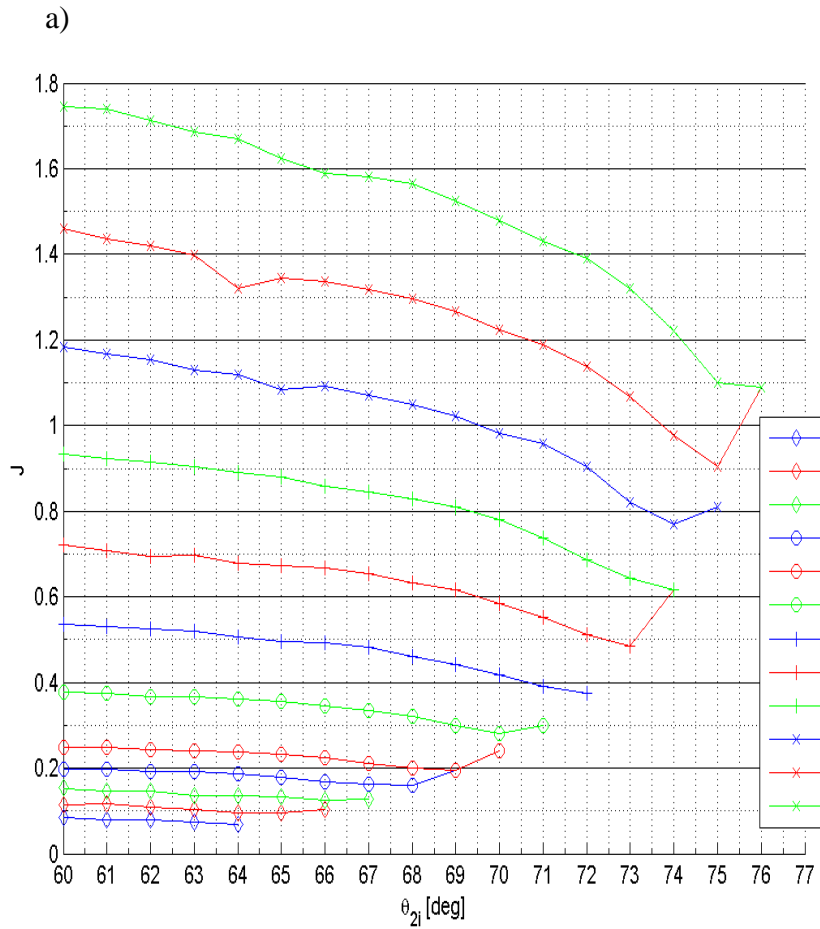
E.2 P$_2$ SMSF's Design Dimensions

Figure P P$_2$ SMSF: Initial state mechanism's constraints.
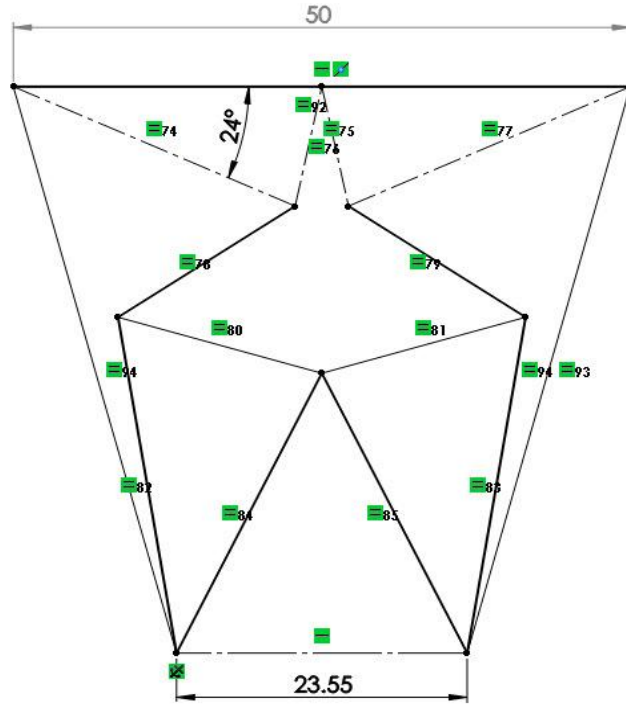
Figure Q P$_2$ SMSF: Final state mechanism's constraints.
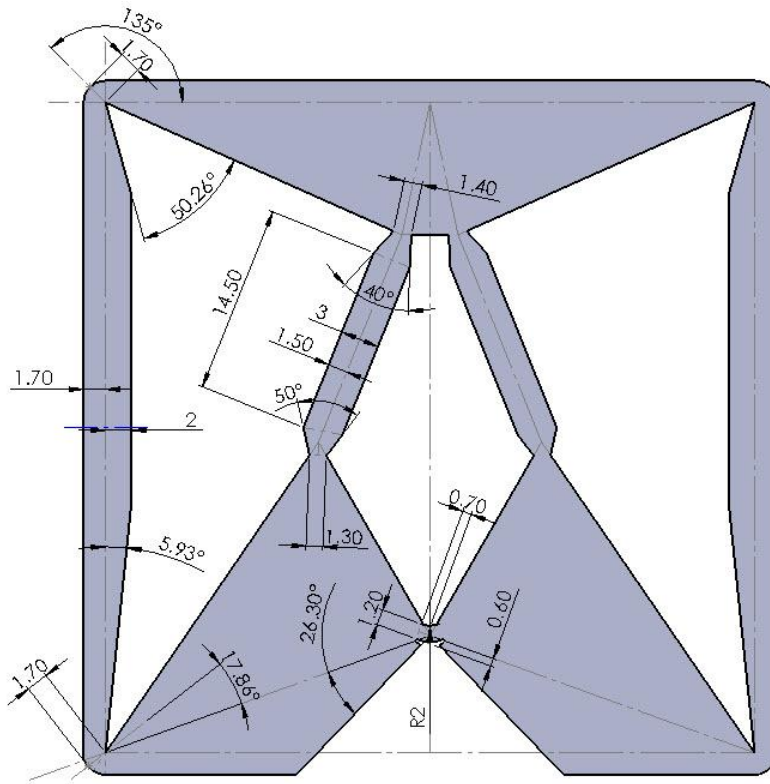
Figure R P$_2$ SMSF: Mechanism's design dimensions.

E.3 PEE Design Dimensions for the P₁ SMSF
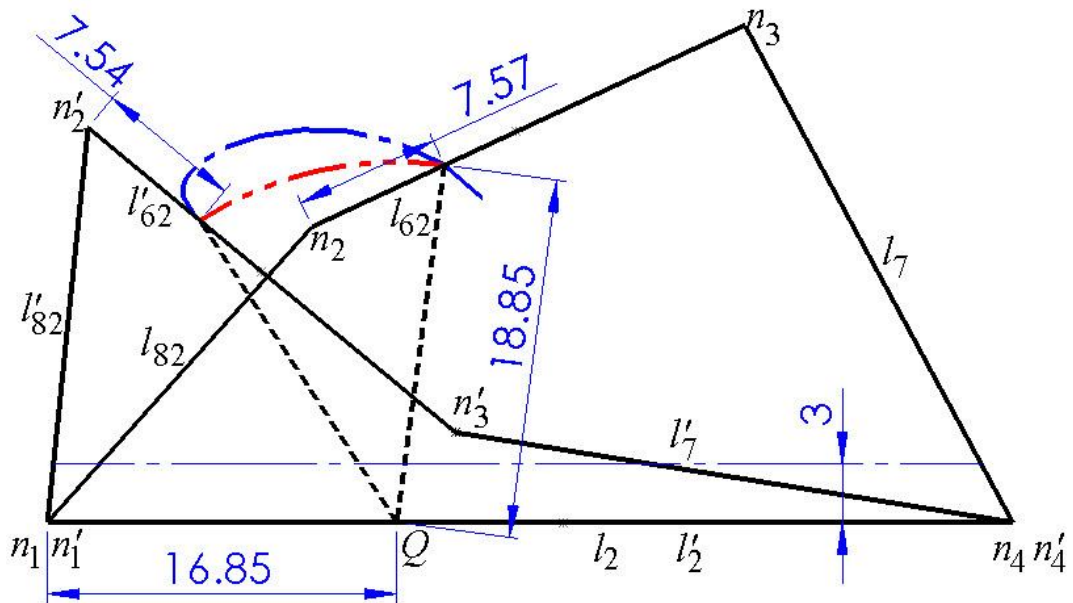
Figure S P1 SMSF: Left half PEE design dimensions.
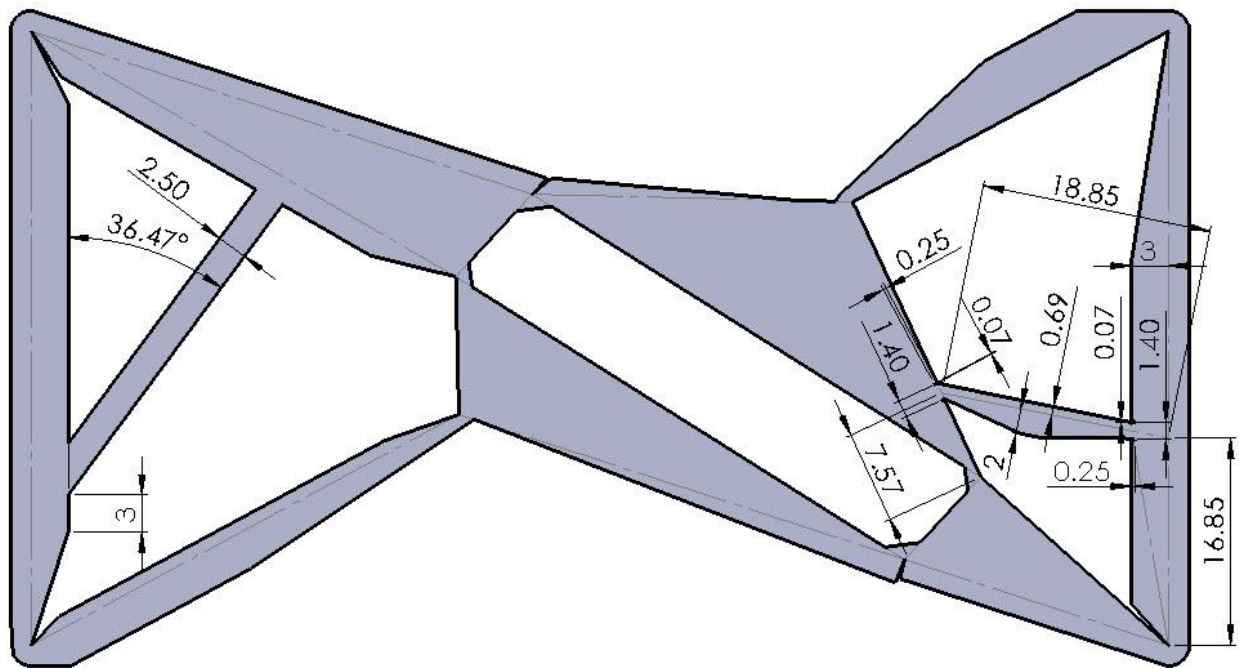
Figure T P₁ SMSF: Mechanism's design dimensions (with bistability).

E.4 Parallel Four-bar Bistable Compliant Mechanism Design Dimensions

Figure U Parallel four-bar bistable mechanism's initial layout dimensions.

Figure V Parallel four-bar bistable mechanism's intermediate dimensions.

Figure W Parallel four-bar bistable mechanism's living hinges dimensions.

APPENDIX F: POLYPROPYLENE COPOLYMER DATASHEET

CORRTEC CHEMICAL & CORROSION RESISTANT MATERIALS

Typical Physical Properties:

PROTEC® COPOLYMER POLYPROPYLENE

Property	Nominal Value	Units	ASTM Test Method
Melt Index	0.5	g/10 min	D 1238
Density	0.9	g/cm³	D 1505
Tensile Strength @ Yield	3,500	psi	D 638
Elongation @ Break	10	%	D 638
Coefficient of Linear Thermal Expansion	6.5×10^{-5}	In./In.°C	D 696
Flexural Modulus	145,000	psi	D 790
Notched Izod Impact	17	fl-lb/in	D 256
Low Temperature Brittleness F$_{50}$			
Heat Deflection Temperature @ 66 psi	86	°C	D 648
Maximum Service Temperature, Air	180		Long Term
Vicat Softening Point	298	°F	D 1525
Hardness, Shore D	72		D 2240
Absorption	Max.0.01%		D 5709(2)
Flammability Rating	UL94 HB		
Compliances	FDA, USDA, NSF(natural only)		

VYCOM OLEFIN AND PVC SOLUTIONS

801 E. Corey Street, Scranton PA 18505
Phone: (800) 235-8320
Fax: (800) 858-9266
www.vycomplastics.com

Physical properties of plastic sheeting are represented as "Typical". Information contained herein is considered accurate to the best of our knowledge. It is offered for your consideration and investigation, and is not to be construed as a representation or warranty expressed or implied. Our warranties are limited to those expressly stated in formal contracts or in conditions of sale on our invoices and order acceptances. Conditions and methods of use may vary and are beyond the control of Vycom; therefore, Vycom disclaims any liability incurred as a result of the use of this product in accordance with the data contained in our physical property charts. No information herein shall be construed as an offer of indemnity for infringement or as a recommendation to use the products in such a manner as to infringe any patent, domestic or foreign.

The "Typical" properties of our plastic sheet cannot be automatically used when engineering finished components; and the fabricator or end user is responsible for insuring the suitability of our products for their specific application or end use!

January 1st, 2012

APPENDIX G: TENSILE TEST DATA

Table A Test data for the displacement load rate 0.081 in/sec.

0.081 (in/sec)

FORCE LBS	DISP IN	FORCE LBS	DISP IN	FORCE LBS	DISP IN	FORCE LBS	DISP IN
7.27	0.14	41.00	3.36	29.47	6.42	70.48	9.58
14.93	0.27	40.77	3.47	25.95	6.53	64.25	9.68
21.10	0.38	39.49	3.57	23.43	6.64	61.43	9.78
26.67	0.48	38.18	3.67	23.83	6.73	66.69	9.89
30.98	0.58	37.19	3.77	23.79	6.83	72.59	9.99
34.88	0.69	36.08	3.87	24.28	6.94	81.15	10.09
37.93	0.79	35.50	3.98	24.59	7.04	87.49	10.19
41.12	0.89	35.37	4.08	24.99	7.14	92.65	10.29
44.49	1.00	34.38	4.18	25.41	7.24	97.06	10.38
47.14	1.10	33.07	4.28	25.57	7.34		
48.90	1.21	31.92	4.38	26.56	7.45		
50.94	1.31	31.16	4.49	27.76	7.55		
52.82	1.41	32.08	4.59	29.84	7.65		
53.80	1.52	31.92	4.69	32.15	7.75		
52.80	1.62	32.05	4.79	35.02	7.85		
48.27	1.72	32.82	4.89	38.03	7.95		
41.63	1.83	32.80	4.99	41.28	8.06		
37.86	1.93	32.57	5.10	44.65	8.16		
35.79	2.04	31.64	5.20	48.94	8.26		
36.50	2.12	32.35	5.30	52.92	8.36		
36.31	2.24	33.34	5.40	56.20	8.46		
36.82	2.34	33.68	5.50	60.00	8.57		
37.12	2.44	34.48	5.60	63.55	8.67		
37.70	2.55	34.07	5.60	66.74	8.77		
38.38	2.65	35.97	5.71	69.83	8.87		
39.40	2.75	37.57	5.81	73.29	8.97		
40.71	2.85	38.94	5.91	76.19	9.07		
41.54	2.95	39.18	6.01	78.59	9.18		
43.03	3.06	38.67	6.12	79.46	9.28		
43.30	3.16	37.04	6.22	78.41	9.38		
42.24	3.26	33.99	6.32	73.86	9.48		

Table B Test data for the displacement load rate 0.188 in/sec.

0.188 (in/sec)

FORCE LBS	DISP IN	FORCE LBS	DISP IN	FORCE LBS	DISP IN	FORCE LBS	DISP IN	FORCE LBS	DISP IN
17.11	0.14	34.23	0.68	44.57	1.21	31.08	2.18	29.26	3.54
17.74	0.16	34.54	0.70	44.76	1.23	31.11	2.22	29.20	3.58
18.36	0.17	34.85	0.71	45.09	1.24	31.04	2.25	29.06	3.62
18.97	0.18	35.51	0.72	45.51	1.27	31.03	2.29	28.86	3.65
19.57	0.20	36.09	0.74	45.97	1.28	30.70	2.32	28.24	3.68
20.14	0.21	36.49	0.75	46.52	1.30	30.61	2.35	28.32	3.72
20.69	0.23	36.59	0.77	46.78	1.32	30.49	2.39	27.96	3.75
21.22	0.24	37.27	0.78	46.86	1.34	30.82	2.42	28.32	3.78
19.77	0.25	37.94	0.79	45.01	1.36	30.91	2.46	28.28	3.82
20.22	0.27	38.46	0.80	45.06	1.38	31.09	2.49	28.05	3.86
21.01	0.28	38.44	0.82	45.07	1.40	31.53	2.52	27.81	3.89
21.70	0.29	38.70	0.83	44.94	1.42	32.52	2.56	27.47	3.93
22.30	0.31	39.01	0.84	44.79	1.44	33.07	2.60	27.21	3.96
22.87	0.32	38.91	0.86	44.91	1.47	33.32	2.63	26.78	4.00
23.32	0.34	38.99	0.87	44.16	1.49	33.98	2.67	26.35	4.04
23.78	0.35	39.06	0.88	42.74	1.52	34.65	2.70	25.74	4.07
24.22	0.37	39.29	0.90	41.32	1.55	34.81	2.74	25.47	4.10
24.74	0.38	39.61	0.91	38.94	1.57	35.07	2.77	25.09	4.14
25.29	0.39	39.87	0.93	36.74	1.59	35.62	2.81	24.45	4.17
25.84	0.41	40.18	0.94	34.27	1.62	35.91	2.84	24.25	4.21
26.30	0.42	40.39	0.95	32.95	1.64	36.28	2.88	24.15	4.25
26.66	0.43	40.41	0.97	31.15	1.67	35.59	2.91	24.47	4.28
27.21	0.45	40.62	0.98	28.64	1.70	34.47	2.94	24.74	4.32
27.64	0.46	40.73	0.99	27.16	1.72	33.99	2.98	24.60	4.36
27.82	0.48	40.82	1.00	26.91	1.73	33.96	3.02	24.32	4.39
28.03	0.49	41.09	1.02	26.97	1.76	34.16	3.05	24.09	4.43
28.57	0.50	41.30	1.03	26.86	1.79	33.86	3.09	24.25	4.46
29.11	0.51	41.74	1.04	27.17	1.82	33.07	3.12	24.66	4.50
29.49	0.53	42.09	1.06	27.66	1.85	32.76	3.16	24.74	4.54
29.80	0.54	42.45	1.07	28.19	1.88	32.76	3.19	25.06	4.57
30.48	0.56	42.93	1.09	28.70	1.90	32.37	3.23	25.07	4.61
31.02	0.57	43.07	1.10	29.35	1.93	32.51	3.27	25.45	4.65
31.51	0.58	43.46	1.11	29.94	1.96	32.45	3.30	25.51	4.69
31.57	0.59	43.64	1.13	30.09	2.00	32.47	3.33	25.26	4.72
32.09	0.61	43.57	1.14	29.93	2.02	32.53	3.37	25.61	4.76
32.69	0.63	43.82	1.15	30.36	2.05	31.72	3.40	25.48	4.79
33.11	0.64	44.19	1.17	30.82	2.09	30.84	3.44	25.42	4.83
33.25	0.66	44.30	1.18	30.53	2.12	30.53	3.48	23.74	4.87
33.72	0.67	44.22	1.19	30.66	2.15	29.66	3.51	23.53	4.90

211

Table B (Continued)

0.188 (in/sec)   Cont.

FORCE LBS	DISP IN	FORCE LBS	DISP IN	FORCE LBS	DISP IN	FORCE LBS	DISP IN
23.86	4.94	24.97	6.35	24.55	7.76	70.51	9.17
24.54	4.98	21.44	6.39	24.93	7.80	71.26	9.19
25.31	5.01	17.52	6.42	25.84	7.84	71.49	9.24
25.66	5.05	16.59	6.46	26.97	7.87	71.95	9.27
25.48	5.09	15.48	6.49	27.80	7.91	72.45	9.31
25.61	5.13	14.93	6.53	29.01	7.94	72.49	9.35
25.49	5.16	14.65	6.56	29.82	7.98	71.91	9.38
25.16	5.19	14.93	6.60	31.01	8.01	71.49	9.42
25.90	5.23	15.28	6.64	32.26	8.03	70.29	9.45
26.39	5.27	15.68	6.67	33.18	8.06	68.55	9.49
26.79	5.30	16.23	6.71	34.74	8.10	66.91	9.53
26.99	5.34	16.51	6.75	35.90	8.14	65.20	9.56
27.77	5.38	16.50	6.78	37.32	8.17	64.23	9.60
28.66	5.42	16.82	6.82	38.91	8.21	61.47	9.63
28.74	5.45	16.58	6.85	40.39	8.25	59.11	9.67
29.55	5.49	17.10	6.89	41.94	8.28	57.20	9.71
30.43	5.52	17.11	6.92	43.16	8.32	56.14	9.74
30.73	5.56	17.35	6.96	44.49	8.36	55.72	9.78
31.61	5.60	17.36	6.99	46.16	8.39	55.65	9.82
31.90	5.63	17.64	7.03	47.86	8.43	56.36	9.85
32.51	5.67	18.16	7.06	49.53	8.47	57.99	9.89
33.45	5.71	18.59	7.10	50.84	8.50	60.51	9.92
34.34	5.74	18.56	7.14	52.22	8.53	63.26	9.96
34.61	5.77	18.74	7.18	53.47	8.57	65.95	10.00
34.51	5.81	19.07	7.21	54.48	8.61	68.55	10.03
34.66	5.85	19.24	7.25	55.41	8.64	70.53	10.07
35.07	5.88	19.22	7.29	56.48	8.68	73.03	10.10
34.80	5.92	18.94	7.32	57.36	8.72	74.11	10.14
34.95	5.95	19.30	7.36	58.91	8.75	74.99	10.16
34.80	5.99	19.22	7.39	60.44	8.79	75.98	10.18
34.82	6.02	19.69	7.43	61.66	8.83	76.97	10.20
34.41	6.06	20.16	7.47	62.59	8.86	76.18	10.22
33.52	6.10	20.70	7.50	63.57	8.90	74.90	10.23
32.76	6.13	20.89	7.54	64.59	8.93	74.06	10.23
32.15	6.17	21.26	7.58	65.61	8.97		
31.45	6.20	21.98	7.61	67.03	9.01		
30.26	6.24	22.48	7.65	67.85	9.05		
29.08	6.28	22.89	7.69	68.81	9.08		
27.11	6.31	23.78	7.73	69.72	9.12		

212

Table C Test data for the displacement load rate 0.275 in/sec.

0.275 (in/sec)

FORCE LBS	DISP IN	FORCE LBS	DISP IN	FORCE LBS	DISP IN	FORCE LBS	DISP IN	FORCE LBS	DISP IN	FORCE LBS	DISP IN	FORCE LBS	DISP IN
15.11	0.36	20.24	1.80	25.99	3.34	19.91	4.90	8.59	6.45	26.82	8.01	41.74	9.60
16.32	0.36	20.82	1.84	25.77	3.38	20.18	4.93	8.85	6.48	28.36	8.05	43.91	9.64
17.59	0.38	22.17	1.87	25.23	3.42	19.97	4.97	9.28	6.53	29.64	8.10	46.24	9.68
18.57	0.41	22.51	1.91	24.52	3.46	20.53	5.02	9.99	6.56	31.11	8.13	49.29	9.72
19.56	0.44	22.91	1.95	23.56	3.50	20.99	5.05	10.74	6.60	32.15	8.17	52.32	9.76
20.89	0.48	23.72	1.99	23.40	3.53	21.30	5.09	11.59	6.64	33.76	8.21	55.28	9.80
22.02	0.51	23.43	2.03	23.44	3.58	21.85	5.14	11.97	6.68	35.08	8.26	58.32	9.84
22.89	0.55	23.57	2.07	22.66	3.62	22.32	5.17	12.45	6.72	36.59	8.30	61.28	9.88
24.30	0.59	24.18	2.11	22.56	3.66	22.49	5.21	12.59	6.76	38.03	8.34	64.17	9.92
25.30	0.63	23.72	2.15	22.76	3.69	22.48	5.25	12.62	6.80	39.26	8.38	66.70	9.96
26.49	0.67	24.17	2.19	22.64	3.73	22.74	5.29	12.68	6.84	40.51	8.42	69.28	10.00
26.99	0.70	24.52	2.23	22.86	3.77	23.15	5.33	12.97	6.88	42.19	8.46	71.61	10.04
28.14	0.75	24.37	2.27	22.89	3.81	23.59	5.38	13.07	6.92	43.91	8.50	73.93	10.08
29.09	0.78	24.66	2.31	22.45	3.85	24.27	5.42	13.45	6.96	45.28	8.54	76.18	10.12
30.06	0.82	24.37	2.34	22.61	3.89	24.61	5.45	13.74	7.00	46.84	8.57	78.29	10.17
30.90	0.86	24.59	2.39	22.55	3.93	25.35	5.49	14.28	7.04	48.27	8.62	79.48	10.20
31.99	0.90	25.16	2.42	22.20	3.97	26.01	5.53	14.74	7.08	49.95	8.66	79.47	10.24
32.97	0.94	25.69	2.46	21.94	4.01	26.47	5.58	14.91	7.12	51.40	8.70	80.28	10.28
33.80	0.97	26.25	2.50	21.98	4.05	26.89	5.61	14.99	7.17	52.66	8.74	81.22	10.32
34.76	1.01	25.40	2.54	20.97	4.09	27.68	5.65	15.31	7.20	53.43	8.78	81.27	10.35
35.30	1.05	26.11	2.58	20.32	4.13	27.82	5.70	15.44	7.24	54.74	8.82	79.56	10.37
36.16	1.09	26.77	2.62	19.57	4.17	28.25	5.73	16.20	7.29	55.78	8.86	78.32	10.39
37.15	1.13	26.93	2.66	19.81	4.21	28.94	5.77	16.78	7.33	57.07	8.90		
37.97	1.17	27.39	2.70	19.57	4.25	29.03	5.81	16.85	7.37	58.28	8.94		
35.70	1.21	26.97	2.74	19.66	4.29	28.73	5.85	17.12	7.41	58.99	8.99		
36.22	1.25	27.23	2.78	19.78	4.33	28.24	5.89	17.57	7.45	59.61	9.03		
36.40	1.29	27.70	2.82	19.91	4.37	28.39	5.93	17.98	7.49	60.11	9.07		
36.82	1.33	27.45	2.86	20.44	4.41	28.21	5.97	18.27	7.53	60.99	9.11		
36.36	1.37	27.45	2.90	20.48	4.45	28.06	6.01	18.43	7.57	60.66	9.15		
36.20	1.41	27.24	2.93	20.32	4.49	26.89	6.05	18.91	7.61	58.60	9.19		
34.90	1.45	26.92	2.98	20.80	4.53	26.32	6.09	19.42	7.65	56.78	9.23		
32.98	1.49	27.31	3.02	20.86	4.57	24.85	6.13	20.09	7.69	54.73	9.27		
29.97	1.53	27.45	3.06	20.94	4.61	23.51	6.17	20.80	7.73	51.11	9.32		
27.87	1.57	27.06	3.10	21.26	4.65	21.56	6.21	21.74	7.77	48.07	9.36		
27.44	1.60	27.18	3.14	21.30	4.69	18.86	6.25	22.66	7.81	46.01	9.39		
26.29	1.64	27.18	3.18	21.54	4.73	14.57	6.29	23.24	7.85	42.72	9.43		
23.30	1.68	26.95	3.22	20.14	4.77	10.86	6.33	24.07	7.89	40.98	9.48		
19.84	1.72	26.14	3.26	19.41	4.81	9.91	6.37	25.14	7.93	39.82	9.52		
20.11	1.76	26.12	3.30	19.59	4.85	9.09	6.41	25.61	7.97	40.34	9.56		

Table D Test data for the displacement load rate 0.391 in/sec.

0.391 (in/sec)

FORCE LBS	DISP IN	FORCE LBS	DISP IN	FORCE LBS	DISP IN
10.35	0.35	16.85	4.22	23.94	8.35
12.32	0.40	15.43	4.33	26.51	8.45
14.27	0.46	13.58	4.44	28.73	8.55
16.34	0.54	12.73	4.54	33.00	8.66
18.81	0.62	12.59	4.65	38.00	8.77
20.56	0.70	12.89	4.75	42.00	8.87
23.09	0.78	13.42	4.86	44.00	8.98
25.04	0.87	14.10	4.97	29.37	9.09
26.73	0.97	15.04	5.07	28.85	9.20
27.46	1.07	15.67	5.18	32.02	9.30
29.19	1.17	16.50	5.28	36.02	9.41
30.23	1.27	16.01	5.39	39.73	9.52
31.17	1.38	16.23	5.50	45.34	9.62
26.44	1.48	15.90	5.60	50.83	9.73
11.33	1.59	14.65	5.71	56.19	9.83
11.50	1.69	13.98	5.81	62.00	9.94
12.77	1.80	12.65	5.91	67.52	10.04
14.85	1.90	11.55	6.02	72.65	10.13
15.58	2.01	9.79	6.12	77.85	10.23
17.19	2.11	8.51	6.23	82.58	10.33
18.41	2.22	8.45	6.33	87.43	10.42
19.15	2.32	7.31	6.44	91.96	10.52
20.31	2.42	8.02	6.54	94.33	10.60
21.05	2.53	8.60	6.64	96.62	10.66
21.02	2.64	9.31	6.75	98.42	10.73
20.90	2.74	9.81	6.85	99.64	10.79
21.10	2.85	10.46	6.96	101.33	10.84
21.70	2.96	11.08	7.07	103.17	10.89
21.40	3.07	11.30	7.17	105.35	10.94
21.00	3.17	11.73	7.28	106.35	10.99
20.70	3.28	11.98	7.38	107.62	11.04
20.00	3.39	12.83	7.50	108.84	11.08
19.80	3.48	12.85	7.60	108.96	11.12
19.48	3.59	13.94	7.71	109.19	11.14
19.91	3.69	13.19	7.82	107.23	11.18
19.83	3.80	14.59	7.92	106.76	11.21
19.69	3.90	16.34	8.03		
19.00	4.01	17.35	8.14		
17.52	4.11	20.70	8.24		

APPENDIX H: COPYRIGHT PERMISSIONS

H.1 Copyright Permission for Material Used in Chapter 3 and Chapter 4

Ahmad Alqasimi <aalqasim@mail.usf.edu>

CONFERENCE PUBLICATIONS PERMISSION REQUEST

Beth Darchi <DarchiB@asme.org>   Tue, Oct 6, 2015 at 2:46 PM
To: Ahmad Alqasimi <aalqasim@mail.usf.edu>

Dear Mr. Alqasimi:

It is our pleasure to grant you permission **to use all or any part of** the following ASME papers:

· "Design of a Linear Bi-Stable Compliant Crank-Slider-Mechanism (LBCCSM)," by Ahmad Alqasimi; Craig Lusk; Jairo Chimento, Paper number DETC2014-34285

· "Shape-Morphing Space Frame (SMSF) Using Linear Bistable Elements," by Ahmad Alqasimi and Craig Lusk, Paper number DETC2015-47526

cited in your letter for inclusion in a Ph.D. Dissertation entitled Design of Shape Morphing Structures Using Bistable Elements to be published by University of South Florida.

Permission is granted for the specific use as stated herein and does not permit further use of the materials without proper authorization. Proper attribution must be made to the author(s) of the materials. **Please note**: if any or all of the figures and/or Tables are of another source, permission should be granted from that outside source or include the reference of the original source. ASME does not grant permission for outside source material that may be referenced in the ASME works. There can be no sales of the ASME papers listed above on ProQuest.

As is customary, we request that you ensure full acknowledgment of this material, the author(s), source and ASME as original publisher. Acknowledgment must be retained on all pages printed and distributed.

Many thanks for your interest in ASME publications.

Sincerely,

ASME
SETTING THE STANDARD

Beth Darchi
Publishing Administrator
ASME
2 Park Avenue, 6th Floor
New York, NY 10016-5990
Tel 1.212.591.7700
darchib@asme.org

From: Ahmad Alqasimi [mailto:aalqasim@mail.usf.edu]
Sent: Sunday, October 4, 2015 12:00 AM
To: permissions@asme.org
Subject: CONFERENCE PUBLICATIONS PERMISSION REQUEST

Dear Permissions Department,

I am a graduate student at the University of South Florida. I'm currently writing my dissertation and I would like to ask permission to include the two conference papers presented in ASME for Mechanisms and Robotics Conference.

The two papers are:
DETC2014-34285
DETC2015-47526

Please see the attached individual permission form for each paper.

I appreciate your time,

Ahmad Alqasimi
PhD Student
Department of Mechanical Engineering
University of South Florida

H.2 Copyright Permission for Material Used in Figure 5.12 and Figure 5.14

Mc Graw Hill Education

PERMISSION LICENSE: EDUCATIONAL ELECTRONIC AND PRINT USE

Request ID/Invoice Number: AHM4768

Date: August 27, 2015

To: Ahmad Alqasimi
         University of South Florida
         4202 E Fowler Ave
         Tampa, FL 33620
         United States
         "Licensee"

McGraw-Hill Education Material

Author: Norton, Robert L.
Title: Design of Machinery, Edition-5
ISBN: 9780077421717
Description of material: Figure 2-11 Part 1(b) on Page 49 and Figure 2-11 Part 2(d) on Page 50

Fee: Waived

Purpose of Reproduction

Course: Dissertation, Ph.D.
School: University of South Florida
Number of Copies: 1
Distribution: One-time educational use in above-referenced course only.

Permission for the use described above is granted under the following terms and conditions:

1.   McGraw-Hill Education hereby grants Licensee the non-exclusive right to use the McGraw-Hill Education Material as outlined and to reproduce and distribute the McGraw-Hill Education Material as outlined on condition that the related textbook is the required text for the course identified above. The McGraw-Hill Education Material may be used only as outlined. All use of the McGraw-Hill Education Material is

216

subject to the terms and conditions of this Agreement. This permission will automatically terminate at such time as the related textbook is no longer required.

2. No changes may be made to the McGraw-Hill Education Material without the prior written consent of McGraw-Hill Education.

3. Licensee will provide to McGraw-Hill Education the URL and password for the web site in which the McGraw-Hill Education Material appears (if applicable).

4. McGraw-Hill Education makes no representations or warranties as to the accuracy of any information contained in the McGraw-Hill Education Material, including any warranties of merchantability or fitness for a particular purpose. In no event shall McGraw-Hill Education have any liability to any party for special, incidental, tort, or consequential damages arising out of or in connection with the McGraw-Hill Education Material, even if McGraw-Hill Education has been advised of the possibility of such damages. All persons provided with the McGraw-Hill Education Material must be provided with written notice of this disclaimer and limitation liability, either in an end-user license and/or with an on-screen notice that is visible each time the end-user initiates access to the McGraw-Hill Education Material.

5. A credit to McGraw-Hill Education shall be visible each time the end-user initiates access to any screen or page containing any of the McGraw-Hill Education Material. Such credit shall include the title and author of the work and a copyright notice in the name of McGraw-Hill Education.

6. A SIGNED COPY OF THIS AGREEMENT should be sent to McGraw-Hill Global Education Holdings, LLC, Attn: Permissions Department, Wells Fargo Bank , Lockbox #6167, PO Box 8500, Philadelphia, Pa. 19178-6167.

7. This permission does not cover the use of any third-party copyrighted material, including but not limited to photographs and other illustrations, which appears in the McGraw-Hill Education Material with a credit to other sources. Written permission to use such material must be obtained from the cited source.

8. McGraw-Hill Education shall have the right to terminate this Agreement immediately upon written notice to Licensee if Licensee is in material breach of this Agreement.

9. Licensee shall indemnify McGraw-Hill Education from any damages, lawsuits, claims, liabilities, costs, charges, and expenses, including attorney's fees, relating to its use of the McGraw-Hill Education Material.

10. This Agreement incorporates the parties' entire agreement with respect to its subject matter. This Agreement may be amended only in writing and signed by both parties and shall be governed by the laws of New York. Licensee may not assign this Agreement or any rights granted hereunder to any third party.

Please sign and return one to the address as outlined in Clause 6 of this agreement.

For McGraw-Hill Education:

Name ___Nandini Acharya_____
Permissions Department
McGraw-Hill Education

For Licensee:

Name _____

Title ___Ph.D. Candidate_____

ABOUT THE AUTHOR

Ahmad Erfan M. Alqasimi was born in Saudi Arabia in 1984. He attended King Fahd University of Petroleum and Minerals (KFUPM) where he earned a Bachelor degree (BS) in Mechanical Engineering in 2006. He then worked as a Field Engineer for Schlumberger, an oil service company, for three years. He pursued his Master's degree (MSc) in Mechanical Engineering Design, from the University of Manchester, in 2010. His passion for the field motivated him to pursue the highest level of education. He joined the University of South Florida in 2011, where he discovered his passion for the Compliant Mechanism field after taking a course with his current supervisor, Dr. Craig Lusk, whose supervisor is the author of the Compliance Mechanism book, Dr. Larry Howell. After five years of hard work and extensive research, he earned his Doctorate of Philosophy (PhD) in Mechanical Engineering in 2015.